Effect of Temperature on Prestressed Concrete Bridge Girder Strand Stress during Fabrication

A Thesis
SUBMITTED TO THE FACULTY OF
UNIVERSITY OF MINNESOTA
BY

Tanner W. Swenson

IN PARTIAL FULFILLMENT OF THE REQUIREMENTS
FOR THE DEGREE OF
MASTER OF SCIENCE

Dr. Catherine E. W. French

October 2015

Acknowledgements

To begin, I would like to thank the Minnesota Department of Transportation for providing me the opportunity to pursue a Master's degree and conduct a research project on their behalf. Their involvement was a critical factor in developing the skills required to begin a successful and satisfying career in structural engineering.

I would also like to thank those who were essential to the completion of the project at the ground level. Nothing could have been done without the willingness of the precasting plant to accommodate my instrumentation of girders during their busy fabrication schedule. I would like to thank the staff and students who sacrificed their own time to help me when no one else would, especially Anna Flintrop, Davide Giannuzzi, Ben Dymond, and Paul Bergson.

I would like to sincerely thank my wife, Jessie, for the continuous encouragement, love, and support during my career as a college student, both during my undergraduate and graduate studies. She continues to inspire me to keep moving forward and grow in all facets of life.

Finally, I would like to thank Dr. Cathy French for her genuine interest in pushing me to get the most out of my experience as a graduate student. Her vast array of knowledge and insight were as invaluable as what she left for me to discover for myself.

Table of Contents

List of Tables

List of Figures

CHAPTER 1. INTRODUCTION

1.1 Introduction and Problem Statement

Before 2007, the Minnesota Department of Transportation (MnDOT) found that many precast, prestressed concrete bridge girders were arriving at the construction site with cambers much lower than predicted. It was thought that the method for estimating the camber at the time of erection was the problem. The method being used at the time was the "PCI multiplier method," which specified that the upward deflection due to initial prestress and downward deflection due to self-weight be multiplied by 1.80 and 1.85, respectively. In 2007, MnDOT began using a single multiplier of 1.5, but observed erection cambers were still lower than predicted.

In a study conducted by O'Neill et al. (2012), it was found that, for 1067 girders produced between 2006 and 2010, the average camber at release on average was only 74% of the predicted design camber. The main factor contributing to the lower than predicted cambers was the underestimation of the concrete elastic modulus at release. The underestimation of the elastic modulus resulted from two factors. First, the relation used to predict the modulus was the ACI 363 equation associated with high strength concrete (i.e., $f'_c \geq 6{,}000$ psi) rather than the Pauw (1960) equation. Second, the concrete compressive strength at release used in the equation was underestimated by approximately 15% on average. These factors accounted for the majority of the difference in the measured to predicted cambers. The remainder of the difference was attributed to possible prestress losses due to thermal effects during fabrication. Because the girders are cast on a fixed bed, changes in temperature during fabrication cause associated changes in stress in the strands. In this study, it was assumed that the temperature changes that occur prior to steel/concrete bond result in unrecoverable changes in prestress force that become locked in the girders. This report summarizes an investigation of these thermal effects on the strand force and girder camber.

1.2 Research Objectives

The primary objective of this study was to determine the effects of temperature on strand force throughout the fabrication process for precast, prestressed concrete girders and to recommend potential improvements to the procedures used to account for the effects, if warranted. The project involved fabricating small prestressed concrete segments, termed "short girders," that were detensioned at early ages to try to determine the time and temperature at which bond occurred. It was assumed that at bond, the prestress force in the strand becomes "locked in" to the concrete section. Any changes in temperature after that time were considered to produce recoverable changes in force. Four full-scale sets of MnDOT girders were instrumented with thermocouples, strain gages, and load cells in some cases, to investigate the temperature effects during fabrication. The four sets of girder productions were selected to investigate parameters believed to influence the temperature effects during fabrication: ambient temperature (cold vs. warm weather), exposure conditions for free length of strand (i.e., covered/uncovered by tarps), and casting with different precasting bed occupancies.

The investigation included the following activities:

- Conduct tests on set of six short girder sections released at early concrete ages to determine the time and temperature associated with bond of the strand to concrete for the typical concrete mix used in MnDOT bridge girders.
- Conduct tests on four full-scale precast, prestressed concrete bridge girder productions to investigate the effects of temperature on the strand force during fabrication; activities included monitoring temperatures along the bed and through the girder sections and force changes in the strands throughout the fabrication process. Girder cambers were measured at release and compared to predicted values.
- Measure concrete compressive strengths and corresponding elastic moduli of concrete cylinder samples to (1) investigate strength and stiffness gain with time, (2) investigate relationship between concrete compressive strength and elastic moduli, and (3) determine measured modulus to be used in elastic shortening and camber calculations.

- Conduct thermal effects analysis to determine strand force changes and initial camber estimates using measured temperature, strand force, and concrete modulus of elasticity data.
- Validate the results of the thermal effects analysis using measured strain, strand force, and camber measurements.
- Conduct parametric study to investigate the effects of ambient temperature at tensioning and release, bed occupancy, and effects of adjustment methods on the prediction of strand force and girder camber.
- Develop potential recommendations for MnDOT and the precasting plant to reduce potential strand force losses due to temperature effects during fabrication and improve initial camber predictions.

1.3 Organization of Report

The report is organized as follows:

- Chapter 2 summarizes previous research pertaining to precast, prestressed concrete girder fabrication and the mechanism of bond between concrete and steel prestressing strand.
- Chapter 3 describes the thermal effects analysis conducted to determine the theoretical strand force changes and initial camber estimates using measured temperature, strains, and concrete elastic modulus data obtained during field tests. The current method used by MnDOT for determining initial camber is also described.
- Chapter 4 describes the instrumentation used in the short girder bond test and the full-scale girder tests. This chapter also describes instrument calibration and data processing.
- Chapter 5 describes the short girder bond test procedure and concrete cylinder tests to determine the time, temperature, and concrete strength, when bond was believed to occur. The thermal effects analysis, described in Chapter 3, is used to predict the strain changes at release, which are compared to the measured results. In addition, the thermal effects analysis is used to investigate the strain changes observed in the free strand during fabrication.

- Chapter 6 describes the full-scale girder test procedure and results. The effects of four parameters on strand force and camber are investigated: casting in cold weather, casting in warm weather, covering portions of the free strand with tarps and steam heating the precasting bed, and bed occupancy. The thermal effects analysis is used to determine theoretical strand force changes due to temperature, concrete strain distributions through the section after release, and cambers, which are compared to measured data.
- Chapter 7 describes a parametric study performed to investigate the effects of ambient temperatures at tensioning and release and concrete temperatures at release on the cambers at release and after the concrete has cooled to ambient temperature. The potential effects of strand force adjustments on camber are also investigated.
- Chapter 8 summarizes the recommendations.

CHAPTER 2. LITERATURE REVIEW

2.1 Introduction

This chapter summarizes some of the previous research pertaining to prestressed concrete girder fabrication and concrete-steel bond. Most of the studies examined girder fabrication as a small portion of a larger study on long-term behavior. The literature review is organized into two sections. The first section reviews previous research pertaining to important variables during prestressed concrete girder fabrication, such as concrete material properties and effects of temperature on strand force. The second section reviews the mechanisms of bond between concrete and prestressing steel. There is little if any research available on the time, temperature, and concrete strength at which bond occurs.

2.2 Prestressed Concrete Girder Fabrication

The following studies investigated the effects of fabrication issues on the initial and long-term behavior of precast, prestressed concrete girders. These issues included effects of temperature and concrete material properties (e.g., compressive strength and modulus of elasticity).

2.2.1 O'Neill et al. (2012)

"Validation of Prestressed Concrete I-Beam Deflection and Camber Estimates"

O'Neill et al. (2012) investigated discrepancies between predicted and measured cambers in prestressed concrete bridge girders for the Minnesota Department of Transportation (MnDOT). Historical girder data revealed that measured release camber values were, on average, only 74% of the design camber values. O'Neill attributed the low camber measurements primarily to concrete strengths at release that exceeded design values, the use of an equation that underestimated the modulus of elasticity of the concrete, and prestress losses due to thermal effects.

O'Neill found that the concrete strength at release was, on average, 15.5% higher than the design strength in the girders constructed from the years 2006 to 2010. Because the concrete elastic modulus is a function of the compressive strength, higher strength concrete would be stiffer, so camber measurements would be lower because camber is inversely related to stiffness. O'Neill conducted a study in which nine models for estimating the elastic modulus of concrete were compared to measured values over time. It was found that the Pauw (1960) equation most closely predicted the modulus.

O'Neill stated that the precasters correct strand stress for strand temperature changes from the time of tensioning to the time of concrete placement, but additional losses could occur because the concrete bonds to the strands at a higher temperature due to hydration. Because the strands are anchored to a fixed-length bed, changes in thermal strain inversely influence mechanical strain, meaning temperature increases cause decreases in strand stress and vice versa. Additional stress changes due to temperature changes occur after the concrete has bonded to the strands because the thermal coefficients of the two materials differ, but as noted in the present study, these changes due to temperature changes after bond should be considered recoverable.

A parametric study was conducted based on studies by Barr et al. (2005) and Erkmen at al. (2008) to investigate prestress and release camber changes due to altering the total strand area, girder size, amount of free length of strand, and concrete and ambient temperatures. It was found that variations in the amount of free length of strand in combination with variations in ambient air temperatures at time of pull and time of bond cause the largest range of prestress and camber changes. High ambient air temperatures at time of bond relative to the time of pull caused the greatest net camber loss.

To more accurately predict the release camber, it was suggested that the design concrete release strength be multiplied by a factor of 1.15 and that the Pauw equation be used to estimate the elastic modulus of concrete instead of the ACI 363 equation used by MnDOT. It was also suggested that the assumed initial strand stress be reduced by 3% from $0.75f_{pu}$ to $0.72f_{pu}$ to account for relaxation and thermal effects. A temperature correction spreadsheet was made available as an option for fabricators, which, if used, eliminated the need for the 3% reduction.

2.2.2 Barr et al. (2000)

"High Performance Concrete in Washington State SR18/SR516 Overcrossing"

The behavior of High-Performance Concrete (HPC) in precast, prestressed bridge girders was investigated. Five girders from the SR18/SR516 overcrossing were instrumented at the time of fabrication and monitored over three years. Vibrating wire strain gages (VWG) were used to measure strain changes and temperatures throughout the girder sections and a stretched-wire system was used to record camber measurements.

During the casting of the girders, Barr observed higher temperatures in the top of the girder section than the bottom. This was attributed to the steam heating process used in the winter months, with heat collecting underneath insulated blankets near the top of the girders and the cold ground drawing heat away from the bottom of the girders. The concrete plant used a Sure-Cure system to regulate the curing temperature of the concrete cylinders tested to determine concrete strength at release. Barr noted that the temperature probe for the Sure-Cure system was typically located at mid-height of the girders. This indicated that the concrete at the bottom of the girder section typically cured at a lower temperature than the cylinders from which the concrete strength at the time of detensioning was determined, so Barr estimated that the cylinders were stronger than the bottom flange concrete.

The detensioning process of each girder was closely monitored. Strain changes were recorded by the VWG during each stage of detensioning. Immediate strain increases were observed in the girder section as sets of strands were released, while gradual strain increases were observed between stages. Barr attributed the gradual strain increases to creep. The cross-sectional strain distributions immediately after destressing were examined to determine if plane sections remained plane. However, Barr observed some non-linearity in the strain distribution and explained that stress concentrations caused by lifting the girder near the end during destressing could have accounted for the nonlinear strain profile.

2.2.3 Barr et al. (2005)

"Effects of Temperature Variations on Precast, Prestressed Concrete Bridge Girders"

Barr et al. (2005) studied the effects of temperature on prestressed bridge girders during fabrication and service. Prestress forces and cambers were affected by temperature during fabrication in three main ways. The first involved temperature changes from time of strand pull to the time of bond. Strand length is fixed between abutments, so changes in thermal strain turn into changes in mechanical strain and, therefore, force. The second way involved the difference in the coefficient of thermal expansion of the strand and the concrete. The concrete hydrates and bonds at a temperature much higher than the typical ambient temperatures that the girder will experience during service. As the girder cools, residual stresses form due to the relative contraction of the steel to the concrete. The third way involved the temperature gradient throughout the girder cross section. As some locations are hotter than others while the concrete hardens, stresses are induced when the section cools to a uniform service temperature.

Temperature and concrete material property data were obtained during fabrication of girders from the WashingtonSR18/SR516 bridge (Barr et al., 2000). The data were used in a thermal effects analysis to estimate the magnitudes of the three temperature effects on the prestress and camber at release. The analysis showed, assuming bond gradually occurs between 6 and 10 hours after the concrete was poured, effects of high fabrication temperatures between tensioning and bond resulted in 3 to 7% losses in prestress at release and 26 to 40% reductions in initial camber compared to what would be expected without considering temperature effects. The first temperature effect was found to have the largest impact on strand stress, but a minimal effect on camber. The second effect was found to be relatively small on both strand stress and camber. The third effect was found to be small on strand stress, but the most significant of the three effects in the reduction of camber. It was determined that the current design procedures, while ignoring thermal effects, were sufficient based on the large number of well-performing girders in service and the conservatism in other components of the design procedure.

2.2.4 Newhouse & Wood (2008)

"The Effect of Temperature on the Effective Prestressing Force at Release for PCBT Girders"

In 2008, Newhouse and Wood investigated the effective prestressing force after losses prior to release. Six full-depth precast concrete bulb tee (PCBT) sections of short length and three full-size beams were monitored during fabrication. Vibrating wire strain gages (VWG) and thermocouples were located at midspan of the six short PCBT specimens. The authors used measured strain changes at release to estimate the amount of force in the strands at that time. Strain changes in the top and bottom of a given beam were used to calculate the change in curvature of the section, which was in turn used to calculate the strain change at the center of the strand group. The elastic shortening losses were then calculated as the product of the strain change at the center of strands and the modulus of elasticity of the strand, taken as 28,500 ksi.

The measured strain data estimated an average of 14.42 ksi (99.4 MPa) in elastic shortening losses, while prestress loss models (i.e., Modified NCHRP 496, AASTHO LRFD, and ZPSW) predicted 10.35 ksi (71.4 MPa) of elastic shortening on average. The observed curvature and modulus of elasticity of concrete were used to calculate the effective prestress in the steel, which was found to be 27.09 ksi (187MPa) higher than the jacking stress. This meant that the strain changes at release recorded in the bottom of the girders were much larger than expected.

The authors discussed three possible explanations for the large strains. First, the modulus of elasticity of the concrete in the beams was lower than that of the concrete test cylinders. The measured modulus of elasticity was 5200 ksi (35.9 GPa) and was consistent with predicted values for concrete with compressive strengths of 7800 psi (53.8 MPa). However, to replicate the observed strain changes with calculations, a modulus of 3460 ksi (23.9 GPa) would have to be used. The authors could not justify such a low modulus of elasticity of concrete to be present in the girders.

The second explanation involved VWG data corrections accounting for difference in the coefficient of thermal expansion between the concrete and the steel wire within the

gage. Studies have shown that the coefficient of thermal expansion of concrete is highly variable during the early hours of curing (Kada, 2002). However, the effects of the different coefficients were believed to be negligible over short time periods, so it would not affect the strain change at release.

The final explanation, which the authors believed was the most logical, was that the concrete achieved an expanded state during the early hours of curing due to increasing temperatures and potentially high coefficients of thermal expansion of concrete in a plastic state. After the initial period of expansion, the concrete was believed to experience shrinkage when it hardened. This could have introduced restraint forces from the strands and formwork, which would have put the concrete in tension. At release, the restraints would be removed and the gages would measure the reduction in tensile strains caused by the restraints in addition to the traditional elastic shortening loss.

2.2.5 Rizkalla et al. (2011)

"Predicting Camber, Deflection, and Prestress Losses in Prestressed Concrete Members"

Rizkalla et al. (2011) investigated the accuracy of camber predictions made by the North Carolina Department of Transportation (NCDOT) because construction problems were arising due to discrepancies between predicted and measured cambers. Site visits to precasting plants were conducted to identify factors during girder fabrication that could affect the accuracy of camber predictions. A large number of concrete cylinders were tested during the site visits and it was found that the concrete compressive strength was, on average, 25% higher than the specified design value at transfer and 45% higher at 28 days. The concrete modulus of elasticity was found to be, on average, only 85% of the value predicted based on the 2004 AASHTO LRFD Specifications (i.e., the Pauw (1960) model, see Equation (5-1) in this report) with a concrete unit weight of 150 pcf (956 kN/m^3). It was noted that the concrete properties can potentially vary between girders cast on the same bed due to the need for multiple concrete batches and the time delays between batches.

Considered to be less significant factors than the concrete properties were the temperatures of the concrete and strands during production and the project schedule.

Temporary thermal gradients due to heat curing or solar effects could temporarily affect camber. The force changes due to the temperature fluctuations between the times of tensioning and transfer were mentioned, but not thoroughly investigated. The production schedule of the precasting plant could cause identical girders to experience different time dependent changes by the time of erection. It was determined that little could be done to mitigate these factors.

2.2.6 Ahlborn et al. *(2000)*

"High-Strength Concrete Prestressed Bridge Girders: Long Term and Flexural Behavior"

In 2000, as part of an investigation of high-strength concrete prestressed bridge girders, Ahlborn et al. studied prestress losses and initial camber. The force in the strand at the time of tensioning was determined from the foil gages on the strands. Low-relaxation 0.6 in. diameter seven-wire prestressing strand was tested for an apparent modulus of elasticity with foil strain gages oriented along the axis of the helical outside wire. Ahlborn found that, when converting strain gage readings to stress values, an apparent modulus of 29,100 ksi (200,700 MPa) should be used.

It was found that foil strain gages attached to the prestressing strand could not be relied upon for accurate prestress loss measurements because they cannot measure losses due to relaxation and drift over time. Equation (2-1) was derived for calculating the force in the strand immediately after release, $P_{after\text{-}release}$, which accounted for stress in the concrete that may have developed before release:

$$P_{after-release} = \left[\frac{1}{\frac{1}{A_{net}} + \frac{e_{net}^2}{I_{net}}}\right]\left(\frac{M_{sw}e_{net}}{I_{net}} - (\Delta\varepsilon_{vw-release}E_{ci}) - \sigma_{before-release}\right) \qquad (2\text{-}1)$$

where:

A_{net}	Net area of concrete
e_{net}	Eccentricity of force from centroid of net concrete section
I_{net}	Net moment of inertia of concrete section
M_{sw}	Moment due to self-weight of girder at midspan
$\Delta\varepsilon_{vw\text{-}release}$	Strain change recorded at release by vibrating wire gage
E_{ci}	Modulus of elasticity of concrete at time of release
$\sigma_{before\text{-}release}$	Concrete stress immediately before release

The concrete stress before release, $\sigma_{before\text{-}release}$, was unknown, so lower and upper bound values were assumed. The lower bound assumed that the concrete was unstressed at the time of release, so $\sigma_{before\text{-}release} = 0$. The upper bound assumed that the girder stress before release was equal to the 28-day cracking strength of the concrete. This was justified because cracks were observed in the girders by the research team prior to release.

Using the lower and upper bound assumptions for the concrete stress before release, the steel stress loss from the time of tensioning until just after release was estimated. Ahlborn found that, for her two girders, the lower bound measured losses were 15.5 and 18.6% and the upper bound measured losses were 29.1 and 29.3%, respectively. Because they were based on measured strain changes, the losses included all changes in stress of the prestressing strand during that time, including relaxation, elastic shortening, and concrete stresses generated from temperature effects and shrinkage.

2.2.7 Kada et al. (2002)

"Determination of the Coefficient of Thermal Expansion of High Performance Concrete from Initial Setting"

Kada et al. (2002) investigated the effects of shrinkage in high performance concrete (HPC) on cracking at early ages. The authors stated that the strains caused by autogenous shrinkage are related to the absolute volume contraction of the hydrated cement paste. Concrete hydration also produces heat, so the volumetric variations due to

thermal expansion must be separated from those due to shrinkage. To do so, the coefficient of thermal expansion of the concrete must be understood during the early stages of curing.

Tests were performed on 4 x 4 x 16 in. (100 x 100 x 400 mm) concrete beams. Three water-to-cementitious ratios (0.45, 0.35, and 0.30) were investigated with six specimens, two for each ratio. Vibrating wire extensometers were installed in each specimen along the longitudinal axis. The specimens were removed from their formwork when the concrete was just strong enough to hold its own shape and wrapped in plastic bags to prevent evaporation and influence of humidity. The samples were then subjected to thermals shocks in heat-controlled water baths of 122°F (50°C) and 50°F (10°C) and vibrating wire extensometer readings were taken. The coefficient of thermal expansion of the concrete at a given time was found as a function of the total strain reading from the extensometer, the coefficient of thermal expansion of the extensometer, and the temperature change.

The results of the tests showed large variations in the coefficient of thermal expansion of the concrete up to approximately 10 hours after casting. The coefficient then leveled off and remained relatively constant at later ages. The authors concluded that the early age variation in concrete coefficient of thermal expansion is caused by the presence of water not yet linked in the system. Since water has a much larger expansion coefficient than concrete, the concrete coefficient of thermal expansion at the beginning of setting should be estimated at 3 to 4 times that of hardened concrete.

2.3 Concrete-Steel Bond

There is little if any research available on the initiation of bond between prestressing strand and concrete during the curing process; that is, when bond occurs . The following studies provide an understanding of the mechanisms of bond between concrete and prestressing strand.

2.3.1 Briere et al. (2013)

“Dilation Behavior of Seven-wire Prestressing Strand – The Hoyer Effect”

Briere et al. (2013) investigated the dilation behavior of seven-wire prestressing strand as it is tensioned and released, specifically the wedging action known as the Hoyer effect. Straight tendons decrease in diameter when tensioned due to the Poisson effect and, upon release, attempt to expand to their original diameter, causing friction that transfers the prestressing force into the concrete. Seven-wire strand diameter is decreased by both the Poisson effect and tightening of the individual wires upon tensioning. When released, the strand wants to expand, causing additional radial forces that result in more friction and a wedging effect within the transfer length, increasing the efficiency of the prestress transfer. However, the increased radial stresses can cause cracking in the concrete if released at an early age.

Briere et al. also discussed strain measurement correction that is necessary when using foil strain gages to monitor seven-wire strand. Gages are applied to the helical wires that twist about the longitudinal axis of the strand at an angle θ (termed β in the paper). For 0.6 in. (15.2 mm) diameter seven-wire prestressing strand, the authors determined an angle of twist of 8.2°. The strain measured along the helical axis, ε_h, must be transformed to determine the strain along the longitudinal axis, ε_c. The authors summarized findings by Machida and Durelli (1973) to determine an expression (Equation (2-2)) for the longitudinal strain:

$$\varepsilon_c = \varepsilon_h / \cos(\theta)^2 \tag{2-2}$$

where:

ε_c	Strain along the longitudinal axis of the strand
ε_h	Measured strain along the axis of the helical wire
θ	Angle of strain gage relative to longitudinal axis of strand

2.3.2 Janney (1954)

"Nature of Bond in Pre-tensioned Prestressed Concrete"

In 1954, Janney studied the bond between pretensioned steel wire reinforcement and concrete. It is important to note that this study was performed on smooth, single strand prestressing wire rather than seven-wire strand that are commonly used in the present day. He outlined three main factors that contribute to bond; adhesion between

concrete and steel, friction between concrete and steel, and mechanical resistance due to deformations in the steel reinforcement. Janney found that adhesion is only a factor in locations where no slip had occurred in the wire in the central region of the test specimen. Mechanical resistance was also deemed negligible because the wire was very smooth and without deformities. Therefore, friction was thought to be the main factor in the stress transfer from steel to concrete.

To test prestress transfer bond, Janney conducted a series of tests on concrete prisms in which he monitored the stress transfer of a single pre-tensioned wire to the concrete. A number of parameters thought to influence bond strength were investigated, including wire diameter, coefficient of friction between the wire and the concrete, surface condition of the wire (clean, lubricated, or rusty), and concrete strength.

A theoretical model for transfer length based solely on friction was developed using Poisson's ratio of steel and concrete to account for the radial expansion of the wire due to a decrease in elongation. The theoretical stress transfer distribution curves generated from the model showed that higher coefficients of friction are more effective at transferring stress into the concrete.

Janney found that larger wire diameters required longer distances to fully transfer stress. However, the small size of the test specimens caused the larger diameter wires to lose more tension force because the concrete stress was considerably higher, so the results were not consistent among wire diameters. It was found that higher concrete strength at release caused the stress transfer to be accomplished over a shorter distance due to the increased ability of the concrete to resist the radial expansion of the wire, leading to higher normal forces and, therefore, friction forces. Finally, Janney found that rusted wire resulted in shorter transfer lengths, while lubricated wire resulted in longer transfer lengths due to reduced friction. These results led to the conclusion that "the prestress transfer bond is largely a result of friction between concrete and steel." While mechanical resistance was not considered to be a large factor by Janney in his study, it could contribute considerably to bond in twisted wire.

2.4 Conclusion

In the studies reviewed in Section 2.2, the discrepancies between predicted and measured concrete properties were a common cause for the poor camber predictions that motivated the investigations. One study investigated the effects of temperature on strand stress and camber and determined that the thermal gradient through the section caused by cooling between bond and release had the greatest effect on camber. While temperature effects on strand force were cited as a potential cause for error in multiple studies, they were not thoroughly investigated. Although the concrete stress just before release is typically assumed to be zero in design calculations, multiple studies commented on potential temperature and shrinkage related tensile stresses in the concrete. The tensile concrete stresses were thought to account for differences in estimated and measured elastic shortening losses.

The mechanisms of bond between concrete and prestressing steel were reviewed in Section 2.3 to better understand the interactions between the concrete and steel, especially during the early stages of curing. This is important in determining the non-recoverable strand force losses due to temperature changes from tensioning to bond. Mechanical resistance of the hardening concrete on the seven-wire strand during curing likely influences the amount of strand force that is lost between tensioning and bond due to temperature effects, as bonding is a gradual process. Very few of the studies addressed the time and temperature at which bond is expected to initiate, which further supported the need for the short girder tests described in Chapter 5 of this study. Barr et al. (2005) assumed that bond occurred between 6 and 10 hours after casting for calculation purposes, as summarized in Section 2.2.3.

The study by Briere et al. (2013) provided a relationship to determine the longitudinal strand strain from measurements obtained on instrumented helical wires. This was useful in interpreting the strand strain gage data in the present study.

CHAPTER 3. METHODOLOGY TO DETERMINE THERMAL EFFECTS ON PRESTRESS FORCE AND CAMBER

3.1 Introduction

This chapter describes the methodology and assumptions used to determine the effect of temperature on strand force throughout the prestressed concrete girder fabrication process. Assumptions used to estimate the force after transfer and associated girder camber are also described. The chapter is arranged in accordance with the steps undertaken during the fabrication process. The following is a brief overview of the process.

During prestressed concrete girder fabrication, temperature changes cause changes in strand force because the strand length is fixed between the abutments on the prestressing bed. Temperature changes are caused by ambient air conditions, solar effects, steam heating, and concrete hydration. It is important to accurately estimate the temperature along the length of the strand to determine the strand force at any given time during the fabrication process.

Although bond between the steel and the concrete is likely a gradual process, for the sake of simplicity, it was assumed that bond occurred at a specific point in time. Prior to that time, the strand was assumed to have a constant force along the length of the precasting bed. At bond, the strand force becomes "locked" into the girder at that temperature, and the concrete and steel are assumed to act compositely from that point. It was assumed that the concrete coefficient of thermal expansion and modulus of elasticity remained constant after bond. Between the time of bond and release, temperature changes can cause stresses to develop in the concrete due to the difference in coefficients of thermal expansion of steel and concrete and due to forces in that develop in the section to equilibrate force changes in the free strand. These stresses may result in prerelease cracks in the girders. Potential bending of the section due to the difference in thermal coefficients of expansion between the steel and the concrete was ignored prior to release.

Just after release, camber is induced in the girder and is a function of the strand force transfer into the section and the girder self-weight. Additionally, the difference between the coefficient of thermal expansion of steel and concrete causes girder deflection based on the change in temperature between bond and release. As the girder continues to cool, further deflection occurs due to the differences in coefficients of thermal expansion between the steel and concrete.

3.2 Thermal Effects Analysis Procedure

To analyze the effects of temperature on strand force, four key points in time were identified in the girder fabrication process: tensioning (*T*), steel-concrete bond (*B*), release (*R*), and normalization (i.e., girder cooling after release) (*N*).

Figures 3.1 and 3.2 show a flowchart and renderings, respectively, that outline the steps followed in the thermal effects analysis and the factors that affect strand force at the key times during the fabrication process. The description of each of the steps, including the detailed description of the notation used in Figures 3.1 and 3.2, is provided in Section 3.3 . This section provides a brief overview.

The forces in the strand inside the girder(s) ($P_{strand,girder}$) and outside the girder(s) in the free strand ($P_{strand,free}$) and in the concrete at the center of gravity of the strands ($P_{concrete,cgs}$) are given during each step in terms of the notation used throughout the chapter. The subscripts "*s*" and "*c*" refer to the steel and concrete, respectively. Various steps in the process and stages between steps are denoted by corresponding subscripts. As an example, "*T-B*" stands for the process between tensioning the strand and bonding of the strand to the concrete. The subscript "*B-R,after*" corresponds to the process between bond and just after release. Camber is denoted with "*C*" and the deflection components are denoted with "*D*."

Besides the determination of the camber at release (C_R) and after cooling to a normalized temperature (C_N), the analysis provides information on the potential tensile forces generated in the concrete that may introduce cracks prior to release and the force in the free strand during that stage. The understanding of these factors can help to prevent cracking in the girder and fracture of the strand due to a large drop in ambient temperature before release.

Because the strand force becomes “locked” into the girder at bond, changes in strand force due to temperature effects between tensioning and bond are not recoverable. Any force change due to temperature that occurs after bond can be recovered if the system returns to the original temperature at the time of bond.

The renderings in Figure 3.2 illustrate the force changes that occur during the fabrication process in the free strand and within the girder at the center of gravity of the strand from tensioning to just before release. After release, the force components are superimposed on the transformed and net girder sections, as appropriate, to determine the camber at release and after the temperature has reached a selected ambient temperature, referred to as “Normalization.” As shown in Figures 3.1 and 3.2, the effect of strand relaxation is ignored until release.

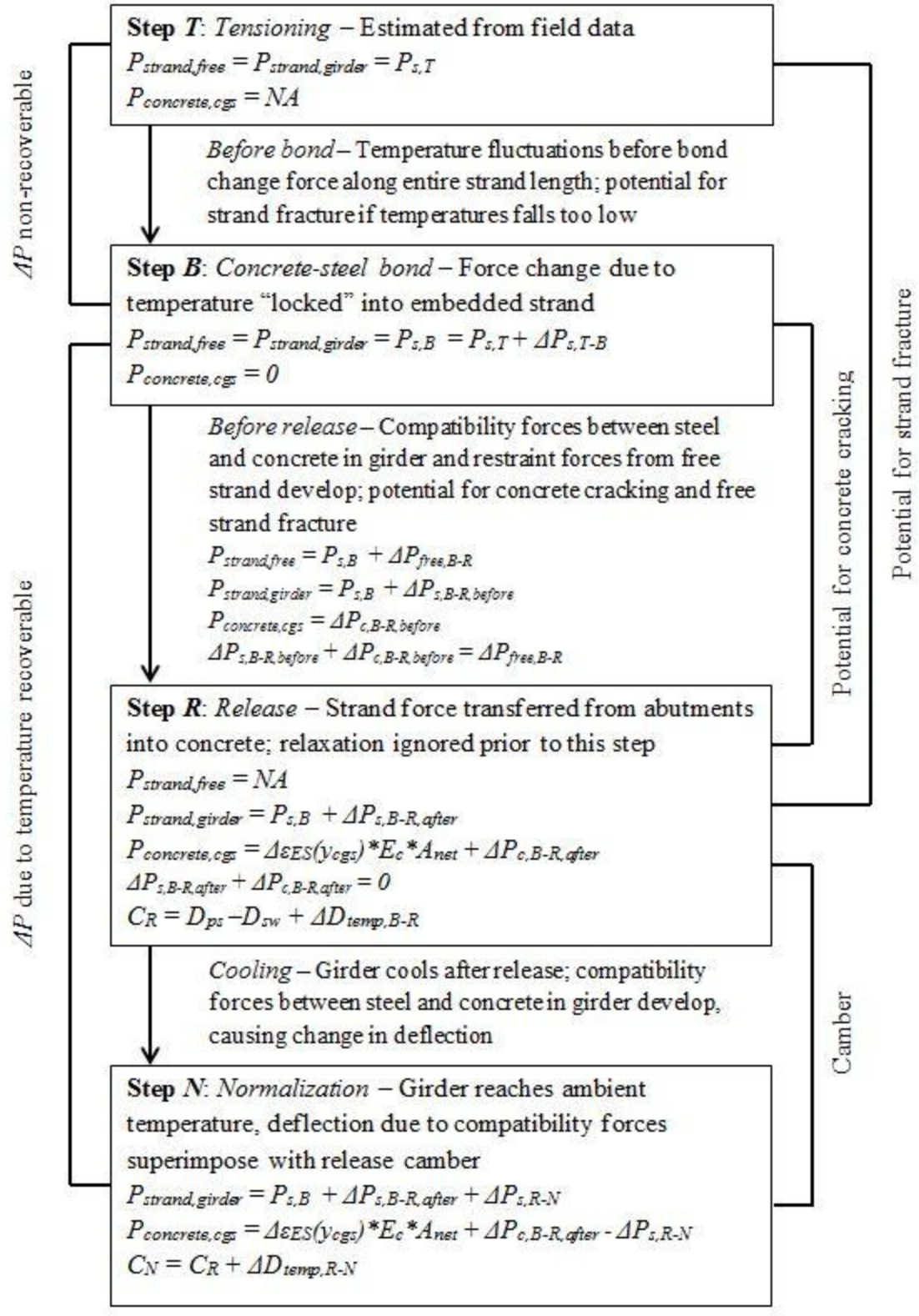

Figure 3.1: Thermal effects analysis flowchart

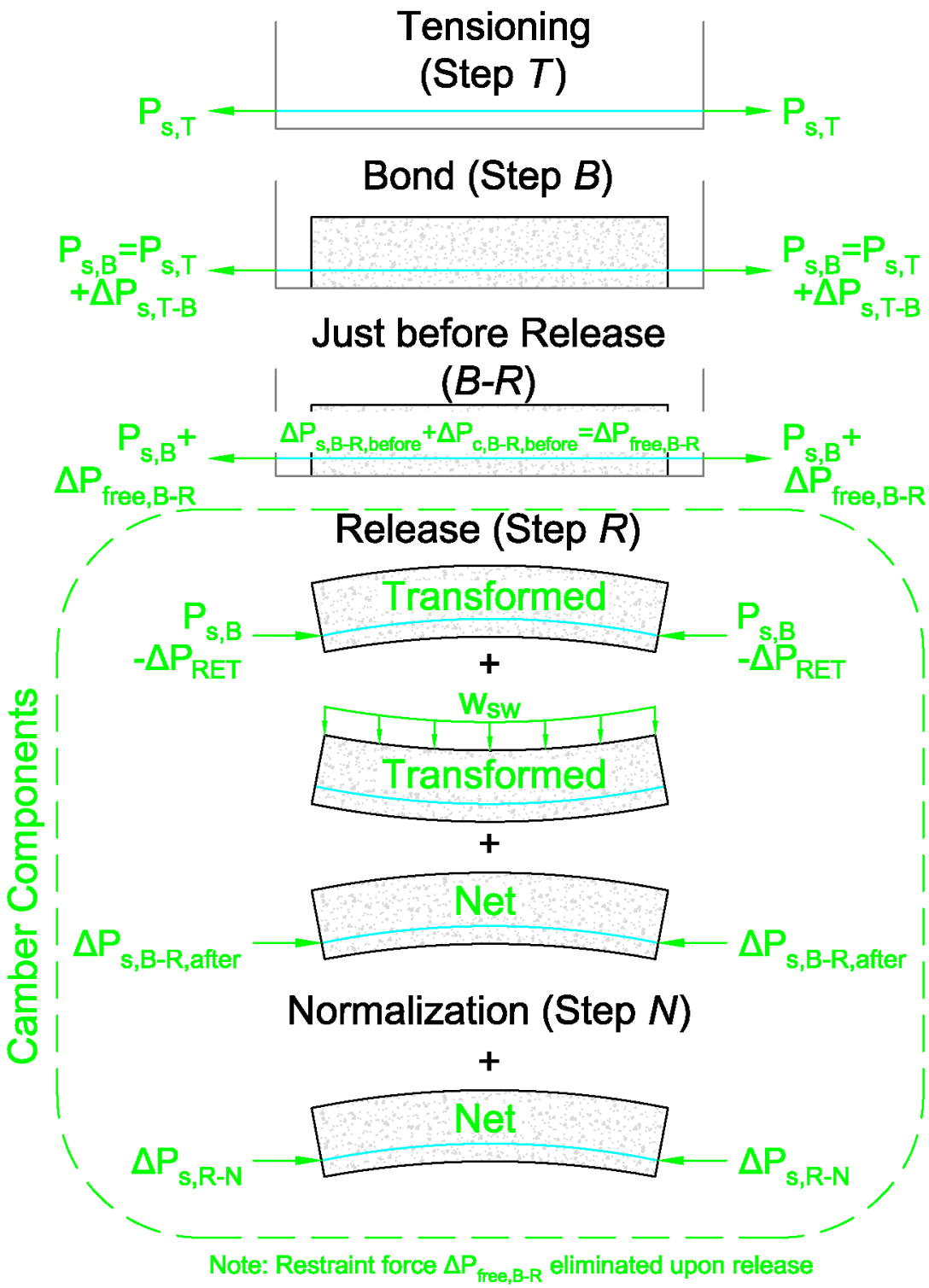

Figure 3.2: Illustration of force changes during fabrication and superposition of force components after release to determine camber

3.2.1 Simplifying Assumptions used in Thermal Effects Analysis

The following assumptions were used to simplify the analysis:

1. The entire length of strand was assumed free prior to bond (i.e., friction due to hold-downs, end forms, and wet concrete were ignored).
2. Strand and concrete temperatures were assumed to be uniform at a section (i.e., the effects of thermal gradients were ignored and changes in strand force due to temperature were assumed the same for all strands, see Appendix B).
3. The concrete coefficient of thermal expansion was assumed constant.
4. The concrete modulus of elasticity was assumed constant from time of bond to normalization and was taken as the average measured value just before release, where available; where not available, the modulus was based on the Pauw equation with the measured concrete compressive stress.
5. The effects of the hold-downs and friction between the precasting bed and the girders were generally ignored (i.e., the girders were assumed to be free to slide along the bed). This assumption is termed "Case A." As described in Section 3.3.3.1, consideration of the hold downs providing restraint was explored with "Case B" assumptions in Section 6.4.1.
6. The effects of the transfer regions of the strands at the girder ends were ignored.
7. Time dependent effects of creep and shrinkage were ignored.

3.2.2 Parameters Assumed in Thermal Effects Analysis

While the variables pertaining to girder geometry were well defined, multiple parameters required reasonable estimations for use in the thermal effects analysis. This section describes the estimations of the average temperature of the prestressing steel at bond based on assumed time of bond, average strand temperature based on measured data, coefficients of thermal expansion of steel and concrete, and the elastic modulus of concrete.

3.2.2.1 Average Temperature of the Prestressing Steel at Bond

Estimating the average temperature of the prestressing steel at bond is required to determine the initial prestress that gets "locked" into the girders. After bond, it was assumed that the steel was perfectly bonded to the concrete and changes in strand strain were associated with equal changes in the concrete strain at the center of gravity of the strands. Changes in temperature after that point were assumed to create compatibility stresses in the strand and concrete due to the differences in coefficients of thermal expansion between the two materials.

To determine the temperature at bond, multiple methods were used to estimate the time at which bond occurs in the fabrication process. Knowing the time at which bond occurs, it is possible to determine the corresponding average temperature in the prestressing steel using a series of thermocouples. One method to determine the time and temperature of bond was to measure the compressive strength and stiffness gains of a series of cylinders as a function of time and temperature during curing. A second method was to release a set of six short prestressed concrete girders at different ages during their curing process (i.e., between 5 and 26 hours after casting) to investigate the force transfer from the strands to the concrete. Based on the cylinder tests and short girder tests described in Chapter 5, it was estimated that bond occurred between 6 and 8 hours after casting. Because full-scale girders can take multiple hours to pour on a single precasting bed, the range was initially expanded to consider that bond occurs between 6 and 10 hours after casting commenced on the bed. Further exploration of the initiation of bond was investigated in Chapter 6 with the full-scale girder tests to investigate which assumed time and temperature of bond best matched the thermal effects analysis. It was observed that if the rate of temperature increase was slowed, so was the strength gain and the initiation of bond. A temperature of 100°F (38°C) generally appeared to correspond with what was deemed to be the initiation of bond for the MnDOT prestressed concrete girder mix used in the study.

3.2.2.2 Average Strand Temperature

The thermal effects analysis is highly dependent on the temperature changes that occur along the length of the strand, both inside the girders and along the free strand. To

accurately determine the average strand temperature during fabrication, thermocouples were placed at multiple locations along at least one strand during each test. A length of strand was assigned to each thermocouple over which the measured temperature was assumed to be constant. For example, one thermocouple could have been assumed to represent a 20 ft segment of strand. Locations that were assumed to be similar to each other, such as the north and south quarter points of a girder, were assumed to have the same temperature. Consequently, data from a thermocouple located at one of those cross sections was assumed to represent the temperature at the mirrored location. Temperature readings over time were used to model the force change in the strand over time.

Because temperature data was sparse during the first three full-scale girder tests, it was important to validate the assumption that the temperatures in the girder were symmetric about midspan. Figures 3.3 and 3.4 show the temperatures on Strand 1 during full-scale girder Test 4 at the girder ends and approximate quarter points, respectively. The figures show that temperatures are generally similar at similar locations. However, the south quarter point of Girder 1 experienced a much lower peak temperature than the other quarter points. This was likely due to the locations of steam heating outlets on the bed. Differences in similar locations could cause inaccuracies in the thermal effects analysis when temperatures had to be assumed at certain locations along the bed due to lack of instrumentation.

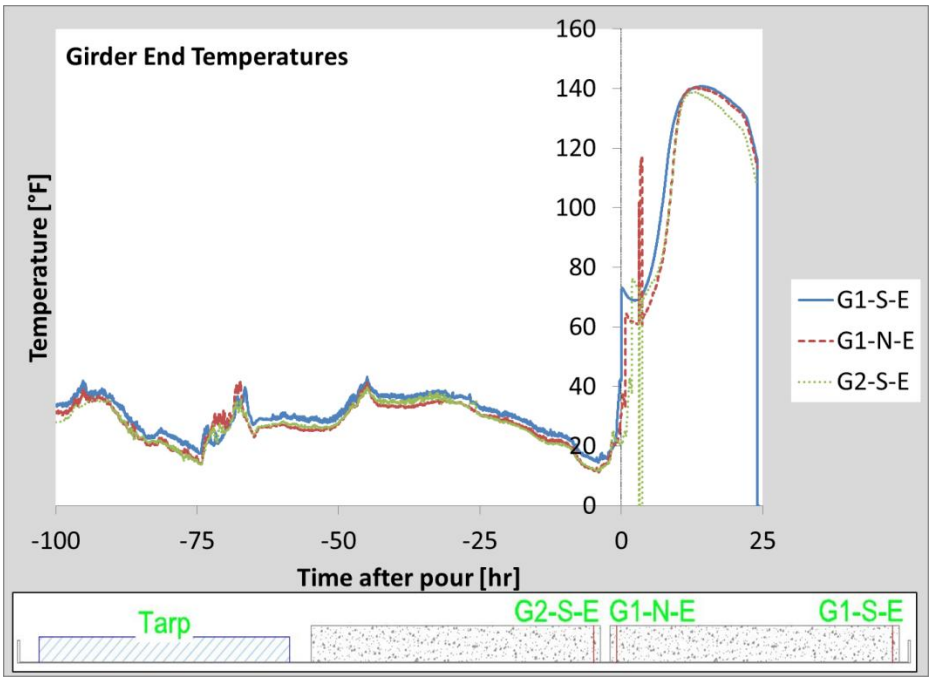

Figure 3.3: Girder end temperatures during full-scale girder Test 4 fabrication

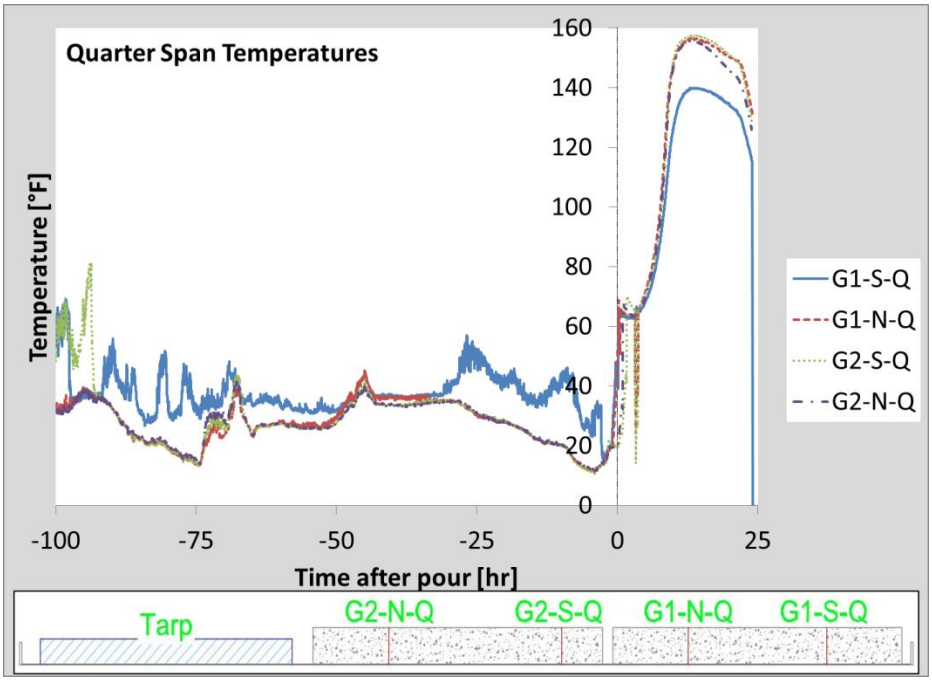

Figure 3.4: Girder quarter span temperatures during full-scale girder Test 4 fabrication

3.2.2.3 Thermal Coefficients of Expansion of Steel and Concrete

The thermal coefficient of expansion was assumed to be 6.78 10^{-6}/°F (12.2 10^{-6}/°C) for steel and 5.78 10^{-6}/°F (10.4 10^{-6}/°C) for concrete. The value assumed for the steel was assumed in previous research (Barr et al. (2000) and O'Neill et al. (2012)). The assumed concrete coefficient of thermal expansion was equal to values used by those authors, but the actual thermal coefficient of concrete is highly variable, particularly during hydration, as discussed in Section 2.2.7. For simplicity, it was assumed that the thermal coefficient of concrete was constant after bond.

3.2.2.4 Elastic Modulus of Concrete

The concrete elastic modulus was measured just before the time of release for all but the first full-scale girder test. Multiple cylinders (2 to 3) were tested and the average measured modulus was used in the camber calculations. Data obtained from cylinder tests described in Section 5.3.2 show that the Pauw (1960) model sufficiently estimated the elastic modulus at the time of bond. This conclusion was also made by O'Neill et al. (2012). Concrete compressive strength values measured by the precasting plant just before release were used with the Pauw (1960) equation to estimate the elastic modulus where values were not measured. It was assumed that the elastic modulus of concrete was constant after bond. These values are given in Chapters 5 and 6 in association with the fabrication process.

3.2.2.5 Strand Relaxation

Strand relaxation between the time of tensioning and release was determined in accordance with the PCI Committee on Prestress Losses (PCI, 1975). Low-relaxation strands were used in this project. The strand force loss due to relaxation between tensioning and release is given by Equation (3-1):

$$\Delta P_{RET} = P_{s,T}\left[\frac{\log t_R - \log t_T}{45}\right] * \left[\frac{P_{s,T}}{A_{ps} f_{py}} - 0.55\right] \quad (3\text{-}1)$$

where:

A_{ps}	Total area of prestressing strands
f_{py}	Yield stress of prestressing strand
$P_{s,T}$	Total strand force after tensioning
t_R	Time of release in hours relative to tensioning
t_T	Time of tensioning taken as 1 hour
ΔP_{RET}	Total force loss due to strand relaxation

and:

$$\frac{P_{s,T}}{A_{ps} f_{py}} - 0.55 \geq 0.05$$

$$f_{py} = 0.9 f_{pu}$$

where:

f_{pu}	Ultimate strength of prestressing strand

The ultimate strength of the prestressing strand used in this project was 270 ksi (1.86 GPa). The methods for determining the total strand force after tensioning are described in Section 3.3.1. The time of tensioning and release were recorded during each fabrication.

3.3 Detailed Description of the Steps in the Thermal Effects Analysis

3.3.1 Tensioning (Step T)

At the beginning of the prestressed girder fabrication process, the prestressing strands were each tensioned with a hydraulic jack. Before each strand was fully tensioned, an approximately 4,000 lb (17.8 kN) preload was introduced into each strand to lift them off the bed and untangle them. The force was then released from the jack and transferred to the chuck holding the strand in place. A string potentiometer was used by the plant personnel to measure the gross and net strand elongations between the preload and after seating. The gross value was recorded when the hydraulic jack was holding the strand at the required tension. The net value was recorded when the jack had been released and the strand had seated in the chuck. Because the string potentiometer was zeroed after the preload was applied, it was assumed that 4,000 lb was the actual load in

the strand before the gross and net elongations were recorded. Equation (3-2) was used to calculate the initial strand force, $P_{s,i}$, in strand *i* after seating:

$$P_{s,i} = \frac{\Delta L_{net,i}}{L_{bed}} E_{ps} A_{strand} + P_{preload} \quad (3\text{-}2)$$

where:

A_{strand}	Area of a single strand
E_{ps}	Strand modulus of elasticity
L_{bed}	Total length of precasting bed
$P_{preload}$	Preload force during tensioning (per strand)
$P_{s,i}$	Tension force after seating in straight strand *i*
$\Delta L_{net,i}$	Net elongation as recorded by precasting plant in strand *i*

The total initial strand force, $P_{s,T}$, was taken as the average initial strand force calculated for the straight strands multiplied by the total number of strands (both straight and draped), shown in Equation (3-3):

$$P_{s,T} = \frac{\sum_{i=1}^{N_{strand,straight}} P_{s,i}}{N_{strand,straight}} N_{strand,total} \quad (3\text{-}3)$$

where:

$N_{strand,straight}$	Number of straight prestressing strands on the precasting bed
$N_{strand,total}$	Total number of prestressing strands (straight and draped) on the precasting bed
$P_{s,T}$	Total strand force after tensioning

The initial strand force for the draped strands was not calculated directly because the strands were not fully tensioned with the hydraulic jack. The draped strands were initially pulled to a lower force than the straight strands, which was determined beforehand based on girder geometry. The workers then positioned “horses” just outside the girder ends and lifted the strands to the correct height with a forklift, so the remaining strand force was induced by the strand elongation in the process. This means that the net elongation recorded for each draped strand in the jacking process was not representative of the total force achieved in that strand, so the average straight strand initial force was assumed for the draped strands.

3.3.2 Bond (Step B)

"Bond" refers to the time at which the concrete has sufficiently hardened and the steel strand and concrete begin to act as a composite material. It is assumed that the strand force at the time of bond is "locked" into the strand within the girder section and any strand force changes beyond that point are recoverable. Between the time of tensioning and the time of bond, temperature changes occur along the length of the bed that result in non-recoverable strand force changes. Assuming the precasting bed is fixed length, the total length change of a strand due to temperature and mechanical strain changes has to sum to zero, as shown in Equation (3-4):

$$\Delta L_{bed} = \sum_{seg=1}^{N_{seg}} \Delta L_{seg} = 0 \tag{3-4}$$

where:

L_{seg} Length of given strand segment *seg*

N_{seg} Total number of strand segments along the bed

Additionally, assuming that the strand is unrestrained between the two abutments (i.e., before bond has occurred), the reactions at the two abutments must be equal and opposite. In other words, the force in the strand must be constant along the length of the bed. This assumption neglects elements that could change the force along the bed, such as friction associated with draping.

Total strain consists of two parts: mechanical strain and thermal strain. For each section of strand, the total change in strand strain for that segment is given by Equation (3-5):

$$\Delta\varepsilon_{Tot,seg,T-B} = \Delta\varepsilon_{mech,seg,T-B} + \Delta\varepsilon_{therm,seg,T-B} = \frac{\Delta P_{s,T-B}}{E_{ps}A_{ps}} + \alpha_s \Delta T_{seg,T-B} \tag{3-5}$$

where:

A_{ps}	Total area of prestressing strands
α_s	Assumed coefficient of thermal expansion of strands
$\Delta P_{s,T\text{-}B}$	Change in girder strand force from tensioning to bond
$\Delta T_{seg,T\text{-}B}$	Change in temperature of strand segment *seg* from tensioning to bond
$\Delta \varepsilon_{mech,seg,T\text{-}B}$	Mechanical strain change in strand segment *seg* from tensioning to bond
$\Delta \varepsilon_{therm,seg,T\text{-}B}$	Thermal strain change in strand segment *seg* from tensioning to bond
$\Delta \varepsilon_{Tot,seg,T\text{-}B}$	Total strain change in strand segment *seg* from tensioning to bond

The change in force, $\Delta P_{s,T\text{-}B}$, must be the same in each segment of strand if the strand is unrestrained between the abutments, even if the temperature changes in the segments are different. The change in length of a strand section is given by the change in total strain multiplied by the length of that section. The sum of all length changes must equal zero because the total strand length is assumed constant between the abutments as shown in Equation (3-6):

$$\begin{aligned} 0 = \sum_{seg=1}^{N_{seg}} \Delta L_{seg} &= \sum_{seg=1}^{N_{seg}} (\Delta \varepsilon_{Tot,seg} L_{seg}) \\ &= \sum_{seg=1}^{N_{seg}} \left(\frac{\Delta P_{s,T-B}}{E_{ps} A_{ps}} L_{seg} + \alpha_s \Delta T_{seg,T-B} L_{seg}\right) \\ &= \frac{\Delta P_{s,T-B}}{E_{ps} A_{ps}} \sum_{seg=1}^{N_{seg}} L_{seg} + \alpha_s \sum_{seg=1}^{N_{seg}} \Delta T_{seg,T-B} L_{seg} \end{aligned} \tag{3-6}$$

Equation (3-6) can be rearranged to solve for the change in strand force due to temperature changes between the time of tensioning and the time of steel-concrete bond, $\Delta P_{s,T\text{-}B}$, as given in Equation (3-7).

$$\Delta P_{s,T-B} = \frac{-\alpha_s \sum_{seg=1}^{N_{seg}} \Delta T_{seg,T-B} L_{seg}}{\sum_{seg=1}^{N_{seg}} L_{seg}} E_{ps} A_{ps} \tag{3-7}$$

The total strand force at the time of bond is given by Equation (3-8):

$$P_{s,B} = P_{s,T} + \Delta P_{s,T-B} \tag{3-8}$$

where:

$P_{s,B}$	Total strand force within girder at bond

This force is equal to the force in the free strand at bond.

3.3.3 Release (Step R)

"Release" refers to the process of cutting the strands and transferring the strand force from the abutments into the girder section, prestressing the girder causing it to camber. The camber is a function of the girder geometry, amount of force in the strands, elastic properties of the steel and concrete, and self-weight of the girder. Additionally, the difference in the coefficients of thermal expansion of the steel strand and the concrete affect the girder forces and deflections based on the difference in temperature between bond and release.

Because restraint forces that can develop in the free strand have the potential to generate cracking in the concrete and potential fracture of the strand prior to release, it is important to also investigate the behavior before release as discussed in 3.3.3.1. The situation after release is described in 3.3.3.2 through 3.3.3.4. Because the system is assumed to be linearly elastic, superposition was used to examine the individual force components due to incompatibility forces and elastic shortening.

3.3.3.1 Concrete and Steel Force Changes with Free Strand Restraint (Just Before Release)

To determine the temperature related force changes in the strand (within girder and free) and the concrete due to the difference in steel and concrete coefficients of thermal expansion (i.e., compatibility forces) and free strand restraint, a system of equations was solved from the following relationships.

After the concrete is bonded to the strands, any change in strain must be equal between the two materials at the center of gravity of the strands (*cgs*). Equation (3-9) shows the strain compatibility relationship between the steel and concrete at the *cgs* ignoring the flexural component due to the eccentricity of the strands:

$$\left(\frac{\Delta P_{s,B-R,before}}{E_{ps}A_{ps}} + \alpha_s \Delta T_{c,B-R}\right) - \left(\frac{\Delta P_{c,B-R,before}}{E_c A_{net}} + \alpha_c \Delta T_{c,B-R}\right) = 0 \qquad (3\text{-}9)$$

where:

A_{net}	Net cross sectional area of concrete girder section
E_c	Modulus of elasticity of concrete
α_c	Assumed coefficient of thermal expansion of concrete
$\Delta P_{c,B\text{-}R,before}$	Resultant concrete force at center of gravity of strands with free strand restraint between bond and just before release
$\Delta P_{s,B\text{-}R,before}$	Change in girder strand force with free strand restraint between bond and just before release
$\Delta T_{c,B\text{-}R}$	Average change in temperature of concrete from bond to release, assuming the steel and concrete have the same temperature at a section

The above equation reflects the behavior in the case where the strands are located at the center of gravity of the concrete. As a simplification, the effect of the gradient due to strand eccentricity was ignored prior to release. Because of the restraint provided by hold downs prior to release, the assumption was considered to be reasonable.

Because the girder(s) is restrained by the free strand, the total change in force in the girder must be equal to the change in force in the free strand, as shown by equilibrium in Equation (3-10):

$$\left(\Delta P_{s,B-R,before} + \Delta P_{c,B-R,before}\right) - \Delta P_{free,B-R} = 0 \qquad (3\text{-}10)$$

where:

$\Delta P_{free,B\text{-}R}$	Change in free strand force between bond and release

Additionally, the total length of strand between the precasting bed abutments cannot change because the bed is a fixed length, so the total length change of the strand in the bed must sum to zero as shown in Equation (3-11):

$$\left(\frac{\Delta P_{s,B-R,before}}{E_{ps}A_{ps}} + \alpha_s \Delta T_{c,B-R}\right) + \left(\frac{\Delta P_{free,B-R}}{E_{ps}A_{ps}} + \alpha_s \Delta T_{free,B-R}\right)\left(\frac{1}{\beta} - 1\right) = 0 \qquad (3\text{-}11)$$

where:

β	Ratio of bed occupancy ($L_{g,tot}/L_{bed}$)
$L_{g,tot}$	Total length of girders on precasting bed
$\Delta T_{free,B\text{-}R}$	Average change in temperature of free strand from bond to release

The three force changes ($\Delta P_{s,B\text{-}R,before}$, $\Delta P_{c,B\text{-}R,before}$, and $\Delta P_{free,B\text{-}R}$) were solved using the previous three equations. Equation (3-12) gives the change in force in the

bonded strands within the girder(s), while Equation (3-13) gives the concrete reaction force generated in the girder(s):

$$\Delta P_{s,B-R,before} = \frac{-\left\{\left(\frac{1}{\beta}-1\right)\left[\frac{(\alpha_s-\alpha_c)\Delta T_{c,B-R}}{K}+\alpha_s\Delta T_{free,B-R}\right]+\alpha_s\Delta T_{c,B-R}\right\}}{\frac{1}{\beta}\left(\frac{1}{K}+1\right)-\frac{1}{K}}E_{ps}A_{ps} \quad (3\text{-}12)$$

$$\Delta P_{c,B-R,before} = \frac{-\left\{\left(\frac{1}{\beta}\right)(\alpha_c-\alpha_s)\Delta T_{c,B-R}+\left(\frac{1}{\beta}-1\right)\alpha_s\Delta T_{free,B-R}+\alpha_s\Delta T_{c,B-R}\right\}}{\frac{1}{\beta}\left(\frac{1}{K}+1\right)-\frac{1}{K}}E_cA_{net} \quad (3\text{-}13)$$

where:

K Relative axial stiffness of steel to concrete ($E_{ps}A_{ps}/E_cA_{net}$)

The concrete reaction force can be determined at any time between bond and release and the potential for cracking in the section can be evaluated. Equation (3-14) gives the change in force in the free strand:

$$\Delta P_{free,B-R} = \frac{-\left\{\left(\frac{1}{\beta}-1\right)\left(\frac{1}{K}+1\right)\alpha_s\Delta T_{free,B-R}+\left(\frac{\alpha_c}{K}+\alpha_s\right)\Delta T_{c,B-R}\right\}}{\frac{1}{\beta}\left(\frac{1}{K}+1\right)-\frac{1}{K}}E_{ps}A_{ps} \quad (3\text{-}14)$$

Note that, in the derivation of the equations in this section, it was assumed the girders were free to slide along the bed. However, in practice, the hold-downs may fix the girder in place on the bed. This could result in interactions between shorter girder and free strand lengths, which could result in different force changes due to temperature between bond and release. The effects of implementing a more complicated assumption regarding the locations of the hold-downs along the bed were investigated in Section 6.4.1, where the assumptions made in this section are referred to as Case A and the assumptions considering the hold-downs are referred to as Case B.

3.3.3.2 Incompatibility Forces due to Temperature (Immediately After Release)

Between bond and release, the incompatibility forces in the girder strand and concrete that develop due to the difference in steel and concrete coefficients of thermal expansion are also influenced by the presence of free strand, so they are not equal and opposite. However, when the free strand is released, the forces that were resisted by the abutments must be applied to the girder, including any changes in the free strand force that occurred between bond and release. This removes the discrepancy between the girder

strand force and the resultant concrete force at the center of gravity of the strands, so equilibrium is satisfied within the girder, as shown in Equation (3-15):

$$\Delta P_{s,B-R,after} = -\Delta P_{c,B-R,after} \tag{3-15}$$

where:

$\Delta P_{s,B\text{-}R,after}$ Change in girder strand force due to compatibility immediately after release

$\Delta P_{c,B\text{-}R,after}$ Resultant concrete force at center of gravity of strands due to compatibility immediately after release

Because the girder is able to deflect after the hold-downs are released, strain due to bending in the concrete portion of the girder section was considered. Strain compatibility between the steel and concrete applies at the center of gravity of the strands (*cgs*), as shown in Equation (3-16). Note that net concrete section properties were used in the equations because the steel and concrete were considered separately. The only unknown was the change in force in the steel, $\Delta P_{temp,B\text{-}R}$, so the strain compatibility expression was rearranged to solve for that value in Equation (3-17):

$$\begin{aligned} 0 = &\left(\frac{\Delta P_{s,B-R,after}}{E_{ps}A_{ps}} + \alpha_s \Delta T_{c,B-R}\right) \\ &- \left(\frac{-\Delta P_{s,B-R,after}}{E_c A_{net}} - \frac{\Delta P_{s,B-R,after}\left(e_{net,midspan}\right)^2}{E_c I_{net,midspan}} + \alpha_c \Delta T_{c,B-R}\right) \end{aligned} \tag{3-16}$$

$$\Delta P_{s,B-R,after} = \frac{-(\alpha_s - \alpha_c)\Delta T_{c,B-R}}{\frac{1}{E_{ps}A_{ps}} + \frac{1}{E_c A_{net}} + \frac{\left(e_{net,midspan}\right)^2}{E_c I_{net,midspan}}} \tag{3-17}$$

where:

$e_{net,midspan}$ Strand eccentricity from centroid of net concrete section at midspan

$I_{net,midspan}$ Moment of inertia of net concrete girder section at midspan

3.3.3.3 Elastic Shortening (Immediately After Release)

Transformed concrete section properties were assumed to determine the mechanical strain changes due to elastic shortening immediately after release assuming the temperature was constant between bond and release. The total strand force at the time of bond was assumed to act at the centroid of the strands calculated at midspan. Strand

relaxation was considered. Equation (3-18) gives the change in strain at a height *y* within the girder section at midspan due to elastic shortening upon release:

$$\Delta\varepsilon_{ES}(y) = -\left[\frac{P_{s,B} - \Delta P_{RET}}{A_{net} + A_{ps}\left(\frac{E_{ps}}{E_c}\right)} + \frac{(P_{s,B} - \Delta P_{RET})e_{t,midspan}(y_{t,NA} - y)}{I_{t,midspan}} - \frac{M_{sw}(y_{t,NA} - y)}{I_{t,midspan}}\right] \quad (3\text{-}18)$$

where:

$e_{t,midspan}$	Strand eccentricity from centroid of transformed concrete section at midspan
$I_{t,midspan}$	Moment of inertia of transformed concrete girder section at midspan
M_{sw}	Self-weight moment of girder
$y_{t,NA}$	Distance from the bottom to the neutral axis of the transformed girder section at midspan
ΔP_{RET}	Total force loss due to strand relaxation
$\Delta\varepsilon_{ES}(y)$	Concrete strain change at midspan due to elastic shortening at height *y* from the bottom of the girder section

3.3.3.4 Total Observed Strain Change at Release at Center of Gravity of Steel

When measuring the strain change at release within a girder with instrumentation, the observed value is the sum of two components: (1) the change in mechanical strain in the composite section due to the change in force in the free strand due to temperature between bond and release, and (2) the change in mechanical strain due to elastic shortening immediately after release.

When the strand bonds to the concrete in the girder, it is "locked in" with non-recoverable strand force losses associated with the changes in temperature between tensioning and bond. Concrete stress is assumed to be equal to zero when the strand bonds to the concrete. Temperature changes in the free strand and girder between bond and release cause changes in the concrete and embedded strand forces due to two factors: (1) the change in free strand force (i.e., "restraint forces"), which must be equilibrated by the concrete and strand within the girder, and (2) incompatibility forces (i.e., equal and opposite forces in the concrete and strand within the girder) generated due to the difference in coefficients of thermal expansion of the steel and concrete. The "restraint forces" have been observed to cause some pre-cracking in girders prior to release.

Assuming release to be an instantaneous process (even though it may take place over the course of an hour), the temperature at release can be assumed constant. Consequently, the incompatibility forces generated due to the differences in coefficients of thermal expansion between the steel and concrete remain the same just before and just after release and do not contribute to the mechanical strain change at release. Upon cutting the strands, the restraint force in the free strand is removed from the composite girder section and creates an associated mechanical strain change in the section. If the restraint force was tensile, the change in mechanical stress would appear compressive. This effect is calculated by applying a negative restraint force to the composite section.

In addition, to the change in strain due to the removal of the restraint forces, the section undergoes elastic shortening due to the force in the prestressing strand that was locked into the strand at bond.

Equation (3-19) gives the observed mechanical strain change at release for an instrument located at the center of gravity of the strands:

$$\begin{aligned}\Delta\varepsilon_{instr,cgs} &= \frac{-\Delta P_{free,B-R}}{E_c\left(A_{net}+A_{ps}\left(\frac{E_{ps}}{E_c}\right)\right)}+\frac{-\Delta P_{free,B-R}e_{t,midspan}{}^2}{E_c I_{t,midspan}}+\Delta\varepsilon_{ES}(y_{cgs})\\ &= -\frac{1}{E_c}\left[\frac{P_{s,B}-\Delta P_{RET}+\Delta P_{free,B-R}}{A_{net}+A_{ps}\left(\frac{E_{ps}}{E_c}\right)}\right.\\ &\quad\left.+\frac{\left(P_{s,B}-\Delta P_{RET}+\Delta P_{free,B-R}\right)e_{t,midspan}{}^2}{I_{t,midspan}}-\frac{M_{sw}e_{t,midspan}}{I_{t,midspan}}\right]\end{aligned} \tag{3-19}$$

where:

y_{cgs}	Distance from the bottom of the girder section to the center of gravity of the strands
$\Delta\varepsilon_{ES}(y_{cgs})$	Change in strain due to elastic shortening at *cgs*
$\Delta\varepsilon_{instr,cgs}$	Expected strain change at release in instrumentation located at the center of gravity of the strands

The temperature related components of the instrument strain change at release may account for some of the differences between estimated and measured elastic shortening losses observed in studies such as Newhouse and Wood (2008).

3.3.4 Camber

Because of the linear elastic assumptions, the camber at release was determined by superposition of the different deflection components: deflection due to the strand force transfer into the concrete, deflection due to the self-weight of the girder, and deflection due to compatibility forces generated by temperature changes between bond and release due to the difference between the thermal coefficients of steel and concrete. The use of draped strands in the girders results in changing transformed and net section properties along the length of the girder as the centroid of the strands shifts. The deflections were determined using the moment area method and assuming symmetry; that is, integrating the moment of the area underneath the curvature diagram from girder end to midspan and multiplying those areas by their distance from the girder end. The effect of the strand transfer length on strand force was neglected.

3.3.4.1 Deflection due to Strand Force Transfer to Concrete

The upward deflection due to the transfer of the strand force into the concrete was determined by assuming that the strand force at the time of bond acted on the transformed section, which varied along the span length due to the change in strand eccentricity. The force loss due to relaxation was included. It was assumed that the strand force was constant along the length of the girder (i.e., transfer lengths and potential force differences along the length of the girder were ignored). Because the strand pattern was symmetrical about midspan, the midspan deflection was taken as the moment of the area underneath the curvature diagram from the girder end to midspan about the support (i.e., the girder end), as shown in Figure 3.5. Equation (3-20) gives the upward deflection at midspan of the girder due to strand force transfer at release:

$$D_{ps} = \frac{(P_{s,B} - \Delta P_{RET})}{E_c} \int_0^{\frac{L_g}{2}} \frac{e_t(x)}{I_t(x)} x dx \tag{3-20}$$

where:

D_{ps}	Upward girder deflection due to strand force transfer to concrete
$e_t(x)$	Strand eccentricity from centroid of transformed concrete section at distance x from girder end
$I_t(x)$	Moment of inertia of transformed concrete girder section at distance x from girder end
L_g	Length of individual girder from end to end
ΔP_{RET}	Total force loss due to strand relaxation
x_{hold}	Distance from girder end to hold-down point for draped strands (used in Figure 3.5 to denote the change in eccentricity and transformed section properties along the length)

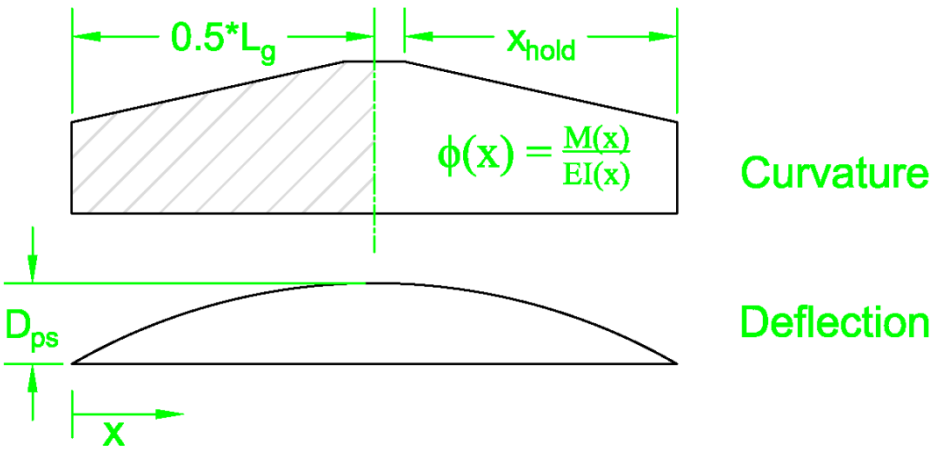

Figure 3.5: Girder curvature and deflection diagrams due to force transfer to concrete

3.3.4.2 Deflection due to Self-Weight of Girder

The downward deflection due to the self-weight of the girder was determined by assuming the girder weight was an external, uniformly distributed load acting on the transformed section. The magnitude of the distributed load was found by assuming a concrete unit weight of 155 pcf (2483 kg/m^3), based on the MnDOT assumption provided on the bridge plans for self-weight, and multiplying that value by the gross area of the girder section. Other concrete unit weight values were considered for estimating the concrete modulus of elasticity during the short girder and full-scale tests, but the MnDOT assumption was a reasonable assumption for self-weight considering the additional weight of reinforcing steel in the girder. The girder was assumed to be a simply-supported member to determine the moment at any point *x* along the length. The downward deflection at midspan due to the girder self-weight just after release was determined as described in the previous section, as shown in Equation (3-17):

$$D_{sw} = \frac{w_{sw}}{2E_c}\int_0^{\frac{L_g}{2}} \frac{(L_g - x)}{I_t(x)} x^2 dx \tag{3-21}$$

where:

D_{sw} Downward girder deflection due to girder self-weight

w_{sw} Uniformly distributed load from girder self-weight

3.3.4.3 Deflection due to Temperature Effects

Temperature changes that occur between bond and release generate forces in the girders to ensure compatibility because of the difference in thermal coefficients of the steel and concrete. To determine this effect on the deflection of the girder at release, the force change in the steel that results from compatibility was assumed to act as a point load at the center of gravity of the strands that is resisted by a coincident force generated in the concrete. A change in curvature in the section is induced because of the eccentricity of the strands. The deflection due to the change in curvature was determined as described in the previous sections, but with net concrete section properties instead of transformed section properties, as shown in Equation (3-22). Similarly to transformed section properties, the net concrete section properties change along the length of the girder because of the draped strands.

$$\Delta D_{temp,B-R} = \frac{\Delta P_{s,B-R,after}}{E_c} \int_0^{\frac{L_g}{2}} \frac{e_{net}(x)}{I_{net}(x)} x dx \quad (3\text{-}22)$$

where:

$e_{net}(x)$ Strand eccentricity from centroid of net concrete section at distance x from girder end

$I_{net}(x)$ Moment of inertia of net concrete girder section at distance x from girder end

$\Delta D_{temp,B-R}$ Change in deflection due to temperature effects between bond and release

Other temperature effects, such as the effect of thermal gradient, were later explored in Section 6.7.2.3 as an additional factor that may affect the measured camber at release.

3.3.4.4 Total Camber at Release

The initial camber (i.e., immediately after release) was determined by superimposing the deflections due to strand force transfer, girder self-weight, and temperature effects, as shown in Equation (3-23):

$$C_R = D_{ps} - D_{sw} + \Delta D_{temp,B-R} \quad (3\text{-}23)$$

where:

C_R Resultant camber immediately after release

3.3.5 Normalization (Step N)

"Normalization" refers to an arbitrary point in time at which the girder has cooled on the precasting bed after release. The equations from Sections 3.3.3.2 and 3.3.4.3, used to determine the change in strand force and deflection due to the difference in the coefficients of thermal expansion of the steel and concrete, can be applied with the change in average girder temperature between release and normalization.

The effects of creep and shrinkage were ignored for simplification, although they likely have some impact on camber. Once the forms are removed, concrete shrinkage is likely to begin and once the strands are released, concrete creep will begin. It was assumed that the girder behaved as a simply-supported member on the bed. When the girders are taken off of the precasting bed and put into storage, the boundary conditions change as the girder is supported on bunks (the ends of the girders typically cantilever beyond the supports when bunked), and aging effects become more significant, so the

equations in this section are only assumed to be valid while the girder is cooling on the precasting bed.

Equations (3-24), (3-25), and (3-26) give the strand force change, change in deflection, and resultant camber, respectively, due to temperature changes after release while the girder is cooling on the precasting bed. Equations (3-24) and (3-25) are identical to Equations (3-17) and (3-22) except that the temperature change considered is between release and normalization rather than between bond and release. The change in deflection is superimposed with the camber at release to determine the camber at normalization.

$$\Delta P_{s,R-N} = \frac{-(\alpha_s - \alpha_c)\Delta T_{c,R-N}}{\frac{1}{E_{ps}A_{ps}} + \frac{1}{E_c A_{net}} + \frac{\left(e_{net,midspan}\right)^2}{E_c I_{net,midspan}}} \tag{3-24}$$

$$\Delta D_{temp,R-N} = \frac{\Delta P_{s,R-N}}{E_c} \int_0^{\frac{L_g}{2}} \frac{e_{net}(x)}{I_{net}(x)} x dx \tag{3-25}$$

$$C_N = C_R + \Delta D_{temp,R-N} \tag{3-26}$$

where:

C_N	Resultant camber after normalization
$\Delta D_{temp,R\text{-}N}$	Change in deflection due to temperature effects between release and normalization
$\Delta P_{s,R\text{-}N}$	Change in girder strand force due to compatibility between release and normalization
$\Delta T_{c,R\text{-}N}$	Average change in temperature of concrete from release to normalization

3.4 Current MnDOT Camber Prediction Method

The Minnesota Department of Transportation (MnDOT) currently uses gross section properties to calculate the expected camber at release for standard girder shapes. The modulus of elasticity and strand stress at the time of release are estimated, so the expected camber is highly variable depending on the quality of those estimations. The girder section is assumed to behave elastically and strand relaxation is ignored. Because transfer takes place shortly after removing the formwork and the camber measurements

are taken almost immediately after release, other time-dependent effects (i.e., creep and shrinkage) are not considered.

The following equations detail the MnDOT approach to calculating elastic shortening and camber for the "MN" series shapes (e.g., the MN54 shapes investigated in this study) that are commonly designed. For the newer, larger "MW" series shapes (e.g., the 82MW shapes investigated in this study), computer programs are used to determine release and long-term camber. The notation used in this section reflects that used by MnDOT. Equivalent notation used in this report parenthetically follows that used by MnDOT, if applicable.

The prestress loss due to elastic shortening, Δf_{ES}, is given by Equation (3-27):

$$\Delta f_{ES} = \frac{\left(A_{ps} f_j (I_c + (e_{mid})^2 A_c)\right) - e_{mid} A_c M_{sw}}{\left(A_{ps}(I_c + (e_{mid})^2 A_c)\right) + \frac{I_c A_c E_{ci}}{E_{ps}}} \quad (3\text{-}27)$$

where:

A_{ps} Total area of prestressing strands

f_j Jacking stress in each strand

I_c Gross concrete moment of inertia

A_c Gross concrete area

E_{ci} Concrete modulus of elasticity at release

E_{ps} Strand modulus of elasticity

e_{mid} Strand eccentricity from centroid of gross concrete girder section at midspan

M_{sw} Self-weight moment

The total prestress force at release, P_{re}, is given by Equation (3-28):

$$P_{re} = A_{ps}(f_j - \Delta f_{ES}) \quad (3\text{-}28)$$

The upward deflection due to prestressing, Δ_{ps}, is given by Equation (3-29):

$$\Delta_{ps} = \frac{P_{re}}{E_{ci} I_c}\left(\frac{e_{mid} {L_{des}}^2}{8} - \frac{(e_{mid} - e_{end}) {x_{hold}}^2}{6}\right) \quad (3\text{-}29)$$

where:

e_{end} Strand eccentricity from centroid of gross concrete girder section at girder end

L_{des} Girder design length (L_g herein)

x_{hold} Distance from girder end to hold-down point for draped strands

The downward deflection due to self-weight, Δ_{sw}, is given by Equation (3-30):

$$\Delta_{sw} = \frac{5 w_{sw} L_{des}^{\ 4}}{384 E_{ci} I_c} \tag{3-30}$$

where:

w_{sw} Concrete self-weight

The total camber at release is given by Equation (3-31):

$$Camber = \Delta_{ps} - \Delta_{sw} \tag{3-31}$$

CHAPTER 4. INSTRUMENTATION

4.1 Introduction

This chapter outlines the instrumentation used in the study and any assumptions and corrections that were required to process the data. The instruments described in this chapter were used in both the short girder tests described in Chapter 5 and the full-scale girder tests described in Chapter 6.

4.2 Data Acquisition for Strain Gages and Thermocouples

Two data acquisition systems were utilized during the field tests for the foil strain gages, concrete strain gages, and thermocouples. The vibrating wire strain gages were read manually with a Model GK-403 Geokon digital readout box. The data acquisition for the load cells is described in Section 4.7.

4.2.1 CR1000

A Campbell Scientific CR1000 datalogger was used as the primary means to obtain foil strain gage, concrete strain gage, and thermocouple measurements. Model AM16/32 multiplexers were connected to the CR1000 through 4WFB120 120-ohm full bridge modules to expand the strain gage capacity of the system. Model AM25T multiplexers were used to record the thermocouple readings.

4.2.2 CR9000X

A Campbell Scientific CR9000X datalogger was used for recording measurements from foil strain gages and thermocouples during the tensioning process. A 4WFB120 120-ohm full bridge module was required for each strain gage. The CR9000X was utilized in addition to the CR1000 to increase the total number of instrument channels available for each test and to provide more flexibility in placing strain gages along the bed, as wire lengths were a limiting factor in placing instrumentation.

4.3 Foil Strain Gages

Tokyo Sokki Kenkyujo Co. (TML) model FLK-1-11-5LT 120-ohm foil strain gages were used to monitor strain changes in the prestressing strand. Factors applied to the data collected from these gages included a correction for apparent strain due to temperature and an apparent modulus of elasticity to convert the strains to stresses. These factors are discussed in the following subsections.

4.3.1 Apparent Strain due to Temperature

Mechanical strain measurements of foil strain gages are based on gage resistance changes. Gage resistance is also a function of temperature and, even though gages are "matched" to the media (e.g., steel) to which they are attached, an apparent strain due to temperature must be accounted for in data reduction if the temperature range over which the gage is used is significant. The manufacturer provided an equation to calculate apparent strain as a function of temperature. The apparent strain was subtracted from the raw strain reading for each point in time.

The apparent strain curve provided by the manufacturer was based on tests performed with gages attached to a specific base material. To verify that the curve was applicable to the gage application on prestressing strand used in this study, small strand samples were instrumented and heated in an oven. Figure 4.1 shows the combined strain readings from four gages on two separate strand samples compared to the curve provided by the manufacturer. While each gage behaved slightly differently and some hysteresis was observed, the manufacturer-provided curve was found to be reasonable due to its similarity to the best-fit line from the strain gage data.

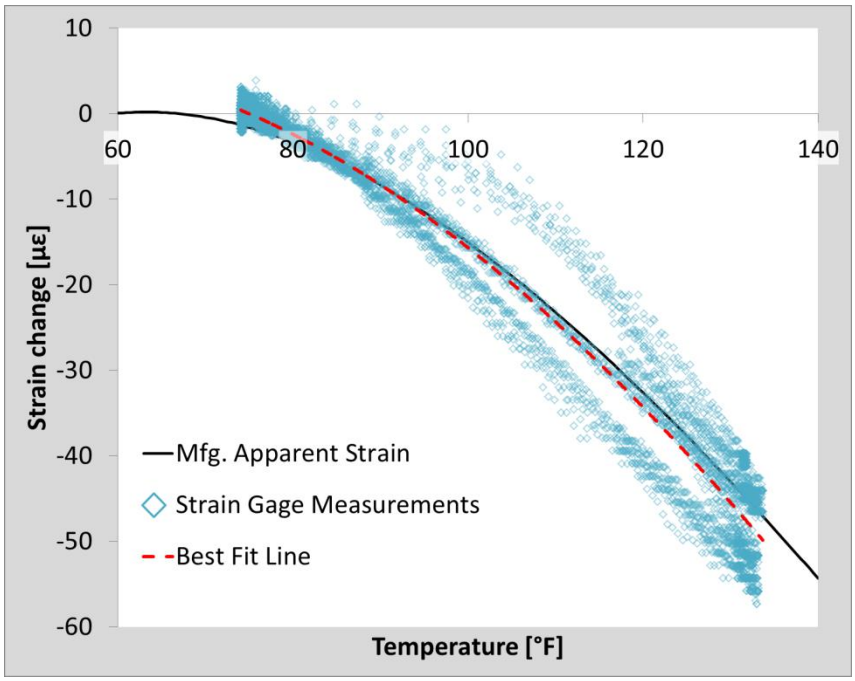

Figure 4.1: Apparent strain due to temperature for foil strain gages

4.3.2 Apparent Modulus of Elasticity

The foil strain gages attached to the prestressing strand were oriented along the axis of individual helical wires. Therefore, the true longitudinal strain was not measured by the strain gage. To convert strains to stresses, an apparent modulus of elasticity was used. The apparent modulus was obtained from precasting plant strand samples subjected to pull tests in the University of Minnesota Galambos Structures Laboratory.

To determine the apparent modulus and potential measurement errors due to variations in gage alignment, the samples were instrumented with foil strain gages attached to the helical wire oriented both along the axis of the wire and along the longitudinal axis of the strand. An extensometer with a gage length of approximately 1 in. (25 mm) was attached to the strand. The elastic stress-strain relationship was plotted for each instrument and the measured apparent modulus of elasticity was taken as the slope of the best fit line. This method was reasonable because the strands were tested within the elastic range and the measured stress-strain relationship was linear.

Figure 4.2 shows the average, minimum, maximum, and estimated apparent modulus of elasticity for strain gages aligned with the wire (aligned gage), strain gages

aligned with the axis of the strand (longitudinal gage), and the extensometer readings (extensometer) for the three strand samples tested. The estimated value for the aligned strain gages was obtained from Equation (2-2) given by Briere et al. (2013) in Section 2.3.1 assuming the angle of the helical wire was approximately eight degrees from the longitudinal axis of the strand. The apparent modulus of elasticity of the longitudinal strain gages was not estimated because it was not clear if the equation was valid for gages not aligned with the helical wire. The estimated modulus of elasticity of the extensometer was the elastic modulus provided by the strand manufacturer.

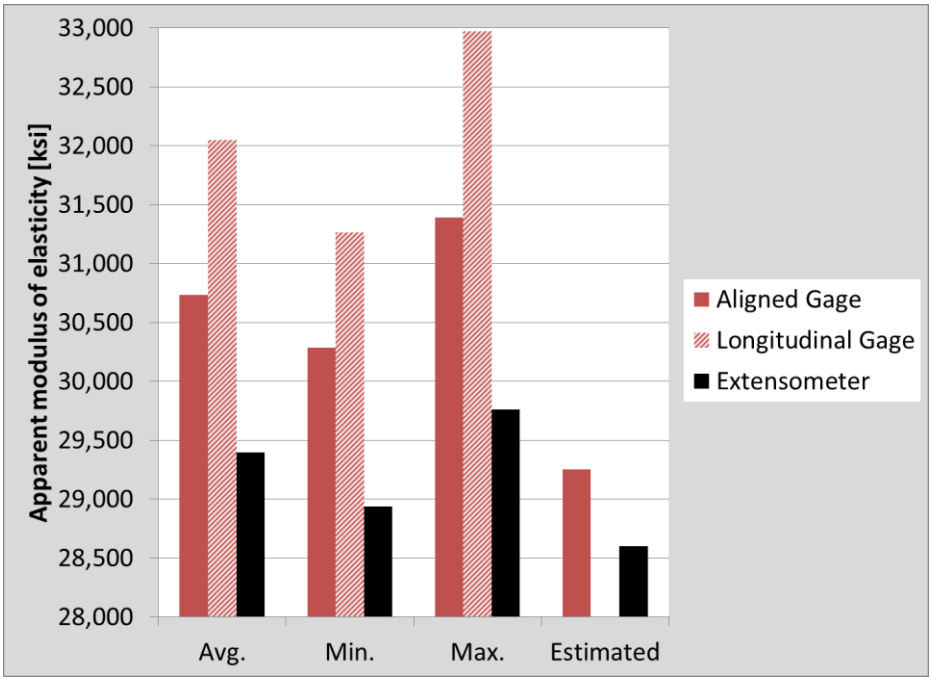

Figure 4.2: Apparent modulus of elasticity for foil strain gages on prestressing strand

The average measured apparent moduli were greater than the estimated values for all instruments. Strain gages were aligned with the helical wire in the field, so the apparent modulus of elasticity for the foil strain gage data in the field was taken as the average apparent modulus of 30,700 ksi (212 GPa) with a coefficient of variation of 1.1%.

4.4 Concrete strain gages

Model PML-60-2LT and PML-120-2LT 120-ohm TML resistive strain gages were used to monitor strain changes in the concrete through the girder cross sections at midspan. The readings obtained from the gages were corrected for temperature using an equation provided by the manufacturer. The gages were suspended within the girder sections with small pieces of fiber reinforced polymer (FRP) bar and rebar ties, as shown in Figure 4.3. It was assumed that the gages were aligned parallel to the length of the beam, but the impact of the concrete being poured into the formwork could have caused the gages to shift.

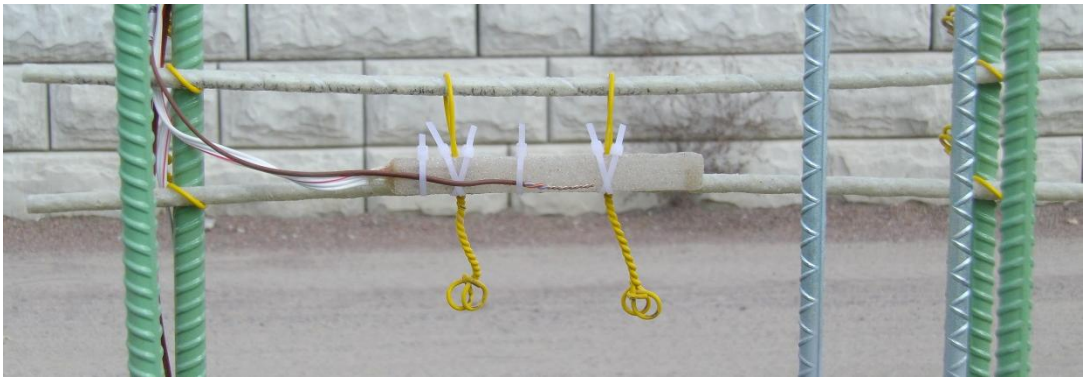

Figure 4.3: Concrete gage with accompanying thermocouple suspended in web of girder section with FRP bars tied to stirrups

4.5 Vibrating wire strain gages

Geokon model 4200 vibrating wire strain gages (VWG) were used to measure concrete strain changes and temperature near the centroid of strands at midspan of the girders. VWGs record strain readings by electromagnetically plucking a steel wire in tension between the two ends of the gage. The changes in resonant frequency of the wire are converted into strain changes. Because the wire is fixed between the two ends of the gage, temperature increases cause decreases in the wire tension, similar to how the prestressing strands experience stress loss due to heating on the precasting bed. Because the VWG are embedded in concrete and the concrete coefficient of thermal expansion is different than that of the steel, additional mechanical strain changes are introduced to the VWG. Equation (4-1), provided by the manufacturer, was used to translate the gage

readings to mechanical strains, termed true, load related strain, ε_{true} [με], by the manufacturer.

$$\varepsilon_{true} = (R_i - R_0)B + (T_i - T_0)(\alpha_{steel} - \alpha_{conc}) \quad (4\text{-}1)$$

where:

R_0: Initial VWG reading, με

R_i: VWG reading at time i, με

B: Batch gage factor

T_0: Initial temperature reading from VWG

T_i: Temperature reading at time i from VWG

α_{steel}: Coefficient of thermal expansion of steel

α_{conc}: Coefficient of thermal expansion of concrete

The manufacturer specified a thermal coefficient of expansion of 6.7 με /°F (12.2 με /°C) for the steel wire inside the VWG. The thermal coefficient of concrete was assumed to be 5.8 με /°F (10.4 με /°C), as discussed in Section 3.2.2.3. The batch gage factor, *B*, is present because the manufacturer's method for clamping the steel wire in the gage slightly shortens the wire, causing readings to read slightly higher. The batch gage factor for the VWGs used was 0.97.

4.6 Thermocouples

Model FF-T-20 thermocouple wire from Omega Engineering, Inc. was used. The wire was gage 20 AWG Type-T, insulated with Neoflon FEP (fluorinated ethylene propylene). A thermocouple was placed near each foil and concrete strain gage to obtain temperature readings that could also be used to correct the respective gage readings due to apparent strain. During preparations for field testing, two thermocouples, one short (less than 1 ft) length and one long (greater than 100 ft), were placed in the same location to test the effects of wire length on the accuracy of the readings. The accuracy of the thermocouple readings was found to be unaffected by the difference in wire lengths.

4.7 Load Cells

Model SST603CHSP load cells from Strainsense Enterprises, Inc. were used to monitor the force on both the dead and live ends of a strand during the final three full-

scale girder tests. The rated capacity of the load cells was 60,000 lb (267 kN). The cells had a maximum outer diameter of 2 in. (50.8 mm), a height of 3 in. (76.2 mm), and a 0.75 in. (19.1 mm) diameter through-hole. The load cells were chosen because they were approximately the size of a chuck, so they fit within the 2 in. (50.8 mm) strand spacing pattern that was standard for the bridge girders fabricated at the precasting plant.

The load cells were conditioned with Vishay model P-3500 and P3 strain indicators, or conditioning boxes. Both systems required the load cell sensitivity, which was provided by the manufacturer, as an input. The P3 also required the full scale range of the cell (60,000 lb). Force readings were directly recorded onto an SD card in the P3 at specified time steps. However, the P-3500 did not have data recording capabilities, so voltage readings were recorded with the CR9000X datalogger and later converted to forces.

Calibration tests were performed on the load cells at the University of Minnesota using two load frames, which will be referred to as Frames 1 and 2, to verify the accuracy of the two load cells under different conditions. Load cell errors measured in two of the tests, which will be referred to as Calibration 1 and Calibration 2, are shown in Figures 4.4 and 4.5, respectively. Calibration 1 was performed by placing one cell at a time in Frame 1 and loading to 60 kips (267 kN) in 5 kip (22.2 kN) increments at a rate of approximately 330 lb/s (1.5 kN/s), then unloading to zero load in 10 kip (44.5 kN) increments at the same rate. The load was held between each increment and the load cell reading from the conditioning box was manually recorded. The difference between the load cell and load frame reading at any given time was called the error. Figure 4.4 plots the error versus the magnitude of the load for Calibration 1 for each load cell in the cases of loading and unloading.

Calibration 2 was performed in Frame 2 as part of the strand pull test described in Section 4.3.2. Both load cells were tested simultaneously, as they were placed at either end of the strand that was pulled. The strand was loaded up to 50 kips (222 kN) in 10 kip (44.5 kN) increments at a rate of 250 lb/s (1.1 kN/s), then twice cycled between 50 and 30 kips (222 and 133 kN) in 5 kip (22.2 kN) increments at the same rate. The strand was unloaded to zero from 50 kips (222 kN) in 10 kip (44.5 kN) increments at the same rate. Loading was paused for 10 seconds between each interval to account for timestamp

mismatching between the load frame readings and the load cell conditioner box readings. Load readings were taken at one second intervals on all systems (i.e., load frame, Cell 1 conditioner, and Cell 2 conditioner), and the error between the readings during the pauses was plotted against the load magnitude in Figure 4.5.

From the figures, it is clear that the error is highly dependent on the magnitude of the load, the loading rate, the direction of loading, the individual cells, and the load frame used. Because the general shape of the error curves for the same cell differed between the two figures, it was possible that some error was introduced due to inaccuracies in the load frame readings. Frame 2 had a much higher load rating (600 kip (2670 kN)) than Frame 1 (220 kip (979 kN)), so the precision of the load frame readings may have been low, causing the large scatter in Figure 4.5.

During girder fabrication, the strands are initially pulled at a relatively fast rate of approximately 45 kips (200 kN) in 20 to 30 seconds, or 1500 to 2250 lb/s (6.7 to 10.0 kN/s). Gradual temperature changes then control the change in force in the strand, so determining the error in the load cell readings from field tests is difficult. Also, no correction for temperature was provided by the load cell manufacturer and the effects of temperature were not investigated during the calibration tests. Therefore, load cell data was assumed to have a tolerance of ± 600 lb (2.7 kN) based on the largest error observed during the calibration tests.

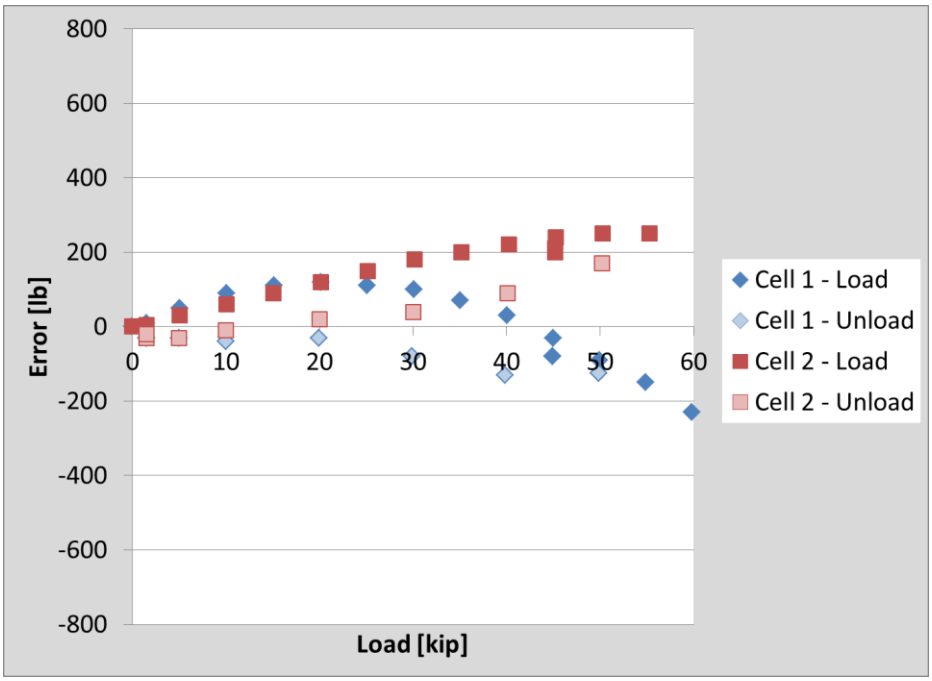

Figure 4.4: Load cell error for Calibration 1

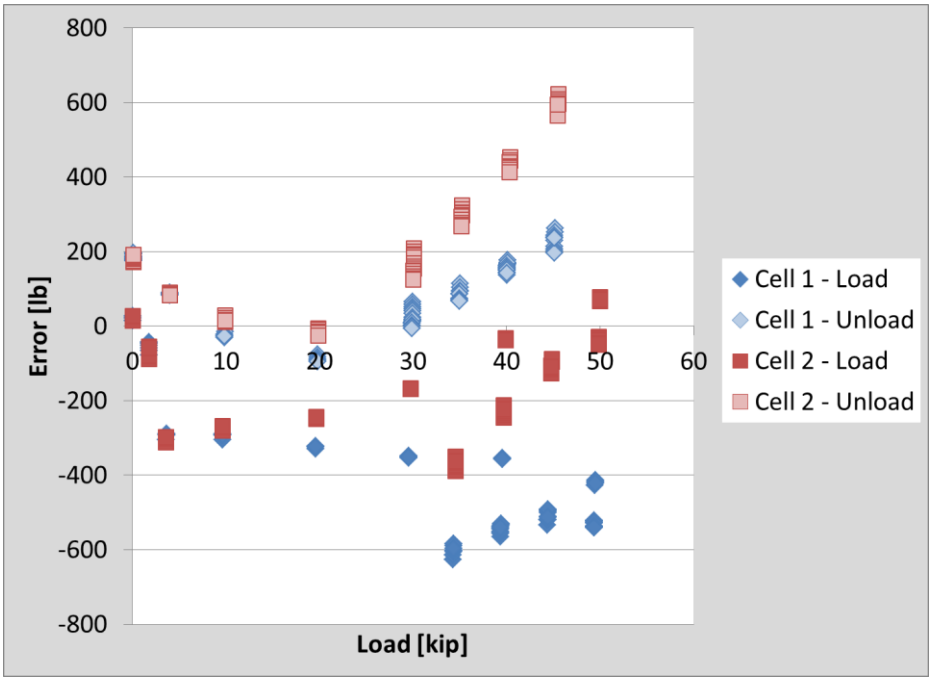

Figure 4.5: Load cell error for Calibration 2

CHAPTER 5. SHORT GIRDER BOND TEST

5.1 Introduction

After tensioning, the steel strand undergoes changes in stress due to the average temperature change along its length because of the fixed strand length in the bed. It is assumed that the concrete is at zero stress when the concrete bonds to the strands and the prestressing force gets "locked in." After that time, any changes in concrete and strand stress due to temperature are considered recoverable. Prior to bond, the prestress changes due to temperature are considered not recoverable. It is important to determine when bond occurs to determine the prestressing force that will be imposed on the girder at release. It is likely that bond is not an immediate phenomenon, and may not simultaneously initiate at all points along and across the member. In addition, bond initiation may vary by time, temperature, concrete mix, concrete strength, and other related factors. For simplicity, it was desired to determine a specific point in time or temperature at which bond could be assumed to occur.

To investigate prestressing strand bond to concrete for the typical MnDOT bridge concrete mix, short concrete "girder" sections were cast on the same bed and released at different times during the early stages of hydration. The "typical MnDOT mix" was that used in the majority of the precast, prestressed bridge girders that the plant was fabricating for MnDOT at the time. Therefore, the behavior of the concrete during these tests was assumed to be similar to that of the concrete used in the bridge girders studied. The short girder test began on July 2, 2014, a mild summer day with high and low temperatures of 73°F (22.8°C) and 53°F (11.7°C), respectively.

5.2 Procedure

Six small, rectangular girder specimens with dimensions HxBxL of 8 x 36 x 96 in. (0.20 x 0.91 x 2.44 m) were cast with the typical bridge concrete mix (called the "normal" mix). The 96 in. length of the short girders was taken as 2.5 times the transfer length specified by ACI 318-11 Section 12.9.1 Eqn. (12-4) to ensure stress transfer at

midspan while maximizing the number of girders on the bed. The girders were cast on the same bed with two batches of concrete; Girders 1 (G1) through 3 (G3) were cast with Batch 1 and Girders 4 (G4) through 6 (G6) were cast with Batch 2. Thick foam sheets were placed over the girders during curing to emulate the blankets that are placed over bridge girder pours to trap heat. Additionally, because the short girders were thin, the foam sheets helped to simulate the MnDOT bridge girder conditions during curing. The bed used to cast the girders was shaded by a tent, but open to the outside on both ends, so the effects of sunlight were not a factor.

To determine when bond occurred, the girders were released at different times during the curing process, with the exception of Girders 4 and 5, which were released simultaneously to provide redundant data for one set of girders. To accommodate releasing girders at different times on the same bed, the bonded strands in each set of girders to be released were debonded in the other girders. The girders were reinforced with two to four straight strands with no eccentricity. A total of 16 strands were tensioned on the bed. The strands that were bonded in individual girders were debonded in the other girders through Schedule 40 ¾" PVC. This PVC was chosen as the debonding agent due to its rigidity and minimal friction with the strands. Figure 5.1 shows the girders positioned along the bed with the PVC utilized for debonding.

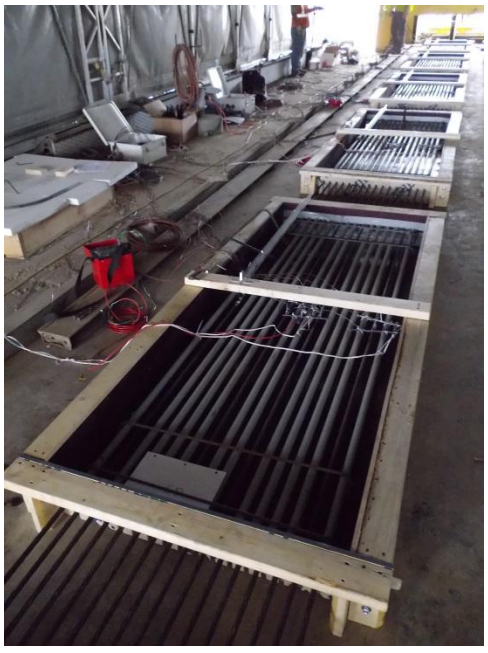

Figure 5.1: Girder setup along bed looking toward dead end

Girders 1 and 2 contained one pair of bonded strands and Girders 3 through 6 contained two pairs. The girder cross section and number of bonded strands within each girder was determined based on the $0.6f'_{ci}$ concrete compressive stress limit at release (ACI 318-11 Section 18.4.1(a)) and the magnitude of strain change the concrete would be expected to experience at release. A relatively large compressive strain was desired to be measured at release to increase the signal-to-noise ratio in the data without exceeding the compressive stress limit in the section for safety reasons.

Figure 5.2 shows the configuration of the girders on the prestressing bed. The bonded strands in each girder were chosen to ensure uniformly distributed loading in each section. The time of release after casting and concrete compressive strength at release are shown below each girder. Figure 5.3 (a) and (b) show cross section and plan views of a girder, highlighting the locations of bent rebar used to prevent strand from rupturing through the section at early age release.

The instrumentation included foil strain gages, concrete strain gages, VWGs, and thermocouples. Four foil gages were attached to the bonded strands in each girder at midspan. One VWG was located near the center of each girder. Two concrete strain gages were placed in each girder; one approximately two inches east of the VWG and one approximately two inches in from the east edge of the girder. Thermocouples were placed alongside each foil and concrete strain gage. Figure 5.4 shows the typical instrumentation setup at midspan of each girder.

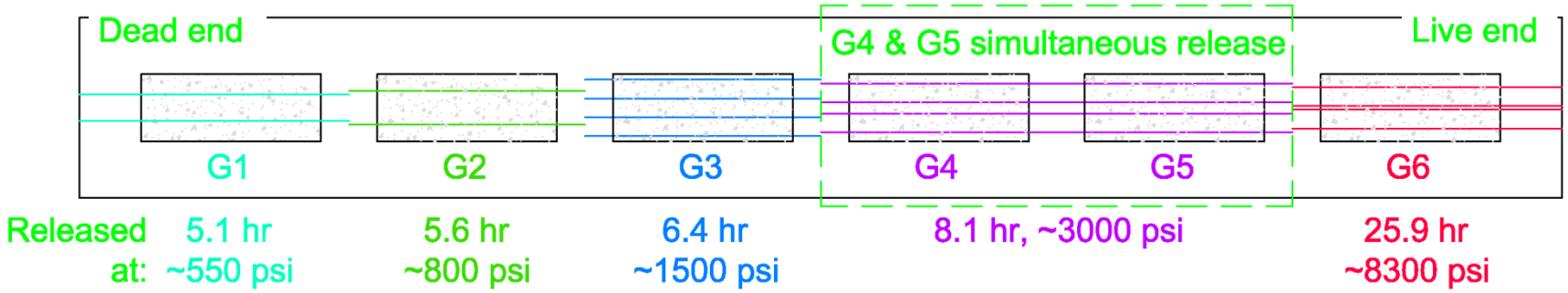

Figure 5.2: Short girder layout on prestressing bed, showing bonded strands, times of release, and approximate concrete compressive strengths at release

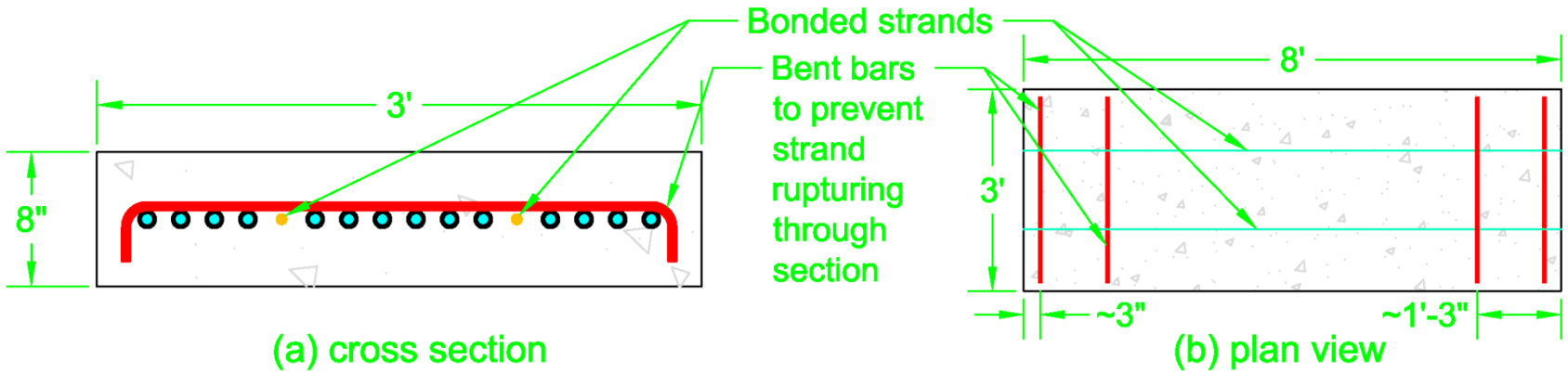

Figure 5.3: Typical short girder cross section and plan view

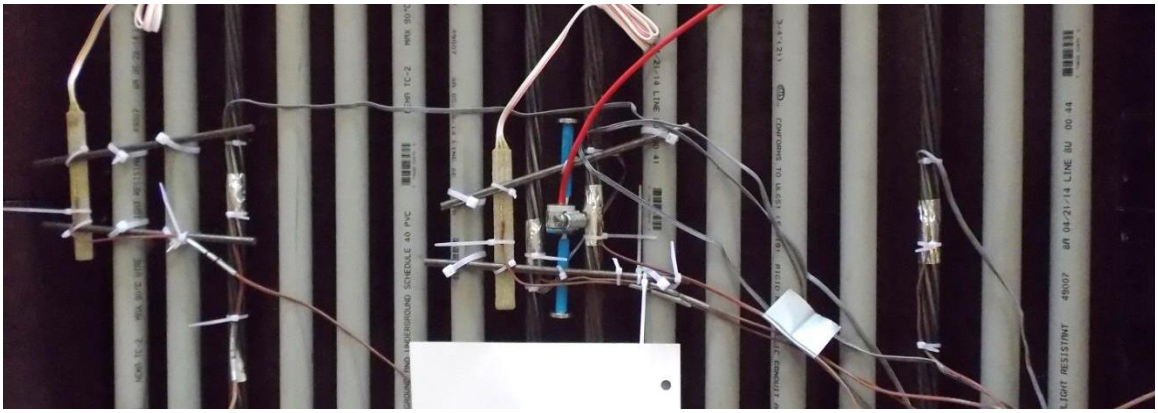

Figure 5.4: Typical instrumentation of short girders, shown at midspan of Girder 6

5.3 Concrete Casting and Cylinder Tests

As noted in Section 5.2, the short girders were cast using two batches of concrete from the dead end to the live end over the course of 30 minutes. A total of 24 4 x 8 in. (100 x 200 mm) companion cylinders were fabricated to measure the concrete compressive strength and modulus of elasticity periodically during the short girder test. The samples were cast in reusable Sure Cure® steel molds that had controllable curing temperatures. The curing temperature is typically driven off of thermocouples located on the side-forms of bridge girders being cast. This allows for more accurate determination of concrete strengths, as the cylinders are cured under similar conditions as the concrete in the larger mass. A Sure Cure mold is shown in Figure 5.5. The sure-cure temperature for all of the short girder tests was driven off of a thermocouple located in the center of Girder 5.

Figure 5.5: Sure Cure® cylinder mold with fresh concrete

5.3.1 Compressive Strength Gain with Time

Concrete compressive strength values for Batches 1 and 2 were measured throughout the course of the short girder tests. This was done to compare modulus of elasticity estimations based on the concrete compressive strength to measured modulus of elasticity values at different points in time during the curing process. Additionally, the rate of concrete strength gain during the short girder tests was compared to similar data obtained during other tests at the precasting plant using the same mix to determine the consistency of strength gain in differing conditions.

Figure 5.6 shows the measured concrete compressive strength during the early portion of the curing process on four different dates. Concrete temperatures are included in the plot where such measurements were taken. The four dates correspond to the following testing events carried out at the precasting plant: a preliminary study conducted during girder casting for an unrelated University of Minnesota project (8/20/2013), full-scale girder Test 1 (11/22/2013), a cast used to practice for the short girder test (7/1/2014), and the short girder test (7/2/2014). The practice test was performed on a block of concrete cast in a wooden form that was one-half the volume of the short girders. The block was covered with foam to replicate the process for the short girders. The temperature increased more quickly and peaked at a higher value during the practice

test because the bottom of the concrete was in contact with wood rather than the steel prestressing bed, so less heat dissipated.

The concrete strengths recorded on each date were consistent up to five hours after casting, at which point the rates of strength increase begin to deviate. Temperature data from the short girder practice test show that the higher temperature caused the concrete to gain strength faster than the lower temperature measured during the short girder test. However, after 24 hours, the concrete strengths were similar despite the difference in early strength gain rate.

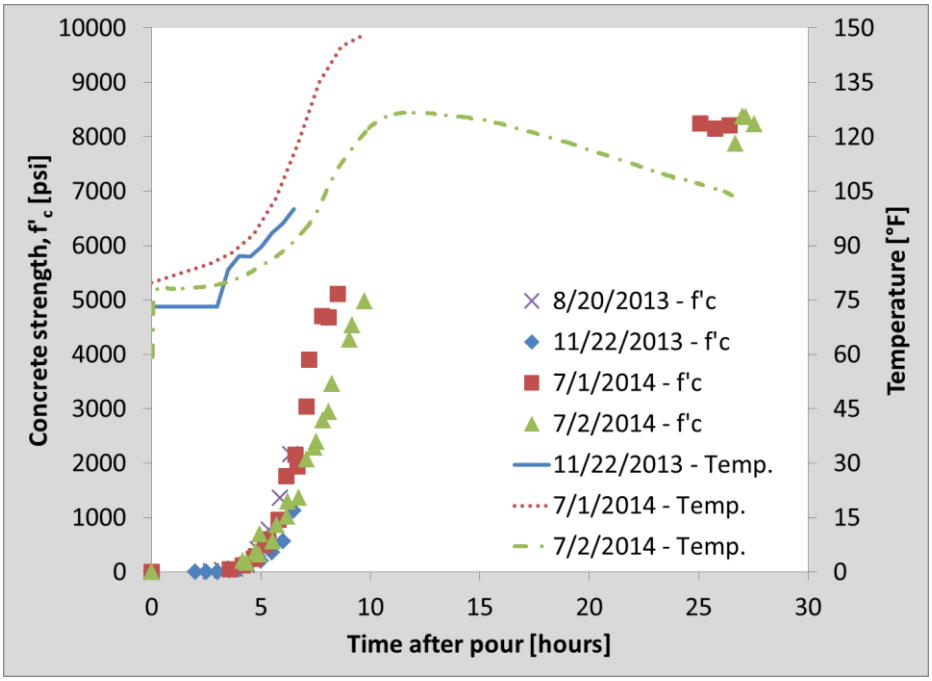

Figure 5.6: Concrete compressive strength and temperature during early stages of curing

5.3.2 Modulus of Elasticity Increase with Time

In addition to compressive strength, concrete modulus of elasticity (MOE) was measured for Batches 1 and 2 throughout the short girder tests. Because the tests for MOE take longer than compressive strength tests, fewer MOE measurements were made. However, the tests are non-destructive, so the cylinders used in the modulus tests were subsequently tested to obtain a compressive strength measurement.

Measured MOE values were compared to estimated values calculated using measured compressive strengths and the Pauw (1960) and ACI 363 (2010) models given in Equations (5-1) and (5-2), respectively. It was suggested by O'Neill et al. (2012) that the Pauw model replace the ACI 363 model currently used by MnDOT to more accurately predict the initial cambers of precast, prestressed concrete bridge girders because it was determined that the Pauw estimation more accurately predicted the MOE of the concrete using measured compressive strengths. The comparison between measured and estimated concrete MOE during the short girder tests was of interest to confirm the findings of O'Neill et al. (2012) and to better understand the discrepancies between predicted and measured initial girder camber. Figures 5.7 and 5.8 show the concrete MOE over the duration of the short girder tests for concrete Batches 1 and 2, respectively. The release times of each short girder are shown as a vertical dashed line labeled with the corresponding girder number.

Pauw (1960) estimation for concrete MOE:

$$E_c = 33w^{1.5}\sqrt{f'_c} \tag{5-1}$$

ACI 363 estimation for concrete MOE:

$$E_c = 1265\sqrt{f'_c} + 1000 \tag{5-2}$$

where:

E_c	Concrete modulus of elasticity; psi in Eqn. (5-1), ksi in Eqn. (5-2)
f'_c	Concrete compressive strength; psi in Eqn. (5-1), ksi in Eqn. (5-2)
w	Unit weight of concrete, pcf

The concrete unit weights for Batches 1 and 2 were 151.6 and 152.6 pcf (2428 and 2444 kg/m^3), respectively.

From Figures 5.7 and 5.8, it is clear that the Pauw (1960) model more accurately estimated the concrete MOE in the later stages of curing (i.e., beyond 8 hours after casting) than the ACI 363 model. In the middle stages (i.e., 5 to 8 hours after casting), both estimations are relatively consistent with the measured values. However, because girders are never released at such early times during curing, the late stage results are the most meaningful for elastic shortening and camber estimations. O'Neill et al. (2012) determined that the underestimation of the concrete MOE at the time of release by the

ACI 363 model was a significant issue associated with initial girder camber over prediction. The data confirmed that the Pauw (1960) model could increase the accuracy of the concrete MOE estimation at release.

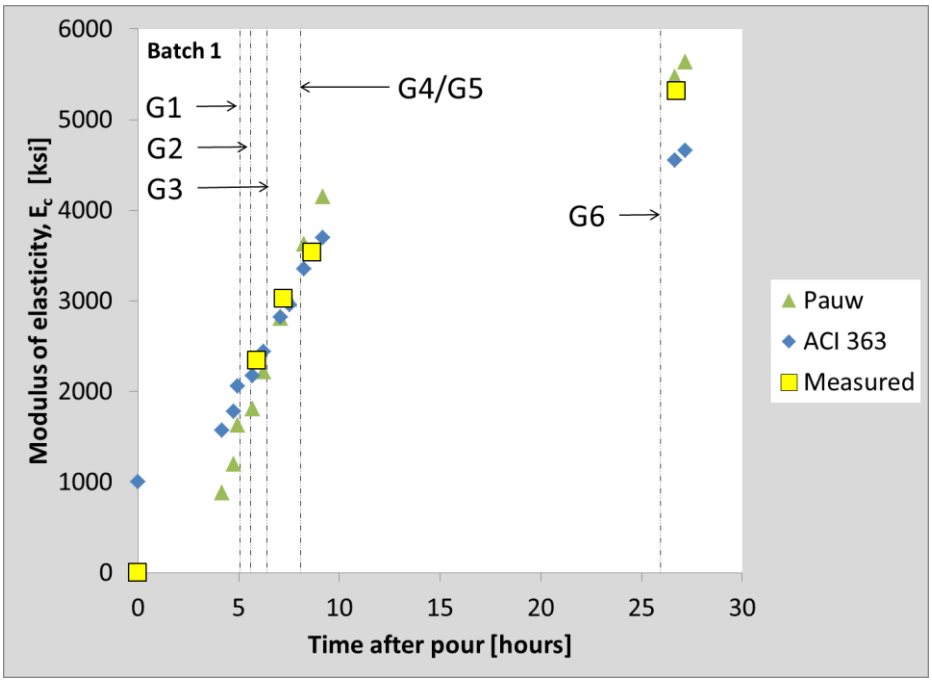

Figure 5.7: Batch 1 concrete modulus of elasticity during short girder test

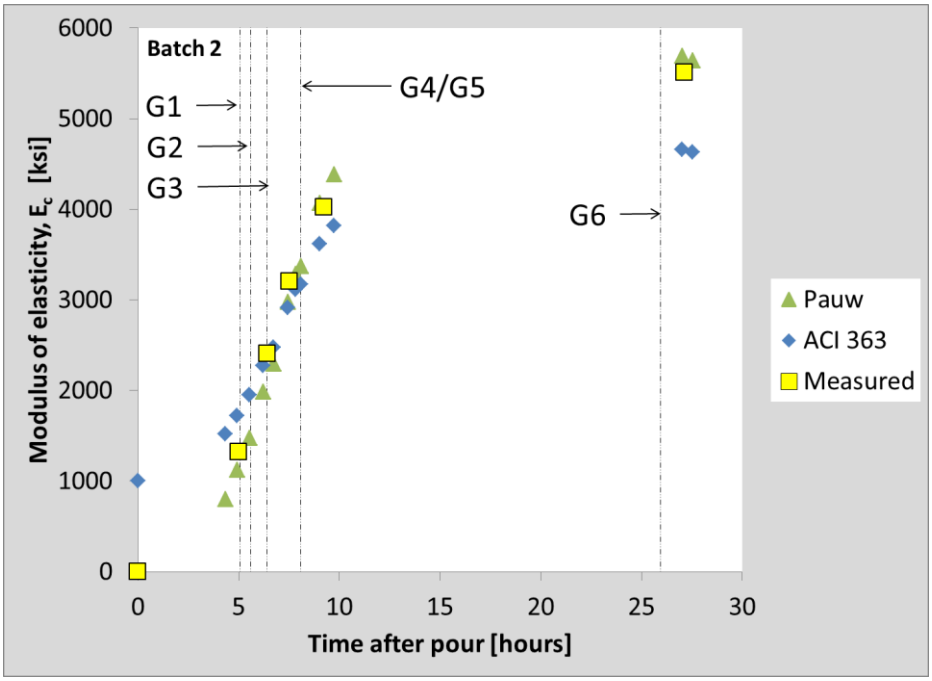

Figure 5.8: Batch 2 concrete modulus of elasticity during short girder test

5.4 Results

During the short girder tests, the times of release for each girder were recorded. For each girder, a target concrete compressive strength was determined before testing began. When the approximate target strength was observed from cylinder tests, the process of releasing that girder began. From the cylinder tests performed throughout the test day, a concrete compressive strength value and MOE value were estimated for each girder at the time of release. This was done by interpolating between the nearest compressive strength measurements from the corresponding batch (Batch 1 for G1, G2, and G3; Batch 2 for G4, G5, and G6). The estimated compressive strength values did not exactly match target values because of the time delay between reaching the approximate target strength and release due to the required preparations, such as stripping formwork and recording VWG readings. The MOE at the time of release was interpolated between the nearest measurement regardless of the batch the cylinder came from because the time between tests was large and the batches were cast only 15 minutes apart. Table 5.1 shows the age of the concrete, target concrete compressive strength, approximate measured concrete compressive strength, and approximate measured MOE at release for each girder.

Table 5.1: Short girder test specimen release times and approximate concrete compressive strengths, and moduli of elasticity at release

Girder No.	**1**	**2**	**3**	**4**	**5**	**6**
Time of release after casting [hr]	5.1	5.6	6.4	8.1	8.1	25.9
Target f'_c at release [psi]	500	1000	1500	3000	3000	7500*
Approximate f'_c at release [psi]	547	803	1465	2945	2945	8307
Approximate E_c at release [ksi]	1275	2199	2594	3408	3408	5408

*Typical MnDOT design concrete compressive strength at release

5.4.1 Strand Temperature Assumptions

Using measured temperature readings along the bed, strand force changes with respect to time were calculated for the short girder tests. Assumptions were made regarding the free strand and concrete temperatures for each girder. To determine the

strand force change due to temperature before bond in accordance with Equation (3-7), the temperatures of the 8 ft (2.4 m) strand segments in each girder were taken as the average of the thermocouple readings from all strain gage locations (both on the strand and embedded in concrete) in the section at midspan of the girder. This resulted in six strand segments with unique temperature profiles that accounted for 48 ft (14.6 m), or 71%, of the total strand length. The remaining free strand length temperature was taken as the ambient temperature recorded by a thermocouple exposed to air next to the precasting bed. The ambient thermocouple was assumed to experience the same temperature changes as the free strand on the bed because the entire bed was shaded, so solar radiation was not an issue.

To determine the free strand force change due to temperature between bond and release in accordance with Equation (3-14), the same temperature assumptions were made for each strand segment, but the free strand corresponding to each of the six girders experienced unique force changes due to the temperature of the bonded strand in the respective girder. Consequently, the free strand force change due to temperature was modeled separately for each girder assuming the average temperature of that girder applied to strand bonded in concrete, while the average temperatures of the other five girders applied to the free strand length, which passed through the other five girders.

5.4.2 Estimated and Measured Free Strand Force Change due to Temperature

To validate the accuracy of the thermal effects analysis described in Chapter 3, the estimated change in free strand force due to temperature using measured temperature data was compared to changes obtained from the free strand mechanical strains of Girder 6. Girder 6 was chosen because it was the last to be released, so data was recorded over a longer time span. Two of the bonded strands from Girder 6 had foil strain gages attached on the free length near the dead end of the bed. Free strand force changes were determined by converting the strain gage readings to forces with an apparent strand modulus of elasticity of 30,700 ksi (212 GPa) (see Section 4.3.2) and a strand area of 0.218 in^2 (141 mm^2). The estimated free strand force change was determined by Equation (3-7) before bond and Equation (3-14) between bond and release.

Figure 5.9 shows the measured and estimated free strand force changes due to temperature for Girder 6. The free strand force changes were zeroed at the time at which all thermocouple data was available along the bed. This plot illustrates how well the thermal effects analysis compared to the measured strain changes. The first two data series (Strand 1 and Strand 2) represent the force changes from the measured strain data. The third and fourth data series (Theo. – 6 hr and Theo. – 10 hr) represent the estimated free strand force change from Equations (3-7) and (3-14) assuming bond occurred at 6 and 10 hours after casting, respectively. The final data series (Theo. w/o Conc.) represents the estimated free strand force change assuming the entire strand length was free, even after bond. That is, it was assumed that the concrete did not bond to the strand, so Equation (3-7) was never replaced by Equation (3-14) in determining the change in force. The force changes are plotted from the time that the thermocouple readings began to be collected at all instrumented locations along the bed.

Because the girders were released at different times on the same bed, the effects of abutment movement were observed in the strain gages on the Girder 6 strands. At the time of each girder release prior to Girder 6, an increase in tensile strain occurred. The thermal effects analysis did not account for these effects, so comparing measured and estimated force changes was difficult without adjusting the measured data. Figure 5.10 shows the measured free strand force changes after the spikes due to abutment movement were removed.

It was observed that the estimated free strand force changes due to temperature were very similar to the measured values in all cases, after removing from the measured data the effect of the measured increase in tensile strains due to the abutment movement as strands were cut. There was very little difference between the three estimated force changes with respect to time. This was due to the short girder length relative to the total strand length (one girder only accounted for approximately 12% of the bed). Additionally, there were no hold downs to mechanically attach the girder to the bed because the strands were straight, so the short girders provided minimal resistance (besides friction) to the movement of the free strand. These assumptions were consistent with the thermal effects analysis.

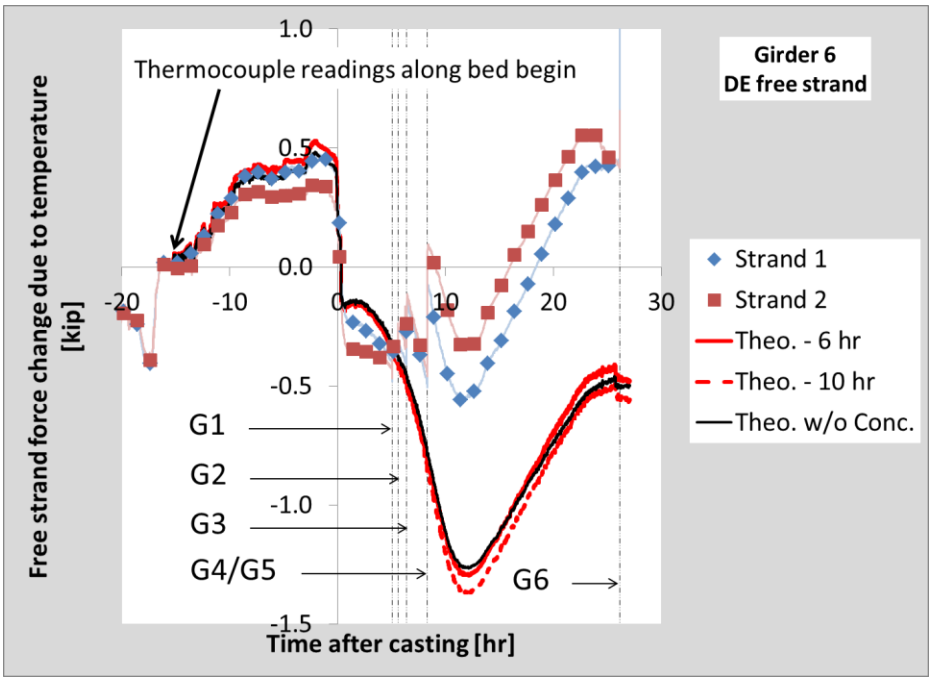

Figure 5.9: Estimated and measured force changes due to temperature in free strand associated with Girder 6 before correction for abutment movement

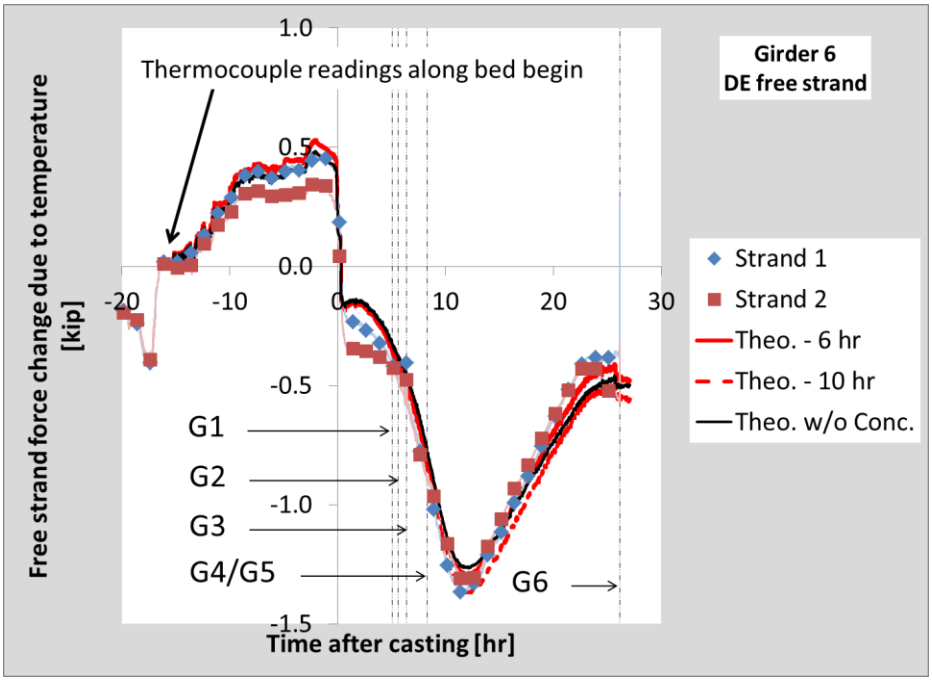

Figure 5.10: Estimated and measured force changes due to temperature in free strand associated with Girder 6 after correction for abutment movement

5.4.3 Stress Transfer at Release

The girders were released beginning at the dead end and moving toward the live end (see Figure 5.2). Pieces of sheet metal were used to separate the strands to be torched from those bonded in adjacent girders to be cut at a later time. Two torch cutters were present to cut the strands symmetrically from one end of the girder. In practice, girders are held in place on the bed by hold-downs used to harp draped strands, so the strands are cut from both ends of the girder. In the short girder tests, there were no draped strands and, consequently, no hold-downs. The short girders were free to slide upon release, so cutting from both sides was dangerous. The strands were cut at locations intended to minimize the amount of sliding (e.g. girders closer to the dead end of the bed were cut out on the live end side of the girder). Because Girders 4 and 5 were released simultaneously, the cuts were made between the two girders, resulting in large sliding distances of up to 40 in. (1 m). After the strands were cut from one side of the girder, the strands were then cut on the other side to release any potential force remaining in the strands, which was found to be negligible.

To determine the time of bond, it was important to analyze the stress transfer from the strands into the short girders upon release. If bond had occurred, the strain change at release measured by the instrumentation embedded in the girder should match the estimated strain change determined using the methods described in Section 3.3.3.4with measured force, temperature, and concrete MOE data.

To estimate the strain change in the girders at release, an assumption for the time of bond was required. Barr et al. (2005) assumed bond likely occurs between 6 and 10 hours after casting, so that time range was assumed to bound the time range at release. Because most of the girders were released before or during that time range, adjustments were made. Table 5.2 shows the assumed lower and upper bound times of bond used to estimate the girder strain change at release for each short girder. Girders 1 and 2 were released before 6 hours, so their times of release were assumed for their times of bond (i.e., 5.1 and 5.6 hours, respectively). Girders 3, 4, and 5 were released between 6 and 10 hours, so the time of release was assumed for the upper bound time of bond. Girder 6 was

released the next day, so 6 and 10 hours were assumed for the lower and upper bound times of bond, respectively.

Table 5.2: Assumed upper and lower bound times of bond for estimating short girder strain change at release

Girder No.	1	2	3	4	5	6
Assumed Time of Bond [hr] - Lower Bound	5.1	5.6	6.0	6.0	6.0	6.0
Assumed Time of Bond [hr] - Upper Bound	5.1	5.6	6.4	8.1	8.1	10.0

Figure 5.11 shows the estimated and measured concrete strain changes at the center of gravity of strand at release for each girder. Because the short girders were rectangular with no strand eccentricity, the strain was assumed to be uniform in the cross sections. The estimated strain change at release was given by Equation (3-19) and consisted of the following: (1) the change in mechanical strain in the composite section due to the release of the restraint force that develops in the free strand due to temperature changes on the bed between bond and release, and (2) the change in mechanical strain due to elastic shortening immediately after release. The measured value was taken as the strain change obtained from the VWG at the center of each girder section at release. Details on the parameters used in the thermal effects analysis for the short girder tests can be found in Appendix A.

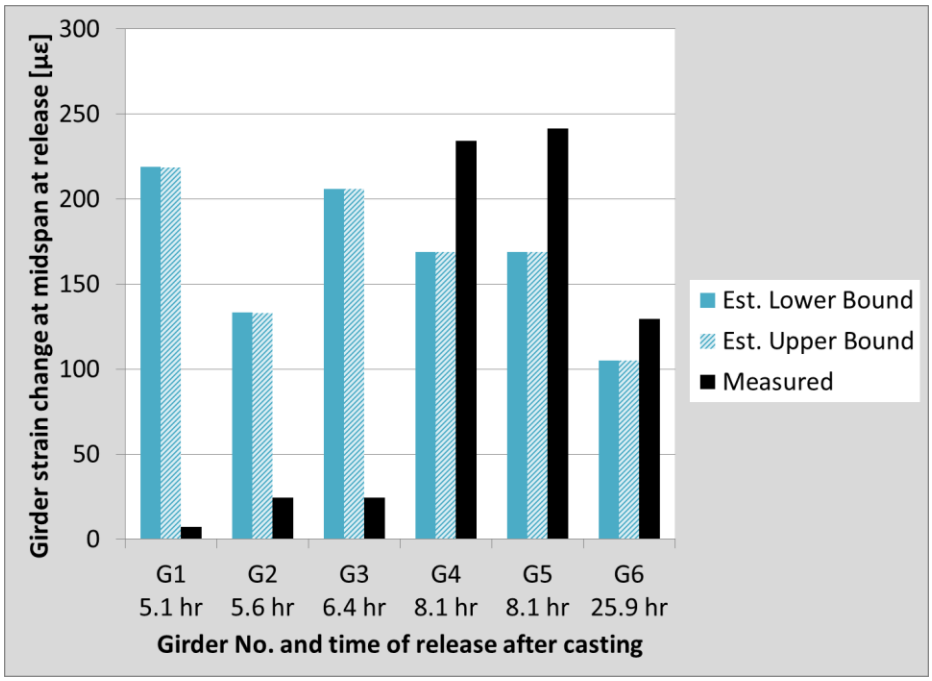

Figure 5.11: Estimated and measured short girder midspan strain changes at release

The figure shows that the measured strain changes in Girders 1 through 3 were much lower than the estimated strain changes. This means that the stress in the strands was not fully transferred to the concrete and, therefore, bond between the steel and concrete had not yet fully developed. The lower and upper bound estimated strain changes in Girders 4 through 6 were lower than the measured values. However, strain data with respect to time shown in Section 5.4.3.1 shows that the estimations may be closer to the measured values than Figure 5.11 depicts, as VWG readings were not taken immediately after release. This is most apparent for Girder 6, for which some of the other instrumentation measured a strain change at release closer to the estimated values. Although the magnitudes of the estimated and measured strain changes are not equal, the pattern of increasing measured strain changes as the girders were released at later points in time suggests that bond had fully developed by approximately 8 hours after casting, which corresponded to an average concrete temperature of approximately 100^{o}F (37.8^{o}C), a concrete compressive strength of approximately 2950 psi (20.3 MPa), and a concrete modulus of elasticity of approximately 3400 ksi (23.4 GPa). The average concrete temperatures were obtained by averaging all of the temperature sensors placed across the short girders at midspan. Concrete temperatures at the time of bond during the short

girder tests are further discussed in Section 5.4.5, which shows the data for the gages located closest to the centroid of the sections at midspan.

5.4.3.1 Observed Steel and Concrete Behavior

The strain changes measured by the VWGs in the girders were analyzed in the previous section, but it was also of interest to investigate the behavior of the other instruments in each girder at release. Figures 5.12, 5.13, and 5.14 show the strain changes recorded by the instruments within Girder 1 (G1), Girder 2 (G2), and Girder 3 (G3), respectively. The estimated strain changes at release from Figure 5.11 are displayed as horizontal dashed lines. Note that, because the lower and upper bound estimated strain changes were found to be similar, only the lower bound value is shown on the plots for simplicity. In each figure, the important data to observe is the jump that occurs at the time of release of each particular girder, further changes in readings beyond that time represent possible shrinkage and creep strains. On each figure, an inset shows the location of each gage within the girder section. Gages labeled GX-E or GX-W were foil strain gages attached to the strands on the east or west side of Girder X. Gages labeled CX-1 or CX-2 were concrete strain gages located near the center or the eastern edge of Girder X. The instrument readings were zeroed just before release of the corresponding girder. Note that the scaling of the plots is not consistent because release times and strain change magnitudes at release vary between girders.

In all three girders, the foil gages located on the strands failed immediately after release. This could have resulted from damage to the gages or the wiring as the strands slid through the girder due to lack of bond between the strand and concrete. The strands were cut from the live end of the bed for safety, and the first three girders were located near the dead end. This means the strands slid through the girders from one direction, rather than compressing toward the center as would be the case if the strands were cut simultaneously from both ends of the girder. Even at low strengths, the concrete is a solid material, so the gage wires could have been torn off.

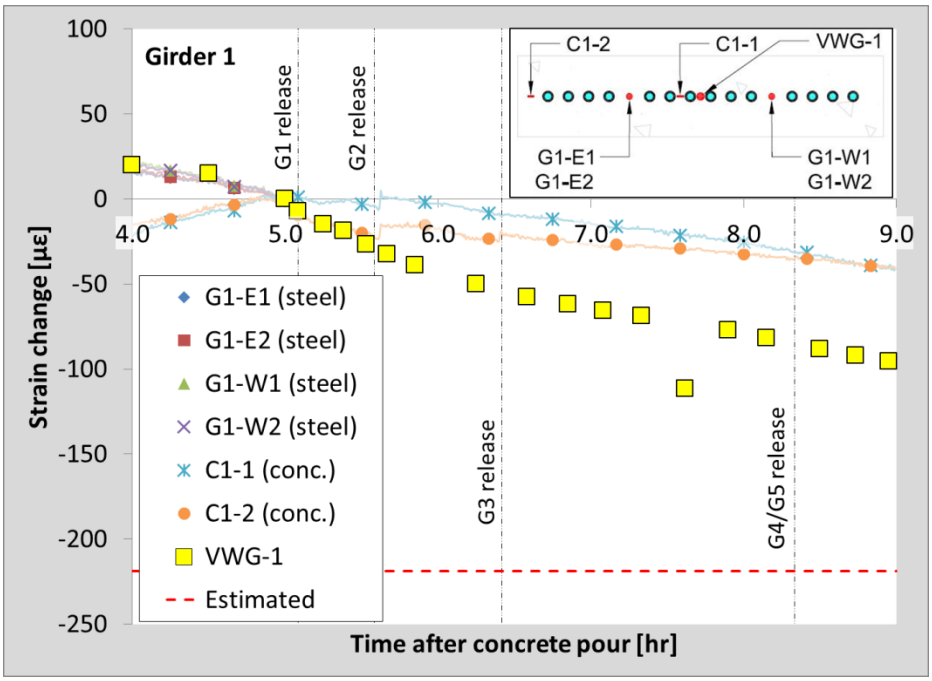

Figure 5.12: Girder 1 measured and estimated strain changes at release

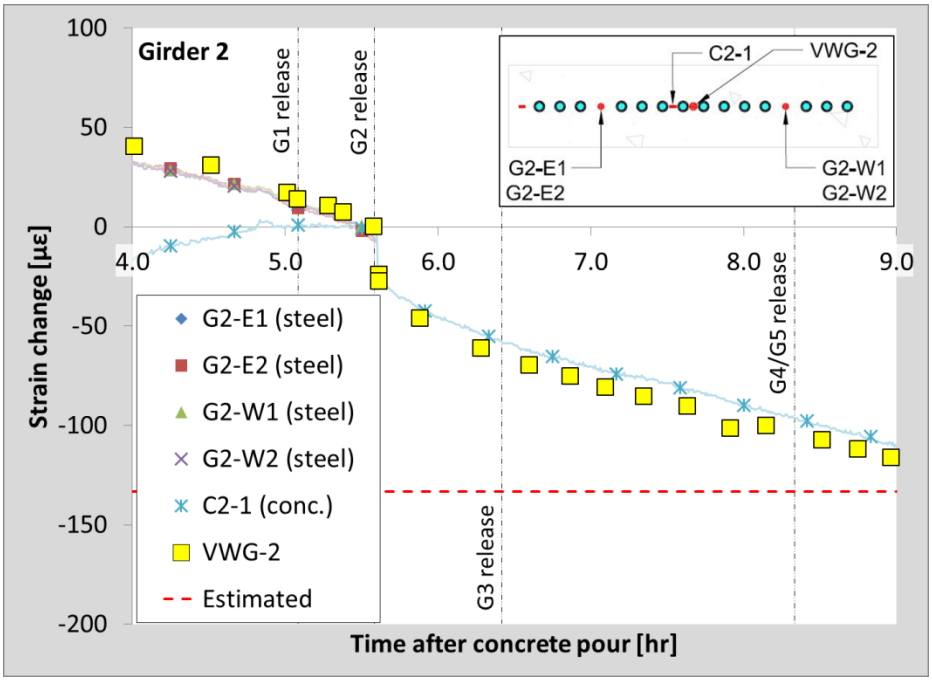

Figure 5.13: Girder 2 measured and estimated strain changes at release

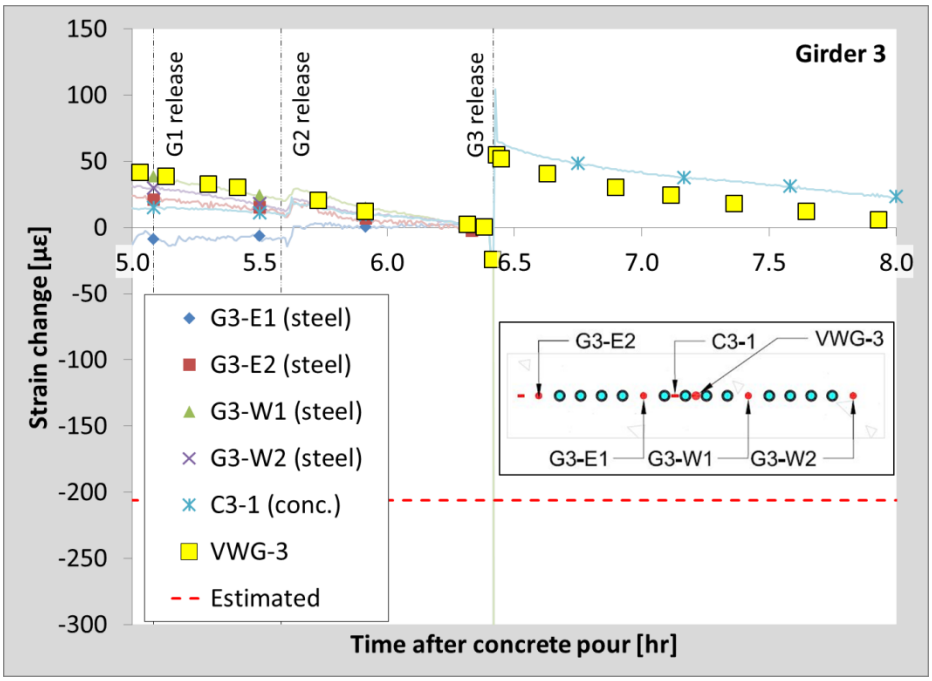

Figure 5.14: Girder 3 measured and estimated strain changes at release

Figures 5.15, 5.16, and 5.17 show the strain changes recorded by the strain gages within Girder 4 (G4), Girder 5 (G5), and Girder 6 (G6), respectively. In all three cases, the concrete gages and VWGs experienced reasonable strain changes relative to the estimated value. G4 and G5 were reinforced identically and released simultaneously, so it was expected that the results would be very similar.

In G4 and G5, all strand strain gages survived release (except G5-W2, which did not function during the test). In both girders, only one of the four strand gages experienced an initial strain change close to the estimated strain change. The remaining gages, with the exception of G4-W1, showed initial strain losses at release up to 10 times larger than the estimated strain losses. This indicates that strand slip had occurred, so the strands did not maintain their original stress after release. However, as noted above, the concrete strain gages and VWGs recorded reasonable strain changes relative to the estimated strain changes, indicating that the estimated stress was transferred into the concrete. This means that bond between the strand and the concrete was almost fully developed at approximately 8 hours after the pour.

Girder 6 was released approximately 26 hours after the pour to provide a control case in which bond had definitely occurred. This release time was close to that of typical

girder production. The data confirmed the assumptions that, when bond had occurred, the concrete and strand strain gages would read the same strain change upon release. Gage G6-W2 behaved abnormally, but was still not far off from the rest of the data and the expected strain change. Approximately 15 minutes elapsed between release and the final VWG reading, which may have contributed to the differences in the estimated and measured strain changes in Figure 5.11, as the section cooled. Similar strain changes were observed in many of the other gages.

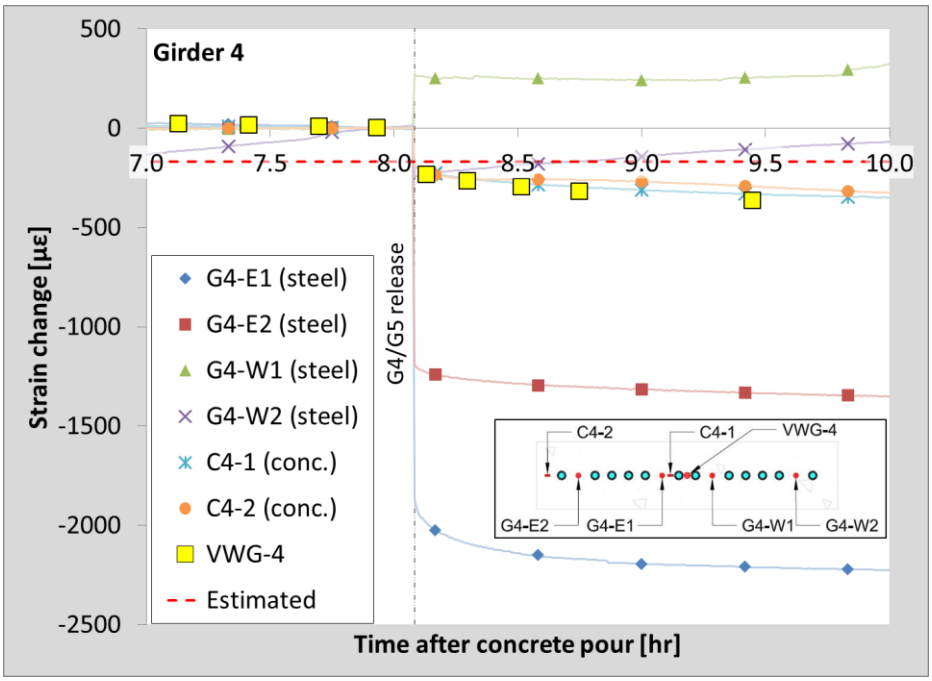

Figure 5.15: Girder 4 measured and estimated strain changes at release

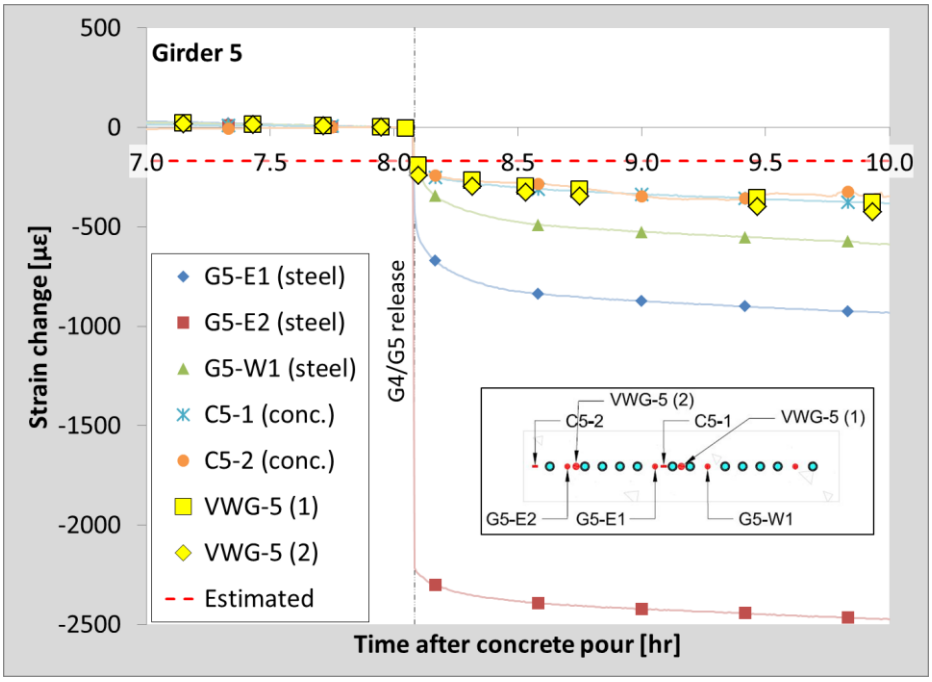

Figure 5.16: Girder 5 measured and estimated strain changes at release

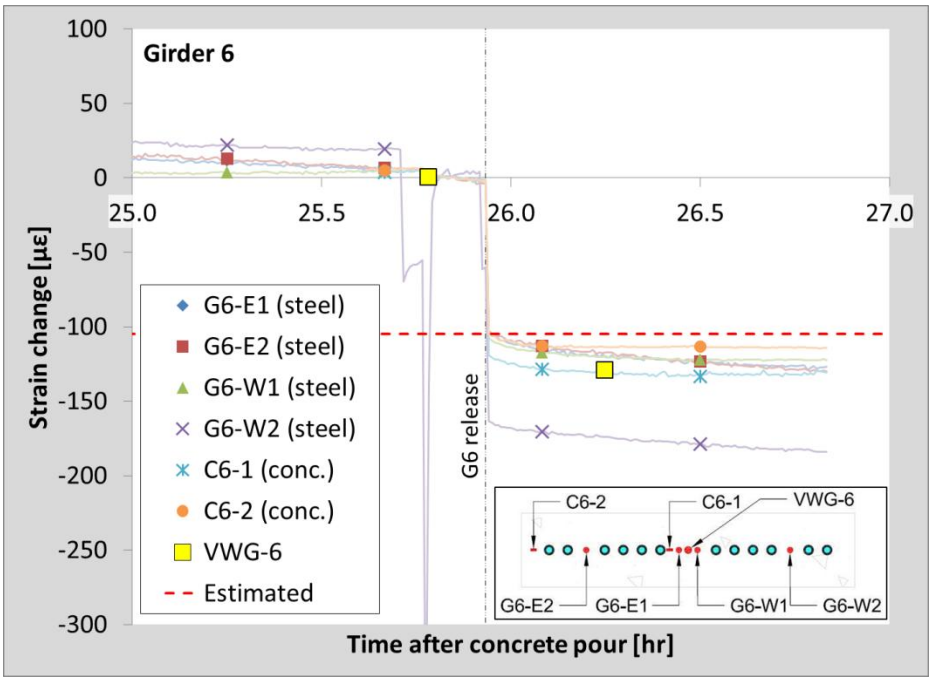

Figure 5.17: Girder 6 measured and estimated strain changes at release

5.4.4 Concrete Cracking

Substantial cracking was observed in Girder 3 after release. Figure 5.18 shows a crack diagram demonstrating the cracks that were discovered upon visual inspection of the girder after release. Figure 5.19 shows pictures that were taken of two cracks, the locations of which are labeled in Figure 5.18.

The presence of cracks in Girder 3 suggests that there was some interaction between the steel and concrete at the time of release, but the concrete strength was not high enough to carry the stress transferred by the strands. This is important to note because the determination of the time of bond is important in determining at what point the strand stress is locked into the girder. Because girders are not released at low concrete strengths in practice, the ability of the concrete to transfer stress at this time is not a concern, but any strand restraint due to concrete-steel interaction influences the amount of non-recoverable strand force losses due to temperature. Based on the observed cracks, bonding between the steel and concrete was likely to have initiated prior to Girder 3 release. The estimation that bond gradually occurs between 6 and 10 hours after the concrete was cast is consistent with Barr et al. (2005).

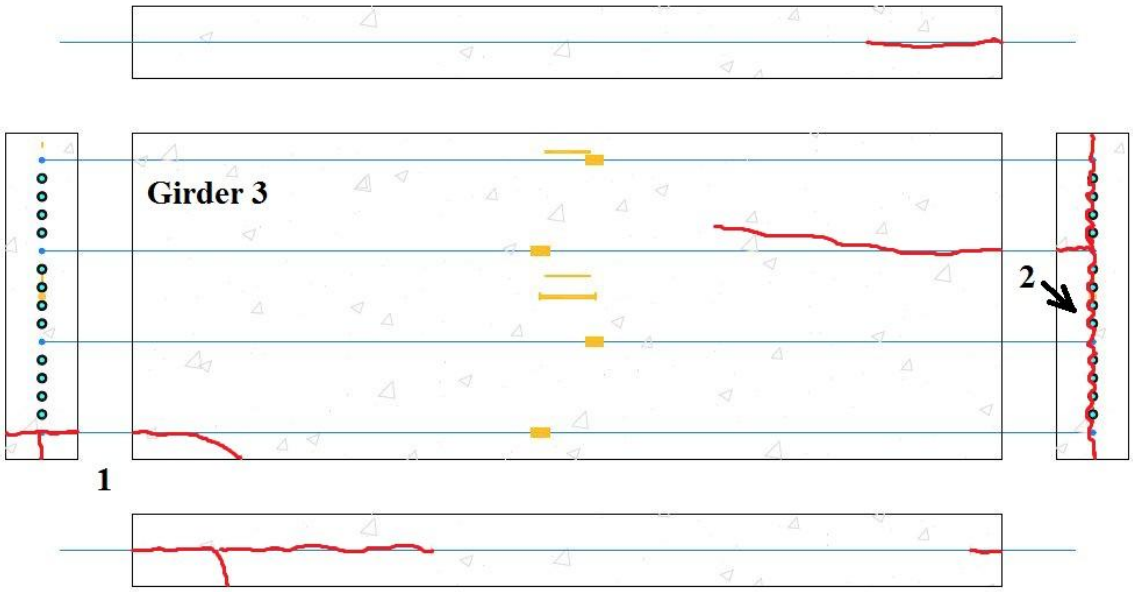

Figure 5.18: Girder 3 crack diagram

Figure 5.19: Girder 3 cracks; Crack 1 (left) and Crack 2 (right)

5.4.5 Concrete Temperature at Time of Bond

The concrete temperature at the time of bond is important in determining the non-recoverable strand force loss due to the temperature change between the time of tensioning and the time of bond. Figure 5.20 shows the concrete temperature profiles of each girder measured at the center of the girder (i.e., centroid of section at midspan) through the duration of the test. The abrupt increase in temperature at 0 hours is

associated with the placement of the wet concrete. The times of release of each girder are represented by vertical dashed lines.

The figure shows that the rates of temperature increase for all girders were similar. Girders that were released later experienced higher peak temperatures than the girders that were released before them because the formwork and foam sheet that covered each girder were removed at the time of release, so heat was allowed to escape. The exception was Girder 5; after release, the formwork was moved back into place and the foam was placed on top to regulate the Sure Cure temperature so the cylinders would be consistent with Girder 6 temperatures overnight. Between the releases of Girders 3 and 4/5, the temperatures of Girders 4, 5, and 6 were between 90 and 110°F (32.2 and 43.3°C). Consequently, the expected temperature at the time of bond for the "normal" concrete mix is expected to be within this range. The temperatures of Girders 1, 2, and 3 were not considered in determining the temperature range because they had already been released and uncovered at the estimated times of bond.

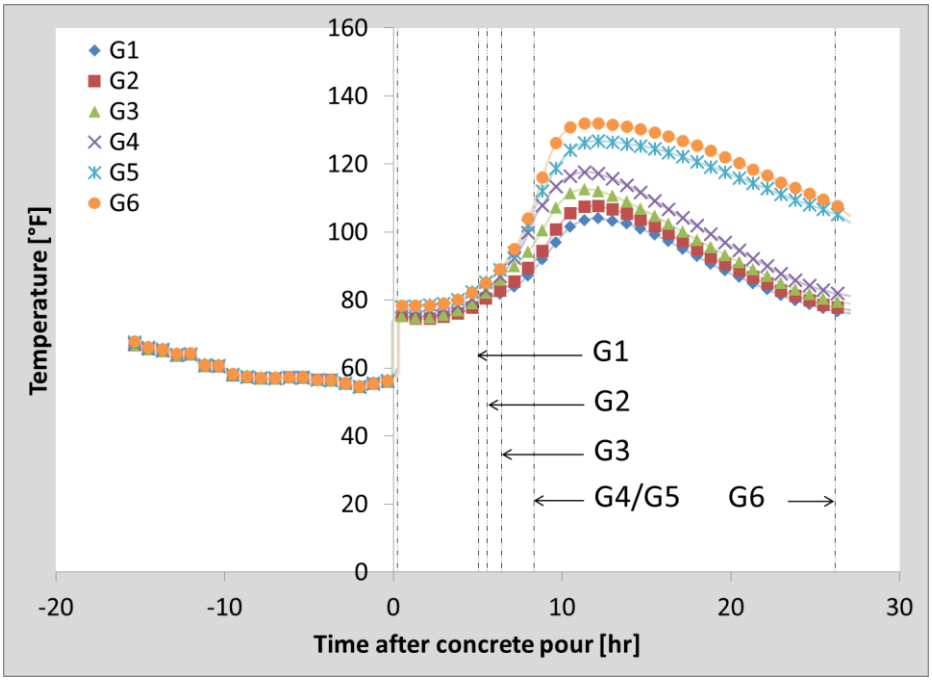

Figure 5.20: Short girder concrete temperatures measured at the center of the girders

5.5 Summary

The temperature associated with bond is an important variable to quantify in determining the amount of strand force that is lost due to temperature change in prestressed bridge girders. Tests were performed on six short girder sections cast with the typical concrete mix used by the precasting plant for fabricating MnDOT precast concrete bridge girders. The girders were released at different times early in the curing process and strain change measurements were analyzed to determine when bond had occurred.

Concrete cylinders were cast with the concrete used during the test and cured in Sure Cure® cylinder molds, which regulate the temperature of the cylinders based on the concrete temperature in the girder. The cylinders were tested for compressive strength and modulus of elasticity continuously throughout the full-scale tests to monitor the strength gain and determine a correlation between time, strength, temperature, and bond. The Pauw (1960) model for estimating the concrete modulus of elasticity was more accurate than the ACI 363 model in the late stages of curing (8 hours after casting and beyond).

Based on comparisons between theoretical and measured stress changes in the girders at release and observed cracking in one of the girders, it was determined that the estimation that bond occurs between 6 and 8 hours after the concrete is poured is reasonable with the MnDOT bridge mix in mild summer weather. The estimated time of bond range corresponded with concrete temperatures of approximately 90 to 110°F (32.2 and 43.3°C), concrete compressive strengths of approximately 1450 to 2950 psi (10.0 to 20.3 MPa), and concrete modulus of elasticity values of approximately 2600 to 3400 ksi (17.9 to 23.4 GPa). The temperature range is particularly important in determining an adjustment procedure for the precasting plant to correct initial strand pull force in order to offset force changes due to temperature between the time of tensioning and time of bond.

CHAPTER 6. FULL-SCALE GIRDER TESTS

6.1 Introduction

Full-scale bridge girders were monitored during the fabrication process at the precasting plant to determine the effect of temperature on strand force and initial camber. The monitored girders were used in bridges designed by the Minnesota Department of Transportation (MnDOT). There are many factors that may affect the amount of prestress loss due to temperature for a given girder set, but four parameters in particular were investigated; casting during a cold season, casting during a warm season, casting with the free length of strand covered, and casting with different bed occupancy during any season.

6.2 Test Details

A total of four sets of bridge girders were instrumented between November 2013 and December 2014. The girder sets were named Test 1 through Test 4 in chronological order and are referred to as such in this report. This section describes the specific details of each test, including general information and instrumentation. Detailed information regarding the girder properties and values assumed in the thermal effects analysis are provided in Appendix A.

6.2.1 General

Table 6.1 summarizes the general details of each test, including the dates, air temperatures, girder geometries, and bed occupancy. Tests 1 through 3 were cured over the course of a weekend, while Test 4 was released the day following casting. The air temperatures during Tests 1, 3, and 4 fell below freezing at some point during the fabrication and steam was used to heat the bed during those tests. Tests 1 and 4 were performed on MN54 girder cross sections, 54 in. (1.37 m) deep, and Tests 2 and 3 were performed on 82MW girder cross sections, 82 in. (2.08 m) deep. Test 3 was the only test in which only one girder was fabricated on the bed. In general, it is most efficient to cast

as many girders at a time that can fit on the bed to speed production and reduce the amount of strand waste, but often during the final production of girders for a specific bridge only one additional girder is needed. Tests 2 and 3 were performed on identical girders from the same bridge, but Test 2 was performed at the beginning of the production cycle and Test 3 was performed at the end. A total of seven girders were needed for the bridge so three casts with two girders on the bed (i.e., Test 2) and one cast with one girder on the bed (i.e., Test 3) were executed. When planning Tests 2 and 3, the goal was to study the effects of bed occupancy on prestress losses due to temperature between two fabrications with identical girders, but the average temperature dropped from 82°F (27.8°C) to 64°F (17.8°C), so steam heating contributed to the differences observed between the two tests in addition to bed occupancy.

Table 6.1: General full-scale test details

Test No.	**1**	**2**	**3**	**4**
Date: Tensioning	Thu., 11-21-13	Wed., 09-24-14	Wed., 10-08-14	Thu., 12-04-14
Date: Casting	Fri., 11-22-13	Fri., 09-26-14	Fri., 10-10-14	Tue., 12-09-14
Date: Release	Mon., 11-25-13	Mon., 09-29-14	Mon., 10-13-14	Wed., 12-10-14
Air Temp: Min.	1°F	44°F	24°F	6°F
Air Temp: Max.	39°F	82°F	64°F	35°F
Air Temp: Avg.	22°F	66°F	44°F	22°F
Steam Heated?	Yes	No	Yes	Yes
Girder Details				
Bridge No.	62925	30001	30001	62921
Girder Shape	MN54	82MW	82MW	MN54
Girder Length [ft]	123.24	180.75	180.75	125.65
No. Girders on Bed	2	2	1	2
% Occupied by Girders	69.1%	93.5%	46.8%	65.0%
% Exposed to Air	14.1%	3.9%	42.9%	7.8%
% Tarped Outside Girders	16.8%*	2.6%**	10.3%	27.2%
Parameters Investigated				
Cold season	X		X	X
Warm season		X		
Free strand covered	X		X	X
Bed occupancy	Medium	High	Low	Medium

*Approximate tarped length of free strand based on typical tarp length of 60 ft

**Due to girder tarp overhang at girder ends and between girders

6.2.2 Instrumentation

To determine the effects of temperature on strand stress, foil strain gages and companion thermocouples were attached to up to four strands at select locations along the length of the bed and through the girder section. One strand in each girder, termed "Strand 1," was instrumented more extensively at points of interest along the bed, including multiple locations between midspan and the girder end, on the free strand near the live and dead ends, and on the free strand between the girders. Additional thermocouples were also placed at locations without strain gages to more completely capture the temperature variations along the bed. Load cells were placed on Strand 1 between the chuck and the abutment at both the dead and live ends of the bed to measure the strand force during fabrication.

Concrete strain gages were suspended throughout the height of the girder section at midspan using a grid of fiber reinforced polymer (FRP) bars and rebar ties attached to the stirrups (see Figure 4.3). Similarly, vibrating wire strain gages (VWGs) were secured at the centroid of the strands at midspan with FRP bars tied to the strands, as shown in Figure 6.1.

Figure 6.1: Vibrating wire strain gage near the center of gravity of the strands at midspan

The instrumented locations along the bed and through the girder sections for the four full-scale tests are shown in Figures 6.2 through 6.9 for the four tests. There are two elevation views shown for each girder in Figures 6.2, 6.4, 6.6, and 6.8. Both elevation views show the instrumented locations, which are symbolized by girder cross sections above the bed and tic marks below the bed. The girder symbols denote the locations along the bed that contained foil strain gages and accompanying thermocouples on one or more strands. The letters associated with the instrumented sections of the girder corresponded with the naming convention used in association with the data acquisition system. The tic marks represented additional thermocouples placed along the bed.

The top elevation views in the figures show the locations of the girders (denoted by G1 and G2, as appropriate); free strand at the live end (LE), between the girders (BG), and at the dead end (DE); and where applicable, the tarps on the free strand during the curing process in relation to the live (LE) and dead (DE) ends. Note that the tarps that covered the girders are not shown in the figures for clarity. The only test that did not utilize tarps on the free strand was Test 2. Although tarps were used in Test 1, their location along the bed was not recorded. The plant personnel noted that the free strand in Test 1 was covered by a single tarp; because a tarp is approximately 60 ft., it was assumed that 16.8% of the bed was covered as noted in Table 6.1. The bottom elevation views in the figures show the division of the prestressing bed into segments for the purpose of determining the weighted average temperature of the strand. The lengths of the segments identified on the bottom elevation views in Figures 6.2, 6.4, 6.6, and 6.8 are centered about a corresponding thermocouple, from which a constant segment temperature was assumed. For segments that did not have a corresponding thermocouple, the temperature was assumed based on data taken from a thermocouple at a similar location as identified with arrows below the figure.

The girder section diagrams (Figures 6.3, 6.5, 6.7, and 6.9) show the instrumentation layouts through the girder sections at midspan; other locations typically contained fewer gages. Foil strain gages are shown as squares surrounding the strand to which they were attached and denoted by an upper-case S followed by the numbering scheme. In the remainder of the report, foil strain gages are identified by their location on the bed followed by the strain gage number (e.g., S1 at midspan of Girder 1 would be

denoted as G1-A-1). The locations of the concrete strain gages and VWGs through the section are also shown; they were only used at midspan.

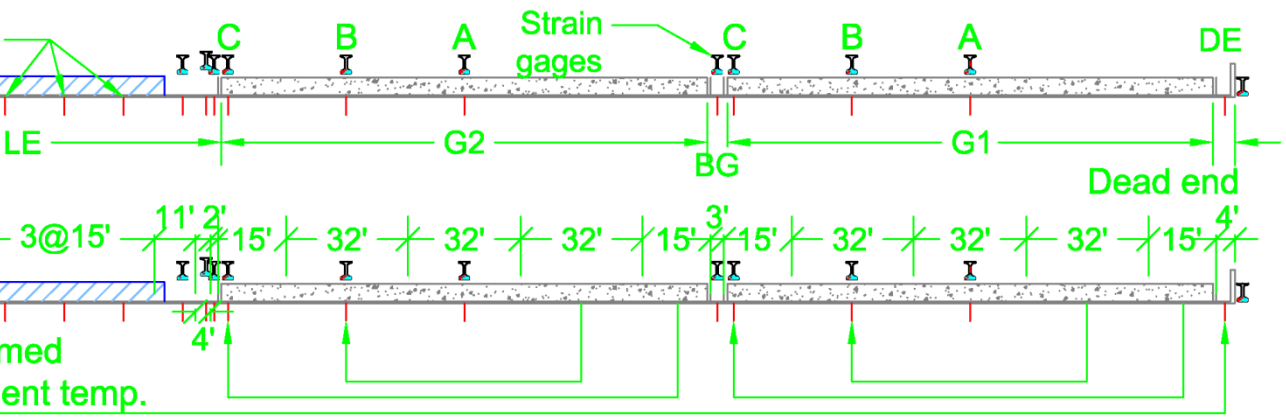

ate tarp length and location

Figure 6.2: Test 1 instrument locations and theoretical temperature sections

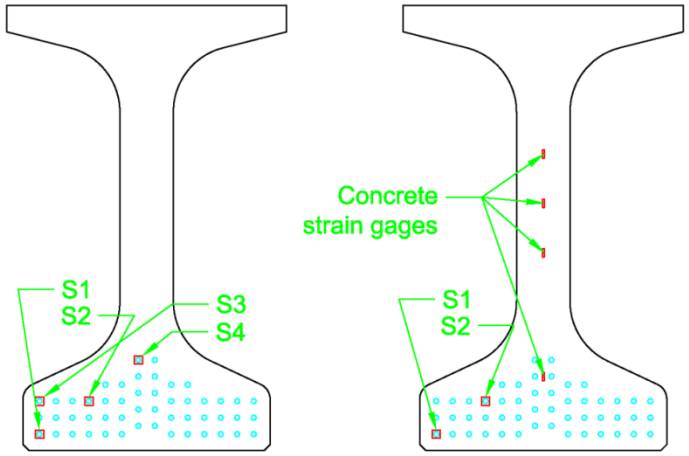

Figure 6.3: Test 1 instrumentation at midspan of Girder 2 (G2-A, left) and Girder 1 (G1-A, right)

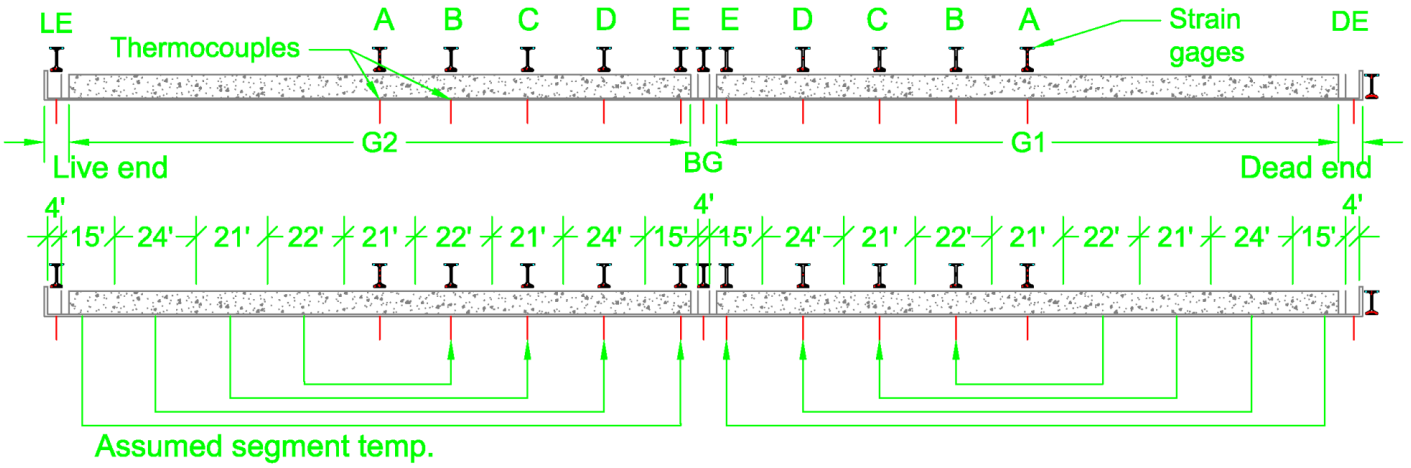
LE
A
B
C
D
E
E
D
C
B
A
DE
Thermocouples
Strain gages
G2
G1
Live end
BG
Dead end
4'
4'
4'
15'
24'
21'
22'
21'
22'
21'
24'
15'
15'
24'
21'
22'
21'
22'
21'
24'
15'
Assumed segment temp.

Figure 6.4: Test 2 instrument locations and theoretical temperature sections

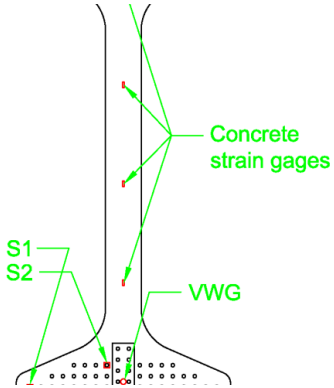

Figure 6.5: Test 2 instrumentation at midspan of Girders 1 and 2 (G1-A and G2-A)

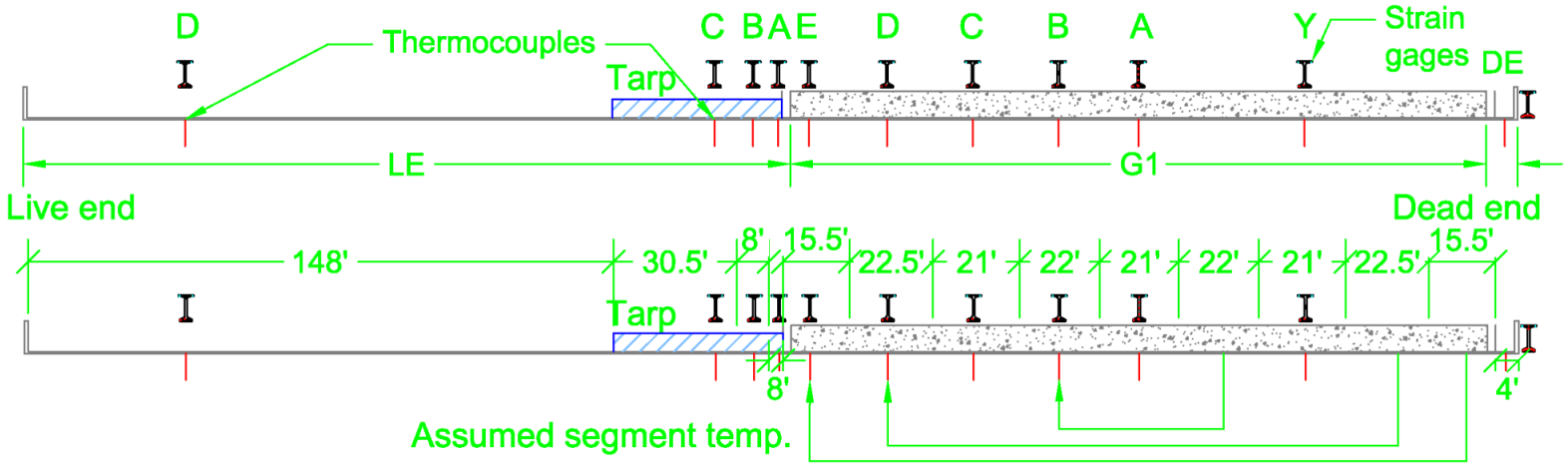
D
Thermocouples
Tarp
C B A E
D
C
B
A
Y
Strain gages
DE
LE
G1
Live end
Dead end
148'
30.5'
8'
15.5'
22.5'
21'
22'
21'
22'
21'
22.5'
15.5'
Tarp
8'
4'
Assumed segment temp.

Figure 6.6: Test 3 instrument locations and theoretical temperature sections

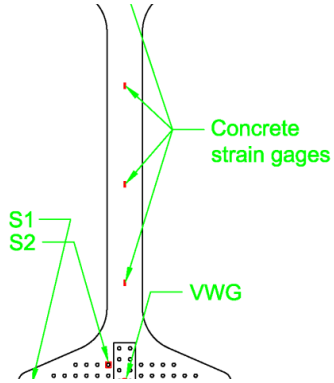

Figure 6.7: Test 3 instrumentation at midspan of Girder 1 (G1-A)

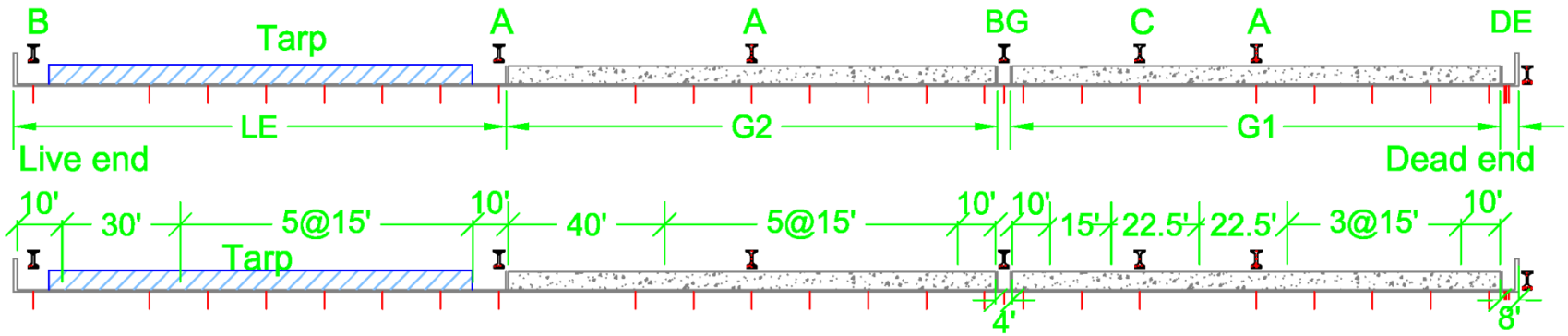
B
Tarp
A
A
BG
C
A
DE
LE
G2
G1
Live end
Dead end
10'
30'
5@15'
10'
40'
5@15'
10'
10'
15'
22.5'
22.5'
3@15'
10'
Tarp
4'
8'

Figure 6.8: Test 4 instrument locations and theoretical temperature sections

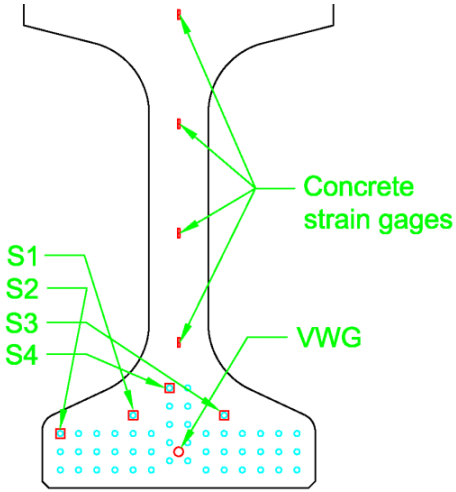

Figure 6.9: Test 4 instrumentation at midspan of Girders 1 and 2 (G1-A and G2-A)

6.3 Initial Strand Force

The following summary describes the strand force correction procedure used by at least one of the precasting plants to fabricate MnDOT prestressed concrete bridge girders. When the precasting plant receives an order for a set of bridge girders from MnDOT, a plan sheet is provided that specifies the required tension force per strand. This is the force that is assumed to be present in each strand at the time of release, so the precasting plant must account for force losses that may occur between the times of tensioning and release. During tensioning, force can be lost due to the strands slipping in the chucks at the dead end of the bed, the chuck seating against the live end abutment upon removal of the hydraulic jack, and the bending of the abutments as force is incrementally applied. After tensioning, temperature changes affect the strand force, which is especially important at the time at which the concrete bonds to the steel, when force loss due to temperature becomes non-recoverable. The precasting plant accounts for the losses due to the differential strand temperature between the time of tensioning to placement of wet concrete. They do not account for the actual length of the strand affected by the temperature differential. Instead they assume the entire strand rather than a portion of it is affected by the temperature differential. They do not account for the temperature differential at bond.

6.3.1 Strand Force Adjustments

This section describes the precasting plant adjustments to the tensioning force to achieve the required strand tension force at the time of release. The adjustments account for expected losses during tensioning (i.e., dead end slippage, abutment movement, and seating) and expected losses due to temperature changes between the times of tensioning and concrete casting. The goal in adjusting the tensioning forces is to offset the expected losses.

6.3.1.1 Losses during Tensioning

To account for losses, the precasting plant increases the initial strand tensioning force specified in the plan sheet. A tensioning sheet with the required strand force and

gross and net elongations is produced for each girder fabrication for use by the tensioning crew. The tensioning crew is required to pull each strand to at least the force and elongation specified on the tensioning sheet, but cannot exceed the values by more than 5%. The plant specifies gross strand elongation based on the assumed seating loss, as well as losses due to slippage of the strand in the chuck at the dead end and the average deflection of the abutments due to the moment of the strand force about their bases, known as abutment movement. The gross elongation is not adjusted in the field to account for strand stress losses assumed to occur due to the difference in temperature at tensioning and the expected concrete placement temperature discussed in Section 6.3.1.2. The gross elongation is used as an approximate check to ensure the tensioning force is met. A required net elongation value, taken as the gross elongation minus the assumed seating loss, is determined to ensure that the force lost due to seating upon releasing the hydraulic jack from the strand is approximately equal to the assumed seating loss. The tensioning crew is required to pull each strand to at least the force and elongation specified on the tensioning sheet, but cannot exceed the values by more than 5%.

Elongation measurements are made with a string potentiometer fixed to the arm of the hydraulic jack used to pull the strands. The strands are initially preloaded to a certain force (typically 4 kips (18 kN)) to untangle them on the bed. The string potentiometer is zeroed after preloading. The gross elongation is measured when the jack is holding the strand at the required force specified on the tensioning sheet. The net elongation is measured after the force has been released from the jack and the chuck has seated against the abutment. Table 6.2 details the assumed losses during tensioning for the precasting beds on which the four full-scale tests were performed. Figure 6.10 compares the assumed seating losses to the average measured seating losses for the straight strands during each test. The measured seating losses were simply taken as the difference in the gross and net elongations that were recorded by the plant for each strand during tensioning.

Table 6.2: Initial force adjustments for losses during tensioning; assumed and measured

Test No.	**1**	**2**	**3**	**4**
Bed No.	6	7	7	7
Plant Adjustments				
Seating, SL [in]	0.375			
Dead End Slip, SD [in]	0.125			
Abutment Movement, AM [in]	0.375	0.25		
Total Adjustment, TA=SL+SD+0.5*AM [in]	0.6875	0.625		
Avg. Measured (gross minus net)				
Seating [in]	0.75	0.68	0.69	0.64

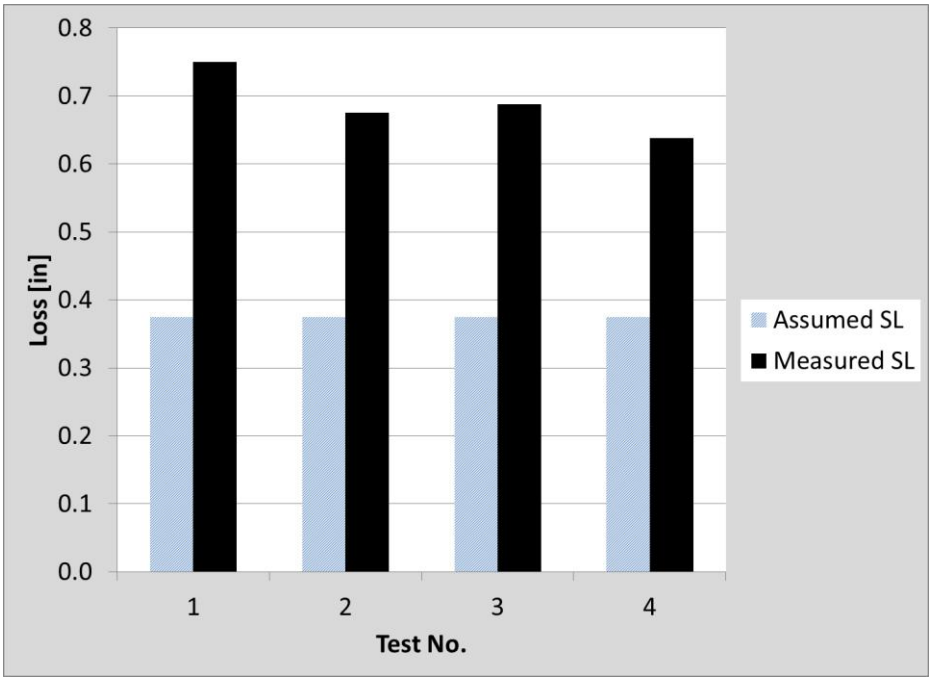

Figure 6.10: Plant assumed live end seating loss adjustment compared to average measured seating loss (gross minus net elongation) for straight strands

From the figure, it can be seen that the average difference between the gross and net elongations was approximately twice as large as the precasting plant's assumption. This difference could result in a 0.5 kip (2 kN), or 1%, reduction in the initial strand force after seating. Dead end slippage and abutment movement were not measured during the full-scale girder tests. However, indications of additional losses after the net elongations

were recorded were observed in load cell readings during and just after tensioning. Figure 6.11 shows the dead (DE) and live (LE) end load cell readings during and just after tensioning for full-scale Test 4. The net measured force for Strand 1, calculated using the net elongations measured by the precasting plant, is shown as a horizontal dotted line. The DE load cell shows that the strand was initially pulled higher than the net force, representing the gross force before seating. The strand then seated to approximately the net measured force. As additional strands were tensioned, the force decreased in a parabolic manner by approximately 0.4 kips (2 kN), which was likely due to abutment movement, as discussed in Section 6.7.2.2.

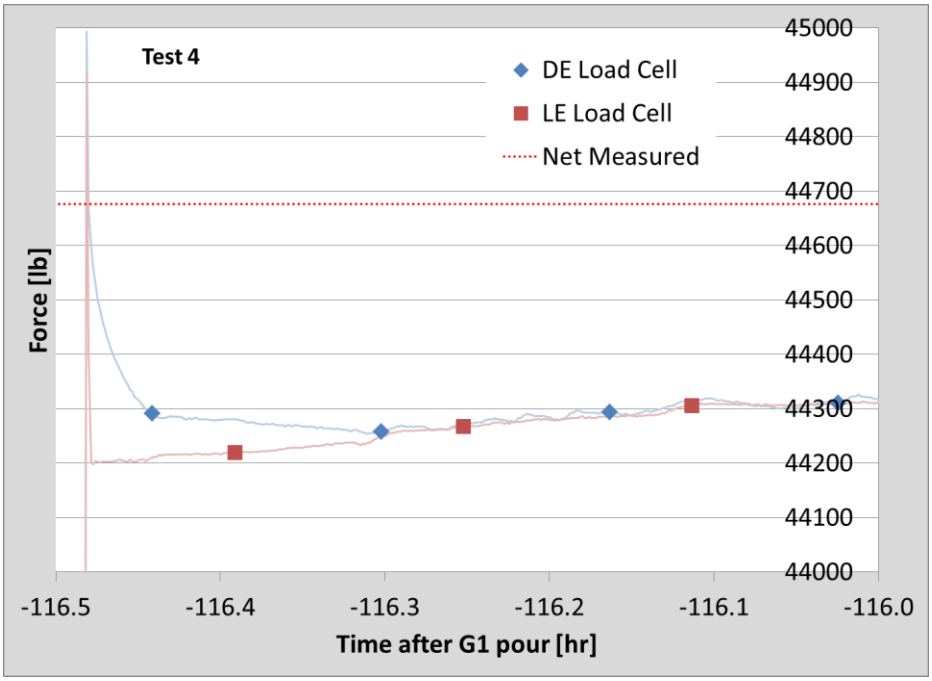

Figure 6.11: Load cell readings during tensioning for Test 4

Additional data regarding initial strand forces derived from multiple field measurements is provided in Appendix D.

6.3.1.2 Losses due to Temperature

Just before tensioning begins, the tensioning crew takes temperature measurements of the strand on the bed at approximately six locations to determine the average strand temperature at the time of tensioning. This value is compared to the temperature of a recent batch of wet concrete, which is generally between 70 and 80°F

(21.1 to 26.7°C). For every 10°F (5.6°C) difference (rounded down) between the average strand and wet concrete temperatures, one percent of the required strand force (after adjusting for losses during tensioning) is added to or subtracted from the initial pull force. The adjustment is approximately equal to the force change that would occur assuming an average temperature change of 10°F (5.6°C) along the entire length of the bed in Equation (3-7), as shown in Equation (6-1):

$$\begin{aligned} \Delta P_{s,T-B} &= -\alpha_s E_{ps} A_{strand} \Delta T_{T-B} \\ &= -6.78x10^{-6}/°F * 28500ksi * 0.218in^2 * 10°F \\ &= 0.42kip \approx 0.01P_{req} \end{aligned} \quad (6\text{-}1)$$

where:

A_{strand}	Area of a single strand
E_{ps}	Strand modulus of elasticity
P_{req}	Required strand force after adjusting for losses during tensioning
α_s	Assumed coefficient of thermal expansion of strands
$\Delta P_{s,T-B}$	Change in girder strand force from tensioning to bond
ΔT_{T-B}	Average change in strand force along bed from tensioning to bond

If the average strand temperature is lower than the wet concrete temperature (e.g., winter), force loss at the time of casting is anticipated, so force is added to the initial pull. If the average strand temperature is higher (e.g., summer) than the wet concrete temperature, force gain at the time of casting is anticipated, so force is subtracted from the initial pull. The temperature correction determined by the tensioning team is noted on the tensioning sheet and the required strand force is adjusted accordingly just before tensioning begins.

6.3.1.3 Safety Issues

Increasing the initial strand force is necessary to offset expected losses as discussed in Sections 6.3.1.1 and 6.3.1.2, but can also pose safety concerns. For example, if the strand temperature is very low compared to the concrete temperature, a large correction may exceed the $0.8f_{pu}$ jacking force limit set in ACI 318-11. To minimize the required adjustments in cold weather, the precasting bed is heated by covering large portions of the bed with insulated blankets and applying steam to raise the average strand temperature at the time of tensioning, decreasing the temperature difference between

tensioning and casting. Heat is applied during the entire fabrication process so the strand temperature does not decrease enough to overstress the strands. During times at which removal of the tarps is required for bed access (i.e., placement of the rebar cages, side form placement, and casting), care is taken to limit the amount of uncovered strand.

6.3.2 Measured Initial Strand Force

Strand forces derived from measured net strand elongations were compared to the MnDOT required strand tension force provided in the bridge plans to estimate the effective temperature adjustments used in the fabrication of the girders. Table 6.3 summarizes the force specified on the MnDOT bridge plan, the precasting plant's target initial tensioning force to account for seating, the precasting plant adjustment to account for temperature effects (based on the difference between the average strand temperature at the time of tensioning and the temperature of the wet concrete, as explained in Section 6.3.1.2), the resulting precasting plant's target initial tensioning force accounting for seating and temperature effects, the average gross and net forces derived from the precasting plant's elongation measurements, and the effective strand force adjustment for temperature.

The precasting plant's target initial tensioning force did not account for potential loss of force due to abutment movement caused by stressing other strands in the tensioning process. The measured gross elongation included dead end slip, the overpull to account for seating, and the elongation due to the applied temperature correction; it did not include the elongation due to the applied 4 kip (18kN) preload nor the abutment movement associated with tensioning other strands. The difference between the net and gross elongation represented the seating loss.

Equation (3-2) was applied to all of the straight strand pull measurements to derive the gross and net average measured forces from the gross and net elongations with consideration for the preload. These derived forces do not account for potential losses due to dead end slip and abutment movement, which are discussed in Section 6.7.2.2. These losses would reduce the effective temperature adjustment in the table, which was taken as the difference between the derived net measured force and the MnDOT plan force. The effective temperature adjustment thus approximately represents the amount of non-

recoverable force per strand that could be lost between tensioning and bond while maintaining the design strand force at release. If the force lost due to temperature was larger than this value, the correction was not large enough. The net measured force was larger than the plan force in all cases, meaning some effective adjustment for temperature was included even for the tests for which no temperature adjustment was specified (ignoring the potential losses due to dead end slip and abutment movement).

Table 6.3: Observed initial strand force and adjustments for temperature for full-scale girder tests

Test No.	1	2	3	4
MnDOT Plan Force [kip]	43.94			
Plant Target Initial Tensioning Force before Temp. Adjustment [kip]*	45	45	45	45
Plant Temp. Adjustment	+2%	0	0	+1%
Plant Target Initial Tensioning Force including Temp. Adjustment*+ [kip]	45.9	45.0	45.0	45.45
Gross Avg. Measured Force [kip]	45.9	45.4	45.4	45.7
Net Avg. Measured Force [kip]	44.8	44.5	44.4	44.9
Effective Temp. Adjustment [kip]	0.8	0.5	0.5	0.9

* Plant target initial tensioning force before temperature adjustment includes the adjustment for assumed seating loss, rounded up to the nearest kip by tensioning crew due to precision of dial gage

+ Additional significant figures are included on precasting plant tensioning sheet, numbers in the table have been rounded because measured precision is lower

6.4 Strand Force Changes due to Temperature

During the fabrication process, temperature changes affect the amount of force in the strands. Before concrete-steel bond, the entire length of strand was assumed to be unrestrained between abutments. Because the bed length was fixed, the total strain change in the strand had to equal zero, so changes in thermal strain due to temperature changes caused changes in mechanical strain and, therefore, strand force. After bond, but before release, the total length change of the strands must be zero, but after bond, some of the strand is embedded in the concrete. Temperature changes in the concrete after bond cause compatibility forces in the girder section due to the different coefficients of thermal expansion between the steel and the concrete. The force change in the free strand due to temperature must be equilibrated by a corresponding resultant force change in the girder

section. Temperature data gathered along the precasting bed during the full-scale tests were used to predict the force change at the time of bond.

6.4.1 Estimations of Strand Force Changes

Load cells were placed at the dead and live ends of Strand 1 during each of the full-scale girder tests (except Test 1) to monitor the strand force throughout the fabrication process. The readings from each cell were expected to be the same before bond, when the strand was unrestrained and equilibrium between the two abutments was required to be satisfied. After bond in the thermal effects analysis (TEA) described in Chapter 3, it was assumed that the girders were unrestrained in the bed (i.e., they could slide). This is referred to as Case A. With these assumptions, the force in the free strand must remain constant across the bed. The free strand can be treated as a single segment between the abutment and girders, and the girders can be treated as one continuous section of concrete that is bordered by the free strand on one side and the other abutment on the other side. With these assumptions, the dead end and live end forces must remain equal.

Because the load cells indicated different free strand force changes in the live and dead ends after casting, a second case, Case B, was also investigated. In Case B, the locations of the hold-downs are considered. It was assumed that the hold-downs behaved as fixed points in the girder, similar to the abutments. A unique free strand force change could then be determined for the live (LE) and dead (DE) ends of the bed.

To determine the strand force changes between tensioning and bond, Equation (3-7) was used. Because the force change in the strand was assumed to be constant along the entire length of the bed before bond, it was expected that the force changes determined with Equation (3-7) would reasonably estimate the changes recorded by the load cells at both ends before bond. To determine the free strand force change between bond and release, Case A and Case B were investigated.

Figure 6.12 shows the differences between Case A and Case B. In Case A, the free strand force change estimation was based on the assumption that the total change in length of the entire precasting bed must equal zero. This implied that the girders were not restrained longitudinally by the hold-downs, so their locations were unimportant. In Case

B, the free strand force change estimation was based on the assumption that the change in length between the abutments and their nearest hold-downs must equal zero. This allowed for unique free strand force change estimations at each end of the bed.

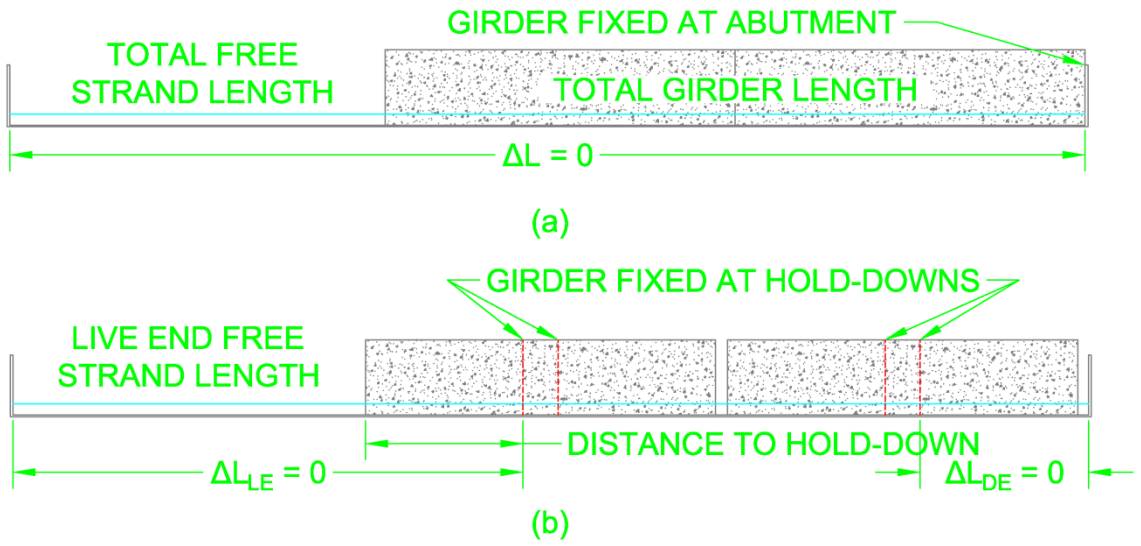

Figure 6.12: Thermal effects analysis assumption diagram comparing (a) Case A and (b) Case B

For both Cases A and B, Equation (3-7) was used to determine the strand force change due to temperature before an assumed time of bond. After the assumed time of bond, the free strand force change with respect to time for Case A was determined by Equation (3-14). The methods for determining the free strand force changes for Case B at

the live and dead ends of the bed are described in Section 6.4.1.3. The following subsections discuss the estimated and measured strand force changes before casting, as well as the effects of Cases A and B on the estimation of the free strand force change after casting. It should be noted that results from Test 1 are not included because load cells were not used and peak temperatures during concrete hydration were not recorded due to an error in the datalogging program, so a complete strand force change profile could not be estimated with the TEA for that test.

6.4.1.1 Strand Force Changes Before Casting

As mentioned earlier, it was expected that the load cells on the live and dead ends of Strand 1 would read similarly before the concrete was cast and that the force changes could be reasonably estimated with Equation (3-7) from the thermal effects analysis (TEA). Figures 6.13, 6.14, and 6.15 show the Strand 1 force changes measured by the load cells and estimated with the TEA between the time of tensioning and casting for full-scale Tests 2, 3, and 4, respectively. Note that time zero on the horizontal axis represents the time that casting (i.e., pouring of concrete) began.

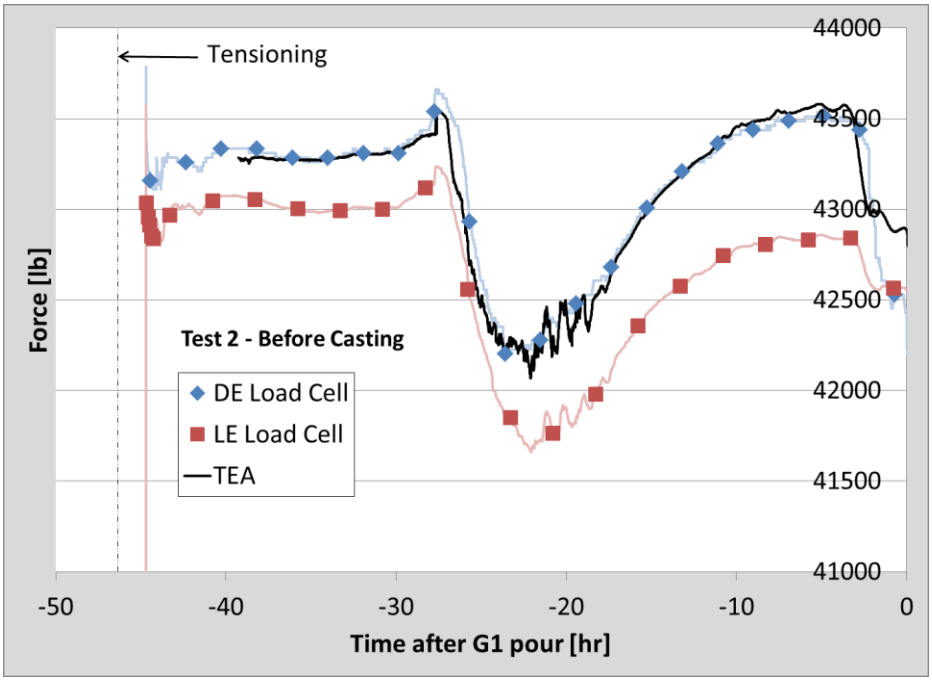

Figure 6.13: Measured and estimated Strand 1 force changes before casting during Test 2

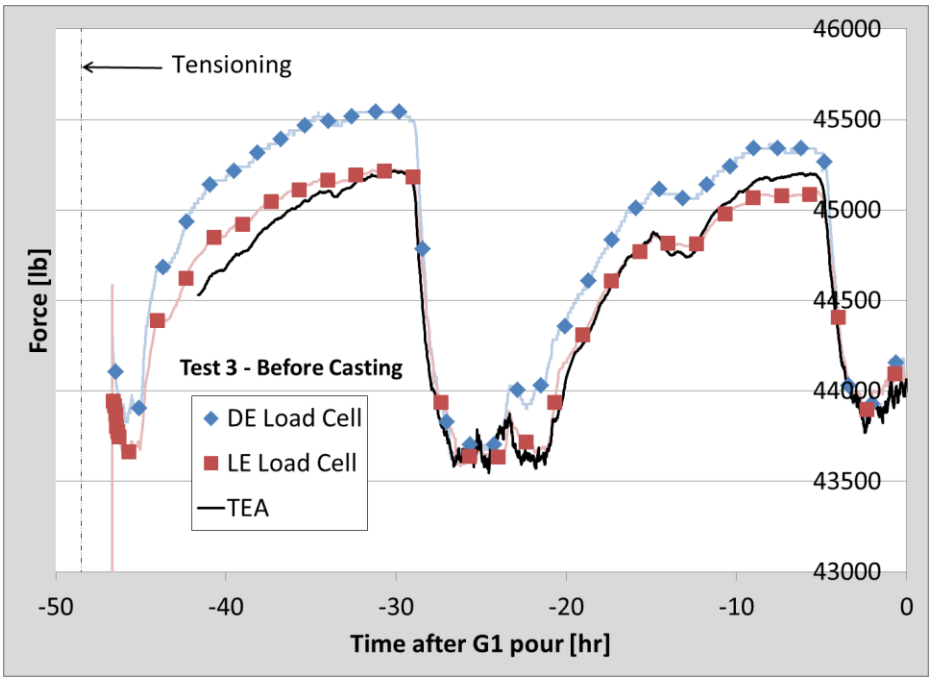

Figure 6.14: Measured and estimated Strand 1 force changes before casting during Test 3

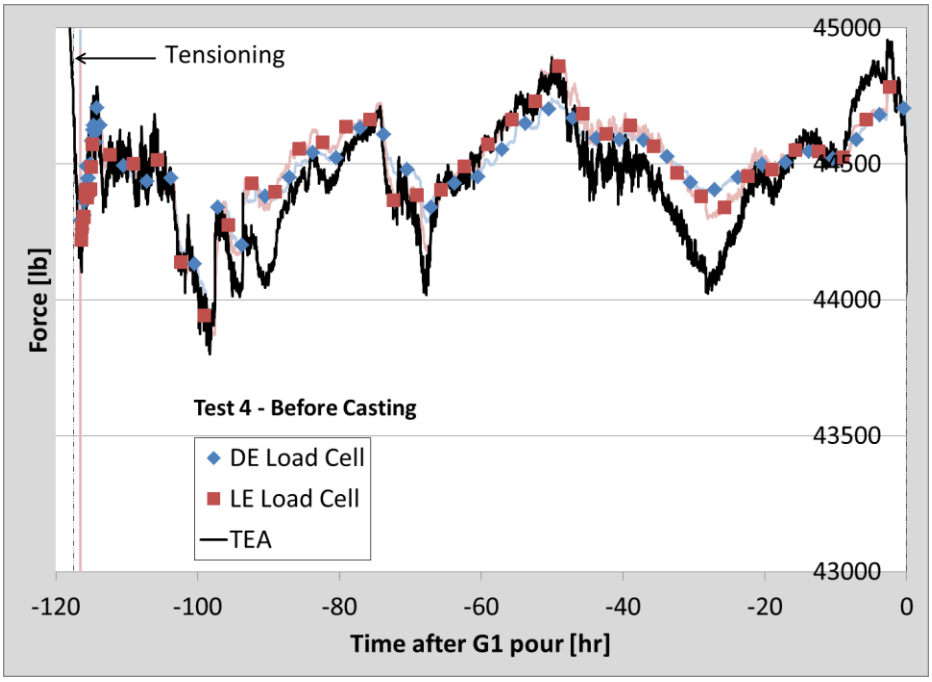

Figure 6.15: Measured and estimated Strand 1 force changes before casting during Test 4

As expected, the LE and DE load cell data were similar before the concrete was cast for all three tests. Although the load cell readings deviate at some points in time before casting, the readings were within the tolerance of ±600 lb (2.7 kN) determined from calibration tests described in Section 4.7. The TEA estimated strand force changes reasonably match the measured values.

6.4.1.2 Strand Force Changes After Casting: Case A – Effects of Ignoring Hold-Downs

To validate the thermal effects analysis (TEA) with the Case A assumptions, estimated and measured free strand force changes were plotted with respect to time for Tests 2, 3, and 4, as shown in Figures 6.16, 6.17, and 6.18, respectively. The datum of the time axis is located at the time casting began for each test. Vertical dashed lines indicate the times of casting the second girder, where applicable, and release. Although the short girder tests described in Chapter 5 concluded that bond occurs between 6 and 8 hours after casting during mild summer weather, the possibility that bond was delayed in some cases was investigated by assuming multiple times of bond in the TEA and determining which assumed time resulted in the best fit between the estimated and measured force changes. The estimated force changes using the TEA with the Case A assumptions are shown as incremental lines representing different assumed times of bond, from 0 up to 12 hours after casting in one hour increments. An arrow indicates the order of the lines, starting from the line representing zero as the assumed time of bond and pointing toward the final assumed time of bond. The arrow is U-shaped in Figure 6.17 because the estimated forces increased from 0 to 3 hours then decreased up to 12 hours assumed time of bond.

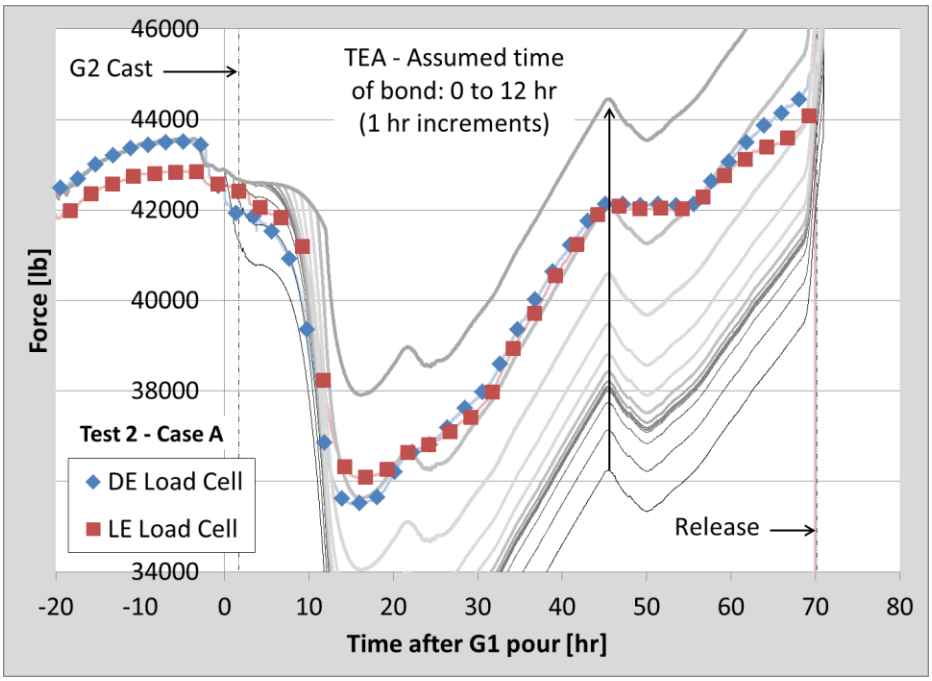

Figure 6.16: Measured and estimated Strand 1 force changes after casting during Test 2 – Case A

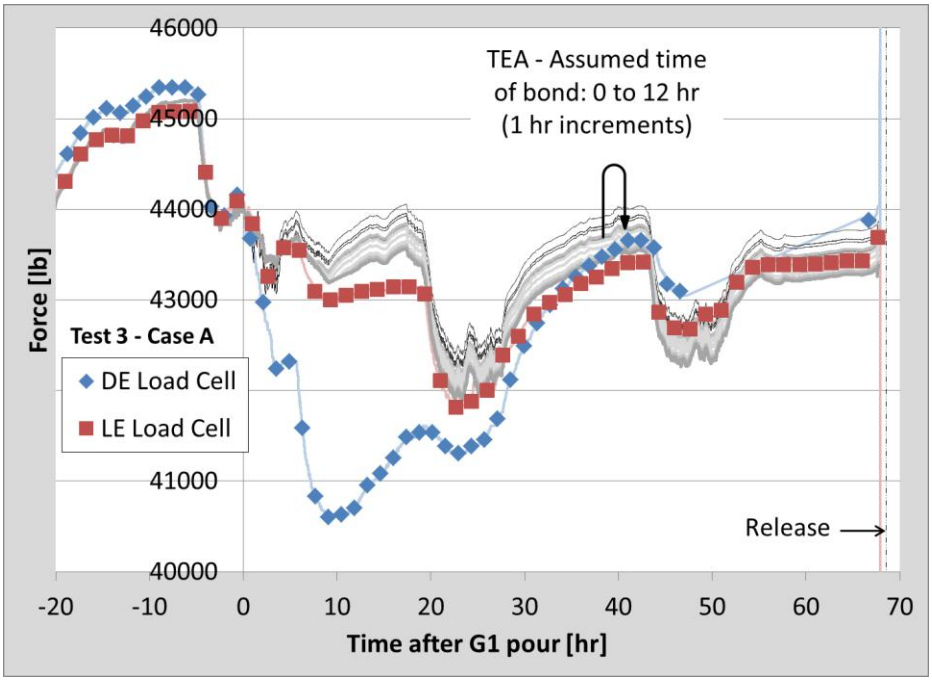

Figure 6.17: Measured and estimated Strand 1 force changes after casting during Test 3 – Case A

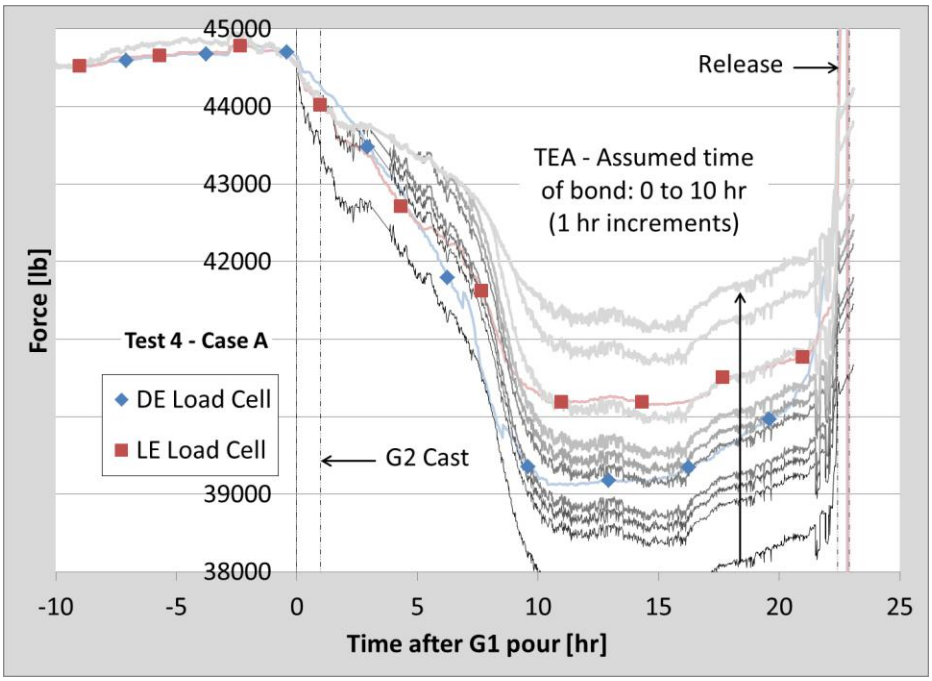

Figure 6.18: Measured and estimated Strand 1 force changes after casting during Test 4 – Case A

After the girders were cast, deviations in load cell readings due to restraint of the concrete on the strands began to occur. The effects were minimal during Test 2 due to the symmetric free strand length at the live and dead ends. The dead end load cells recorded more severe free strand force losses during Tests 3 and 4, likely because the dead end free strand length was much shorter than the live end length and the expansion of the girder due to the heat of concrete hydration, in addition to possible increases in free strand temperature, resulted in a larger strain change relative to the shorter free strand length.

The fit of the TEA estimated force changes after casting was highly dependent on the assumed time of bond. The best fit for Test 2 occurred when the time of bond was assumed to be 11 hours after casting, which suggested that bond occurred later than the initially assumed time range of 6 to 10 hours in accordance with Barr et al. (2005). Test 3 contained the largest continuous length of free strand of the four full-scale tests (approximately 200 ft (60 m) from the girder end to the LE abutment), so it was reasonable that the TEA with the Case A assumptions more closely estimated the free strand force changes recorded by the LE load cell. The TEA was also less sensitive to the

assumed time of bond during Test 3. Test 4 also contained a large amount of free strand between the girder end and LE abutment, so the TEA was expected to more closely estimate the LE load cell readings. The best fit between the Test 4 estimated and LE measured strand force changes occurred when the assumed time of bond was 8 hours after casting. It should be noted that, although later assumed times of bond (8 to 11 hours) better fit the overall measured strand force profile, earlier assumed times of bond (1 to 4 hours) better captured the strand force changes during the hydration process (0 to 12 hours after casting). This could be a result of the assumption that bond is an instantaneous phenomenon, when in reality it is a gradual process.

For Test 2, it was found that the best estimation for the strand force changes after casting using the TEA occurred when a time of bond of 11 hours after casting was assumed, which was later than expected. To investigate the likelihood that bond the concrete in Test 2 cured more slowly than normal, the temperatures of Strand 1 at midspan of Girder 1 for each full-scale girder test during hydration were examined, as shown in Figure 6.19. Table 6.4 summarizes the concrete temperatures in the figure at times of interest after casting and shows the time after casting at which the concrete temperatures reached 100°F (37.8°C) for each full-scale girder test.

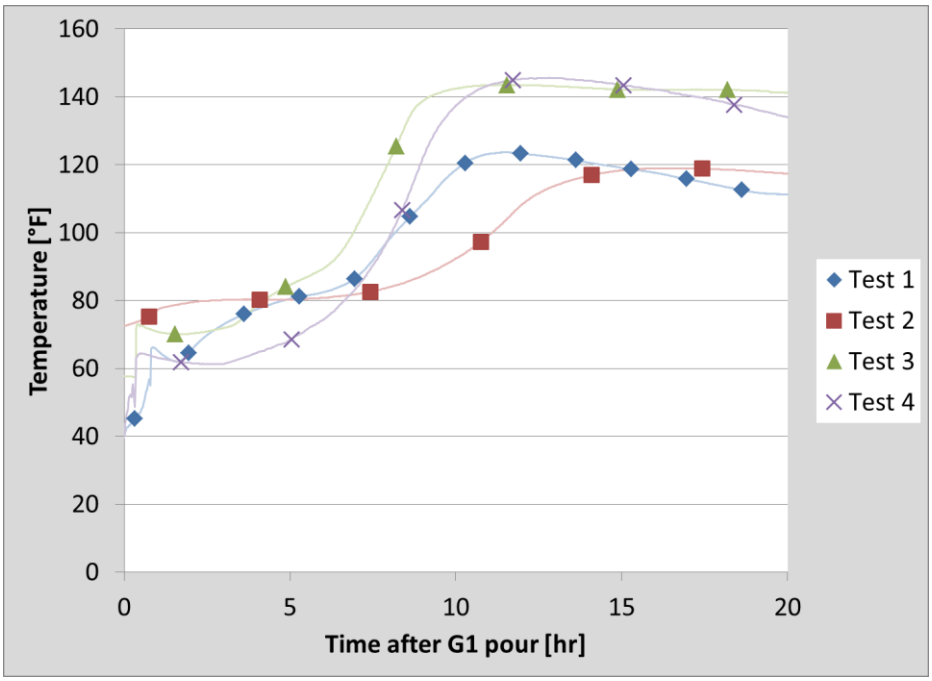

Figure 6.19: Strand 1 temperatures at midspan of Girder 1 during concrete hydration for all full-scale tests

Table 6.4: Concrete temperatures at midspan on Strand 1 at various times after casting and the time at which the temperature reached 100°F for each full-scale test

Time After Casting [hr]	Midspan Concrete Temperature [°F]			
	Test 1	Test 2	Test 3	Test 4
3	73	80	72	61
6	83	81	89	74
8	98	84	121	99
10	119	92	142	137
12	123	108	144	145
Time After Casting [hr] at which Temperature Reached 100°F				
100°F at:	8.2	11.1	6.9	8.0

The rate of increase in concrete temperature was slowest during Test 2, reaching 100°F (38°C) at approximately 11 hours after casting compared to 7 to 8 hours during the other three tests. This can be attributed to the lack of steam heating during Test 2, as well as the large amount of time it took to cast the girders, as Test 2 required the largest amount of concrete among the four full-scale tests. Cylinder tests described in Section

5.3.1 showed a correlation between the rates of concrete compressive strength gain and temperature increase; consequently, the low rate of concrete temperature increase observed during Test 2 may have resulted in a lower rate of concrete strength gain, which would have delayed the time of bond. Based on observed concrete temperatures during the short girder tests in Section 5.4.5, it was concluded that bond likely occurs when the concrete has reached a temperature between 90 and 110°F (32.2 and 43.3°C). The estimated free strand force changes under the Case A assumptions and assuming the time at which the concrete temperature reached 100°F was the time at which bond occurred were reasonable when compared to load cell data from full-scale Tests 2, 3, and 4.

6.4.1.3 Strand Force Changes After Casting: Case B – Effects of Considering Hold-Down Restraints

In typical prestressed concrete girder production, a number of strands are raised at the girder ends to reduce the strand eccentricity. This is referred to as "draping" the strands and its purpose is to reduce the tensile and compressive stresses in the top and bottom flange of the girder ends, respectively, due to strand eccentricity because stresses at the girder ends due to self-weight and external loads are zero in simply-supported members. Draping strands allows economic design of prestressed concrete girders without exceeding tensile and compressive stress limits defined by bridge design codes in the girder ends.

To produce draped strands, mechanical anchors, called "hold-downs," are fixed to the precasting bed at the "harp" points specified on the girder plans. The hold-downs contain rollers to minimize friction with the prestressing strands. During tensioning, the draped strands are pulled to a lower force than the straight strands. The remaining force is introduced when the draped strands are lifted to the correct height just outside the girder ends to achieve the proper eccentricity. To accomplish this, the draped strands are fed through a mechanical "horse" during fabrication that is lifted into proper position by a forklift. The assumptions in Case B consider the hold-downs as fixed points on the bed that prevent the girder from sliding and resist any force changes due to temperature.

The free strand, girder strand, and concrete forces between bond and release with the Case B assumptions were determined in a similar manner to the forces with the Case

A assumptions. The only difference was in the free strand and girder lengths assumed in the calculations; consequently, the temperature profiles were different in Case B from Case A to reflect the average measured temperatures of the Case B assumed girder and free strand lengths. In Case A, the total length of the girders on the bed and the total length of free strand were considered. In Case B, only the free strand length from the abutment to the girder end and the girder length from the end to the nearest hold-down were considered. To reflect the Case B assumptions in estimating strand and concrete force changes, the equations in Section 3.3.3.1 were modified.

Equation (3-9), representing strain compatibility between the steel and concrete at the center of gravity of the strands (*cgs*), was unchanged with the exception of the notation for the force changes in the girder strand and concrete, which were modified for Case B to reflect the consideration of the hold-downs, as shown in Equation (6-2). As in Equation (3-9), bending due to the eccentricity of the strands was ignored, and it was assumed that the change in length of the steel and concrete at the *cgs* are equal.

$$\left(\frac{\Delta P_{s,B-R,hold}}{E_{ps}A_{ps}} + \alpha_s \Delta T_{c,B-R}\right) - \left(\frac{\Delta P_{c,B-R,hold}}{E_c A_{net}} + \alpha_c \Delta T_{c,B-R}\right) = 0 \qquad (6\text{-}2)$$

where:

A_{net}	Net cross-sectional area of concrete girder section
A_{ps}	Total area of prestressing strands
E_c	Modulus of elasticity of concrete
E_{ps}	Modulus of elasticity of prestressing strand
α_c	Assumed coefficient of thermal expansion of concrete
α_s	Assumed coefficient of thermal expansion of steel
$\Delta P_{c,B\text{-}R,hold}$	Resultant concrete force at center of gravity of strands with free strand restraint between bond and just before release considering hold-downs
$\Delta P_{s,B\text{-}R,hold}$	Change in girder strand force with free strand restraint between bond and just before release considering hold-downs
$\Delta T_{c,B\text{-}R}$	Average change in temperature of concrete from bond to release between the end of the bed and the first hold-down

Equation (3-10), showing that the force changes in the free strand and girder strand and the resultant concrete force must be in equilibrium, was also unchanged with the exception of the notation, as shown in Equation (6-3):

$$\left(\Delta P_{s,B-R,hold} + \Delta P_{c,B-R,hold}\right) - \Delta P_{free,B-R,hold} = 0 \tag{6-3}$$

where:

$\Delta P_{free,B\text{-}R,hold}$ Change in free strand force between bond and release considering hold-downs

Equation (3-11) showed that the change in length of the girder strand must be equal and opposite to the change in length of the free strand. The Case B assumptions state that the change in length of the free strand between the abutment and the girder end must be equal and opposite to the change in length of the girder strand from the girder end to the hold-down, as shown in Equation (6-4):

$$\left(\frac{\Delta P_{s,B-R,hold}}{E_{ps}A_{ps}} + \alpha_s \Delta T_{c,B-R}\right) x_{hold} + \left(\frac{\Delta P_{free,B-R,hold}}{E_{ps}A_{ps}} + \alpha_s \Delta T_{free,B-R}\right) L_{free} = 0 \tag{6-4}$$

where:

L_{free} Length of free strand between the abutment and the nearest girder end

x_{hold} Distance from girder end to hold-down

$\Delta T_{free,B\text{-}R}$ Average change in temperature of free strand between the precasting bed end and adjacent girder from bond to release

The three unknown force changes ($\Delta P_{s,B\text{-}R,hold}$, $\Delta P_{c,B\text{-}R,hold}$, and $\Delta P_{free,B\text{-}R,hold}$) were solved using the previous three equations. The force change in the girder strand and the resultant force in the concrete considering the hold-downs are given by Equation (6-5) and (6-6), respectively. The free strand force change considering the hold-downs is given by Equation (6-7):

$$\Delta P_{s,B-R,hold} = \frac{-\left\{\left[\frac{(\alpha_s - \alpha_c)\Delta T_{c,B-R}}{K} + \alpha_s \Delta T_{free,B-R}\right] L_{free} + \alpha_s \Delta T_{c,B-R} x_{hold}\right\}}{x_{hold} + \left(\frac{1}{K} + 1\right) L_{free}} E_{ps}A_{ps} \tag{6-5}$$

$$\Delta P_{c,B-R,hold} = \frac{-\left\{\left[(\alpha_c - \alpha_s)\Delta T_{c,B-R} + \alpha_s \Delta T_{free,B-R}\right] L_{free} + \alpha_c \Delta T_{c,B-R} x_{hold}\right\}}{x_{hold} + \left(\frac{1}{K} + 1\right) L_{free}} E_c A_{net} \tag{6-6}$$

$$\Delta P_{free,B-R,hold} = \frac{-\left\{\left(\frac{1}{K} + 1\right) \alpha_s \Delta T_{free,B-R} L_{free} + \left(\frac{\alpha_c}{K} + \alpha_s\right) \Delta T_{c,B-R} x_{hold}\right\}}{x_{hold} + \left(\frac{1}{K} + 1\right) L_{free}} E_{ps}A_{ps} \tag{6-7}$$

where:

K Relative axial stiffness of steel ($E_{ps}A_{ps}/E_cA_{net}$)

To determine the effects of the Case B assumptions, estimated free strand force changes were determined using measured temperature data from full-scale girder Test 4. Test 4 was examined due to the large amount of temperature measurements taken along the bed. Unique free strand force changes were found for the live (LE) and dead (DE) ends of the precasting bed by assuming different free strand lengths and temperature profiles in Equation (6-7). The free strand length was approximately 125 ft (38.1 m) between the LE abutment and the nearest girder end and 8 ft (2.4 m) between the DE abutment and the nearest girder end. The distance from the girder ends to the hold-downs was approximately 57 ft (17.4 m).

Figures 6.20, 6.21, and 6.22 show measured and estimated free strand force changes on Strand 1 during full-scale girder Test 4 for both Case A and Case B (DE and LE) assumptions assuming bond occurred at 3, 6, and 8 hours after casting, respectively. The three assumptions for the time of bond were chosen to bound the potential time of bond and appeared to best correlate the Case A strand force estimations with the measured values as shown in Figure 6.18.

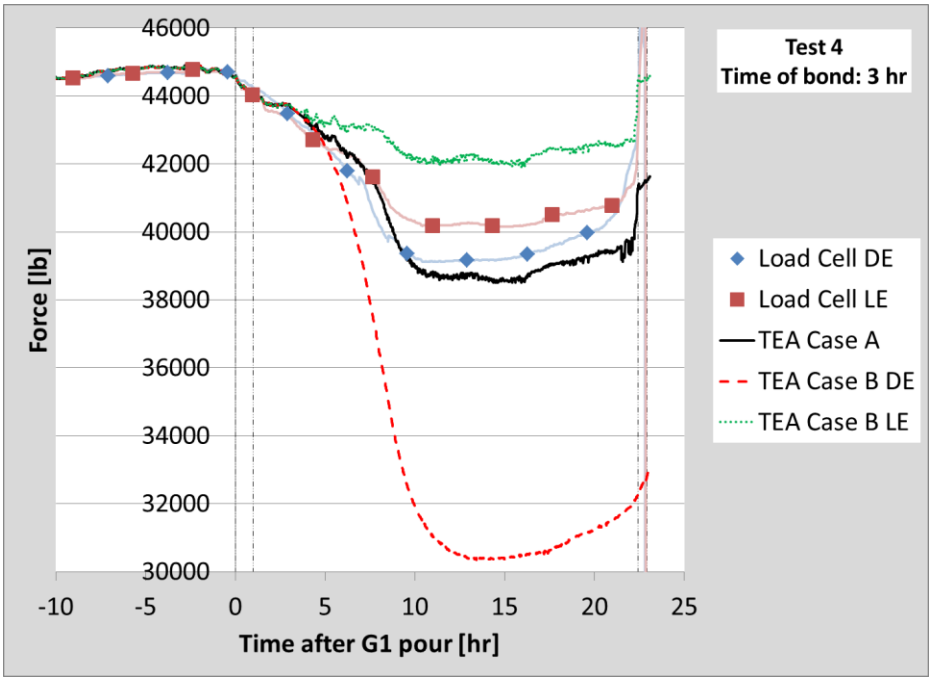

Figure 6.20: Measured and estimated Strand 1 force changes after casting during Test 4 assuming bond occurred at 3 hours – Case B

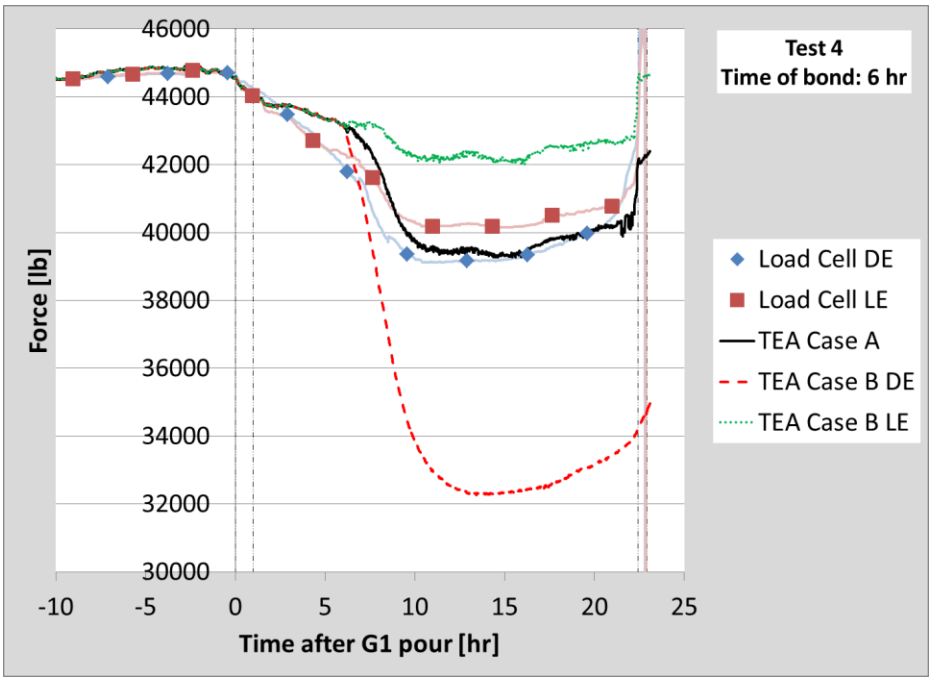

Figure 6.21: Measured and estimated Strand 1 force changes after casting during Test 4 assuming bond occurred at 6 hours – Case B

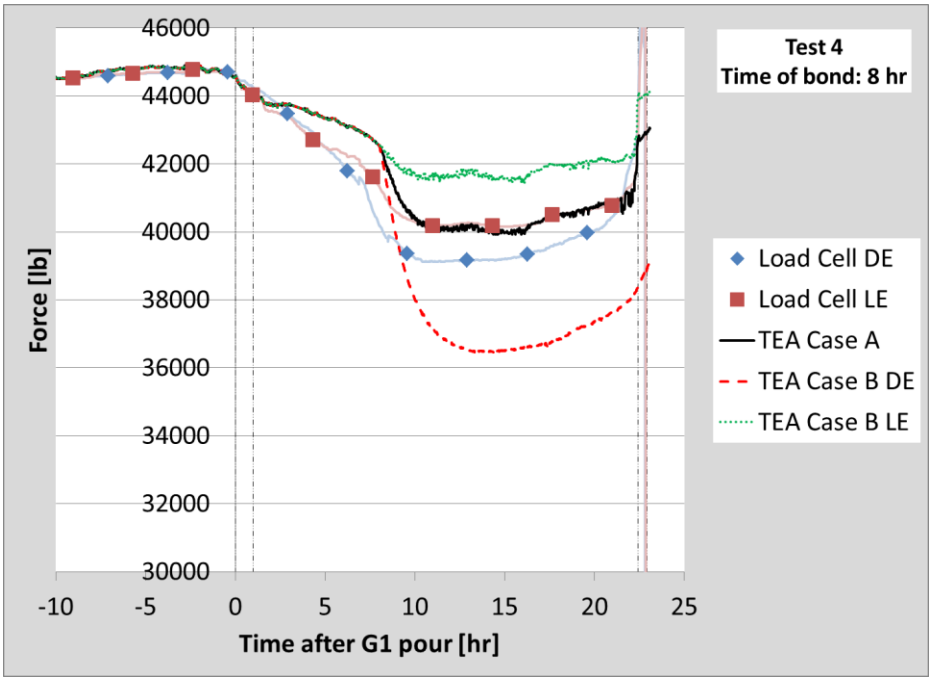

Figure 6.22: Measured and estimated Strand 1 force changes after casting during Test 4 assuming bond occurred at 8 hours – Case B

It was expected that the estimated LE and DE free strand force changes under the Case B assumptions would reasonably match the LE and DE load cell readings, respectively. From the figures, it can be seen that the estimations of the free strand force changes vary significantly between Case A and Case B. With the Case B assumptions, the LE free strand force changes were consistently underestimated and the DE free strand force changes were severely overestimated. The Case A assumptions more reasonably estimated the free strand force change for both the LE and DE for all assumed times of bond. These observations suggest that the hold-downs may not act as fixed points on the bed that resist all girder movement and forces. The slots through which the hold-downs are attached to the precasting bed are not cut to perfectly fit around the base of the hold-down, so some sliding is possible. However, the load cell readings showed differences in the free strand force changes at the LE and DE, which suggests that the girders are not free to slide along the bed, likely due to friction between the concrete and precasting bed. Because the Case A assumptions were found to better estimate the free strand force changes between bond and release, they were used in the thermal effects analysis for the remainder of this report.

6.4.2 Non-recoverable Strand Force Losses

Changes in strand force that occur due to temperature changes between tensioning and bond are considered non-recoverable because the strand force at the time of bond becomes "locked" into the girder strand when the concrete hardens. To determine the approximate effectiveness of the plant tensioning force adjustments in offsetting losses due to temperature, temperature data were used in the thermal effects analysis (TEA) to estimate the amount of non-recoverable force loss that had occurred at the time of bond for each full-scale test. Estimations of the strand force changes with respect to time using the TEA in Section 6.4.1 indicated that the time of bond likely varied for each full-scale girder test, in some cases outside the assumed range of 6 to 10 hours after casting (Barr et al., 2005), so non-recoverable force losses were determined for assumed times of bond between 0 and 12 hours after casting. As noted in Table 6.4, the assumed times of bond for Tests 1 through 4 were 8.2, 11.1, 6.9, and 8.0 hours after casting, respectively, based

on the time at which the concrete temperature at midspan was determined to be 100°F (37.8°C).

Figure 6.23 shows the estimated non-recoverable strand force changes due to temperature for each full-scale girder test. The magnitudes of the force changes are shown on the primary vertical axis and the force changes as a percentage of the MnDOT plan force (i.e., the force assumed in the strand just before release in MnDOT design calculations, typically 43.94 kips (195.5 kN)) are shown on the secondary vertical axis. Figure 6.24 shows the estimated strand force at the time of bond for each full-scale test. The force was estimated by adding the estimated non-recoverable force change using the TEA at the assumed times of bond to the net average measured force from Table 6.3. The plant tensioning force adjustment is considered approximate because the potential losses due to dead end slip and abutment movement were not considered in determining the net average measured force. The horizontal dashed line represents the MnDOT design force.

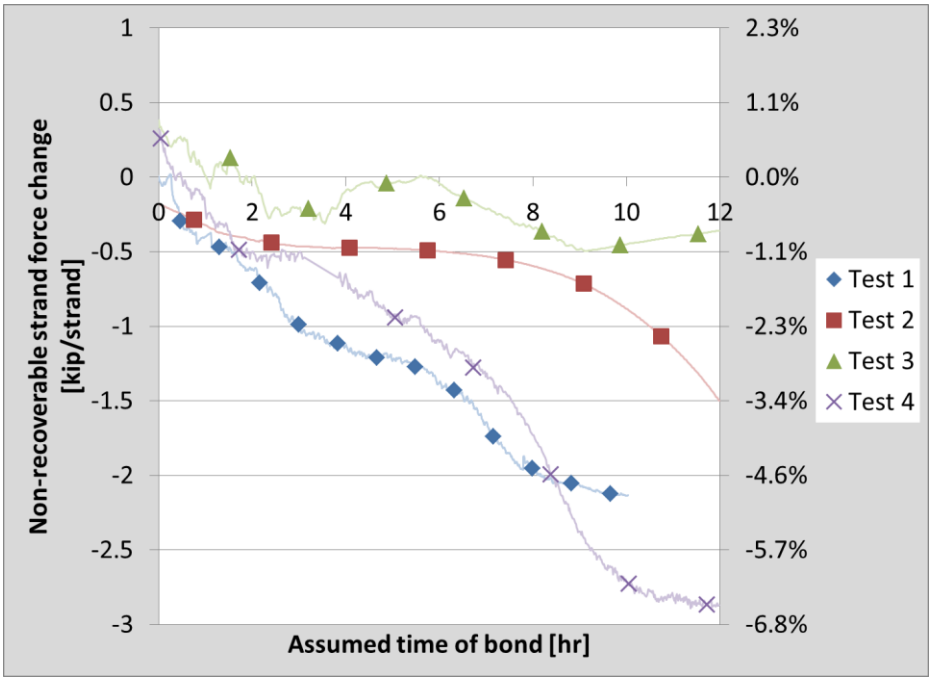

Figure 6.23: Estimated non-recoverable strand force changes for full-scale girder tests

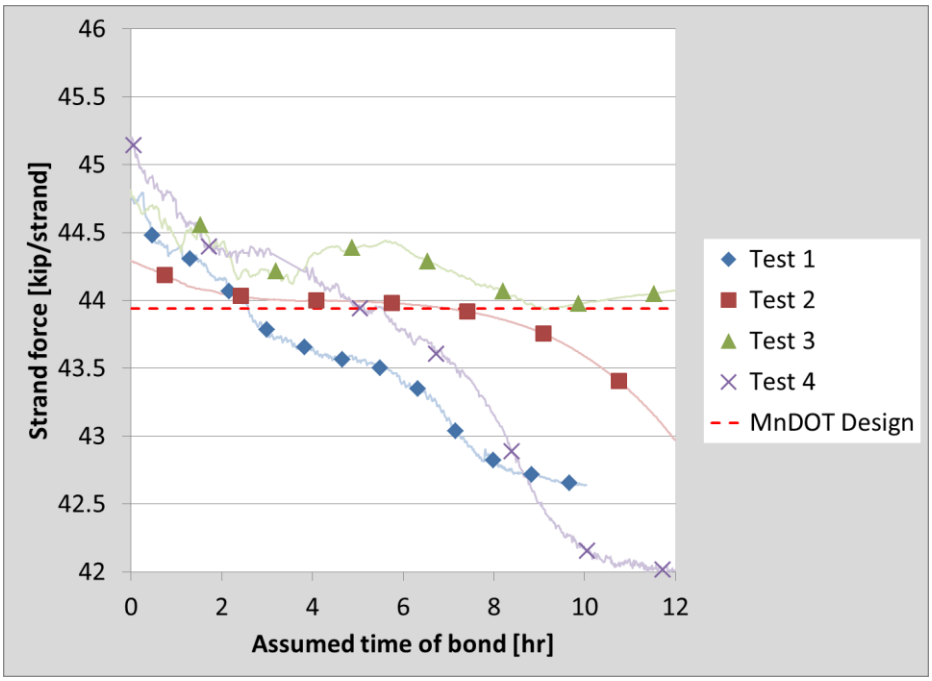

Figure 6.24: Estimated strand force at time of bond for full-scale girder tests

Figure 6.23 shows that non-recoverable strand force losses were larger during Tests 1 and 4 than during Tests 2 and 3 due to the low average strand temperature at the time of tensioning relative to the concrete temperature during hydration. Because steam heating was not used during Test 2, the estimated force changes were inversely proportional to the concrete temperature increase in the girders (see Figure 6.19); consequently, the strand force was relatively constant until decreasing rapidly after 8 hours. Ambient temperatures during Test 3 were not as low as those observed during Tests 1 and 4 and only one girder was cast on the bed, so the strand force losses were not as large. It should be noted that the temperatures used to estimate the strand force changes due to temperature with the TEA were measured on a single strand; consequently, different force losses may have occurred on other strands if the temperatures differed.

When analyzing Figure 6.24, it is important to note that the MnDOT design force line represents the "target" strand force at release. That is, the MnDOT design calculations for elastic shortening and camber assume that value for strand force, so the precasting plant attempts to adjust the strand force during tensioning such that the design force is "locked" into the girder at release. It was observed that the strand force typically

fell below the design force before the assumed time of bond, but the effective temperature adjustment by the precasting plant (i.e., the difference between the average net measured strand force and the MnDOT design force) appeared to offset the force losses due to temperature during Tests 2 and 3 relatively well. A larger amount of strand force was lost during Tests 1 and 4 due to the cold weather conditions. Ideally, the estimated forces at bond would be equal to the design force.

6.4.3 Implications on Girder Quality

6.4.3.1 Pre-release Cracking

A potential cause of cracking comes from the changes in force in the free strand during hydration. If the outside temperature decreases, the free strand force will increase, and the force change must be equilibrated by the girder. Tensile stresses may develop in the concrete that could cause cracking. In addition, after the peak temperature due to hydration has been reached, the concrete begins to cool on the precasting bed. Side forms and heat blankets retain heat relatively well, but cooling becomes more rapid when those elements are removed just before release. Shrinkage may also initiate when the concrete is exposed. Because the concrete is restrained by the hold-downs and free strand, tensile stresses can develop which may cause vertical cracks to form near the harp points prior to release.

To investigate the potential for cracking during the four full-scale tests, the concrete stresses between bond and release due to incompatibility (i.e., the difference between the coefficients of thermal expansion of steel and concrete) and free strand restraint were determined using the thermal effects analysis (TEA) under the Case A assumptions. The time of bond was assumed at the time which the Strand 1 temperature at midspan reached 100°F (37.8°C), as shown in Table 6.4. Figure 6.25 shows the estimated concrete stresses from bond to release due to temperature changes with free strand restraint for the four full-scale girder tests. The dashed horizontal line represents the tensile stress limit from ACI 318-11, as shown in Equation (6-8), which is the limit in regions away from simply-supported ends at transfer. This limit is half the value that would be expected to cause cracking. The concrete compressive strength at release was conservatively assumed as the value in the MnDOT plans of 7500 psi (51.7 MPa).

$$f_t = 3\sqrt{f'_{ci}} \tag{6-8}$$

where:

f'_{ci} Concrete compressive strength at release (psi)

f_t Concrete tensile stress limit (psi)

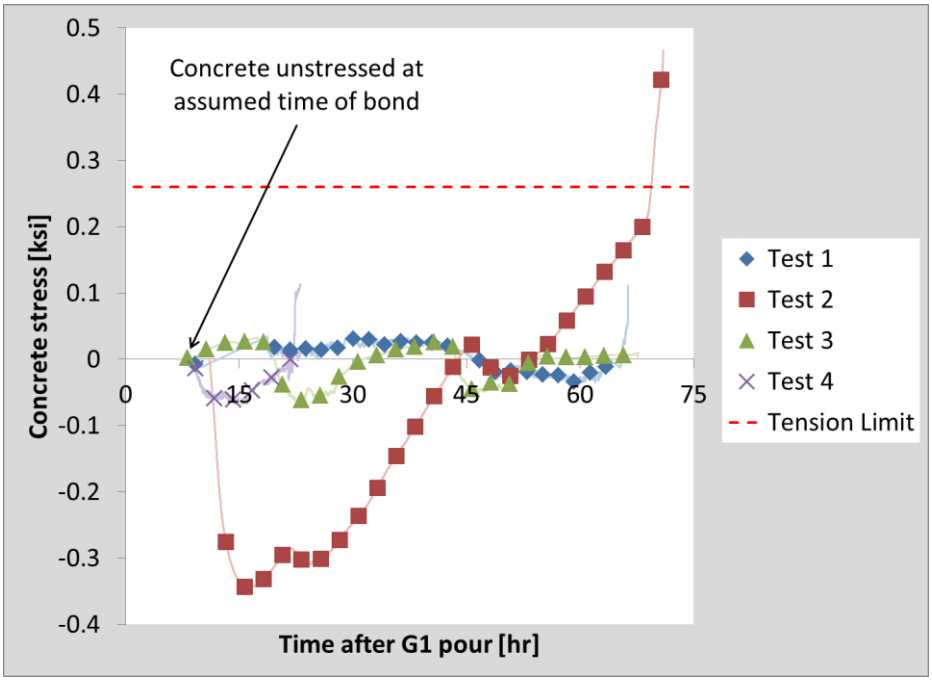

Figure 6.25: Estimated concrete stresses due to temperature changes with free strand restraint during full-scale girder tests

Based on the figure, cracking should only have been observed during Test 2. Cracks were not observed after the forms were removed, but it should be noted that the research team was not actively searching for cracks at this time. However, cracking was observed during Tests 1 and 3 near the hold-downs. Figure 6.26 shows a crack observed during Test 1. The TEA was highly dependent on the assumed time of bond and was shown to have deficiencies in estimating strand force losses between casting and bond due to the gradual hardening of the concrete, which may have affected the quality of the concrete stress estimates. However, the general behavior was reasonable, as tensile stresses increased just before release when the tarps and formwork were removed and the girders rapidly cooled. The observation of tensile concrete stress just before release was

consistent with observations made by Newhouse and Wood (2008) and Ahlborn et al. (2000).

Figure 6.26: Observed concrete cracking near hold-down just before release during Test 1

6.4.3.2 Constructability and Service Load Capacity

Non-recoverable prestress force losses due to temperature reduce the amount of compressive stress that is transferred into the concrete upon release. This can cause lower cambers and reduced service load capacity. Cambers that are lower than expected can result in constructability issues which require extension of the hooks that interact with the bridge deck, while reduced service load capacity is a serviceability concern (i.e., the concrete may crack at lower than anticipated loads).

6.5 Concrete Material Properties

Errors in estimating initial camber were found to be largely caused by poor estimations of the strand force and concrete elastic modulus (MOE) at the time of release (O'Neill, 2012). The model used to estimate the MOE can have a large impact on the accuracy of the estimation, but the concrete is subject to many other factors during fabrication that make its properties difficult to quantify. Each girder that is cast contains numerous batches of concrete, each with slight variances in mix properties that can cause

different rates of strength gain. Weather influences the potential need for steam heating on the bed, which can heat some portions of the girders more than others based on the locations of the steam outlets along the bed, which can cause variations in strength gain along the length of the girder.

Perhaps the largest influence on the modulus of elasticity of the concrete at release is the amount of time between casting and release. The precasting plant prefers short turnaround times to maintain high efficiency, so girders are released as soon as possible. The girders can be released when the concrete strength has met or exceeded the release strength, which often occurs approximately 24 hours after the concrete is poured. However, many girders are cast on a Friday, meaning the earliest they will be released is three days later on Monday, so the concrete may be stiffer than anticipated.

Recommendations have been made by previous studies to improve the quality of concrete MOE estimations in order to improve camber estimations. Concrete compressive strength and MOE data obtained from cylinder tests performed during the full-scale tests were compared to estimations made with the current and recommended methods for verification.

6.5.1 Previous Recommendations for Improving Elastic Modulus Estimation

In a previous camber study, O'Neill at al. (2012) studied historical prestressed bridge girder data to investigate the factors responsible for poor camber estimations. It was determined that one of the largest factors was the underestimation of the concrete material properties at release. Based on their findings, the following recommendations for improving the initial camber prediction were made:

1. Multiply the assumed concrete compressive strength at release, f'_{ci}, by a factor of 1.15 to account for higher concrete strengths observed in the field.
2. Replace the ACI 363 equation for estimating the concrete MOE with the Pauw (1960) (ACI 318-08, AASHTO LRFD 2010) equation.

It was concluded from the short girder tests that the Pauw (1960) estimation better predicted the concrete MOE at approximately 24 hours after casting than the ACI 363 estimation (see Section 5.3.2). This supports the second recommendation made by O'Neill et al. (2012).

6.5.2 Estimated and Measured Compressive Strengths and Elastic Moduli

The recommendations for increasing the assumed concrete compressive strength at release and substituting the Pauw (1960) MOE estimation for the ACI 363 estimation were compared to compressive strength and MOE measurements made during the full-scale girder tests. For a typical girder fabrication, three concrete cylinders are tested for compressive strength on the morning of the anticipated girder release; one each from the north and south ends and one from the middle of the bed. The concrete MOE was measured at approximately the same time on two to three cylinders from different batches.

For reference, a range of estimated concrete MOE were determined for each test based on the average measured compressive strength. The Pauw (1960) equation was used and a range of unit weights from 144-155 pcf (2306-2483 kg/m^3) was assumed. The lower bound of the unit weight range is based on the assumed unit weight in the simplification of the Pauw (1960) equation from ACI 318-11 for normalweight concrete, given by Equation (6-9):

$$E_c = 57000\sqrt{f_c'} \tag{6-9}$$

where:

E_c Concrete modulus of elasticity; psi

f'_c Concrete compressive strength; psi

Table 6.5 shows the MnDOT design values for concrete compressive strength ($f'_{ci,design}$) and MOE ($E_{ci,design}$) at release and MOE values that reflect the recommendations made by O'Neill et al. (2012). It was recommended that the ACI 363 equation should be replaced by the Pauw (1960) equation for predicting the MOE. The Pauw equation was used to estimate the MOE at release using the design compressive strength at release ($E_{ci,Pauw}$) and 1.15 times the design compressive strength at release ($E_{ci,Pauw+1.15f'ci}$). The concrete unit weight was assumed to be 155 pcf (2483 kg/m^3). The average measured compressive strengths ($f'_{ci,meas}$) and MOE ($E_{ci,meas}$) for each of the four full-scale tests are shown, as well as the range of MOE values based on measured compressive strength values described in the previous paragraph ($E_{ci,Pauw+f'ci,meas}$). Note

that Test 1 did not include testing for MOE. The ratios of the design and recommended compressive strength and MOE values relative to the measured values are shown.

Table 6.5: Concrete compressive strength and modulus of elasticity at release

Test No.	**1**	**2**	**3**	**4**
$f'_{ci,design}$ [psi]	7500			
$E_{ci,design}$* [ksi]	4464			
$E_{ci,Pauw}$** [ksi]	5515			
$E_{ci,Pauw+1.15f'ci}$$^{+}$ [ksi]	5914			
Avg. Measured				
$f'_{ci,meas}$ [psi]	9087	9858	10213	8430
$E_{ci,meas}$ [ksi]	NA	6186	5834	5153
$E_{ci,Pauw+fci,meas}$$^{++}$ [ksi]	5436-6070	5662-6323	5763-6435	5236-5847
Ratios of Measured to Predicted Values				
$f'_{ci,meas}/f'_{ci,design}$	1.21	1.31	1.36	1.12
$E_{ci,meas}/E_{ci,design}$	NA	1.39	1.31	1.15
$E_{ci,meas}/E_{ci,Pauw}$	NA	1.12	1.06	0.93
$E_{ci,meas}/E_{ci,Pauw+1.15f'ci}$	NA	1.05	0.99	0.87

*Calculated with ACI 363 equation

**Calculated with Pauw (1960) equation with design f'_{ci} and w_c = 155 pcf

$^{+}$Calculated with Pauw (1960) equation with 1.15 times design f'_{ci} and w_c = 155 pcf

$^{++}$Calculated with Pauw (1960) equation with measured f'_{ci} and w_c = 144-155 pcf

Currently, MnDOT assumes an initial concrete compressive strength of 7500 psi (51.7 MPa) and estimates the MOE with the ACI 363 model given in Equation (5-2). When the second recommendation (i.e., replace ACI 363 with Pauw (1960) MOE estimation) was implemented alone, the design MOE at release was 5515 ksi (38.0 GPa), as opposed to 4464 ksi (30.8 GPa) estimated by the ACI 363 equation. When both recommendations were implemented, the MOE increased to 5914 ksi (40.8 GPa). A unit weight of concrete of 155 pcf (2483 kg/m^3) was assumed in the Pauw (1960) equation, as it is the value assumed by MnDOT in calculating the self-weight of the girder and the

value assumed by O'Neill et al. (2012). This unit weight is typically used as a simplification for the weight of concrete with embedded steel, so it may be larger than the actual concrete unit weight.

The average measured concrete compressive strengths for the four full-scale tests ranged from 8430 to 10213 psi (58.1 to 70.4 MPa), with all values being larger than the specified release strength of 7500 psi (51.7 MPa). The average measured compressive strengths ranged from 12 to 36% higher than the specified release strength, compared to an average of 15% observed by O'Neill et al. (2012). Tests 1 and 4, during which lower compressive strengths were measured, were the coldest fabrications monitored, which may have lowered the rate of concrete hydration. Additionally, Test 4 was the only fabrication without a curing period that extended over a weekend, so the concrete was two days younger at release than the other tests. For Tests 2 and 3, implementing both recommendations resulted in average measured MOE values within 5% of the predicted value. However, Test 4 produced lower MOE values than predicted because of the short curing time and low temperatures. The data in Table 6.5 show that the recommendations made by O'Neill et al. (2012) sufficiently increase the predicted MOE at release to better represent the values typically observed in the field.

6.6 Girder Strain Distribution after Release

The precasting plant cuts the strands when the concrete compressive strength has met or exceeded the minimum required release strength. This can occur less than 24 hours after the girders are cast due to the high rate of hydration that is achieved from a combination of the concrete mix properties and steam heating. Just before release, the blankets covering the girders and free strand are removed, followed by the formwork. The detensioning crew then places one worker at each end of the girder(s) and one worker between the girders, if multiple girders are present. Each worker is equipped with a torch and a diagram detailing the order in which the strands will be cut. The workers will cut the same group of strands simultaneously and pause between groups to ensure that the other workers are ready to begin cutting the next strand group.

Figures 6.27 through 6.30 show the girder strain distributions after release for full-scale Tests 1 through 4, respectively. The strain changes measured by foil strain

gages, concrete strain gages, and vibrating wire strain gages (VWGs) from the time detensioning began to times shortly after detensioning was completed are plotted with respect to the vertical location of the instrument in the girder section. Multiple points in time were plotted, measured in hours from the time detensioning was finished, to investigate the effects of cooling on girder strains. Both Girders 1 and 2 were analyzed for Tests 1 and 2 because concrete strain gages were placed through the cross sections of both girders. Test 3 involved the casting of a single girder on the bed and time only allowed Girder 1 to be instrumented with concrete strain gages during Test 4, so the strain distributions in Figures 6.29 and 6.30 only include measurements from one girder. VWGs were not used in Test 1. Error bars representing 50 microstrain are included on some of the measured data series for visual reference.

For each test, the thermal effects analysis (TEA) was used to estimate the strain changes at release through the height of the girder section with measured temperatures, measured concrete modulus of elasticity values, and net average measured strand forces. The data series "TEA (ES)" represents the estimated strain change due only to strand force transfer into the concrete upon release (i.e., elastic shortening), as determined by Equation (3-18). The data series "TEA (ES,restr.)" represents estimated instrument strain, ε_{instr}, as determined by Equation (3-19), which considers forces generated due to the removal of the free strand restraint at release.

The TEA assumes that stress transfer from the steel to the concrete occurs instantaneously at the time that detensioning begins; however, detensioning can take up to an hour, so some girder cooling occurs during the process. Because the coefficient of thermal expansion of concrete is typically lower than that of steel, cooling will cause compressive stresses in the concrete unrestrained by the free strand. The effects of cooling on the strain distributions through the depth of the sections during detensioning were found to be negligible and are not included in the figures.

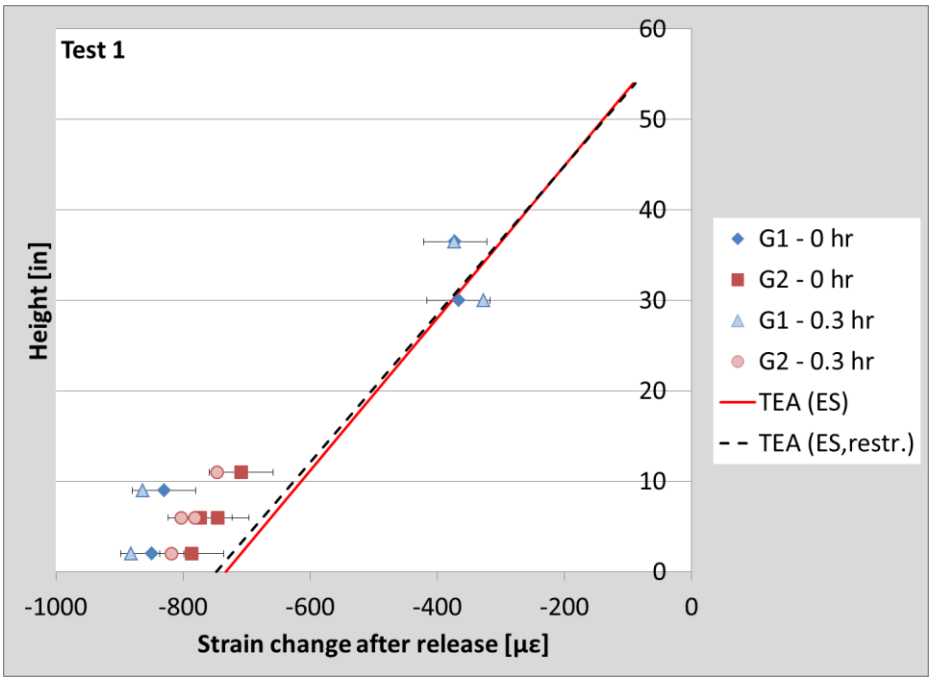

Figure 6.27: Strain distributions after release for Test 1

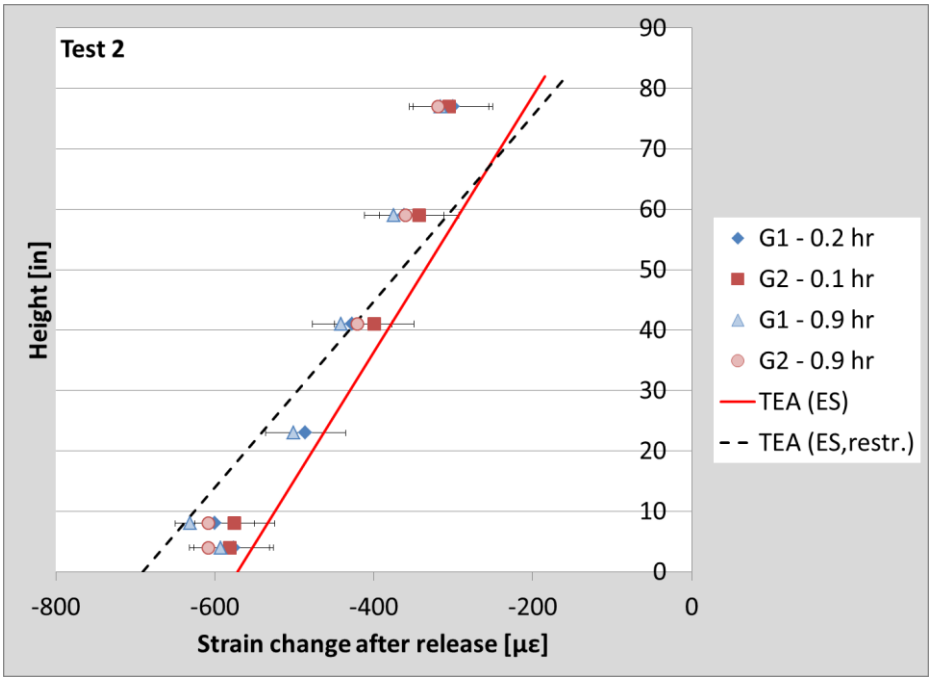

Figure 6.28: Strain distributions after release for Test 2

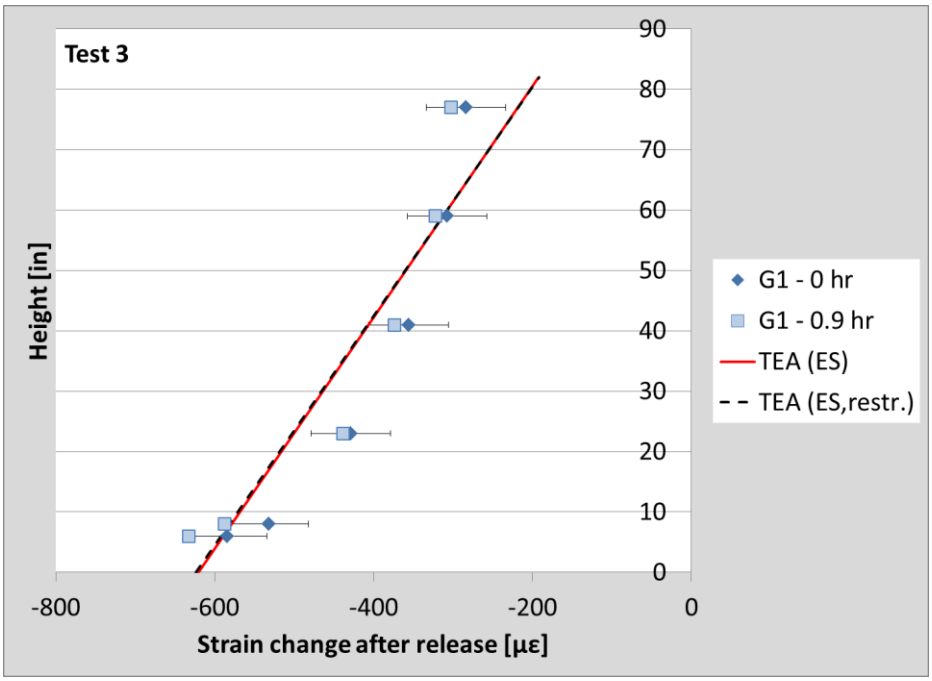

Figure 6.29: Strain distributions after release for Test 3

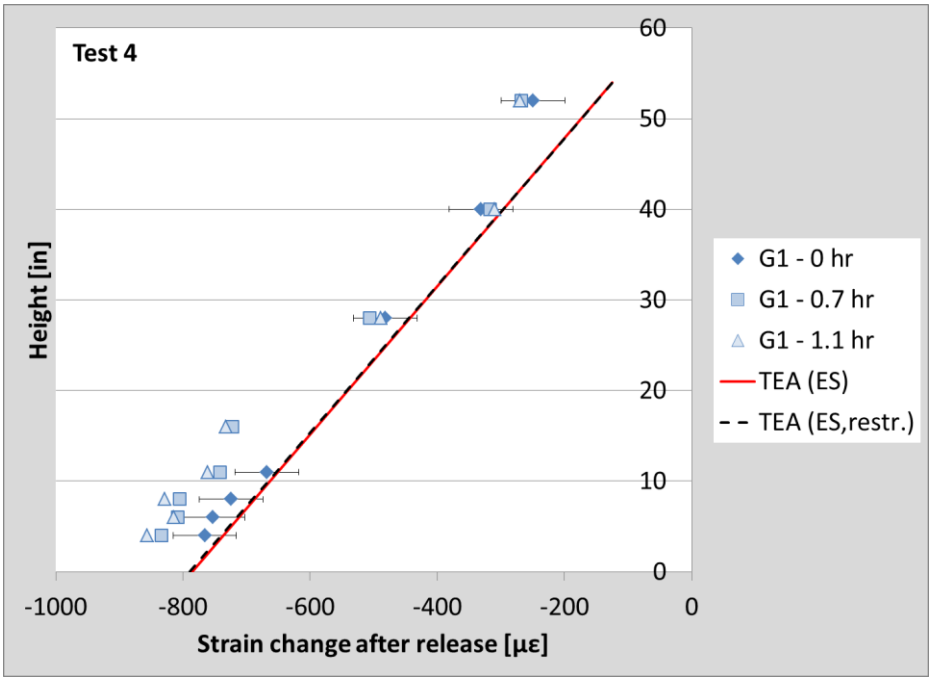

Figure 6.30: Strain distributions after release for Test 4

The TEA reasonably estimated the strain distributions after release for the four full-scale tests. The effects of free strand restraint on the estimated strains were negligible

for all tests except Test 2. Table 6.6 shows the average free strand and concrete temperatures assumed at bond and release on Strand 1 during each full-scale girder test, and it can be seen that the largest decrease in concrete temperature between bond and release occurred during Test 2. The bed occupancy was also high during Test 2. Consequently, the relatively large temperature drop after the formwork was removed affected almost the entire length of the bed, causing total girder length to reduce and the mechanical strain in the relatively short length of free strand to significantly increase.

Table 6.6: Average free strand and concrete temperatures at bond and release on Strand 1 during full-scale girder tests

Test No.	**1**	**2**	**3**	**4**
Assumed Time of Bond* [hr]	8.2	11.1	6.9	8.0
Bond				
Average Free Strand Temp. [°F]	41°F	85°F	57°F	80°F
Average Concrete Temp. [°F]	116°F	97°F	96°F	108°F
Release				
Average Free Strand Temp. [°F]	27°F	66°F	53°F	44°F
Average Concrete Temp. [°F]	115°F	79°F	99°F	127°F

*Assumed time of bond when concrete temperature at midspan on Strand 1 reached 100°F

In almost all cases, the measured compressive strains increased with time. The instruments near the bottom of the section experienced larger increases in compressive strain than those near the top. This indicated that girder cooling caused additional compressive stresses and curvature to develop in the concrete due to incompatibility stresses that developed due to the difference between the concrete and steel coefficients of thermal expansion. In the TEA, it is assumed that the coefficient of thermal expansion of the steel is greater than that of the concrete, so the steel would like to contract more than the concrete upon cooling. Because strain compatibility must exist between the two materials at the center of gravity of the steel, the concrete resists the contraction of the steel and induces additional tension in the strands and compression in the concrete. The behavior of the measured strain readings was consistent with the assumptions, but the magnitudes of the measured strain changes due to incompatibility were much larger than the estimated values, which were negligible.

In some cases, the measured strain distribution was slightly nonlinear. This was consistent with strain distributions observed by Barr et al. (2000), which the authors believed was caused by stress concentrations due to lifting the girder ends during release. However, the girders were not lifted during the full-scale girder tests performed in this study, so the behavior was likely due to another factor, such as compatibility stresses developed due to a nonlinear thermal gradient through the depth of the section. Figure 6.31 shows measured temperatures through the Girder 1 section at midspan during detensioning for Test 3. The figure indicates that the temperature decreases more rapidly in the web than in the centers of the flanges. The web wants to contract more than the flanges, but the flanges resist the movement, causing less compression to develop in the web. This is most clearly demonstrated in Figure 6.29. The TEA used to estimate the strain distributions does not consider stresses caused by thermal gradients through the height of the girder sections.

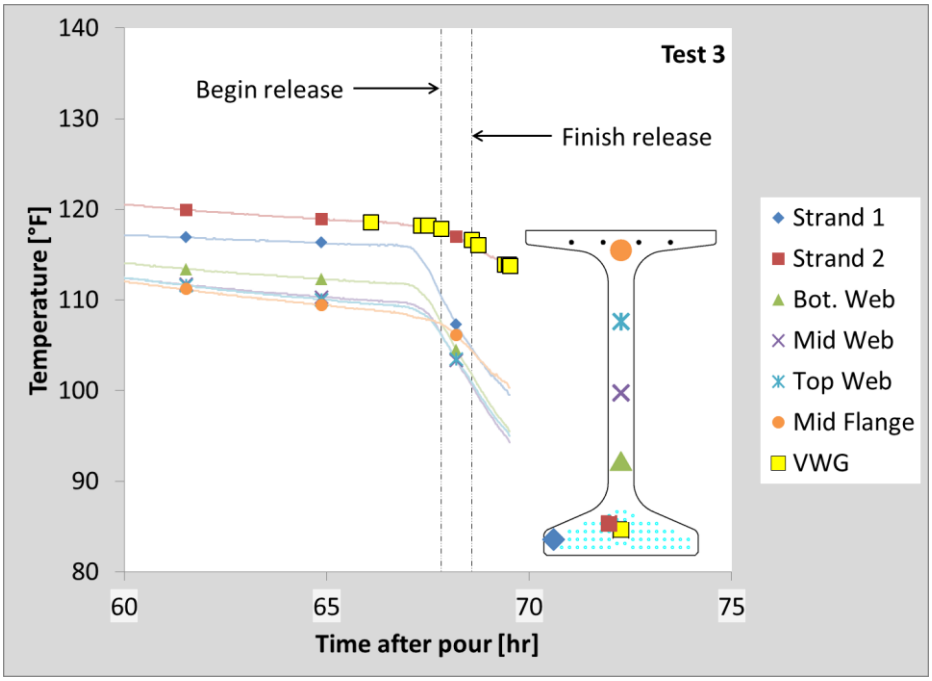

Figure 6.31: Temperature distribution through Girder 1 section at midspan during Test 3 release

6.6.1 Shrinkage and Creep

Shrinkage and creep were also investigated as potential causes for the appearance of increasing compressive strains observed while the girders were cooling on the bed. Strain gages capture not only mechanical strains, they also capture strains due to time-dependent effects such as creep and shrinkage. To estimate the effects of shrinkage and creep, equations found in the AASHTO LRFD Bridge Design Specifications 5th Edition (2010) were used. The results from Test 4 were used as a sample case for the calculations.

6.6.1.1 Shrinkage

The predicted shrinkage strain in the girder was given by Equation (6-10):

$$\varepsilon_{sh} = k_s k_{hs} k_f k_{td} * 0.48 * 10^{-3} \quad (6\text{-}10)$$

where:

k_f	Factor for the effect of concrete strength
k_{hs}	Humidity factor for shrinkage
k_s	Factor for the effect of the volume-to-surface ratio of the girder
k_{td}	Time development factor

The factors for calculating the shrinkage strain were determined by Equations (6-11) through (6-15). The volume-to-surface ratio was given by Equation (6-11):

$$V/S = \frac{A_g L_g}{d_{per} L_g} = \frac{A_g}{d_{per}} = \frac{749 in^2}{201 in.} = 3.7 in. \quad (6\text{-}11)$$

where:

A_g	Gross area of concrete girder section
d_{per}	Perimeter of girder section
L_g	Length of girder from end to end
V/S	Volume to surface ratio in inches

The factor for the effect of volume-to-surface ratio of the girder was given by Equation (6-12):

$$\begin{aligned} k_s &= 1.45 - 0.13(V/S) \geq 1.0 \\ &= 0.97 < 1.0 \\ k_s &= 1.0 \end{aligned} \quad (6\text{-}12)$$

The factor for the effect of concrete strength was given by Equation (6-13). The concrete compressive strength at release was taken as the average measured cylinder strength taken just before release.

$$k_f = \frac{5}{1 + f'_{ci}} = \frac{5}{1 + 5.15ksi} = 0.53 \quad (6\text{-}13)$$

where:

f'_{ci} Concrete compressive strength at release

The humidity factor was given by Equation (6-14). The relative humidity was taken as 91% on the day of release (12/10/2014) based on online weather archives from Weather Underground (wunderground.com).

$$k_{hs} = 2.0 - 0.014H = 0.73 \quad (6\text{-}14)$$

where:

H Relative humidity in percentage (%)

The time development factor was given by Equation (6-15). For shrinkage calculations, the age of the concrete is measured from the end of curing. It was assumed that the end of curing was when peak hydration temperature was reached at approximately 12 hours after casting. Typically, the end of curing would be assumed at the time at which the girders are uncovered just before release, but assuming an earlier time results in conservative estimates of the shrinkage strains.

$$k_{td} = \frac{t}{61 - 4f'_{ci} + t} \quad (6\text{-}15)$$

where:

t Maturity of the concrete in days, defined as the age of the concrete from the end of curing

Table 6.7 shows the estimated shrinkage strain for the MN54 girders monitored during full-scale Test 4 at different times. The magnitude of the shrinkage strain is small until 5 days after curing had completed, so it is unlikely that shrinkage had an effect on the girder strains just after release.

Table 6.7: Estimated shrinkage strains over time for Test 4 girders

Time after Release [day]	Shrinkage Strain [με]
0	3.3
1/24	3.6
1	9.6
5	31.0
10	51.4
28	94.4

6.6.1.2 Creep

The creep coefficient was given by Equation (6-16). The factors for the effects of the volume-to-surface ratio and concrete strength were identical to those used to estimate shrinkage. Equation (6-15) was used to determine the time development factor for creep, but concrete age was defined from the time of loading for creep rather than from the end of curing for shrinkage. The age of the concrete at the time of loading, t_i, was taken as the time between the peak hydration temperature of the concrete and the time of release (approximately 0.5 days).

$$\Psi(t, t_i) = 1.9 k_s k_{hc} k_f k_{td} t_i^{-0.118} \quad (6\text{-}16)$$

where:

k_f	Factor for the effect of concrete strength
k_{hc}	Humidity factor for creep
k_s	Factor for the effect of the volume-to-surface ratio of the girder
k_{td}	Time development factor
t	Maturity of the concrete in days, defined as the age of the concrete from the time of loading
t_i	Age of concrete at time of loading in days

The humidity factor for creep was given by Equation (6-17):

$$k_{hc} = 1.56 - 0.008H = 0.83 \quad (6\text{-}17)$$

The estimated axial creep strain at the center of gravity of the strands (*cgs*) was determined by multiplying the creep coefficient at a given time with the strain change due to elastic shortening from Section 3.3.3.3, as given by Equation (6-18). The effects of temperature were not considered.

$$\varepsilon_{cr} = \Delta\varepsilon_{ES}(y_{cgs})\Psi(t, t_i) \quad (6\text{-}18)$$

where:

$\Delta\varepsilon_{ES}(y_{cgs})$ Concrete strain change at midspan due to elastic shortening at the center of gravity of the strands from Equation (3-18)

Table 6.8 shows the estimated creep strain for the MN54 girders monitored during full-scale Test 4 at different times. Like the shrinkage strain, the creep strain within one day of release was small. However, the combined magnitudes of the shrinkage and creep strains at one day after release account for approximately 50% of the compressive strain increase observed in Figure 6.30 at the midspan *cgs* of the girders that occurred over the course of approximately one hour. It is possible that the estimations for creep and shrinkage are not accurate for such short time intervals and the observed strain changes reflect the "real" effects of creep and shrinkage.

Table 6.8: Estimated creep strains over time for Test 4 girders

Time after Release [day]	Creep Strain [με]
0	0
1/24	1.0
1	23.1
5	101.1
10	175.0
28	330.5

6.7 Release Camber

Knowledge of the strand force is important for predicting the camber upon releasing the girders on the prestressing bed. The initial camber is estimated in the planning phase of girder fabrication, and the estimated initial camber is used to estimate the camber at the time of bridge erection. The camber at erection is based on the multiplication of the initial camber by factors associated with time-dependent effects (i.e., creep and shrinkage). Any error made in estimating the initial camber is therefore amplified when estimating the camber at erection. Comparisons of measured to predicted camber values were made to validate the thermal effects analysis performed for each test.

Factors that affect the initial camber and the ability to accurately predict it are discussed. Finally, the current and recommended camber estimations are compared to the measured values and those estimated using the thermal effects analysis.

6.7.1 Estimated and Measured Release Cambers

During the full-scale tests, camber measurements were made just after cutting the strands was complete. Camber was measured at midspan of each girder with a tape measure, so the accuracy of the measurements was considered to be within approximately 1/8 in. (3 mm). Just before release, concrete cylinders were tested for compressive strength and modulus of elasticity (MOE). The average measured MOE values, along with strand forces determined from net elongation measurements, were used to estimate the camber at release. The estimations were compared to the measured release cambers.

To investigate the effects of non-recoverable strand force losses on release camber, two estimations were compared: the first ignoring non-recoverable strand force losses due to temperature changes between tensioning and bond ("No Temp Effects"), and the second, considering them using the thermal effects analysis ("TEA"). The same mechanical theory was used to calculate camber for both cases (i.e., assuming changing transformed section properties and integrating curvature along the girder length) and the same concrete MOE at release and initial strand force were assumed. The difference between the two estimations shows the effects of temperature on camber (i.e., non-recoverable prestress force losses due to bonding at a higher temperature and deformations due to incompatibility between the coefficients of thermal expansion between the steel and concrete in the case of the TEA). The release camber estimated with the TEA including the non-recoverable force losses was expected to most closely match the measured release camber.

For the TEA, the time of bond was assumed to be the time at which the concrete temperature on Strand 1 at midspan of Girder 1 reached 100°F (37.8°C) for each full-scale test (see Table 6.4). It should be noted that although the change in deflection due to incompatibility forces between bond and release (see Section 3.3.4.3) were considered in the TEA, they were found to be negligible. Because the concrete MOE was not measured during Test 1, the Pauw (1960) model was used with measured compressive strength

values and a concrete unit weight of 152 pcf (2435 kg/m^3). The assumed unit weight was based on concrete unit weights measured during the short girder tests (see Section 5.3.2).

Table 6.9 shows the measured concrete compressive strength and MOE at release and the initial strand force for each full-scale test. Figure 6.32 shows the estimated cambers compared to the measured camber for each full-scale test.

Table 6.9: Measured concrete compressive strength and modulus of elasticity at release and initial strand force for full-scale tests

Test No.	1	2	3	4
f'_{ci} [psi]	9087	9858	10213	8430
E_{ci} [ksi]	5895**	6186	5834	5153
P_i* [kip/strand]	44.8	44.5	44.4	44.9

*Average strand force from measured net elongations (see Table 6.3)
**Modulus of elasticity measurements not taken during Test 1, so MOE was calculated with Pauw (1960) equation with measured f'_{ci} and w_c = 152 pcf

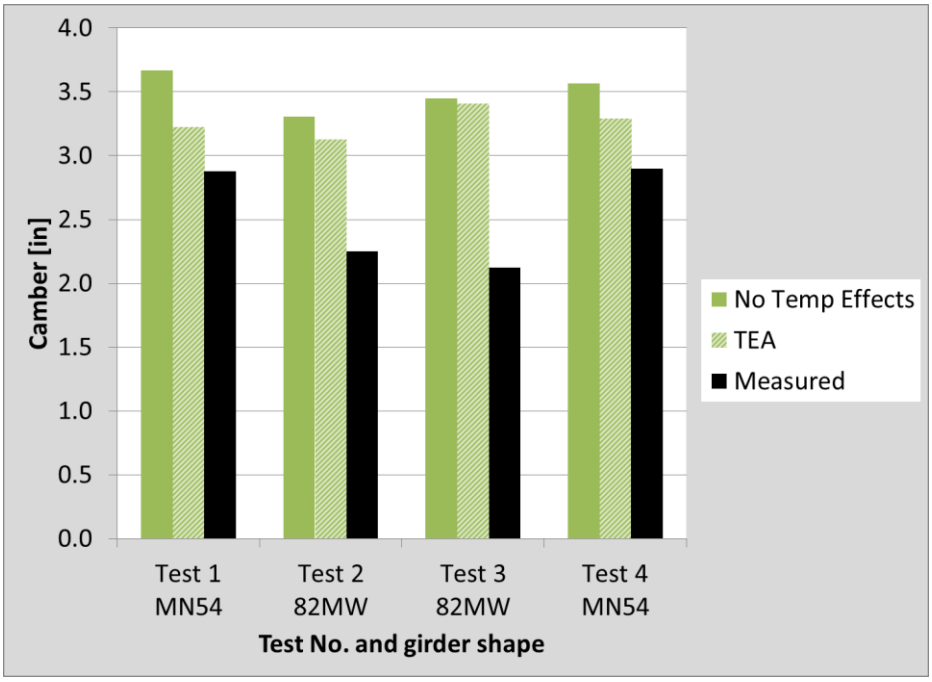

Figure 6.32: Estimated and measured cambers at release for full-scale tests

From the figure, it is clear that the measured cambers were consistently lower than the estimated cambers. It was expected that the TEA would more accurately estimate

the release camber because the effects of temperature were considered using measured temperature data. Other factors that may contribute to the remaining discrepancies between the estimated and measured cambers are discussed in the next section.

6.7.2 Factors Affecting Initial Camber

Results from the full-scale girder tests showed that the thermal effects analysis overestimated the measured initial camber values in all cases. Multiple factors were not considered in the thermal effects analysis that could affect the camber in the field and are described in this section.

6.7.2.1 Concrete Modulus of Elasticity

Because it is highly dependent on the concrete modulus of elasticity, inaccurate assumptions regarding the material stiffness may have a large impact on estimated cambers. Up to 30 batches of concrete are poured over the course of multiple hours during fabrication, so the material properties may vary by batch and, therefore, along the length of the precasting bed. When measuring the modulus of elasticity in the field, only a small sample of concrete was tested, so the likelihood that the average measured elastic modulus was representative of the entire bed was difficult to quantify. If the concrete within the girders was, on average, stiffer than the measured values, the camber would be lower than expected. However, it is could have been just as likely that the concrete was less stiff.

The average measured concrete modulus of elasticity (MOE) at release was used to estimate the camber with the thermal effects analysis (TEA) for each full-scale girder test. As an example, the difference in estimated camber was determined when using the maximum measured MOE in the TEA for Test 2 (i.e., 82MW girder shape) and Test 4 (i.e., MN54 girder shape), as shown in Table 6.10. The potential reductions in camber when using the maximum measured MOE at release were relatively small for both tests, so the likelihood that this effect contributed significantly to the discrepancies between the estimated and measured cambers is low.

Table 6.10: Differences in estimated cambers using average and maximum measured concrete modulus of elasticity

Test No.	2	4
Girder Shape	82MW	MN54
Avg. Measured MOE [ksi]	6186	5153
Max. Measured MOE [ksi]	6559	5305
Difference in Est. Camber [in]	-0.15	-0.08

6.7.2.2 Strand Force

Inaccuracies in the assumed strand force could affect the camber estimation. The measured strand force has potential for error in the accuracies of the elongation measurements, assumed preload forces, and potential abutment movement losses that occurred after measurements were recorded. Also, strand force changes due to temperature at the time of bond may vary among strands. This is due to the fact that the thermal effects analysis (TEA) only considered temperatures along the bed on one strand. Other strands may experience different temperature changes, which are not considered in the analysis.

To determine the initial strand force, net elongation measurements, taken by the precasting plant during tensioning, were converted to forces. The net elongation measurements take into account the losses due to seating of each strand as the hydraulic jack is released, but additional losses may occur due to dead end slippage and abutment movement. As the strand is tensioned, the strand may slip in the chuck at the dead end as the strand diameter decreases (Briere et al., 2013) and the wedge tightens around the strand. This effect causes the strand elongation to appear larger than the corresponding strand force, resulting in an overestimation of the strand force when converting the elongations.

Abutment movement affects the strand group as a whole. As the strands are tensioned, the abutment increasingly deflects due to the total strand force. Strands that are tensioned early in the process lose elongation and, therefore, force. This effect is not captured in the net elongation measurements because they are taken on a per strand basis immediately after the strand was tensioned.

Table 6.11 shows the assumed dead end slip and abutment movement losses for each precasting bed. The values with units of length were originally presented in Table 6.2. The changes in force resulting from the assumed values are shown. Note that the force change due to abutment movement is considered in an average sense, assuming zero deflection at the bottom of the abutment and the full assumed abutment movement value at the top layer of strands. Consequently, the average effect of abutment movement was taken as one-half of the assumed value. Finally, the reduction in camber as a result in the force loss was determined for each full-scale test. From the table, it is clear that the reduction in camber associated with dead end slip and abutment movement was insignificant.

Table 6.11: Potential reductions in strand force and camber due to abutment movement and dead end slippage

Test No.	**1**	**2**	**3**	**4**
Bed No.	6	7	7	7
Plant Adjustments				
Dead End Slip, SD [in]	0.125			
Abutment Movement, AM [in]	0.375	0.25		
Potential Loss in Net Average Measured Force due to:				
Dead End Slip, SD [kip]	0.18	0.17	0.17	0.17
Abutment Movement, AM* [kip]	0.27	0.17	0.17	0.17
Total [kip]	0.45	0.33	0.33	0.33
Potential Reduction in Camber due to:				
Total Potential Force Loss [in]	0.05	0.06	0.06	0.04

*Taken as the average abutment movement loss over the total number of strands, or 0.5AM

The TEA performed to estimate the force changes in the strands during girder fabrication assumes that the strand force is constant along the length of the bed before bond occurs because the strand is not restrained except by the dead and live end abutments. Load cells were attached to the dead and live end of the same strand during three of the four full-scale tests to monitor the force changes over time. If the assumption was reasonable, the load cells should read very similar forces at the time of bond. Figure

6.33 shows the difference in load cell readings for each full-scale test, taken as the live end load cell reading minus the dead end reading. The differences at 10 hours are significantly larger than those at 6 hours in all cases, meaning the strands have been restrained by concrete-steel bond at some point during that time period, if not before. As shown in Figure 6.17, Test 3 shows a significant difference in load cell readings even at 6 hours, which indicates that the concrete provides some restraint even before it has fully hardened.

In calculating camber, it is assumed that the strand force is constant along the length of the girder, so symmetry can be assumed to find the midspan deflection. However, Figure 6.33 shows that the force may change by up to 2.5 kips (11.1 kN) along the length of the girder. Because this effect may be caused by the gradual hardening of the concrete, the strand force differences "locked" into the girders could be different along the length of the girder.

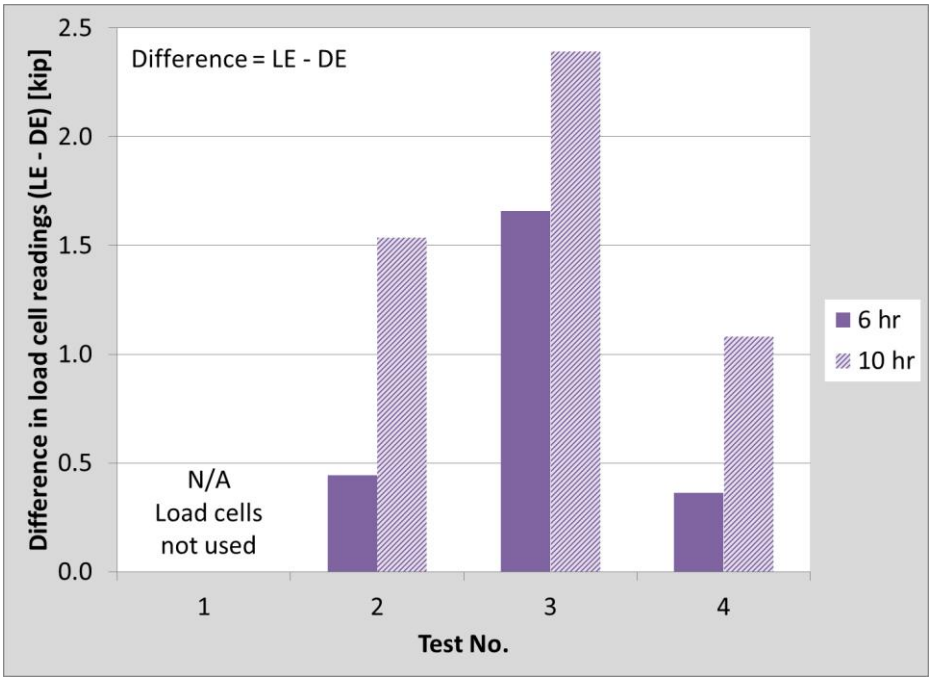

Figure 6.33: Differences in dead and live end load cell readings at assumed times of bond (6 and 10 hours after casting) during full-scale girder tests

6.7.2.3 Bed Friction

Friction between the girder and the precasting bed was neglected in the thermal effects analysis, but it could restrict the girder ends from sliding on the bed as the strands

are cut, which would reduce the initial camber. A short study was performed to determine the potential effect of friction on initial camber. The coefficient of static friction, μ, of a concrete-steel interface was assumed to range from 0.57 to 0.70 (Rabbat and Russell, 1985). Both the MN54 and 82MW girder shapes were instrumented during the full-scale girder tests, so both shapes were considered in the study. It was assumed that the friction force was equal to the total girder weight associated with the end reaction ($0.5\ W_{total}$) multiplied by the friction coefficient and acted as a tensile point force on the bottom fiber of the girder. The downward deflection due to the eccentricity of the force was determined by assuming the force acted on the transformed section.

For MN54 shape with concrete unit weight, w_c = 155 pcf:

- Girder self-weight distributed load, w_{sw} = 0.07 k/in.
- Length of girder, L = 1508 in.
- Total girder weight, W_{total} = 101.3 kip
- Friction force, $P_{friction}$ ($\mu * 0.5 W_{total}$) = 28.9 to 35.5 kip
- Downward deflection at midspan: 0.13 to 0.15 in.

For 82MW shape with w_c = 155 pcf:

- Girder self-weight distributed load, w_{sw} = 0.10 k/in.
- Length of girder, L = 2169 in.
- Total girder weight, W_{total} = 206.6 kip
- Friction force, $P_{friction}$ ($\mu * 0.5 W_{total}$) = 58.9 to 72.3 kip
- Downward deflection at midspan: 0.21 to 0.25 in.

Based on the calculations above, the friction between the girder and the precasting bed could significantly decrease the initial camber. In an attempt to measure the effects of friction, camber was measured before and after a "lift-set," during which the precasting plant used cranes to lift one end of the girder and set it back down, relieving the friction forces between the girder and bed. However, depending on the location at which the girder was lifted (i.e., lift hooks), the boundary conditions may have changed in the transition from being supported by the bed (i.e., simply-supported) to being supported by the crane (i.e., girder end overhang). This could induce friction in the opposite direction upon setting the girder back down, which would exaggerate the effects of the initial

friction forces. After lift-set during the full-scale tests, no more than a 1/8 in. (3 mm) increase in camber was observed, so the effects of friction appeared to be small.

6.7.2.4 Thermal Gradient

At the time of bond, the concrete in the girder is assumed to have zero stress. A thermal gradient can form if the temperature does not change uniformly through the depth of the section. The thermal gradient can cause mechanical stresses in the section required to achieve compatibility, additional curvature and, therefore, camber. Figure 6.34 and Figure 6.35 show how the temperature varied through the depth of Girders 1 and 2, respectively, at midspan changed between the times of bond and release, which was approximately 24 hours after casting for full-scale girder Test 4. Data points missing through at particular depths were associated with faulty gages. The temperature gradient at the time of release is a function of the temperature profile at the time of bond. It can be seen that there is a large temperature range that falls within the assumption that bond occurred between 6 and 10 hours after casting. In either case, the girder appears to cool more quickly at the top of the section, so the change in curvature due to the thermal gradient would cause the girder to deflect downward.

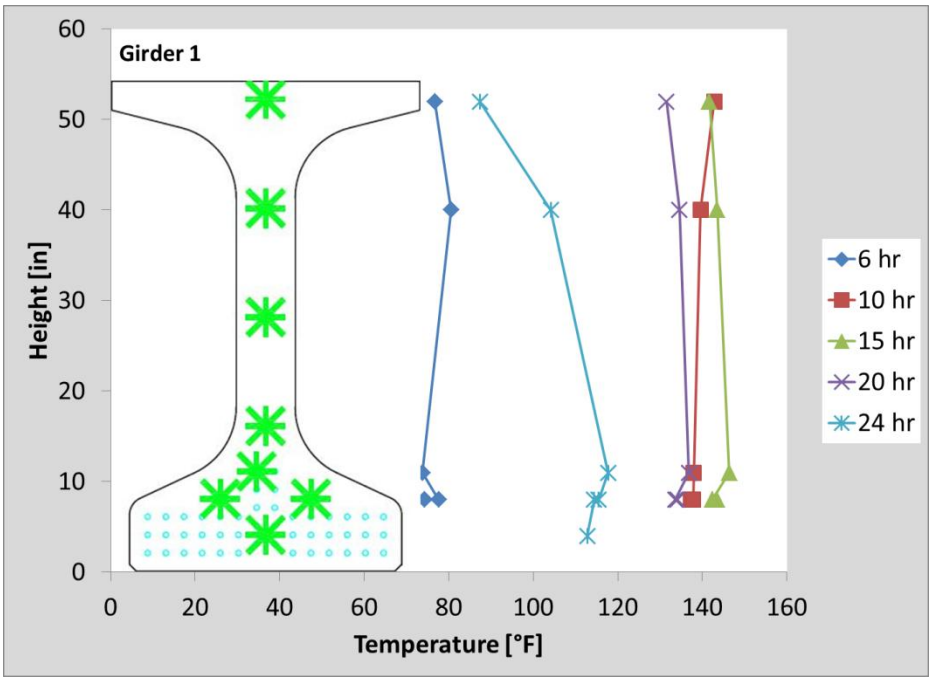

Figure 6.34: Temperature through Girder 1 section at midspan at various time steps during Test 4 fabrication

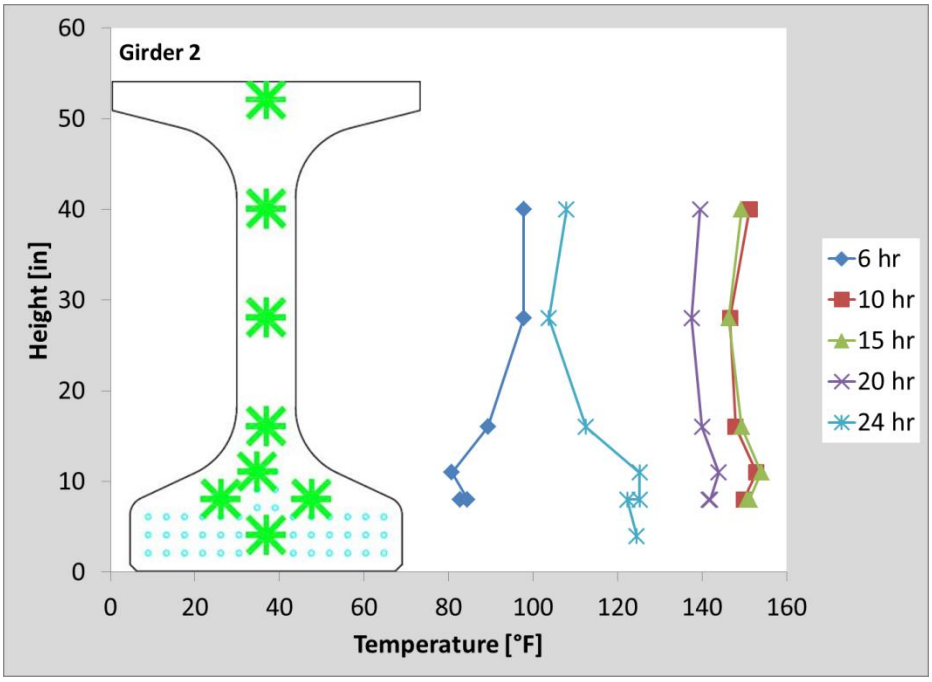

Figure 6.35: Temperature through Girder 2 section at midspan at various time steps during Test 4 fabrication

To determine the effects of the thermal gradient on camber, temperature changes through the girder sections from bond to release were analyzed to determine the curvature induced by the thermal gradient, as given by Equation (6-19) derived by Barr et al. (2005). In the equation, positive curvature is defined in the same sense as is positive moment. That is, positive curvature corresponds to downward deflection.

$$\phi_0 = \frac{\sum_i \alpha_i E_i \int \Delta T(y) y dA_i}{\sum_i E_i I_i} \tag{6-19}$$

where:

A_i	Cross-sectional area of material *i*
E_i	Modulus of elasticity of material *i*
I_i	Moment of inertia of material *i* about the composite centroid
y	Vertical coordinate measured downward from composite centroid
α_i	Coefficient of thermal expansion of material *i*
$\Delta T(y)$	Change in temperature at height *y* relative to temperature at the time of bond
ϕ_0	Curvature induced by thermal gradient

For each full-scale test, the girder cross section was divided into sections based on the locations of thermocouples through the height. The temperature in each section at a given point in time was assumed to be uniform. For each division of the girder area, the concrete and steel were considered separately and the net sectional properties of each material about the composite centroid of the entire girder section were determined.

The deflection induced by the thermal gradient was determined by integrating the curvatures along the length of the simply-supported girder. Because the temperature through the depth of the section was only monitored at midspan, the curvature was assumed to be constant along the length of the girder. Equation (6-20) gives the deflection based on those assumptions:

$$\delta = \frac{\phi_0 L_g^2}{8} \tag{6-20}$$

where:

L_g	Length of girder from end to end
δ	Midspan deflection due to thermal gradient

The assumed time of bond significantly affects the potential effects of thermal gradient on deflection just after release. Figure 6.36 shows the estimated deflections due

to the difference in temperature between bond and release for each full-scale girder test assuming times of bond ranging from 6 to 12 hours after casting to account for the later time at which it was believed the strand in Test 2 bonded (approximately 11 hours after casting). Test 1 was omitted due to lack of data through the depth of the girder sections. The direction of the deflections in the figure correspond to the convention used when describing girder camber (i.e., positive upward).

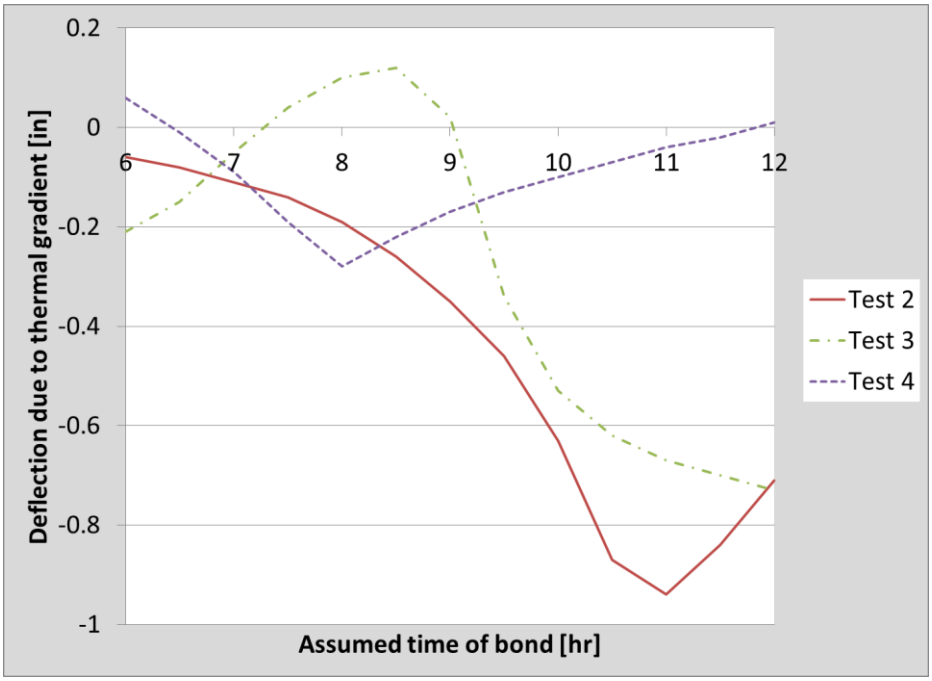

Figure 6.36: Estimated deflections due to thermal gradient between bond and release for full-scale tests

It is clear that the estimated deflection depends greatly on the assumed time of bond (i.e., when the concrete is assumed to have hardened and have zero stress). However, within the assumed time of bond range, the estimated deflections indicate that much of the difference in estimated and measured camber at release for each full-scale test could be accounted for by considering the effects of the thermal gradient. It should be noted that the estimated deflections due to thermal gradients in the figure were determined with many underlying assumptions that were made due to lack of data. The calculations were based on no more than seven thermocouples through the section and the curvature due to the thermal gradient was assumed constant along the girder length.

6.7.2.5 Summary

Multiple factors that could account for differences between estimated and measured release cambers were discussed in the previous subsections, including variations in concrete MOE at release, losses in strand force due to abutment movement and dead end slip, variations in strand force along the length of the bed as the concrete hardens, friction between the girders and the precasting bed, and thermal gradient through the depth of the girder. The factors that are believed to be the most significant are the reduction in camber due to the non-recoverable loss of prestress force and the thermal gradient effect. The other factors are believed to be unlikely to have a large effect on camber.

To demonstrate the potential effects of the thermal gradient on release camber, the estimated deflections due to thermal gradient shown in Figure 6.36 were superimposed with the estimated release cambers shown in Figure 6.32 and compared with the measured release cambers for the full-scale tests. Table 6.12 shows the maximum, minimum, and expected downward deflections due to thermal gradient. Note that negative values represent downward deflections. The expected downward deflection is based on the assumption that bond occurred when the concrete temperature at midspan on Strand 1 reached 100°F. Figure 6.37 shows the estimated release cambers without considering the deflection due to thermal gradient (i.e., the values from Figure 6.32) compared with the TEA estimated camber considering the maximum and expected downward deflections due to thermal gradient.

Table 6.12: Maximum, minimum, and expected downward deflection due to thermal gradient

Test No.	**1**	**2**	**3**	**4**
Max. Downward Deflection [in]	NA	-0.94	-0.73	-0.28
Min. Downward Deflection [in]	NA	-0.06	0.12	0.06
Expected Downward Deflection* [in]	NA	-0.94	-0.11	-0.19

*Assuming bond occurred when concrete temperature at midspan on Strand 1 reached 100°F

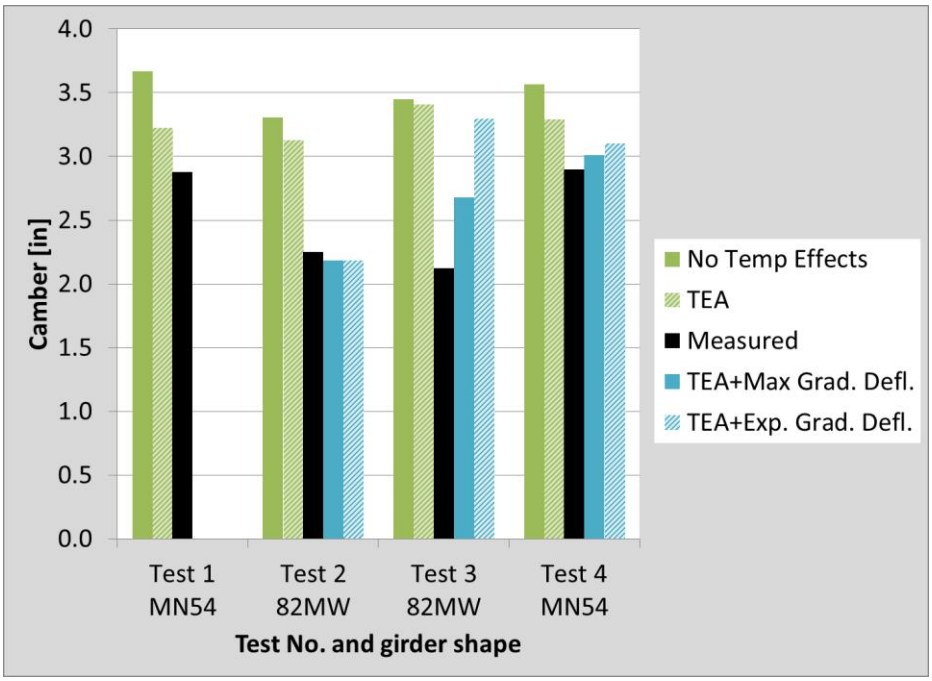

Figure 6.37: Estimated cambers considering deflection due to thermal gradient

The estimated camber considering the expected downward deflection due to thermal gradient was very close to the measured release camber for Tests 2 and 4. The expected deflection due to thermal gradient was not close for Test 3, but the maximum downward deflection was reasonable. It should be noted that the estimated deflections due to thermal gradient were based on multiple assumptions and are not expected to be accurate. However, the estimations were expected to provide the potential magnitudes of the effects of thermal gradient. Based on the information in Figure 6.37, it is reasonable to believe that the effects of thermal gradient could significantly affect girder camber at release and account for differences between estimated and measured cambers.

6.7.3 Other Camber Estimations

In addition to comparing estimated cambers using the thermal effects analysis (TEA) to measured cambers, camber predictions made using current MnDOT methods were also compared to measured cambers with and without implementing the recommendations made by O'Neill et al. (2012) for adjusting the design modulus of elasticity (MOE) estimate. The estimations introduced in this section were calculated

using gross concrete section properties as described in Section 3.4 and assuming the MnDOT plan force was achieved.

Table 6.13 shows the assumed concrete compressive strength, concrete MOE, and strand force values for each of the release camber estimations. The data series titled "ACI 363 – f'_{ci}" represents the current MnDOT method for estimating release camber, for which the MOE was estimated with the ACI 363 equation (see Section 5.3.2, Equation (5-2)). The data series titled "Pauw – f'_{ci}" and "Pauw – 1.15f'_{ci}" represent the release camber estimation recommendations from O'Neill et al. (2012) discussed in Section 6.5.1. It was recommended that the Pauw (1960) model for estimating the concrete MOE replace the ACI 363 model and that the concrete strength at release assumed by MnDOT be increased by 15% in calculating the release camber. The release camber estimated with both the current MnDOT assumed compressive strength at release (7500 psi (51.7 MPa)) and the increased compressive strength at release (8625 psi (59.5 MPa)) using the Pauw model (assuming a concrete unit weight of 155 pcf (2483 kg/m^3)) for estimating the MOE were examined using the current MnDOT calculation method in Section 3.4.

Table 6.13: Camber estimation parameters for data series in Figure 6.38

Data Series	ACI 363 - f'_{ci}	Pauw - f'_{ci}	Pauw - 1.15f'_{ci}
f'_{ci} [psi]	7500	7500	8625
E_{ci} [ksi]	4464	5515	5914
$P_{release}$ [kip/strand]	43.94*	43.94*	43.94*

*MnDOT plan force

Figure 6.38 shows the release cambers estimated with the parameters outlined in Table 6.13 compared to the measured cambers at release for each full-scale test. Figure 6.39 shows the percent difference between the estimated release cambers and the measured values (given by $\frac{(estimated-measured)}{measured} * 100$). Tests 2 and 3 were performed on a relatively new girder cross section, the MW shape. For this reason, MnDOT used computer software to model the behavior of the girders to obtain the camber estimates that appeared on the bridge plans. Outputs from two programs, Midas and RM Bridge, are included in the figures for the 82MW shape. The results from RM Bridge were used

in the final MnDOT bridge plans for the girders tested. The figure also contains the camber estimations described in Section 6.7.1 (i.e., “No Temp Effects” and “TEA”).

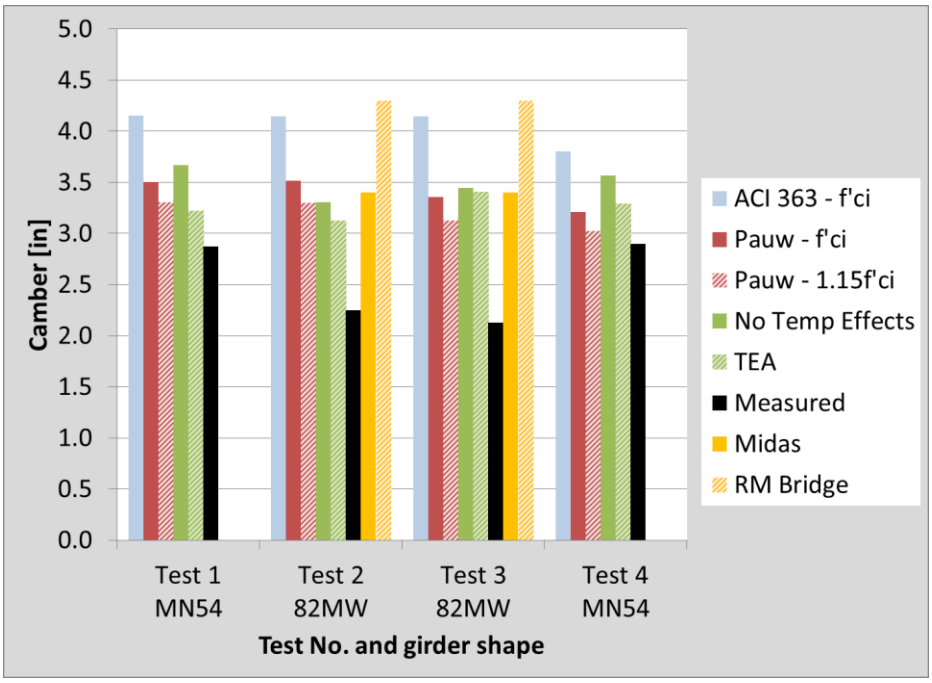

Figure 6.38: Estimated and measured cambers at release

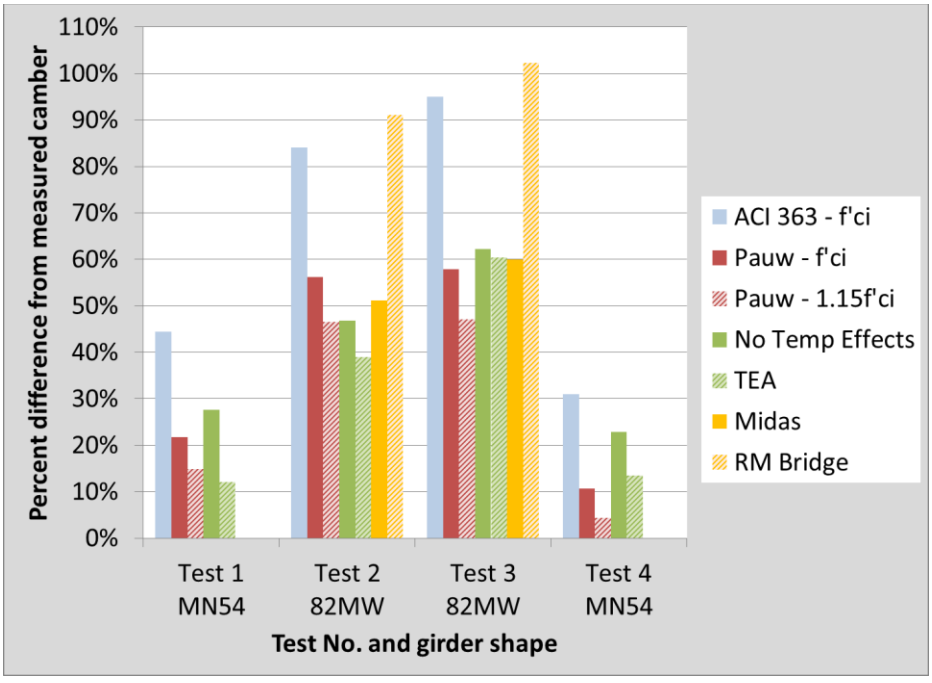

Figure 6.39: Percent difference between estimated and measured cambers

From Figures 6.38 and 6.39, it is clear that the estimations from the MnDOT plans were significantly higher than the measured initial camber. The current MnDOT design method using the ACI 363 equation overestimated the release camber by 44 and 31% of the measured value for Tests 1 and 4 and by 84 and 95% for Tests 2 and 3, respectively. The estimations were significantly improved by implementing the recommendations made by O'Neill et al. (2012), estimating release cambers 15 and 4% higher than the measured values for Tests 1 and 4, respectively, and 47% higher for both Tests 2 and 3.

For Tests 3 and 4, the estimations implementing both recommendations made by O'Neill were closer to the measured results than those obtained with the TEA based on measurement parameters. However, the effects of thermal gradient on camber, as described in Section 6.7.2.4, were not considered in Figures 6.38 and 6.39. The reduction in camber due to thermal gradient was found to reasonably account for the discrepancies between the estimated camber using the TEA and the measured value. In addition, for Tests 3 and 4, the measured concrete MOE were lower than the estimated MOE using the Pauw model with 15% increased compressive strength, resulting in higher estimated cambers with the measured data.

The computer software programs used by MnDOT, Midas and RM Bridge, also overestimated the release camber. The detailed methods used by the program to determine the release camber were unknown, but from the information provided by MnDOT it was found that approximately 0.6 in. (15 mm) of the 3.4 in. (86 mm) release camber estimated by Midas was attributed to creep. However, creep would not likely have such a large effect on camber at release. If creep had not been considered, the release camber predicted by Midas for Tests 2 and 3 would have been the most accurate estimation at approximately 2.8 in. (71 mm).

6.8 Summary of Temperature Effects on Strand Force and Release Camber

The objective of the full-scale girder tests was to determine the effects of temperature on strand force and release camber. Table 6.14 summarizes the observed non-recoverable strand force changes due to temperature changes from tensioning to bond. The total non-recoverable strand force changes that were "locked" into the girders

were determined using the thermal effects analysis (TEA) for each test, as described in Section 6.4.2. The time of bond was assumed to be when the concrete temperature on Strand 1 at midspan of Girder 1 reached 100°F (37.8°C). The effective temperature adjustment, described in Section 6.3.2, was taken as the difference between the average measured net force and the MnDOT plan force. The effective non-recoverable force change due to temperature was taken as the total non-recoverable force change plus the effective temperature adjustment (ignoring the potential losses due to dead end slip and abutment movement, as noted in Section 6.3.2). Ideally, this value would be zero, which would mean that the precasting plant had reasonably adjusted the strand force during tensioning to offset the force changes due to temperature.

Table 6.14: Summary of total and effective non-recoverable strand force changes due to temperature for full-scale girder tests

Test No.	**1**	**2**	**3**	**4**
Assumed Time of Bond* [hr]	8.2	11.1	6.9	8.0
Avg. Temp. at Tensioning [°F]	46°F	69°F	66°F	57°F
Avg. Free Strand Temp. at Bond [°F]	41°F	85°F	57°F	80°F
Avg. Concrete Temp. at Bond** [°F]	116°F	97°F	96°F	108°F
Total Non-recoverable Force Change [kip]	-2.0	-1.2	-0.2	-1.8
Total Non-recoverable Force Change^{+} [%]	-4.5%	-2.7%	-0.5%	-4.0%
Effective Temp. Adjustment*** [kip]	0.8	0.5	0.5	0.9
Effective Non-recoverable Force Change [kip]	-1.2	-0.6	0.3	-0.8
Effective Non-recoverable Force Change^{+} [%]	-2.6%	-1.4%	0.7%	-1.9%

*Assumed time of bond when concrete temperature at midspan on Strand 1 reached 100°F
**Weighted average concrete temperature for all embedded thermocouples on Strand 1 when midspan gage read 100°F
***Average net measured force minus MnDOT design force
$^{+}$Percent of MnDOT plan force

It was found that the effective non-recoverable strand force changes were relatively low during Tests 2 and 3 and slightly larger during Tests 1 and 4. The precasting plant's strand force adjustments were reasonable, limiting the "locked" in strand force loss to 2.6% in the worst case. For reference, the average force loss due to strand relaxation during fabrication was determined to be approximately 2.7 ksi (19 MPa) for the full-scale tests, or approximately 1.3% of the MnDOT plan force. The non-

recoverable strand force change due to temperature can be significantly larger than the loss due to relaxation, but plant adjustments were observed to reasonably offset those losses.

Table 6.15 summarizes the effects of non-recoverable strand force losses on release camber. The estimated cambers without and with temperature effects correspond to the estimated cambers shown in the data series "No Temp Effects" and "TEA" in Section 6.7.1, respectively.

Table 6.15: Summary of effects of temperature on release camber for full-scale girder tests

Test No.	1	2	3	4
Estimated Camber w/o Temperature Effects [in]	3.49	3.30	3.45	3.56
Estimated Camber with Temperature Effects*+ [in]	3.22	3.13	3.41	3.29
Difference [in]	-0.27	-0.18	-0.04	-0.27
Difference [%]	-7.6%	-5.4%	-1.1%	-7.7%

*Assumed time of bond when concrete temperature at midspan on Strand 1 reached 100°F

+Includes effects of recoverable strand force changes due to incompatibility

The effects of temperature resulted in a decrease in release camber of approximately 1/4 in. (6 mm) during Tests 1 and 4, 3/16 in. (5 mm) during Test 2, and 1/16 in. (2 mm) during Test 3. Because differences in camber smaller than 1/8 in. (3 mm) are difficult to observe with a tape measure, they were considered to be insignificant. The upward deflection is directly proportional to the prestressing force at bond (see Section 3.3.4.1), whereas the downward deflection due to self-weight is constant for a given girder. This means that the percent difference in total camber was amplified relative to the percent of total non-recoverable strand force change. The camber at release was reduced by as much as 7.7% due to temperature changes between tensioning and bond during the full-scale girder tests.

6.9 Summary of Full-Scale Girder Tests

Tests were performed on full-scale girder fabrications to monitor the effects of temperature on strand force and initial camber. Four sets of girders were instrumented with foil strain gages, concrete strain gages, vibrating wire gages, load cells, and

thermocouples from the time the strands were tensioned until the girders were released and removed from the precasting bed. The tests were performed with the goal of monitoring the effects of cold and warm weather casts, as well as the effects of bed occupancy and externally heating the strands, on strand force and release camber.

Before tensioning began, adjustments were made by the precasting plant to the initial strand force at the time of tensioning to account for expected losses that occur during tensioning, as well as losses due to the temperature increase associated with the placement of concrete. Net strand elongation measurements recorded by the precasting plant during tensioning were used to derive the average initial strand force. The elongation measurements captured the initial strand force adjustments for temperature and seating losses, but did not account for potential losses due abutment movement and dead end slip, which were determined to be relatively small. The effective temperature adjustment was taken as the difference between the average initial strand force derived from the net elongation measurements and the MnDOT plan force (i.e., 43.94 kips (195.5 kN)). This value represented the maximum amount of non-recoverable force loss due to temperature the strands could experience between tensioning and bond while maintaining a force greater than or equal to the MnDOT plan force at release, even if no temperature adjustment was specified (i.e., due to incidental over- or under-stressing).

Non-recoverable strand force changes due to temperature changes between tensioning and bond, as well as free strand force changes between bond and release, were estimated with the thermal effects analysis (TEA) using temperature data measured at multiple points along the length of the precasting bed. The estimated changes were compared to force measurements recorded by load cells on the dead and live ends of Strand 1 during each test (except Test 1). The assumed time of bond significantly affected the results of the TEA, so multiple cases were examined for each test. It was found that the best fit between the estimated and measured force changes occurred when the concrete temperature reached approximately 100°F (37.8°C). For simplicity, the time of bond for each full-scale test was assumed when the concrete temperature at midspan of Girder 1 on Strand 1 was 100°F. This corresponded to weighted average concrete temperatures of 116, 97, 96, and108°F (46.7, 36.1, 35.6, and 42.2°C) and assumed times of bond of 8.2, 11.1, 6.9, and 8.0 hours after casting for Tests 1 through 4, respectively.

With the exception of Test 2, the assumed times of bond for the full-scale tests reasonably aligned with the assumption that bond occurred between 6 and 8 hours during the short girder tests. Because Test 2 was the only fabrication during which steam heating was not used, it took more time for the concrete temperature to reach 100°F. The later assumed time of bond for Test 2 suggested that bond is more dependent on temperature than time. The comparison of the TEA results with measured strand force data also served to validate the model.

The total non-recoverable strand force changes due to temperature with the assumed times of bond ranged from -0.5 to -4.5% of the MnDOT plan force. However, strand force adjustments made during tensioning resulted in initial forces higher than the MnDOT plan force. The effective non-recoverable strand force change due to temperature, taken as the total non-recoverable strand force change plus the effective temperature adjustment, ranged from 0.7 to -2.6% of the MnDOT plan force. For comparison, strand relaxation losses for the full-scale tests during fabrication were approximately equal to 1.3% of the MnDOT plan force. The non-recoverable effects of temperature on strand force can be significantly larger than those due to relaxation during fabrication and their effects on serviceability should be considered (e.g., potential cracking at service), but current plant adjustments were found to reasonably minimize those losses. Additionally, restraint forces that can develop between bond and release have the potential to contribute to concrete cracking before release, as was observed during some full-scale tests.

Concrete material properties at the time of girder release were measured and compared to design values and values recommended by previous research. The measured concrete compressive strengths were 12 to 36% larger on average than the plan release values for each test, while the average measured elastic moduli were 15 to 39% larger than plan values. Recommendations were made by O'Neill et al. (2012) to increase the concrete compressive strength at release by 15% and replace the ACI 363 model for modulus of elasticity (MOE) at release with the Pauw (1960) model when predicting the release camber. When the recommendations were implemented, the estimated elastic moduli for tests during which the girders were cured over a weekend increased to within 5% of the measured values, while the measured MOE for Test 4 was only 87% of the

estimation because the concrete was only cured overnight. The recommended method for estimating the MOE at release by O'Neill et al. (2012) was found to be reasonable for the full-scale tests.

Measured strain distributions through the girder sections at midspan were compared to estimated strain distributions determined using the TEA with measured temperatures, strand forces, and concrete properties. The instrument strain changes at release were a function of (1) restraint forces that developed in the free strand between bond and release acting on the composite girder section as the strands were cut and (2) elastic shortening caused by the force "locked" into the girder at bond, after considering non-recoverable force losses due to temperature. It was found that the former component was insignificant for all tests except for Test 2, which was the only fabrication during which steam heating was not used to moderate the temperature of the free strand on the bed, resulting in a large ambient temperature decrease. This decrease caused large tensile restraint forces in the free strand that were equilibrated in the composite section. Upon release, the restraint forces were removed from the composite girder section. The tensile strain in the concrete just before release appears to be additional compressive strain due to elastic shortening when viewing the strain change at release, but the effect does not contribute to camber.

Using the average strand force derived from net elongation measurements, measured temperature data, assumed times of bond when Strand 1 temperatures at midspan reached 100°F, and measured MOE values with the TEA, two release camber estimates were made for each test; the first ignoring the effects of temperature on strand force and incompatibility (i.e., where incompatibility represents the forces generated within the concrete and steel due to differences between the coefficients of thermal expansion of the two materials), and then considering the effects of temperature. The latter case was expected to more accurately depict the release camber. The difference between the two scenarios demonstrated the effect of total non-recoverable strand force changes due to temperature on the release camber. It was found that non-recoverable strand force changes of -4.5, -2.7, -0.5, and -4.0% the MnDOT plan force resulted in deflection changes of approximately -7.6%, -5.4%, -1.1%, and -7.7% of the TEA estimated release camber for full-scale Tests 1 through 4, respectively. Because strand

force is directly proportional to upward deflection, but camber is also a function of downward deflection due to self-weight, non-recoverable strand force changes are not proportional to reductions in camber due to the non-recoverable strand force changes. The component of camber due to incompatibility was found to be negligible.

The estimated cambers described above were compared to measured values. For all full-scale tests, the estimated cambers were larger than the measured values. Multiple factors that could affect the release camber were investigated, including variations in concrete MOE, inaccurate assumed strand forces, friction between the girders and the precasting bed, and deflections due to thermal gradients caused by cooling of the girder. It was found that the potential reduction in camber due to thermal gradients was significant and reasonably accounted for the remaining discrepancies between the estimated and measured release cambers.

Finally, other release camber estimations were compared to the TEA estimates and measured values. The other estimations included the current MnDOT prediction method, MnDOT prediction methods implementing recommendations made by O'Neill et al. (2012), and estimations made with computer software used by MnDOT for 82MW shape girders. It was found that the current MnDOT and computer software methods significantly overestimated the release camber, while the methods implementing the recommendations made by O'Neill et al. (2012) estimated release cambers much closer to the measured values.

CHAPTER 7. PARAMETRIC STUDY

7.1 Introduction

A parametric study was performed to investigate the effects of temperature changes during fabrication and tension force adjustments made by the precasting plant on camber. The thermal effects analysis (TEA) described in Chapter 3 was performed with the girder properties from Test 4 of the full-scale girder tests, which can be found in Appendix A. The ambient temperature was assumed constant throughout the hypothetical fabrication and applied to the entire free strand length (i.e., strand not embedded in concrete). The temperature of the strand at the time of tensioning was assumed to be the specified ambient temperature, which was varied to simulate possible cases in which the strands were tensioned in different weather conditions. Concrete temperatures at the time of bond and release were assumed and applied to the total length of embedded strand. The concrete temperature at the time of bond was assumed to be 100°F (37.8°C), while the concrete temperature at release varied. A final temperature, representing a point in time at which the girder had normalized to the ambient temperature, was assumed to be 75°F (23.9°C). The variations in concrete temperature at release in combination with the final concrete temperature were useful in investigating the effects of girder cooling on camber. Because the average strand temperature along the bed is a function of the length of embedded strand (i.e., the number of girders on the bed), two different bed occupancies, 33% and 65% occupied by girders, were examined to simulate casting a single girder and two girders simultaneously, respectively. It was assumed that corrections for initial losses (i.e., seating, dead end slippage, and abutment movement) were already taken into account, so the initial strand force was assumed to be 45 kips (200 kN) per strand.

The current strand force adjustment used by the precasting plant to offset losses due to temperature was examined and compared to a proposed adjustment method, which considers bed occupancy and a higher concrete temperature at bond, rather than the wet concrete temperature assumed in the plant's current method. The two methods were

compared in the context of both the parametric study and the full-scale girder tests in Section 7.5.1.

7.2 Control Case

A control case was implemented to represent the case in which no strand force changes due to temperature occurred. The strand force was assumed constant at 45 kips (200 kN) per strand and the final camber was assumed to be equal to the camber just after release. The control case camber was compared to the cambers resulting from various temperature scenarios to determine the effects of those temperatures on the release and final cambers.

7.3 Thermal Effects

Two factors affecting camber were investigated; ambient temperature at the time of tensioning and concrete temperature at release. Precasting plants experience a wide temperature range over the course of a year, especially in Minnesota. Low ambient temperatures at the time of tensioning can lead to large strand force losses when the warmth of the concrete increases the strand temperature prior to bond, leading to lower cambers. Girder cooling after hydration can cause additional changes in deflection due to stresses that develop at the center of gravity of the strands due to incompatibility (i.e., the difference between the coefficients of thermal expansion of the steel and concrete), which were found to be negligible as described in 6.7.1, evident in the following figures as the difference between the release and final cambers. Thermal gradient, which was found to have a potentially significant effect on camber, was not investigated as part of the parametric study.

7.3.1 Temperature at Time of Tensioning

Four ambient temperatures were assumed and camber results compared to determine the impact of the strand temperature at the time of tensioning on camber. The ambient temperature for each case was assumed for all free strand length and remained constant until the final camber was calculated. Table 7.1 shows the temperatures assumed for each case and the impact they had on strand force at the time of bond, associated with

a non-recoverable force change, and the release and final camber values for a precasting bed with 33% occupancy (i.e., amount of the total bed length containing girders) and 65% occupancy. Figure 7.1 shows the resulting release and final camber values for the four cases compared to the control case. Note that in this chapter the scale of the plots ranges from 2.5 to 3.2 in. (64 to 81 mm), which exaggerates the differences in camber among cases; the accuracy of camber measurements in the field were approximately to the nearest 1/8 in. (3 mm).

For every 25°F (13.9°C) difference between the ambient (i.e., temperature at the time of tensioning) and concrete bond temperatures, the 33% occupancy case experienced a strand force loss of approximately 0.8%. This doubled for the 65% occupancy case, meaning the force change was linearly related to both the temperature change and bed occupancy. The largest observed difference in camber of approximately 1/4 in. (6 mm) was between the control case (i.e., no temperature effect) and the case with 65% bed occupancy and ambient temperature of 25°F (-3.9°C), which was the largest difference between ambient temperature and temperature at bond,. This represented a difference of approximately 9% of the control camber (2.88 in. (73.1 mm)). An ambient temperature of such low magnitude is unlikely during production due to the measures taken by the precasting plant to mitigate strand force losses due to temperature by covering and heating portions of the bed at all times.

Table 7.1: Effects of strand temperature at time of tensioning on strand force and camber

Tension at Different Ambient Temperatures					
Ambient temperature		25°F	50°F	75°F	100°F
Concrete temp. at bond		100°F			
Concrete temp. at release		100°F			
Final concrete/ambient temp.		75°F			
33% Occupancy					
Total non-recoverable force change	kip/strand	-1.0	-0.7	-0.3	0.0
	% pull	-2.3%	-1.5%	-0.8%	0.0%
Camber [in]	Release	2.75	2.79	2.84	2.88
	Final	2.77	2.82	2.86	2.90
65% Occupancy					
Total non-recoverable force change	kip/strand	-2.1	-1.4	-0.7	0.0
	% pull	-4.6%	-3.0%	-1.5%	0.0%
Camber [in]	Release	2.62	2.71	2.79	2.88
	Final	2.64	2.73	2.82	2.90
Control Camber [in]		2.88			

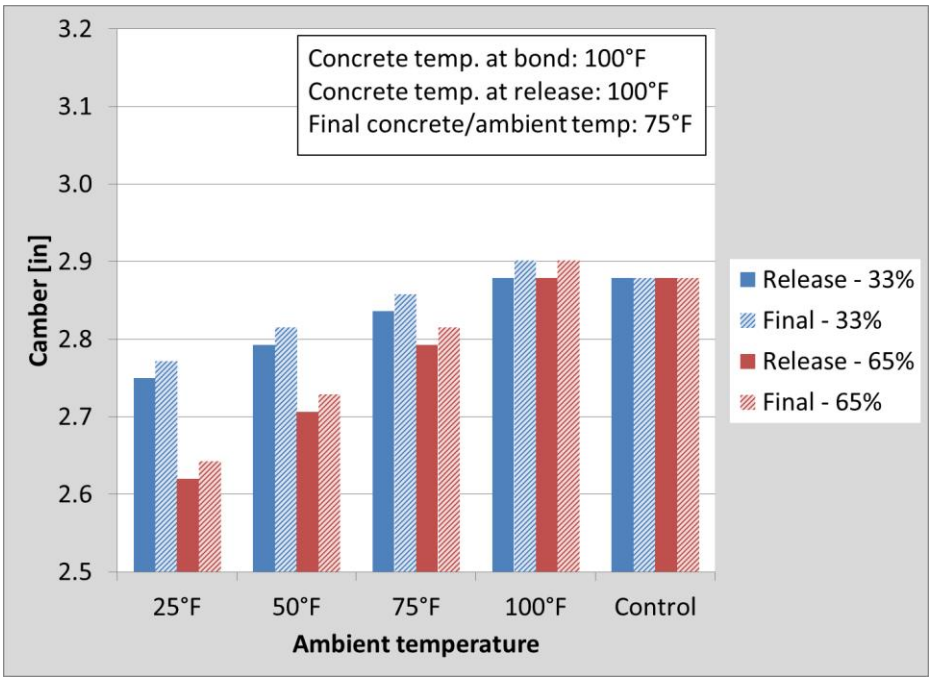

Figure 7.1: Effects of ambient temperature on release and final camber for 33% and 65% bed occupancy

7.3.2 Temperature at Time of Release

Four concrete temperatures at release were assumed and camber results compared to determine the impact on camber. A constant ambient temperature of 75°F (23.9°C) was assumed, meaning each bed occupancy case experienced non-recoverable strand force loss due to the difference between the ambient temperature and the concrete temperature at bond (100°F (37.8°C)). Table 7.2 shows the temperatures assumed for each case and the impact they had on the release and final camber values for a precasting bed with 33% occupancy and 65% occupancy. Figure 7.2 shows the resulting release and final camber values for the four cases compared to the control case.

The effect of release temperature on camber was much less significant than the effect of temperature at the time of tensioning discussed in Section 7.3.1. Once the girders have been released, the bed occupancy does not affect the difference in release and final camber values because the girders act independently from each other upon release, no matter how many girders were cast together on the bed. The magnitudes of the

difference were insignificant and would likely not be noticed during inspection by the precasting plant.

Table 7.2: Effects of concrete temperature at release on camber

Release at Different Concrete Temperatures					
Ambient temperature		75°F			
Concrete temp. at bond		100°F			
Concrete temp. at release		50°F	75°F	100°F	125°F
Final concrete/ambient temp.		75°F			
33% Occupancy					
Total non-recoverable force change	kip/strand	-0.3	-0.3	-0.3	-0.3
	% pull	-0.8%	-0.8%	-0.8%	-0.8%
Camber [in]	Release	2.88	2.86	2.84	2.81
	Final	2.86	2.86	2.86	2.86
65% Occupancy					
Total non-recoverable force change	kip/strand	-0.7	-0.7	-0.7	-0.7
	% pull	-1.5%	-1.5%	-1.5%	-1.5%
Camber [in]	Release	2.84	2.82	2.79	2.77
	Final	2.82	2.82	2.82	2.82
Control Camber [in]		2.88			

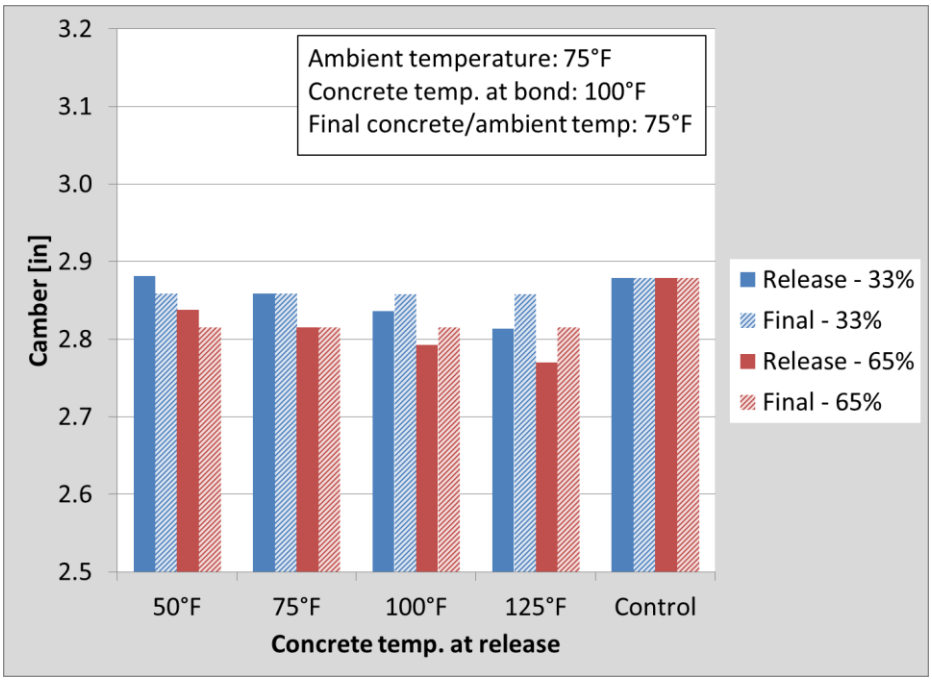

Figure 7.2: Effects of release temperature on release and final camber for 33% and 65% bed occupancy

7.4 Plant Temperature Adjustment Method

The precasting plant anticipates strand force loss due to temperature changes between the times of tensioning and casting. To offset these losses, the plant adjusts the initial jacking force based on the difference between the average strand temperature at the time of tensioning and the anticipated temperature of the wet concrete at the time of casting. This adjustment method is described in detail in Section 6.3.1.2. The effects of varying ambient temperatures on camber were investigated in Section 7.3.1, and this section investigates the effects of the current force adjustment method on camber for the same temperature scenarios that were examined in that section.

Table 7.3 details the strand force adjustments and resulting camber from the assumed temperature scenarios with the current strand force adjustment method applied. The wet concrete temperature shown represents the final temperature assumed by the precasting plant when adjusting the strand force for prestress losses due to temperature. The difference between the wet concrete temperature and the average strand temperature at the time of tensioning is used to determine the percentage of strand force that will be

added or subtracted from the target jacking force (i.e., the force adjustment). For both occupancy cases (i.e., 33 and 65%), the total non-recoverable strand force due to temperature is listed, then superimposed with the force adjustment made to offset the effects of temperature. The difference in these percentages (i.e., effective non-recoverable strand force change) can be used to determine the effectiveness of the adjustment in offsetting force losses due to temperature at the time of bond. If the amounts are equal and opposite (i.e., the effective non-recoverable strand force change is equal to zero), the adjustment perfectly offset the losses. If the effective non-recoverable strand force change is positive, the adjustment overcompensated for the losses due to temperature.

It was observed that the 33% bed occupancy case was more affected by the strand force adjustment than the 65% occupancy case because the losses due to temperature are a function of bed occupancy, so smaller losses occurred with 33% occupancy, but the force adjustment remained the same for both cases (i.e., the plant makes the adjustment assuming the temperature change affects the entire bed length).

Figures 7.3 and 7.4 show the release and final cambers resulting from the temperature scenarios from Table 7.1 with and without the application of the plant force adjustment for 33% and 65% bed occupancy, respectively. The correction was too large for the 33% occupancy case when the ambient temperature was low due to the assumption of a fully occupied bed in the precasting plant's temperature adjustment. The force adjustment was more reasonable for the 65% occupancy case because the bed occupancy was closer to the assumed occupancy. It should be noted that even the largest difference was of small magnitude, approximately 0.15 in. (3.8 mm), so the use of the plant force adjustment method was not unreasonable for the 33% occupancy case.

Table 7.3: Effects of current strand force adjustment method for losses due to temperature on release and final cambers

Tension at Different Ambient Temperatures					
Ambient temperature		25°F	50°F	75°F	100°F
Concrete temp. at bond		100°F			
Concrete temp. at release		100°F			
Final concrete/ambient temp.		75°F			
Current Temperature Correction					
Wet concrete temperature		75°F			
Ambient - wet concrete temp.*		-50°F	-25°F	0°F	25°F
Force adjustment		5%	2%	0%	-2%
33% Occupancy					
Total non-recoverable force change		-2.3%	-1.5%	-0.8%	0.0%
Effective non-recoverable force change**		2.7%	0.5%	-0.8%	-2.0%
Camber [in]	Release	3.03	2.91	2.84	2.77
	Final	3.06	2.93	2.86	2.79
Control camber [in]		2.88			
65% Occupancy					
Total non-recoverable force change		-4.6%	-3.0%	-1.5%	0.0%
Effective non-recoverable force change**		0.4%	-1.0%	-1.5%	-2.0%
Camber [in]	Release	2.90	2.82	2.79	2.77
	Final	2.93	2.84	2.82	2.79
Control camber [in]		2.88			

*Ambient temperature minus the wet concrete temperature

**Sum of the force adjustment and the total non-recoverable force change due to temperature

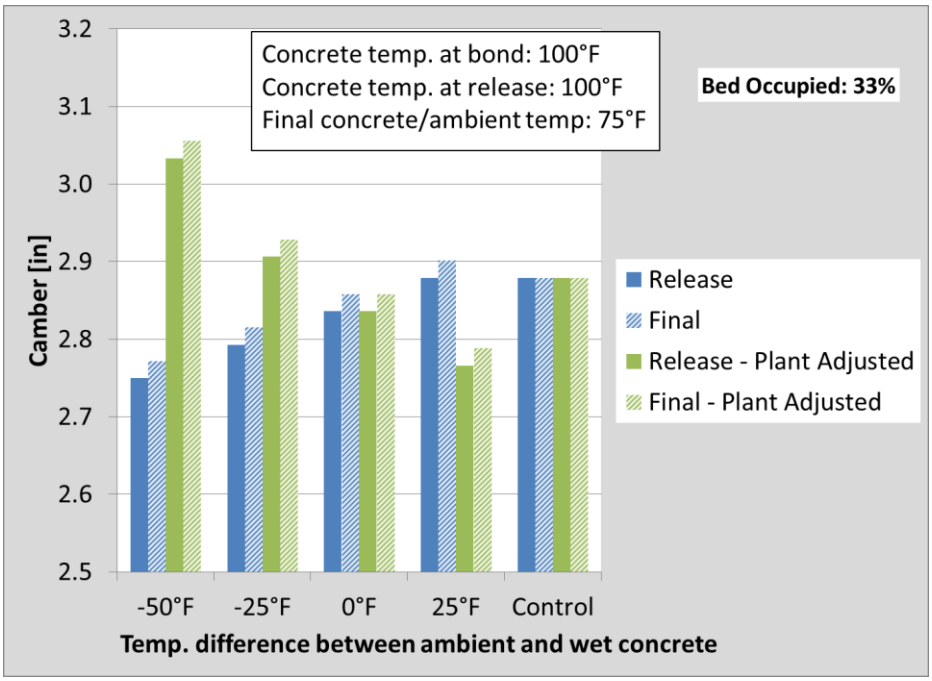

Figure 7.3: Effects of current strand force adjustment method for losses due to temperature on release and final cambers for 33% bed occupancy

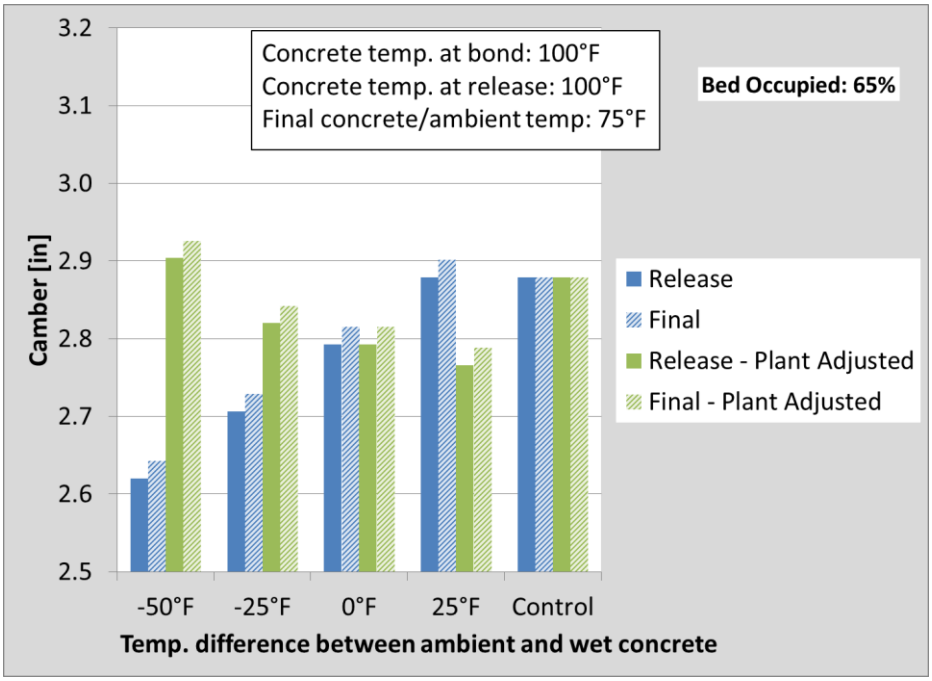

Figure 7.4: Effects of current strand force adjustment method for losses due to temperature on release and final cambers for 65% bed occupancy

7.5 Proposed Temperature Correction Method

The precasting plant currently adjusts the initial force put into each strand during tensioning based on the average strand temperature just before tensioning (taken by measuring with a temperature gun at approximately six locations along the bed) and the temperature of the wet concrete to be poured (taken as the temperature of recent batches, generally 70-80°F (21-27°C)), assuming the bed is fully occupied. Because the average temperature of the bed and, subsequently, the strand force loss due to temperature are directly related to the amount of the bed occupied by girders, a new method for adjusting the initial strand force at tensioning is proposed.

Equation (3-7) was simplified into Equation (7-1), which is proposed for use by the precasting plant in place of their current method for adjusting the tensioning force based on the temperature of the wet concrete. The force adjustment, ΔP, is a function of the amount of the bed that is occupied by girders (i.e., $\frac{L_{in}}{L_{bed}}$) and the temperature difference between the time of tensioning and time of bond.

$$\Delta P = \alpha_s E_{ps} A \frac{L_{in}}{L_{bed}} (T_{bond} - T_{tension}) \quad (7\text{-}1)$$

where:

- α_s: Coefficient of thermal expansion of steel
- E_{ps}: Strand modulus of elasticity
- A: Strand area
- L_{in}: Total length of girders on the bed (i.e., length of strand inside girders)
- L_{bed}: Length of the bed
- T_{bond}: Average temperature of the concrete at bond
- $T_{tension}$: Average temperature of the strand before tensioning

A tensioning sheet is created by the engineers at the precasting plant for each fabrication that includes important information for the field workers, such as the strand pattern and required jacking forces and elongations. The required forces and elongations on the tensioning sheet account for seating, slippage, and abutment movement losses, while the force adjustment for losses due to temperature are performed in the field just before tensioning by the worker supervising the tensioning process.

The quantity $\alpha_s E_{ps} A \frac{L_{in}}{L_{bed}}$ would be included on the tensioning sheet as a factor to be applied to the anticipated strand temperature difference between the time of tensioning and time of bond. The same average temperature measurement taken by the field worker for the current adjustment method would be used for the proposed method, but, instead of adding a set percentage to the target jacking force based on the difference between the average strand temperature and the temperature of the wet concrete, the difference between the average strand temperature and the assumed concrete temperature at the time of bond (i.e., $(T_{bond} - T_{tension})$) would be multiplied by the factor from Equation (7-1) (i.e., $\alpha_s E_{ps} A \frac{L_{in}}{L_{bed}}$) to obtain the force adjustment. The proposed method more accurately predicts the strand force loss due to temperature before bond without much, if any, additional work required in the field and without altering the physical process of tensioning the strands.

Figures 7.5 and 7.6 compare the current and proposed plant strand force adjustment methods for losses due to temperature for 33% and 65% bed occupancy, respectively. The temperature scenarios were the same as those in the previous section. It can be seen that the proposed adjustment method matches the control release camber for all cases because it is a function of the bed occupancy and temperature of the concrete at bond (as opposed to 100% bed occupancy and the wet concrete temperature).

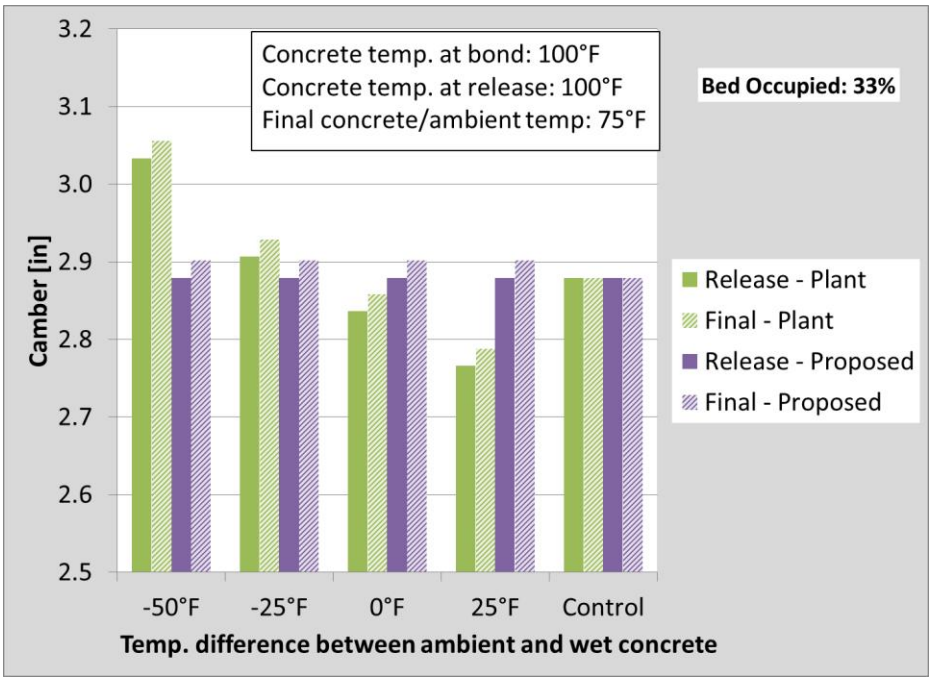

Figure 7.5: Effects of current and proposed strand force adjustment methods for losses due to temperature on release and final cambers for 33% bed occupancy

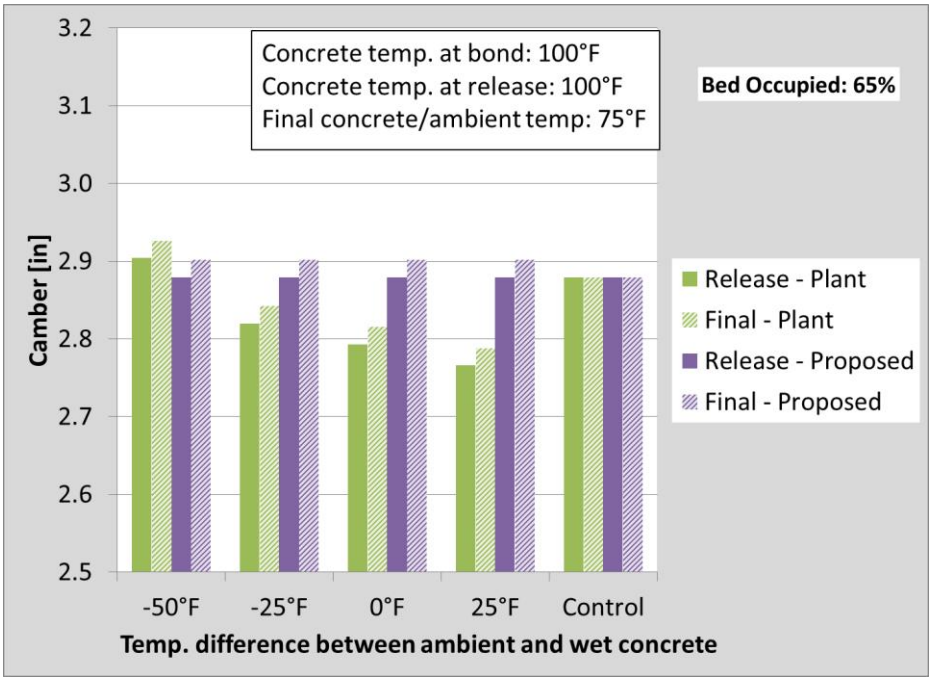

Figure 7.6: Effects of current and proposed strand force adjustment methods for losses due to temperature on release and final cambers for 65% bed occupancy

7.5.1 Effects of Ambient Temperature Changes

The proposed strand force adjustment for temperature does not consider the change in temperature of the free strand after the concrete is cast. However, free strand temperature changes were observed during the full-scale girder tests. Figure 7.7 shows the average measured Strand 1 temperature before the concrete was cast during each full-scale test. The average temperature was determined from all thermocouples located along the length of the bed on Strand 1. Figure 7.8 shows the average measured temperature of the embedded portion of Strand 1 after casting during each full-scale test. The temperature was determined only from thermocouples located within the girders on Strand 1. Figure 7.9 shows the average measured temperature of the free portion of Strand 1 after casting during each full-scale test.

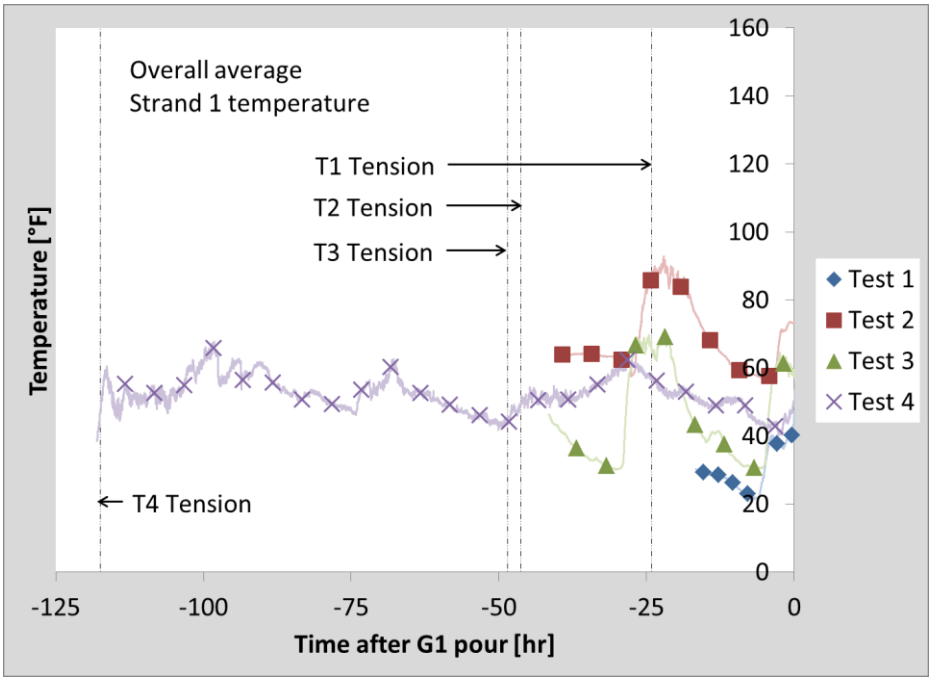

Figure 7.7: Average Strand 1 temperature before casting during full-scale girder tests

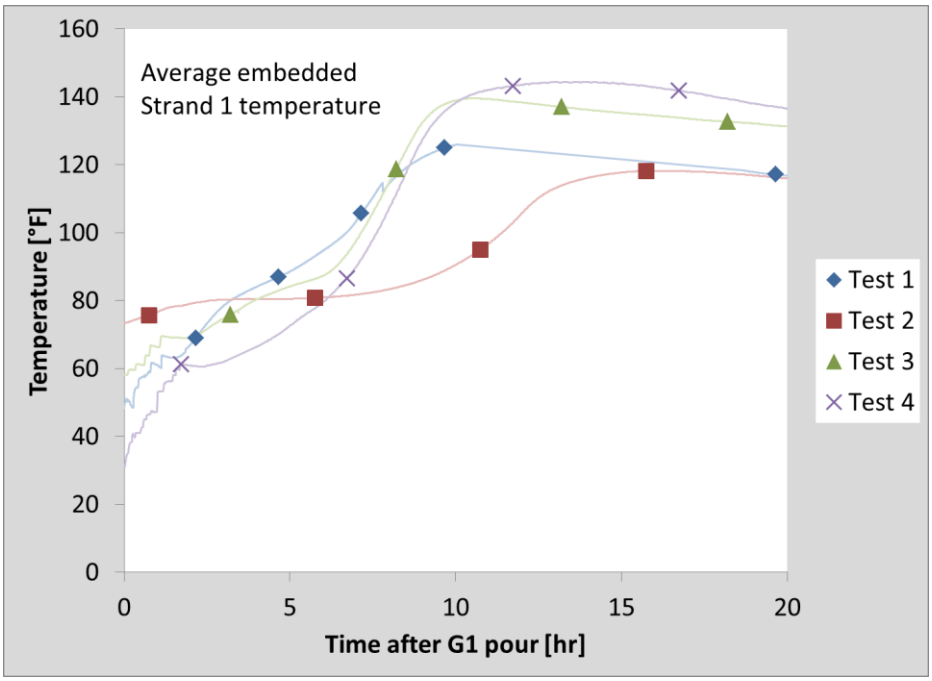

Figure 7.8: Average embedded Strand 1 temperature after casting during full-scale girder tests

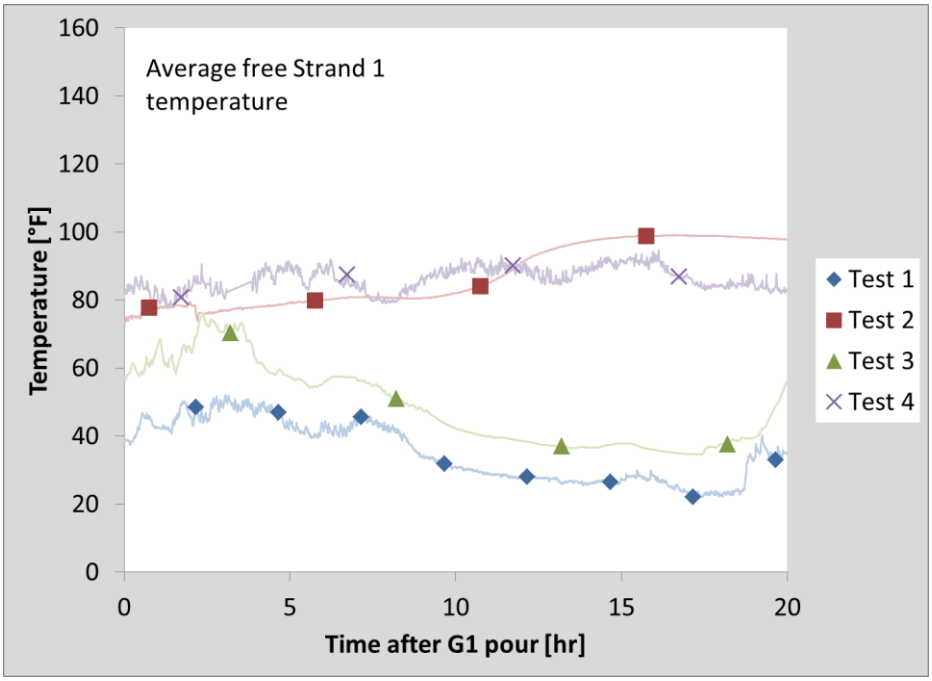

Figure 7.9: Average free Strand 1 temperature during full-scale girder tests

The figures above show that the temperature of the free strand at bond was not necessarily the same as the average strand temperature at tensioning. To determine the

effects of ignoring the free strand temperature change in the proposed strand force adjustment method and also to compare the current plant and proposed adjustments, temperatures measured during the full-scale girder tests were used to determine the hypothetical effectiveness of each adjustment method. The initial strand force was assumed to be the MnDOT plan force (43.94 kip (195.5 kN)) and adjustments for losses during tensioning (i.e., seating, abutment movement, dead end slip) were not considered. Table 7.4 summarizes the comparison between the current plant adjustment and the proposed adjustment. It should be noted that the average strand temperature at the time of tensioning not directly measured for Tests 1 through 3, as shown in Figure 7.7. The average temperature at tensioning shown in the table was determined by utilizing data from strain gages that began recording before tensioning began. The methodology is described in detail in Appendix B.

The time of bond was assumed when the Strand 1 concrete temperature at midspan of Girder 1 reached 100°F (37.8°C) during each full-scale test. The concrete temperatures at bond listed in the table do not equal 100°F because they consist of all thermocouples located within a girder on Strand 1 at that time. The total non-recoverable strand force changes shown are equal to the values from Table 6.14 in Section 6.7.2.5. The effective non-recoverable strand force change for each adjustment method was given by the sum of the total non-recoverable strand force change and the adjustment for each full-scale test.

Table 7.4: Effective non-recoverable strand force loss during full-scale tests; comparing current plant adjustment method with proposed method

Test No.	**1**	**2**	**3**	**4**
Assumed Time of Bond* [hr]	8.2	11.1	6.9	8.0
Avg. Temp. at Tensioning [°F]	46°F	69°F	66°F	57°F
Avg. Free Strand Temp. at Bond [°F]	41°F	85°F	57°F	80°F
Avg. Concrete Temp. at Bond** [°F]	116°F	97°F	96°F	108°F
Total Non-recoverable Force Change [kip/strand]	-2.0	-1.2	-0.2	-1.8
Non-recoverable Force Change (no adjustment) [%]	**-4.5%**	**-2.7%**	**-0.5%**	**-4.0%**
Current Plant Adjustment Method				
Wet Concrete Temperature*** [°F]	70°F	69°F	70°F	72°F
Temperature Difference[+] [°F]	-24°F	0°F	-4°F	-15°F
Adjustment [kip/strand]	0.88	0	0	0.44
Adjustment %	2%	0%	0%	1%
Effective Non-recoverable Force Change [%]	**-2.5%**	**-2.7%**	**-0.5%**	**-3.0%**
Proposed Adjustment Method				
Temperature Difference[++] [°F]	-54°F	-31°F	-34°F	-43°F
Bed Occupancy[+++]	0.69	0.94	0.47	0.65
Adjustment [kip/strand]	1.58	1.22	0.46	1.19
Adjustment %	3.6%	2.8%	1.0%	2.7%
Effective Non-recoverable Force Change [%]	**-0.9%**	**0.1%**	**0.6%**	**-1.3%**

*Assumed time of bond when concrete temperature at midspan on Strand 1 reached 100°F

**Weighted average concrete temperature for all embedded thermocouples on Strand 1 when midspan gage read 100°F

***Taken as values written on tensioning sheets provided by the precasting plant

[+]Average strand temperature at tensioning minus wet concrete temperature

[++]Average strand temperature at tensioning minus 100°F, which was the assumed concrete temperature at bond for proposed adjustment method

[+++]Total length of girders divided by bed length

Despite the assumption that the free strand temperature remains constant from tensioning to bond, the proposed strand force adjustment method more accurately corrected the initial strand force for temperature than the current plant adjustment method for three of the four full-scale girder tests. The strand force was over-corrected for Test 3

with the proposed method by approximately the same amount as it was under-corrected with the current plant method. The hypothetical scenario using measured fabrication temperatures shows that the proposed strand force adjustment method could slightly increase the accuracy of the temperature correction over the current plant adjustment method.

7.6 Safety Concerns when Adjusting Strand Force

Safety is always a concern during the production of prestressed concrete bridge girders due to the large forces applied to the strands. ACI 318-11 specifies a limit for the initial jacking force that can be applied of 80% of the ultimate tensile strength of the strand to minimize the risk of overstressing and fracturing the strands. In MnDOT design, the initial strand stress is specified to be approximately 75% of the ultimate tensile strength, so only a 5% increase will bring the strand stress to the limit. When adding initial strand force to compensate for losses during tensioning and temperature-related losses it is important not to exceed this limit.

After tensioning, the precasting bed must be prepared for casting the concrete. Rebar cages are tied to the strands and side forms are positioned. Depending on the casting schedule, multiple days may pass between tensioning and casting. Overnight temperatures are often lower than daytime temperatures, so strand forces may increase during the night. This effect is mostly taken care of by regulating the temperature of portions of the bed with tarps and steam heating, but can still be present in warm months when steam is not used.

7.7 Conclusion

It was determined that the temperature difference between the time of tensioning and the time of bond has a significant effect on the final camber. The plant practice of covering and heating the strands when ambient temperatures are low reduces the potential non-recoverable strand force loss due to the reduction in temperature change between tensioning and bond. The plant method for adjusting strand force for losses due to temperature was found to be reasonable, but, because the correction is not a function of bed occupancy, it is better suited for larger bed occupancy ratios. An adjustment method

was proposed that is a function of the bed occupancy, so non-recoverable strand force losses due to temperature can be more accurately taken into consideration.

The proposed adjustment method was found to more accurately offset the non-recoverable strand force changes due to temperature when the ambient temperature was constant, but data from the full-scale girder tests showed that the ambient (i.e., free strand) temperature varied during fabrication. The plant and proposed adjustment methods were compared by using measured temperatures and bed occupancies for the four full-scale tests. Although the proposed method assumes a constant ambient temperature, it was more effective in offsetting the non-recoverable strand force changes than the plant adjustment method.

CHAPTER 8. SUMMARY, CONCLUSIONS, AND RECOMMENDATIONS

8.1 Summary

The Minnesota Department of Transportation (MnDOT) reported erection cambers of many precast, prestressed concrete bridge girders that were much lower than anticipated, resulting in construction delays and increased costs. In a study by O'Neill et al. (2012), it was found that the girder cambers at release were, on average, only 74% of the predicted values on the MnDOT plans. This was attributed to inaccurate estimates of the concrete material properties and prestress losses due to temperature during fabrication. The purpose of the present study was to investigate prestress losses due to temperature during girder fabrication in order to improve release camber predictions and reduce constructability issues during erection.

To determine the effects of temperature on strand force and camber, a thermal effects analysis (TEA) was developed. The analysis used measured temperature and concrete elastic moduli data from field tests to estimate strand force changes throughout the fabrication process, as well as camber at release and after cooling. The estimates from the analysis were validated by comparing them with measured strand force changes, girder strain changes at release, and cambers.

The temperature at bond was an important variable in the thermal effects analysis. Six short girder sections were cast simultaneously and released at different times early in the curing process to determine the time and temperature at which bond was assumed to have developed for the typical concrete mix used in MnDOT prestressed bridge girders. Based on observations made during the tests and comparisons between measured and estimated strain changes at release, it was determined that bond generally occurred between 6 and 8 hours after casting for the MnDOT bridge mix in mild summer weather. This corresponded with concrete temperatures in the range of 90 to 110°F (32.2 and 43.3°C).

Concrete cylinders were periodically tested for compressive strength and modulus of elasticity during the short girder tests to determine the early strength gain behavior of the concrete. To determine their accuracy, estimated elastic moduli values obtained using the Pauw (1960) and ACI 363 models with measured concrete compressive strengths were compared to measured moduli. It was found that both models sufficiently estimated the modulus of elasticity during the very early stages of curing (i.e., 5-8 hours after casting), but the Pauw model was more accurate later in the curing process, when girders are typically released.

Four full-scale girder fabrications were monitored from the time of tensioning to release. The four tests were selected to represent casting during a cold season, casting during a warm season, casting with the free length of strand covered, and casting with different bed occupancy during any season. Temperature readings were taken at many points along the length of the precasting bed and concrete cylinders were tested at release to determine compressive strength and modulus of elasticity. The temperature readings were used in the TEA to estimate free strand force changes (i.e., free strand represented the entire length of bed before bond and the portion of strand outside the girder after bond). The estimated free strand force changes were compared to those measured by load cells located on the dead and live ends of the strand. The comparison showed a correlation between the assumed time of bond at which the estimated force changes best matched the measured values at concrete temperatures of approximately 100°F (37.8°C), measured on Strand 1 at the center of Girder 1 for each test (i.e., weighted average concrete temperatures of 116, 97, 96, and108°F (46.7, 36.1, 35.6, and 42.2°C) for Tests 1 through 4, respectively). This was consistent with temperatures measured during the short girder tests when bond was believed to occur.

Using the measured data from each test in the TEA and assuming bond occurred when the concrete reached approximately 100°F, it was found that the effective non-recoverable strand force changes due to temperature among the four tests ranged from -2.6 to 0.7%. The effective non-recoverable strand force change was taken as the sum of the total non-recoverable strand force change due to temperature from tensioning to bond and the effective temperature adjustment made by the precasting plant (i.e., the difference between the average net measured strand force after tensioning and the MnDOT design

force). Tests 1 and 4 were performed in the coldest weather with approximately 2/3 of the bed occupied by girders. Although the precasting bed was tarped and heated prior to tensioning, the non-recoverable strand force changes due to temperature were the largest observed during these tests. Larger non-recoverable strand force changes were observed during Test 2 than Test 3, which was attributed to the bed occupancy for Test 2 being twice that of Test 3.

Two of the four full-scale girder tests were performed on MN54 shapes (i.e., 54 in. (1.37 m) deep) and the other two were performed on 82MW shapes (i.e., 82 in. (2.08 m) deep). The current MnDOT method described in Section 3.4 overestimated the release camber by up to 44% of the measured value for the MN54 shapes and up to 95% for the 82MW shapes. By implementing design recommendations made by O'Neill et al. (2012) with the MnDOT calculation method, the estimated release cambers were no more than 15% higher than the measured values for the MN54 shapes and no more than 47% higher for the 82MW shapes. The TEA for each full-scale test estimated release cambers similar to the values estimated by the MnDOT method with O'Neill's recommendations.

A number of factors not considered in the TEA were investigated to determine their potential effect on camber. These included varying concrete material properties and non-uniform strand force along the girders, deflection due to thermal gradients through the girder sections, and friction between the girders and the precasting bed. The thermal gradient was determined to be the factor most likely to reduce the camber at release. Recoverable strand force changes due to incompatibility (i.e., the difference between the coefficients of thermal expansion of concrete and steel) were considered in the TEA, but were found to be small and their effects on camber were negligible.

The TEA was found to reasonably estimate strand force changes due to temperature and camber, so a parametric study was conducted to determine the effects of temperature at different steps in the fabrication process. The current method used by the precasting plant to adjust the strand force during tensioning to account for thermal effects was compared to a proposed method that considers the amount of bed occupied by the girders. The proposed adjustment method was shown to more accurately correct the initial strand force for any bed occupancy.

Based on the conclusions made in this study, recommendations are made to improve release camber predictions and control over the fabrication process.

8.2 Conclusions

8.2.1 Temperature and Time of Concrete/Steel Bond

- Based on observations made during the short girder and full-scale tests, bond is believed to occur when the concrete temperature reaches approximately 100°F (37.8°C). Only the typical concrete mix used by the precasting plant to fabricate MnDOT bridge girders was investigated during this study, and the relationship between bond and temperature may vary between mixes.
- The time of bond based on the 100°F assumption typically fell within the range of 6 to 10 hours assumed by Barr et al. (2005), but values were observed outside of that range in cases where steam curing wasn't used.

8.2.2 Non-recoverable Strand Force due to Temperature

- Because bond is believed to occur when the concrete reaches approximately 100°F (37.8°C), lower average strand temperatures during tensioning result in larger non-recoverable strand force losses. Additionally, higher bed occupancy results in higher average strand temperatures due to concrete hydration, also resulting in larger non-recoverable strand force losses.
- The effective non-recoverable strand force changes due to temperature (i.e., the effective temperature adjustment plus the total non-recoverable strand force change due to temperature) were observed to be of similar magnitude of typical assumed strand relaxation losses during fabrication (approximately 1.3% of the MnDOT plan force).
- The current plant tensioning and force adjustment procedures were found to result in initial net strand forces that were higher than the MnDOT plan force, even when a temperature adjustment was not specified. Part of the increase was applied to account for losses during tensioning and roundup of the force in the field by the tensioning crew. The adjustments were found to reasonably reduce the effective

non-recoverable strand force losses due to temperature changes between tensioning and bond.

- The precasting plant's method of covering and heating the strands reduces the potential temperature change between tensioning and bond, thereby reducing potential non-recoverable strand force losses. In addition, it prevents low temperatures at tensioning that would require extreme strand force adjustments that could cause unsafe overstress conditions.

8.2.3 Strand Force Changes due to Restraint of Free Strand

- Temperature changes between bond and release cause force changes in the free strand and the composite girder section. The change in free strand force (i.e., "restraint force") must be equilibrated by the composite girder section. The difference in coefficients of thermal expansion of the steel and concrete in the girder also generate incompatibility forces (i.e., equal and opposite forces in the concrete and strand within the girder).
- The restraint forces, particularly due to large temperature changes due to cooling after the forms are removed, can result in large tensile stresses in the girder, which can cause cracks to develop in the concrete prior to release. This was observed in multiple girders during the full-scale tests.
- Upon cutting the strands, the restraint force in the free strand is released from the composite girder section. The portion of the strain change due to the removal of the restraint force is captured by instrumentation at release, and can be difficult to distinguish from the portion of the strain change due to elastic shortening.

8.2.4 Camber

- The measured release cambers were found to be significantly lower than estimated values using the current MnDOT estimation method and the values estimated by the computer software used by MnDOT for the 82MW girder shape.
- The current MnDOT estimation method was significantly improved by implementing recommendations made by O'Neill et al. (2012) to increase the assumed concrete compressive strength at release by 15% and replacing the ACI

363 concrete modulus of elasticity (MOE) estimation with the Pauw (1960) model. The recommendations were compared with measured concrete compressive strengths and MOE values and were found to be reasonable.

- Release camber estimations made using the TEA were found to be higher than measured values. This was attributed primarily to the reduction in deflection due to thermal gradient through the depth of the section during cooling that was not considered in the TEA. At bond, the concrete is at a zero-stress state and the temperature is relatively high and non-uniform through the section. As cooling occurs, the non-uniform temperature changes in the section can cause significant deflections. This is the same effect that causes girders exposed to sunlight on the top flange to deflect upward.
- The non-recoverable strand force changes due to temperature were found to significantly affect release camber, which could result in construction and serviceability issues if not considered. Non-recoverable strand force changes resulted in reductions in camber of 1.1 to 7.7%
- Another component of camber considered in the TEA was the change in deflection due to incompatibility forces, or forces generated within the concrete and embedded strand due to the difference between the coefficients of thermal expansion of the two materials. This deflection was found to be negligible for the full-scale tests.

8.3 Recommendations

8.3.1 Recommendations for Release Camber Prediction

To improve the prediction of camber at release, the following recommendations, originally made by O'Neill et al. (2012), should be implemented into all design calculations:

1. Increase the design concrete compressive strength at release, f'_{ci}, by a factor of 1.15 to account for higher release strengths observed during girder fabrication.

2. Replace the ACI 363 equation for estimating the modulus of elasticity of concrete at release, E_{ci}, with the Pauw (1960) equation to account for stiffer concrete observed during girder fabrication.

8.3.2 Recommended Strand Force Adjustment for Temperature

8.3.2.1 Current Procedure

Prior to tensioning, the precasting plant measures the average strand temperature with a temperature gun at approximately six locations along the bed and compares the value with the anticipated wet concrete temperature (typically between 70 and 80°F (21.1 to 26.7°C)). For every 10°F (5.6°C) difference (rounded down) between the average strand and wet concrete temperatures, one percent of the required strand force (after adjusting for losses during tensioning) is added to or subtracted from the initial pull force.

8.3.2.2 Proposed Procedure

The proposed strand force adjustment for temperature and bed occupancy described in Section 7.5, as shown in Equation (8-1), more accurately accounts for the non-recoverable strand force loss by considering the temperature change between tensioning and bond and accounting for the percent of the precasting bed occupied by girders. The average temperature of the strand in the bed at bond should be considered relative to the average temperature of the strand in the bed at tensioning. A reasonable assumption for the average concrete temperature at bond is believed to be approximately 100°F (37.8°C). It should be noted that the proposed method ignores any temperature change in the strand outside the girders between tensioning and bond.

$$\Delta P = \alpha_s E_{ps} A \frac{L_{in}}{L_{bed}} (T_{bond} - T_{tension}) \quad (8\text{-}1)$$

where:

α_s:	Coefficient of thermal expansion of steel
E_{ps}:	Strand modulus of elasticity
A:	Strand area
L_{in}:	Total length of girders on the bed (i.e., length of strand inside girders)
L_{bed}:	Length of the bed
T_{bond}:	Average temperature of the concrete at bond, 100°F (37.8°C)
$T_{tension}$:	Average temperature of the strand before tensioning

The recommended procedure to account for non-recoverable strand force loss due to temperature is compared to the plant's current procedure in Figure 8.1. The strand force adjustment for temperature is shown on the vertical axis and the average strand temperature at tensioning (i.e., the average temperature that the plant would measure along the bed prior to tensioning) is shown on the horizontal axis. The forces were determined assuming a strand area of 0.218 in^2 (141mm^2), which is that of a 0.6 in. (15 mm) diameter strand. For this example, the wet concrete temperature for the plant's current adjustment method was assumed to be 75°F (23.9°C) and the average concrete temperature at bond for the recommended method was assumed to be 100°F (37.8°). The recommended method is shown as a series of five lines, each representing a bed occupancy value ranging from 0 to 1 (representing 0 to 100% of the bed occupied by girders).

To simplify the recommended method and parallel the current procedure used by the plant, an average temperature of the strand in the bed at bond was assumed to be 95°F (35.0°C). This is shown as "Simplified Rec." in Figure 8.1. The average strand temperature at bond was selected to best match the recommended adjustment method for bed occupancies of approximately 75% and above for cases in which the average strand temperature at tensioning is lower than that at bond. This procedure is identical to the current plant procedure, except that the wet concrete temperature is replaced with the assumed average strand temperature in the bed at bond of 95°F (35.0°C).

The tension stress limit of $0.8f_{pu}$ is represented by a horizontal dashed line, assuming an initial strand pull of 45 kips (200 kN) per strand. This value should not be exceeded for code and safety considerations.

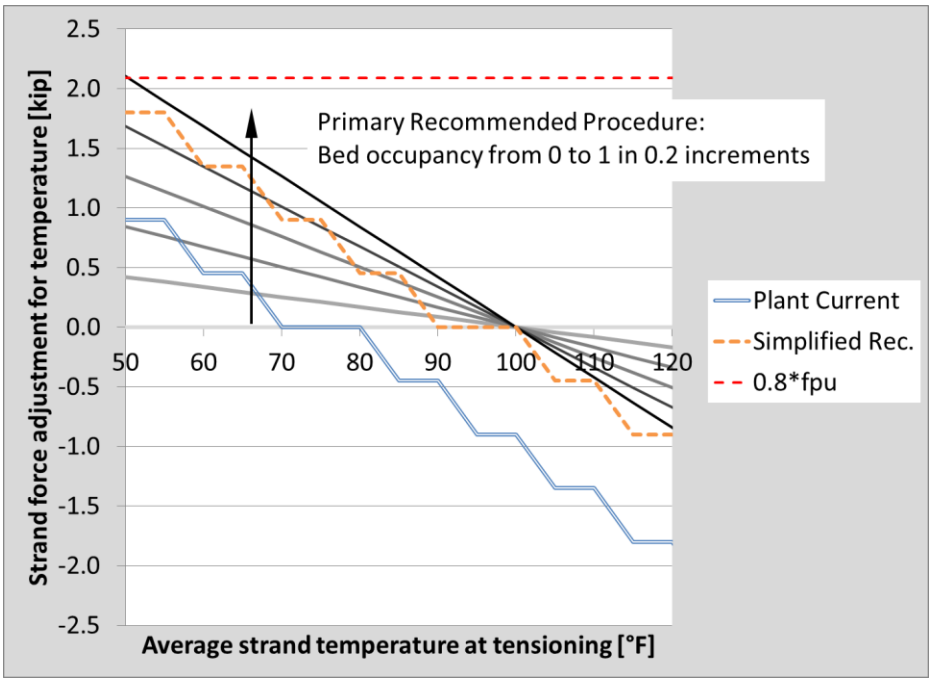

Figure 8.1: Current and recommended plant adjustment methods for losses due to temperature

8.3.3 Other Recommendations for Girder Fabrication

8.3.3.1 Tensioning

When ambient temperatures are low enough to warrant use of steam heating, the precasting plant should continue to cover the strands before tensioning and during the entire fabrication. Keeping the strand temperature relatively close to the concrete temperature at the time of bond reduces the amount of non-recoverable strand force loss due to temperature. Additionally, maintaining a constant temperature reduces the risk of the strand temperature cooling enough to overstress the strands, which is a safety concern.

The precasting plant should continue to accurately read the dial gage showing the level of preload and initial prestress. If the gage is not read straight on, the strand force

could differ from the expected force by up to 1 kip (4.4 kN), or approximately 2% of the design strand force.

8.3.3.2 Release

Girders should continue to be released as quickly as possible after the covers and formwork have been removed to reduce the effects of cooling on concrete stresses. Cooling of the concrete and free strand restraint could result in tensile stresses that could cause cracking in the girder, especially near the hold-downs.

8.3.4 Recommendation for Future Research

The effects of thermal gradients through the depth of the girder sections from bond to release were found to potentially have a significant effect on the camber at release. However, limited data was gathered for accurately estimating the effects, so multiple assumptions were made. Additional research into the effects of thermal gradients on release camber could be beneficial.

REFERENCES

AASHTO. (2010). LRFD Bridge Design Specification, 5th Edition. Washington, DC: American Association of State Highway and Transportation Officials.

ACI Committee 318. (2011). ACI 318-11 Building Code Requirements for Structural Concrete and Commentary. Farmington Hills, MI: American Concrete Institute.

ACI Committee 363. (2010). ACI 363R-10 State-of-the-Art Report on High-Strength Concrete. Farmington Hills, MI: American Concrete Institute.

Ahlborn, T., French, C., & Shield, C. (2000). *High-Strength Concrete Prestressed Bridge Girders: Long Term and Flexural Behavior*. MnDOT Report No. MN/RC 2000-32. Minnesota Department of Transportation Research Services. St. Paul, MN.

Barr, P., Eberhard, M., Stanton, J., Khaleghi, B., & Hsieh, J. C. (2000). *High Performance Concrete in Washington State SR18/SR516 Overcrossing*. Washington State Transportation Commission. Seattle, WA.

Barr, P., Stanton, J., & Eberhard, M. (2005). Effects of Temperature Variations on Precast, Prestressed Concrete Bridge Girders. *Journal of Bridge Engineering*, *10*(March), 186–194.

Briere, V., Harries, K. A., Kasan, J., & Hager, C. (2013). Dilation Behavior of Seven-wire Prestressing Strand – The Hoyer Effect. *Construction and Building Materials*, *40*, 650–658.

Erkmen, B., Shield, C. K., & French, C. E. (2008). Self-Compacting Concrete (SCC) for Prestressed Bridge Girders. MnDOT Report No. MN/RC 2008-51. Minnesota Department of Transportation Research Services. St. Paul, MN.

Janney, J. (1954). Nature of Bond in Pre-tensioned Prestressed Concrete. *ACI Journal Proceedings*, *25*(9), 717–736.

Kada, H., Lachemi, M., Petrov, N., & Aitcin, P.-C. (2002). Determination of the coefficient of thermal expansion of high performance concrete from initial setting. *Materials and Structures*, *35*(February), 35–41.

Machida, S., & Durelli, A. J. (1973). Response of a strand to axial and torsional displacements. *ARCHIVE: Journal of Mechanical Engineering Science 1959-1982 (vols 1-23)*, *15*(4), 241–251.

Newhouse, C., & Wood, T. (2008). The Effect of Temperature on the Effective Prestressing Force at Release for PCBT Girders. In *Structures Congress 2008* (pp. 1–10). Reston, VA: American Society of Civil Engineers.

O'Neill, C., & French, C. E. (2012). *Validation of Prestressed Concrete I-Beam Deflection and Camber Estimates*. MnDOT Report No. MN/RC 2012-16. Minnesota Department of Transportation Research Services. St. Paul, MN.

Pauw, A. (1960). Static Modulus of Elasticity of Concrete as Affected by Density. *ACI Journal*, *32*(6), 679–687.

PCI Committee on Prestress Losses. (1975). Recommendations for Estimating Prestress Losses. *PCI Journal*, (July-August), 43–75.

Rabbat, B. G., & Russell, H. G. (1985). Friction Coefficient of Steel on Concrete or Grout. *Journal of Structural Engineering*, *111*(3), 505–515.

APPENDIX A. DETAILED TEST PARAMETERS

A.1 General Test Parameter Values

Table A.1 lists the values of the general parameters used to perform calculations for each full-scale girder test. Table A.2 and Table A.3 provide information regarding the strand patterns at midspan and the girder ends, respectively, for each full-scale test. Table A.4 lists the values of the general parameters used to perform calculations for the short girder tests.

Table A.1: General full-scale test parameter values

Test No.	**Notation in Report**	**1**	**2**	**3**	**4**	**units**
Girder Shape		MN54	82MW	82MW	MN54	
Girder length	L_g	123.24	180.75	180.75	125.65	**ft**
No. girders on bed		2	2	1	2	
Total length of girders	$L_{g,tot}$	246.48	361.50	180.75	251.29	**ft**
Bed length	L_{bed}	356.75	386.5	386.5	386.5	**ft**
Distance from girder end to hold-down	x_{hold}	49.29	72.46	49.29	49.29	**ft**
Strand properties						
Total strand force at tensioning	$P_{s,T}$	2240.0	2848.0	2841.6	2160.0	**kip**
Ultimate tensile strength	f_{pu}	270	270	270	270	**ksi**
Modulus of elasticity	E_{ps}	28500	28500	28500	28500	**ksi**
Coefficient of thermal expansion	α_s	6.78	6.78	6.78	6.78	**με/°F**
Area of single strand	A_{strand}	0.218	0.218	0.218	0.218	**in^2**
Total area of strands	A_{ps}	10.90	13.95	13.95	10.46	**in^2**
Number of strands (total)	$N_{strand,total}$	50	64	64	48	
Number of strands (straight)	$N_{strand,straight}$	40	54	54	38	
Distance to *cgs* from bottom of section (midspan)		4.92	5.03	5.03	4.79	**in**
Distance to *cgs* from bottom of section (girder end)		12.92	15.66	15.66	13.13	**in**

Relaxation						
Yield stress	f_{py}	243	243	243	243	**ksi**
Time of tensioning	t_T	1	1	1	1	**hr**
Time of release	t_R	91	116	116	140	**hr**
Ratio of initial stress to yield stress	$P_{s,T}/A_{ps}f_{py}$	0.85	0.84	0.84	0.85	
Force loss due to relaxation	ΔP_{RET}	28.84	37.90	37.56	30.85	**kip**
Concrete material properties						
Coefficient of thermal expansion	α_c	5.67	5.67	5.67	5.67	**με/°F**
Unit weight of concrete	w_c	155	155	155	155	**pcf**
Concrete strength	f'_c	9087	9858	10213	8430	**psi**
Concrete modulus of elasticity	E_c	5895	6186	5834	5153	**ksi**
Self-weight distributed load	w_{sw}	0.067	0.095	0.095	0.067	**k/in**
Moment due to self-weight	M_{sw}	18367	56020	56020	19091	**k-in**
Gross concrete section properties						
Cross-sectional area	A_g	749	1062	1062	749	**in^2**
Moment of inertia	I_g	285230	1010870	1010870	285230	**in^4**
Distance to centroid from bottom of section	y_g	24.63	38.37	38.37	24.63	**in**
Strand eccentricity at midspan	e_{mid}	19.71	33.34	33.34	19.84	**in**
Strand eccentricity at girder end	e_{end}	11.71	22.71	22.71	11.51	**in**

Note: Sufficient information is provided in the tables to calculate net and transformed section properties for the girder sections. The net and transformed section properties are not tabulated because they change along the length of the girder due to the draped strands.

Table A.2: Strand patterns at midspan for full-scale girder tests

	Number of strands for Test No. (midspan)				
Height [in]	**1**	**2**	**3**	**4**	
2	12	16	16	12	
3	2	2	2	2	draped
4	12	16	16	12	
5	2	2	2	2	draped
6	12	12	12	12	
7	2	2	2	2	draped
8	4	8	8	2	
9	2	2	2	2	draped
10	0	2	2	0	
11	2	2	2	2	draped

Table A.3: Strand patterns at girder ends for full-scale girder tests

	Number of strands for Test No. (girder end)				
Height [in]	**1**	**2**	**3**	**4**	
2	12	16	16	12	
4	12	16	16	12	
6	12	12	12	12	
8	4	8	8	2	
10	0	2	2	0	
43	2	0	0	2	draped
45	2	0	0	2	draped
47	2	0	0	2	draped
49	2	0	0	2	draped
51	2	0	0	2	draped
71	0	2	2	0	draped
73	0	2	2	0	draped
75	0	2	2	0	draped
77	0	2	2	0	draped
79	0	2	2	0	draped

Table A.4: General short girder test parameter values

Short Girder No.	**Notation in Report**	**1**	**2**	**3**	**4**	**5**	**6**	**units**
Release Time After Casting		5.1	5.6	6.4	8.1	8.1	25.9	**hr**
Girder length	L_g	8	8	8	8	8	8	**ft**
Bed length	L_{bed}	76.68	76.68	76.68	76.68	76.68	76.68	**ft**
Strand properties								
Number of bonded strands	N_{strand}	2	2	4	4	4	4	
Total strand force at tensioning	$P_{s,T}$	82.6	85.6	158.6	170.9	170.9	165.8	**kip**
Ultimate tensile strength	f_{pu}	270	270	270	270	270	270	**ksi**
Modulus of elasticity	E_{ps}	28500	28500	28500	28500	28500	28500	**ksi**
Coefficient of thermal expansion	α_s	6.78	6.78	6.78	6.78	6.78	6.78	**με/°F**
Area of single strand	A_{strand}	0.218	0.218	0.218	0.218	0.218	0.218	**in^2**
Total area of bonded strands	A_{ps}	0.436	0.436	0.872	0.872	0.872	0.872	**in^2**
Distance to *cgs* from bottom of section (midspan)		4	4	4	4	4	4	**in**
Relaxation								
Yield stress	f_{py}	243	243	243	243	243	243	**ksi**
Time of tensioning	t_T	1	1	1	1	1	1	**hr**
Time of release	t_R	47	48	49	51	51	68	**hr**
Ratio of initial stress to yield stress	$P_{s,T}/A_{ps}f_{py}$	0.78	0.81	0.75	0.81	0.81	0.78	
Stress loss due to relaxation	ΔP_{RET}	1.62	1.89	1.35	1.90	1.90	1.80	**ksi**

Concrete material properties								
Coefficient of thermal expansion	α_c	5.67	5.67	5.67	5.67	5.67	5.67	**με/°F**
Concrete compressive strength at release	f'_c	547	803	1465	2945	2945	8307	**psi**
Concrete modulus of elasticity at release	E_c	1275	2199	2594	3408	3408	5408	**ksi**
Concrete section properties								
Width		36	36	36	36	36	36	**in**
Height		8	8	8	8	8	8	**in**
Distance to centroid from bottom of section	y_g	4	4	4	4	4	4	**in**
Gross concrete area	A_g	288	288	288	288	288	288	**in^2**
Area of PVC for debonded strands		0.442	0.442	0.442	0.442	0.442	0.442	**in^2**
Total area of PVC		6.185	6.185	5.301	5.301	5.301	5.301	**in^2**
Net concrete area (includes reduction in area for PVC on debonded strands)	A_{net}	281.38	281.38	281.83	281.83	281.83	281.83	**in^2**
Transformed section area	A_{trans}	291.12	287.03	291.41	289.12	289.12	286.42	**in^2**

A.2 Thermal Effects Analysis

The values used to perform the thermal effects analysis (TEA) for each full-scale test are detailed in Table A.5. The values used to perform the TEA for the short girder tests are detailed in Table A.6.

Table A.5: Thermal effects analysis details for full-scale tests

Thermal Effects Analysis

Test No.	**Notation in Report**	**1**	**2**	**3**	**4**	**units**
Tensioning (Step T*)*						
Total strand force at tensioning	$\mathbf{P_{s,T}}$	2240.0	2812.2	2812.2	2160.0	**kip**
Average strand temperature (full bed length)	$\mathbf{T_T}$	45.8	69.1	66.5	56.6	**°F**
Bond (Step B*)*						
Assumed time of bond		8.2	11.1	6.9	8.0	**hr**
Average concrete temperature	$\mathbf{T_{c,B}}$	116.5	97.5	138.9	107.4	**°F**
Average free strand temperature	$\mathbf{T_{free,B}}$	42.1	85.5	42.4	79.5	**°F**
Average concrete temperature change	$\mathbf{\Delta T_{c,T-B}}$	70.7	28.4	72.4	50.8	**°F**
Average free strand temperature change	$\mathbf{\Delta T_{free,T-B}}$	-3.8	16.4	-24.1	23.0	**°F**
Strand force change due to temperature from tensioning to bond	$\mathbf{\Delta P_{s,T-B}}$	-100.4	-74.6	-28.9	-83.0	**kip**
Total strand force at bond	$\mathbf{P_{s,B}}$	2139.6	2737.6	2812.7	2077.0	**kip**
Release (Step R*)*						
Average concrete temperature	$\mathbf{T_{c,R}}$	115.2	78.6	98.8	127.4	**°F**
Average free strand temperature	$\mathbf{T_{free,R}}$	26.9	66.1	52.6	44.1	**°F**
Average concrete temperature change	$\mathbf{\Delta T_{c,B-R}}$	-1.3	-18.9	-40.1	20.0	**°F**
Average free strand temperature change	$\mathbf{\Delta T_{free,B-R}}$	-15.2	-19.4	10.2	-35.4	**°F**
Just before release						

Change in free strand force due to temperature	$\Delta P_{free,B-R}$	32.3	368.2	9.5	6.8	**kip**
Resultant concrete force at *cgs* due to temperature	$\Delta P_{c,B-R,before}$	29.7	338.1	10.1	12.5	**kip**
Change in girder strand force due to temperature	$\Delta P_{s,B-R,before}$	2.6	29.1	-0.6	-5.7	**kip**
Immediately after release						
Change in girder strand force due to temperature	$\Delta P_{s,B-R,after}$	0.4	7.4	-1.1	-5.7	**kip**
Change in strain at midspan at *cgs* due to elastic shortening	$\Delta\varepsilon_{ES}(y_{cgs})$	-674.4	-547.7	-594.2	-726.8	**με**
Upward deflection due to strand force transfer at midspan	D_{ps}	5.60	7.30	7.85	6.24	**in**
Downward deflection due to self-weight at midspan	D_{sw}	2.38	4.20	4.44	2.93	**in**
Change in deflection due to temperature effects at midspan	$\Delta D_{temp,B-R}$	0.00	0.02	0.00	-0.02	**in**
Camber	C_R	3.22	3.13	3.41	3.29	**in**

Table A.6: Thermal effects analysis details for short girder tests

Thermal Effects Analysis

Girder No.		**1**	**2**	**3**	**4**	**5**	**6**	
Tensioning (Step T*)*								
Total strand force at tensioning	$\mathbf{P_{s,T}}$	82.6	85.6	158.6	170.9	170.9	165.8	**kip**
Average strand temperature (full bed length)	$\mathbf{T_T}$	67.0	66.7	66.7	66.9	67.5	67.6	**°F**
Bond (Step B*)*								
Assumed time of bond		5.1	5.6	6.0	6.0	6.0	6.0	**hr**
Average concrete temperature	$\mathbf{T_{c,B}}$	78.3	78.4	81.6	82.2	84.1	85.5	**°F**
Average free strand temperature	$\mathbf{T_{free,B}}$	76.0	77.3	77.8	77.8	77.5	77.3	**°F**
Average concrete temperature change	$\mathbf{\Delta T_{c,T\text{-}B}}$	11.3	11.7	14.9	15.3	16.7	17.9	**°F**
Average free strand temperature change	$\mathbf{\Delta T_{free,T\text{-}B}}$	9.0	10.6	11.2	10.9	10.0	9.7	**°F**
Strand force change due to temperature from tensioning to bond	$\mathbf{\Delta P_{s,T\text{-}B}}$	-0.8	-0.9	-1.9	-1.9	-1.8	-1.8	**kip**
Total strand force at bond	$\mathbf{P_{s,B}}$	81.8	84.7	156.7	169.0	169.1	164.1	**kip**

Release (Step R*)*								
Average concrete temperature	$\mathbf{T_{c,R}}$	78.3	78.4	83.8	95.5	98.2	104.2	**°F**
Average free strand temperature	$\mathbf{T_{free,R}}$	76.0	77.3	79.3	85.2	84.9	77.7	**°F**
Average concrete temperature change	$\mathbf{\Delta T_{c,B\text{-}R}}$	0.0	0.0	2.2	13.3	14.0	18.7	**°F**
Average free strand temperature change	$\mathbf{\Delta T_{free,B\text{-}R}}$	0.0	0.0	1.4	7.5	7.4	0.4	**°F**
Just before release								
Change in free strand force due to temperature	$\mathbf{\Delta P_{free,B\text{-}R}}$	0.00	0.00	-0.28	-1.48	-1.47	-0.37	**kip**
Resultant concrete force at *cgs* due to temperature	$\mathbf{\Delta P_{c,B\text{-}R,before}}$	0.00	0.00	-0.21	-1.08	-1.06	0.14	**kip**
Change in girder strand force due to temperature	$\mathbf{\Delta P_{s,B\text{-}R,before}}$	0.00	0.00	-0.07	-0.40	-0.41	-0.51	**kip**
Immediately after release								
Change in strain at midspan at *cgs* due to elastic shortening	$\mathbf{\Delta \varepsilon_{ES}(y_{cgs})}$	-218.8	-133.2	-206.3	-170.4	-170.5	-105.2	**με**

APPENDIX B. STRAIN GAGE DATA DURING TENSIONING

During full-scale girder Tests 1 through 3, temperature data was not recorded along the length of the bed during tensioning. Because the strands lay tangled on the bed prior to tensioning (see Figure B.1), foil strain gages and accompanying thermocouples were attached to the strand just inside the dead end (DE) abutment, where the strand pattern was still discernable (see Figure B.2, showing the strands before gages were applied). These gages were used to obtain strain readings during tensioning, as well as during the remainder of the fabrication. After tensioning was completed, the remainder of the foil strain gage and thermocouples were placed at the desired locations along the length of the bed. This often took several hours, during which the temperature profile of the strands could change significantly. Because the thermal effects analysis (TEA) described in Chapter 3 was dependent on the average strand temperature change between tensioning and bond to determine the non-recoverable force change due to temperature that was "locked" into the girders, it was important to determine the average temperature of the strands at tensioning.

To determine the average temperature of the strands at tensioning, the readings from the foil strain gages on the DE were used to determine the point in time at which the strand strain returned to the observed values just after tensioning. Before casting the concrete, the strand force must be equilibrated by the abutments on either end of the bed and constant along its length. Consequently, the average temperature change along the strand dictates the strain changes that occur and the strain changes are measurable at any point along the length of the strand. Therefore, when the measured strain at the DE of the strand returned to the value just after tensioning, the average strand temperature was assumed to have been the same, as well.

Figure B.3 shows the dead end foil strain gage readings during and shortly after tensioning with respect to time for Test 1. Figure B.4, Figure B.5, Figure B.6, and Figure B.7 show the dead end foil strain gage readings with respect to time from tensioning until the time casting began for Tests 1, 2, 3, and 4, respectively. For Test 1, it was determined that the average strand temperature returned to the temperature during tensioning just before casting began, so the average strand temperature at 0 hours was assumed to be the

datum temperature. Note that the time of zero corresponded to the beginning of casting, so any time before casting was negative. For Test 2, it was determined that the strand temperature was relatively constant during and just after tensioning because external heating was not used. The temperature measured by the thermocouple located on Strand 1 at the dead end of the bed at the time of tensioning was assumed as the temperature datum for Test 2. For Test 3, the temperature datum was assumed to be the average strand temperature at -23 hours. For Test 4, the average strand temperature was recorded before tensioning began, so no assumptions using the DE strain gage readings were made.

Figure B.1: Strands lying on precasting bed near hold-down prior to tensioning

Figure B.2: Straight strands fed through dead end abutment prior to tensioning (before gages were applied)

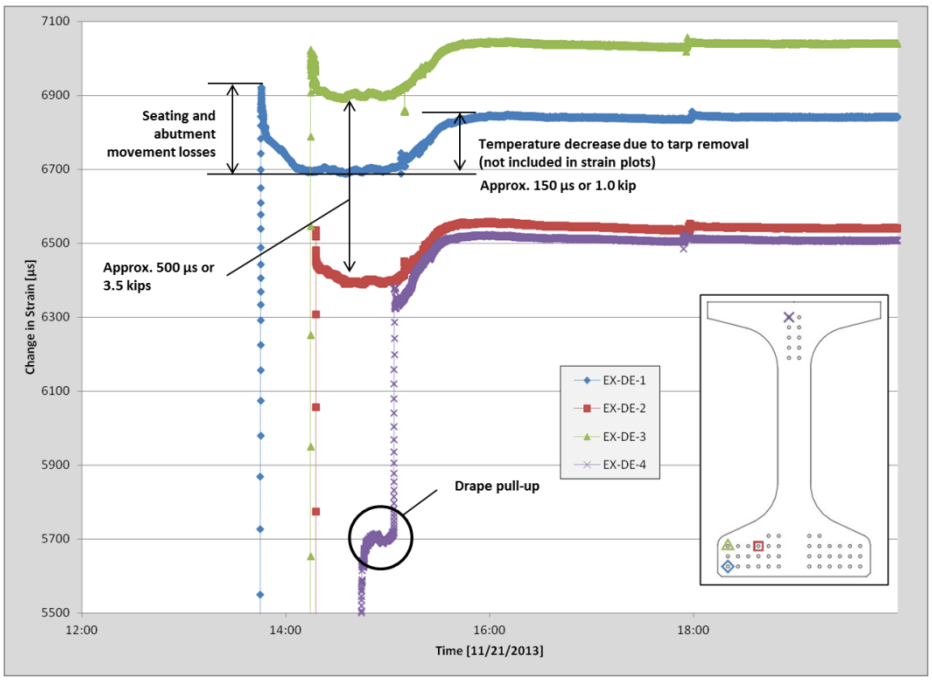

Figure B.3: Dead end foil strain gage readings during tensioning for Test 1

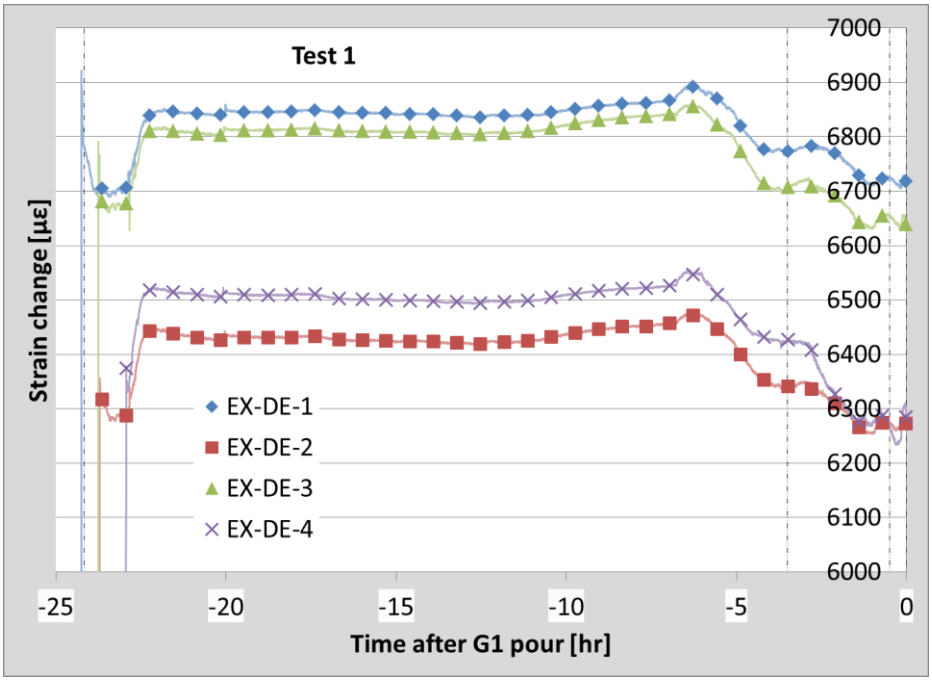

Figure B.4: Dead end foil strain gage readings from tensioning to casting for Test 1

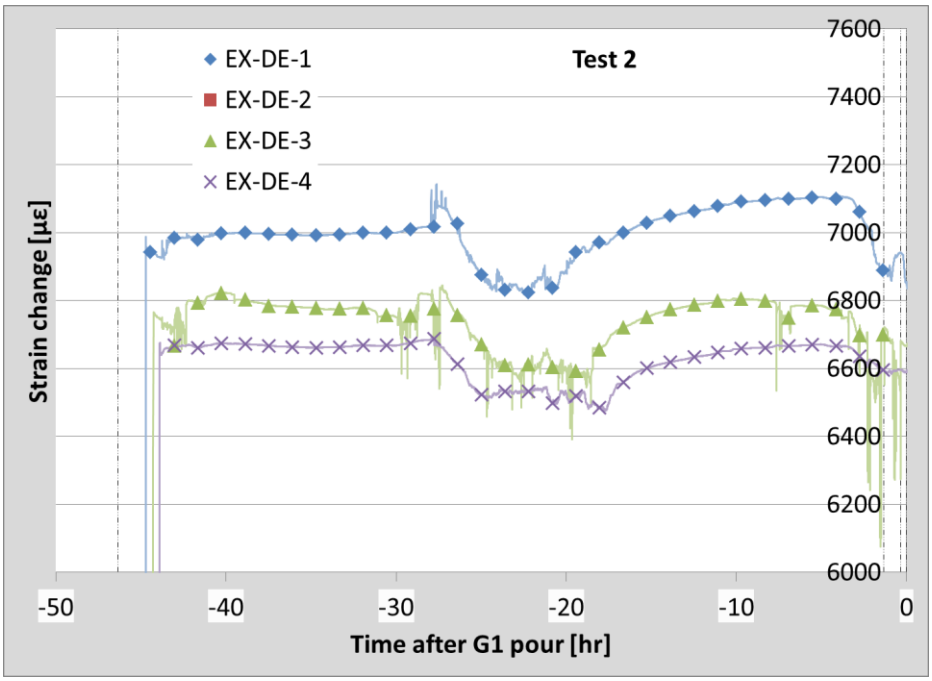

Figure B.5: Dead end foil strain gage readings from tensioning to casting for Test 2

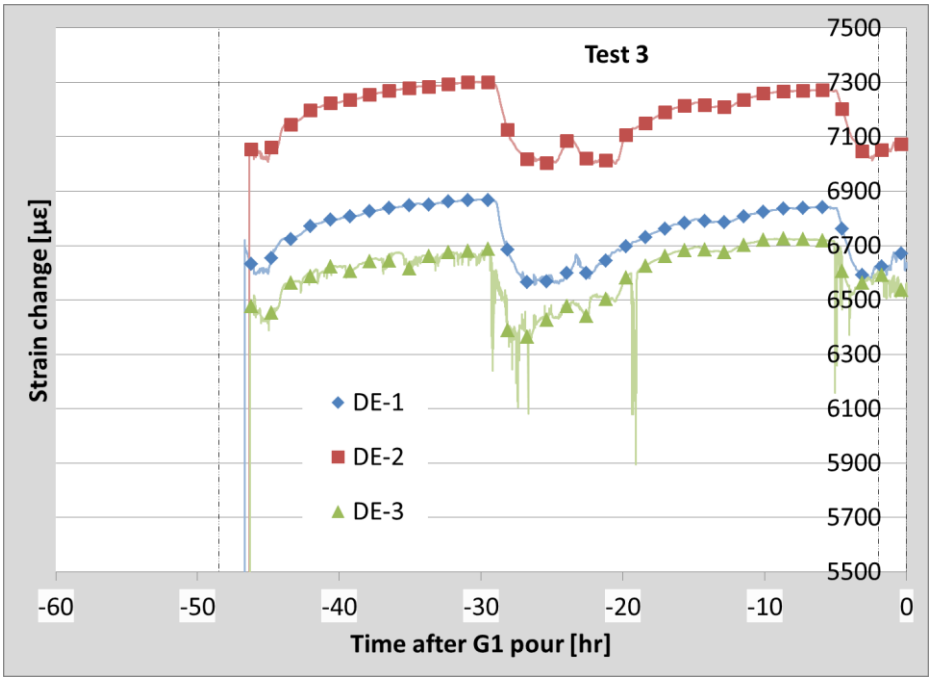

Figure B.6: Dead end foil strain gage readings from tensioning to casting for Test 3

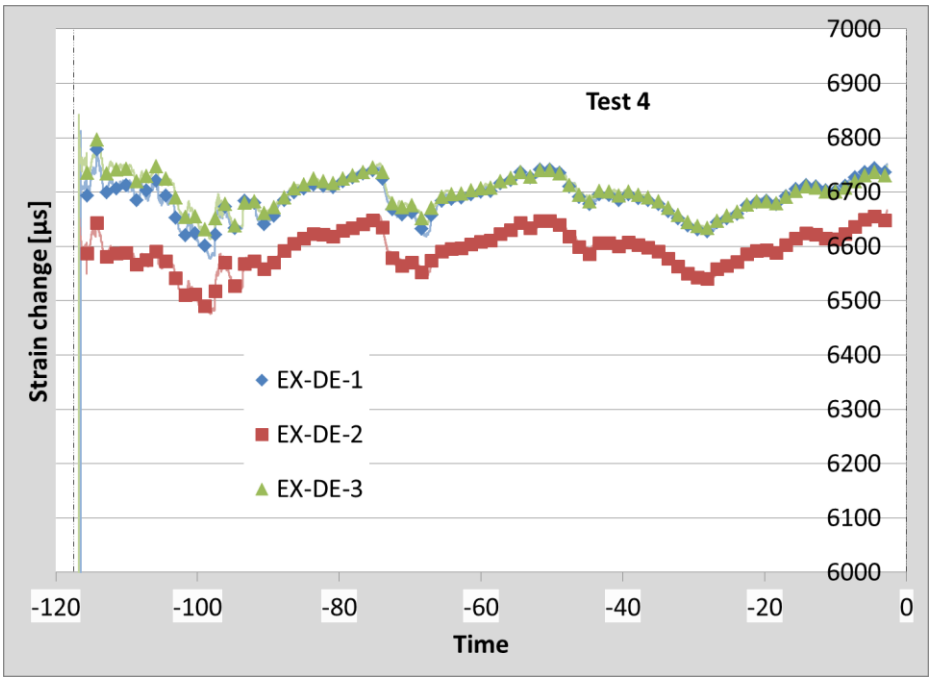

Figure B.7: Dead end foil strain gage readings from tensioning to casting for Test 4

APPENDIX C. TENSIONING SHEETS

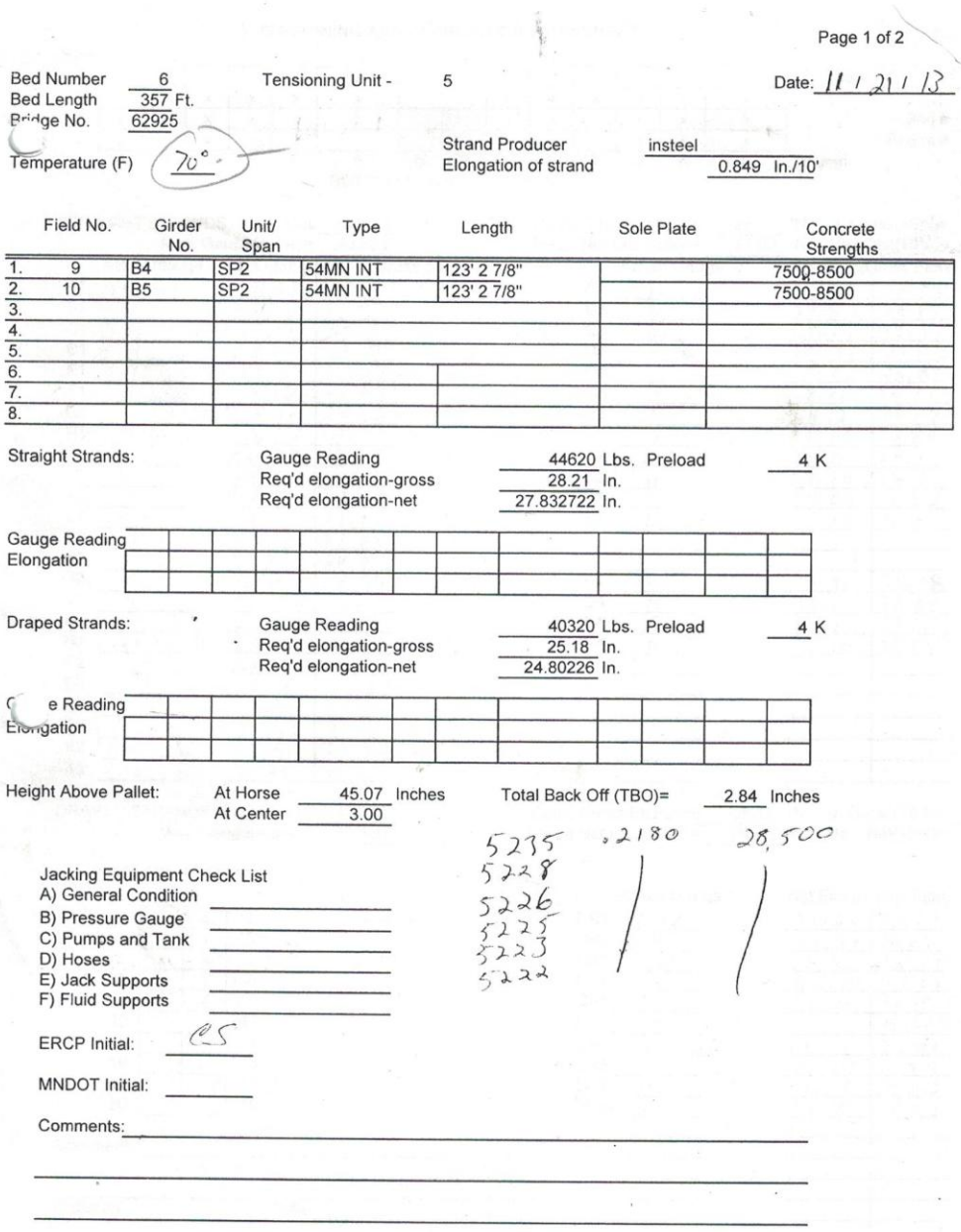

Page 1 of 2

Bed Number 6 Tensioning Unit - 5 Date: 11/21/13
Bed Length 357 Ft.
Bridge No. 62925
Temperature (F) 70°
Strand Producer insteel
Elongation of strand 0.849 In./10'

	Field No.	Girder No.	Unit/ Span	Type	Length	Sole Plate	Concrete Strengths
1.	9	B4	SP2	54MN INT	123' 2 7/8"		7500-8500
2.	10	B5	SP2	54MN INT	123' 2 7/8"		7500-8500
3.							
4.							
5.							
6.							
7.							
8.							

Straight Strands:
Gauge Reading 44620 Lbs. Preload 4 K
Req'd elongation-gross 28.21 In.
Req'd elongation-net 27.832722 In.

Gauge Reading												
Elongation												

Draped Strands:
Gauge Reading 40320 Lbs. Preload 4 K
Req'd elongation-gross 25.18 In.
Req'd elongation-net 24.80226 In.

Gauge Reading												
Elongation												

Height Above Pallet: At Horse 45.07 Inches At Center 3.00
Total Back Off (TBO)= 2.84 Inches

5235 .2180 28,500
5228
5226
5225
5223
5222

Jacking Equipment Check List
A) General Condition
B) Pressure Gauge
C) Pumps and Tank
D) Hoses
E) Jack Supports
F) Fluid Supports

ERCP Initial: CS

MNDOT Initial:

Comments:

Figure C.1: Test 1 tensioning sheet – page 1 of 2

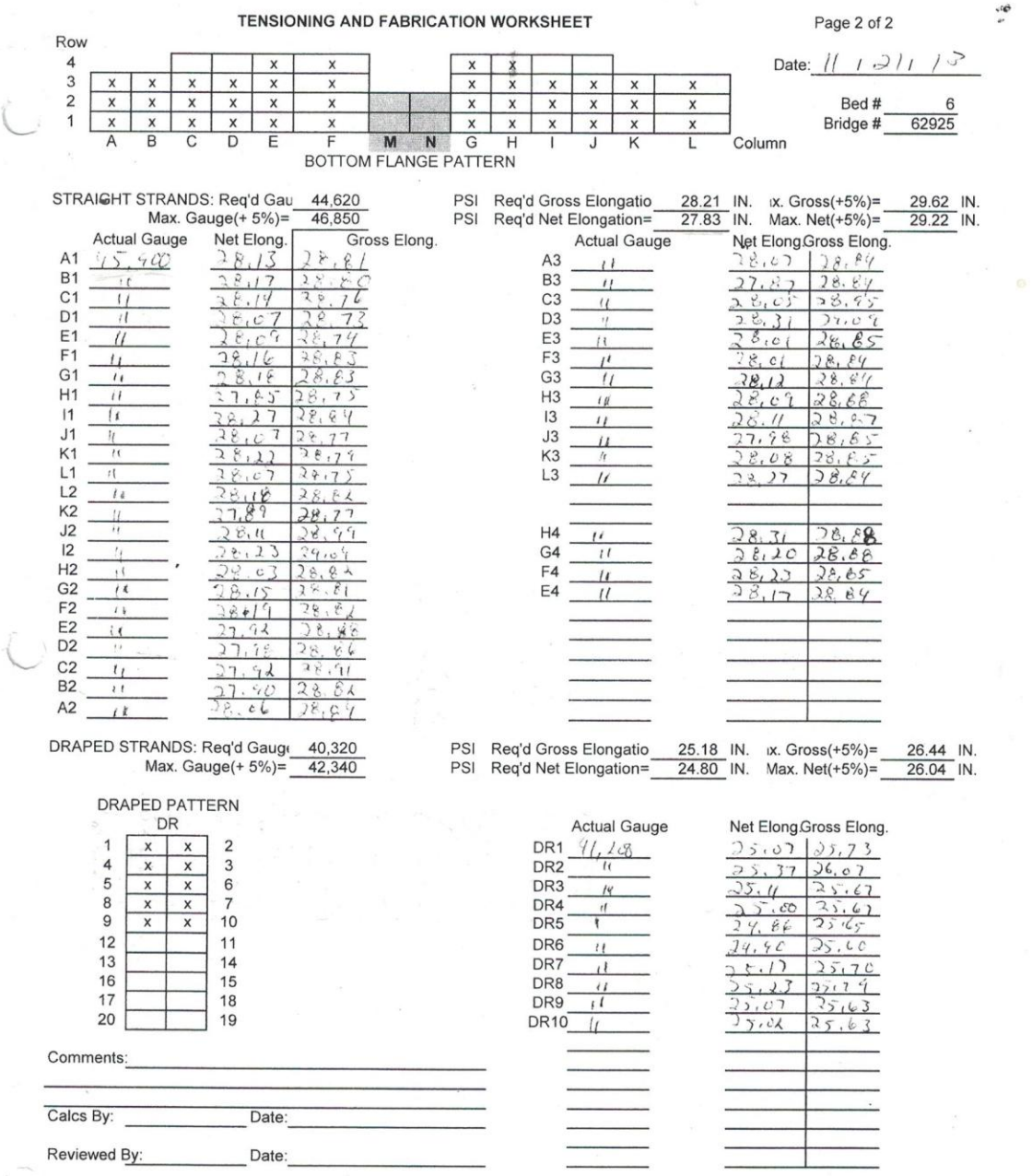

TENSIONING AND FABRICATION WORKSHEET

Page 2 of 2

Date: 11/21/13

Bed # 6

Bridge # 62925

Row

Row	A	B	C	D	E	F	M	N	G	H	I	J	K	L
4					x	x			x	x				
3	x	x	x	x	x	x			x	x	x	x	x	x
2	x	x	x	x	x	x			x	x	x	x	x	x
1	x	x	x	x	x	x			x	x	x	x	x	x

Column

BOTTOM FLANGE PATTERN

STRAIGHT STRANDS: Req'd Gau 44,620 PSI Req'd Gross Elongatio 28.21 IN. ıx. Gross(+5%)= 29.62 IN.

Max. Gauge(+ 5%)= 46,850 PSI Req'd Net Elongation= 27.83 IN. Max. Net(+5%)= 29.22 IN.

	Actual Gauge	Net Elong.	Gross Elong.
A1	45,400	28.13	28.81
B1	"	28.17	28.85
C1	"	28.14	28.76
D1	"	28.07	28.73
E1	"	28.07	28.74
F1	"	28.16	28.83
G1	"	28.18	28.83
H1	"	27.85	28.75
I1	"	28.27	28.84
J1	"	28.07	28.77
K1	"	28.22	28.79
L1	"	28.07	28.75
L2	"	28.18	28.82
K2	"	27.89	28.77
J2	"	28.11	28.79
I2	"	28.23	29.04
H2	"	28.03	28.82
G2	"	28.15	28.81
F2	"	28.19	28.82
E2	"	27.92	28.86
D2	"	27.79	28.86
C2	"	27.92	28.91
B2	"	27.90	28.82
A2	"	28.06	28.84

	Actual Gauge	Net Elong.	Gross Elong.
A3	"	28.07	28.84
B3	"	27.87	28.84
C3	"	28.05	28.95
D3	"	28.31	29.09
E3	"	28.04	28.85
F3	"	28.04	28.84
G3	"	28.12	28.84
H3	"	28.09	28.88
I3	"	28.11	28.87
J3	"	27.98	28.85
K3	"	28.08	28.85
L3	"	28.27	28.84
H4	"	28.31	28.88
G4	"	28.20	28.88
F4	"	28.23	28.85
E4	"	28.17	28.84

DRAPED STRANDS: Req'd Gaug 40,320 PSI Req'd Gross Elongatio 25.18 IN. ıx. Gross(+5%)= 26.44 IN.

Max. Gauge(+ 5%)= 42,340 PSI Req'd Net Elongation= 24.80 IN. Max. Net(+5%)= 26.04 IN.

DRAPED PATTERN

DR			
1	x	x	2
4	x	x	3
5	x	x	6
8	x	x	7
9	x	x	10
12			11
13			14
16			15
17			18
20			19

	Actual Gauge	Net Elong.	Gross Elong.
DR1	41,208	25.07	25.73
DR2	"	25.37	26.07
DR3	"	25.11	25.67
DR4	"	25.60	26.27
DR5	"	24.86	25.65
DR6	"	24.40	25.60
DR7	"	25.17	25.70
DR8	"	25.23	25.79
DR9	"	25.07	25.63
DR10	"	25.02	25.63

Comments: _____

Calcs By: _____ Date: _____

Reviewed By: _____ Date: _____

Figure C.2: Test 1 tensioning sheet – page 2 of 2

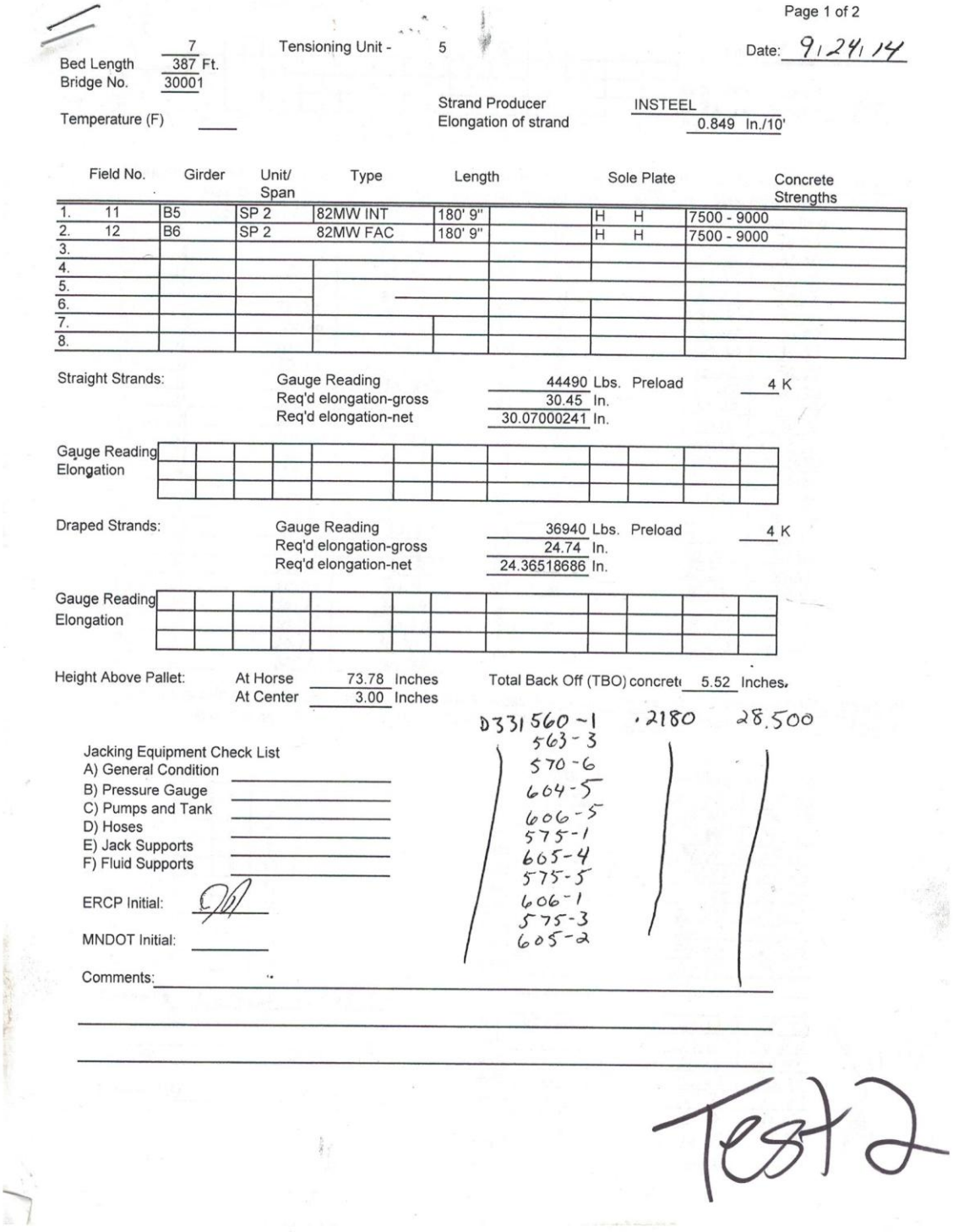

Page 1 of 2

Date: 9/24/14

7 Tensioning Unit - 5

Bed Length 387 Ft.
Bridge No. 30001

Temperature (F) ____

Strand Producer INSTEEL
Elongation of strand 0.849 In./10'

	Field No.	Girder	Unit/ Span	Type	Length		Sole Plate		Concrete Strengths
1.	11	B5	SP 2	82MW INT	180' 9"		H	H	7500 - 9000
2.	12	B6	SP 2	82MW FAC	180' 9"		H	H	7500 - 9000
3.									
4.									
5.									
6.									
7.									
8.									

Straight Strands:
Gauge Reading 44490 Lbs. Preload 4 K
Req'd elongation-gross 30.45 In.
Req'd elongation-net 30.07000241 In.

Gauge Reading												
Elongation												

Draped Strands:
Gauge Reading 36940 Lbs. Preload 4 K
Req'd elongation-gross 24.74 In.
Req'd elongation-net 24.36518686 In.

Gauge Reading												
Elongation												

Height Above Pallet: At Horse 73.78 Inches
At Center 3.00 Inches

Total Back Off (TBO) concrete 5.52 Inches

D331560-1 .2180 28.500
563-3
570-6
604-5
606-5
575-1
605-4
575-5
606-1
575-3
605-2

Jacking Equipment Check List
A) General Condition ____
B) Pressure Gauge ____
C) Pumps and Tank ____
D) Hoses ____
E) Jack Supports ____
F) Fluid Supports ____

ERCP Initial: ____

MNDOT Initial: ____

Comments: ____

Test 2

Figure C.3: Test 2 tensioning sheet – page 1 of 2

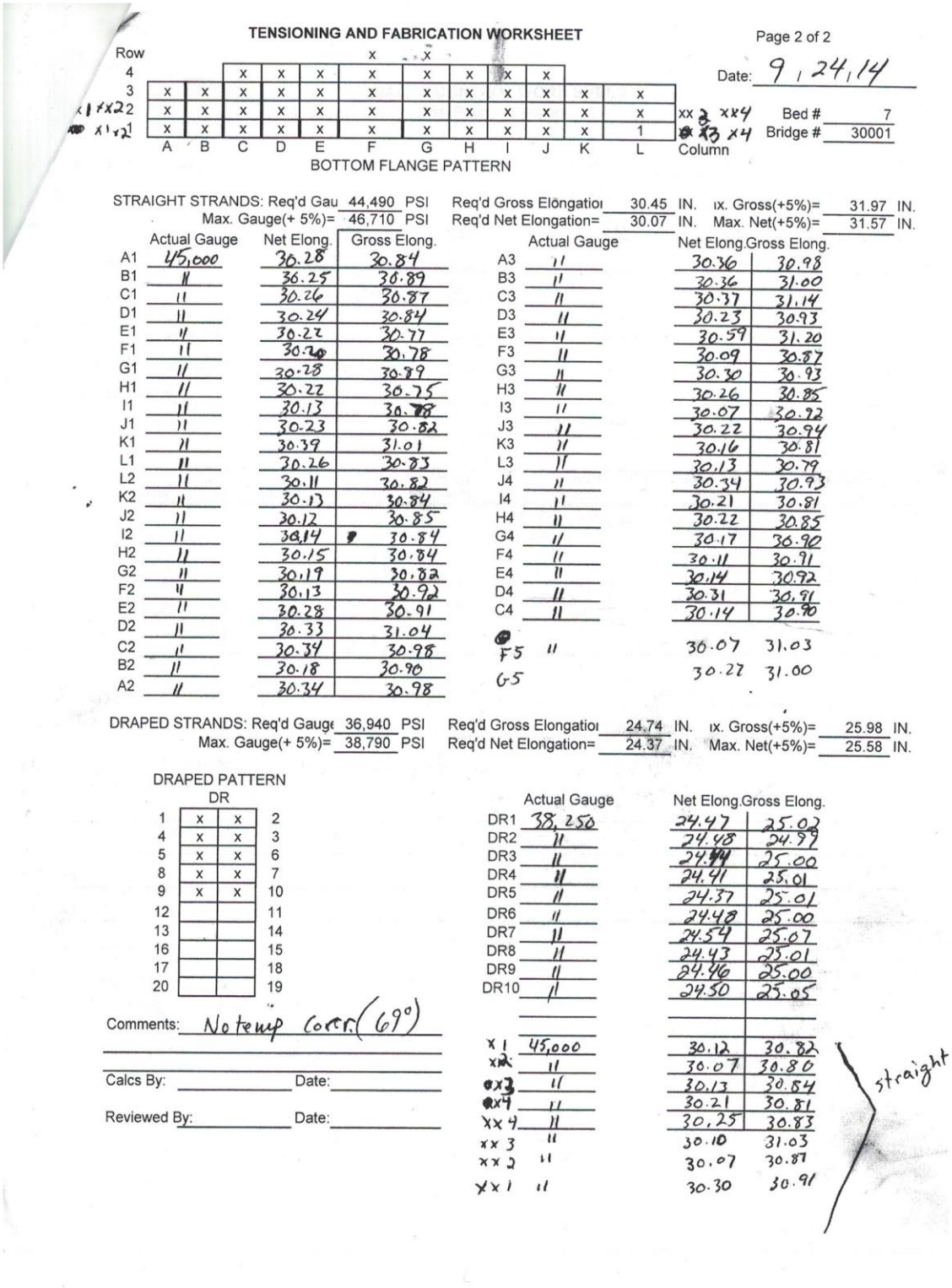

TENSIONING AND FABRICATION WORKSHEET

Page 2 of 2

Date: 9 / 24 / 14

Bed # 7

Bridge # 30001

BOTTOM FLANGE PATTERN

Row	A	B	C	D	E	F	G	H	I	J	K	L
4			x	x	x	x	x	x	x	x		
3	x	x	x	x	x	x	x	x	x	x	x	x
2	x	x	x	x	x	x	x	x	x	x	x	x
1	x	x	x	x	x	x	x	x	x	x	x	1

Column

STRAIGHT STRANDS: Req'd Gau 44,490 PSI Max. Gauge(+ 5%)= 46,710 PSI

Req'd Gross Elongatio 30.45 IN. Req'd Net Elongation= 30.07 IN.

Max. Gross(+5%)= 31.97 IN. Max. Net(+5%)= 31.57 IN.

	Actual Gauge	Net Elong.	Gross Elong.
A1	45,000	30.28	30.84
B1	"	30.25	30.89
C1	"	30.26	30.87
D1	"	30.24	30.84
E1	"	30.22	30.77
F1	"	30.20	30.78
G1	"	30.28	30.89
H1	"	30.22	30.75
I1	"	30.13	30.88
J1	"	30.23	30.82
K1	"	30.39	31.01
L1	"	30.26	30.83
L2	"	30.11	30.82
K2	"	30.13	30.84
J2	"	30.12	30.85
I2	"	30.14	30.84
H2	"	30.15	30.84
G2	"	30.19	30.82
F2	"	30.13	30.92
E2	"	30.28	30.91
D2	"	30.33	31.04
C2	"	30.34	30.98
B2	"	30.18	30.90
A2	"	30.34	30.98

	Actual Gauge	Net Elong.	Gross Elong.
A3	"	30.36	30.98
B3	"	30.36	31.00
C3	"	30.37	31.14
D3	"	30.23	30.93
E3	"	30.59	31.20
F3	"	30.09	30.87
G3	"	30.30	30.93
H3	"	30.26	30.85
I3	"	30.07	30.72
J3	"	30.22	30.94
K3	"	30.16	30.81
L3	"	30.13	30.79
J4	"	30.34	30.93
I4	"	30.21	30.81
H4	"	30.22	30.85
G4	"	30.17	30.90
F4	"	30.11	30.91
E4	"	30.14	30.92
D4	"	30.31	30.91
C4	"	30.14	30.90
F5	"	30.07	31.03
G5		30.27	31.00

DRAPED STRANDS: Req'd Gauge 36,940 PSI Max. Gauge(+ 5%)= 38,790 PSI

Req'd Gross Elongatio 24.74 IN. Req'd Net Elongation= 24.37 IN.

Max. Gross(+5%)= 25.98 IN. Max. Net(+5%)= 25.58 IN.

DRAPED PATTERN

DR

1	x	x	2
4	x	x	3
5	x	x	6
8	x	x	7
9	x	x	10
12			11
13			14
16			15
17			18
20			19

	Actual Gauge	Net Elong.	Gross Elong.
DR1	38,250	24.47	25.02
DR2	"	24.48	24.97
DR3	"	24.44	25.00
DR4	"	24.41	25.01
DR5	"	24.37	25.01
DR6	"	24.48	25.00
DR7	"	24.54	25.07
DR8	"	24.43	25.01
DR9	"	24.46	25.00
DR10	"	24.50	25.05
x1	45,000	30.12	30.82
x2	"	30.07	30.80
x3	"	30.13	30.84
x4	"	30.21	30.81
xx4	"	30.25	30.83
xx3	"	30.10	31.03
xx2	"	30.07	30.87
xx1	"	30.30	30.91

straight

Comments: No temp corr. (69°)

Calcs By: Date:

Reviewed By: Date:

Figure C.4: Test 2 tensioning sheet – page 2 of 2

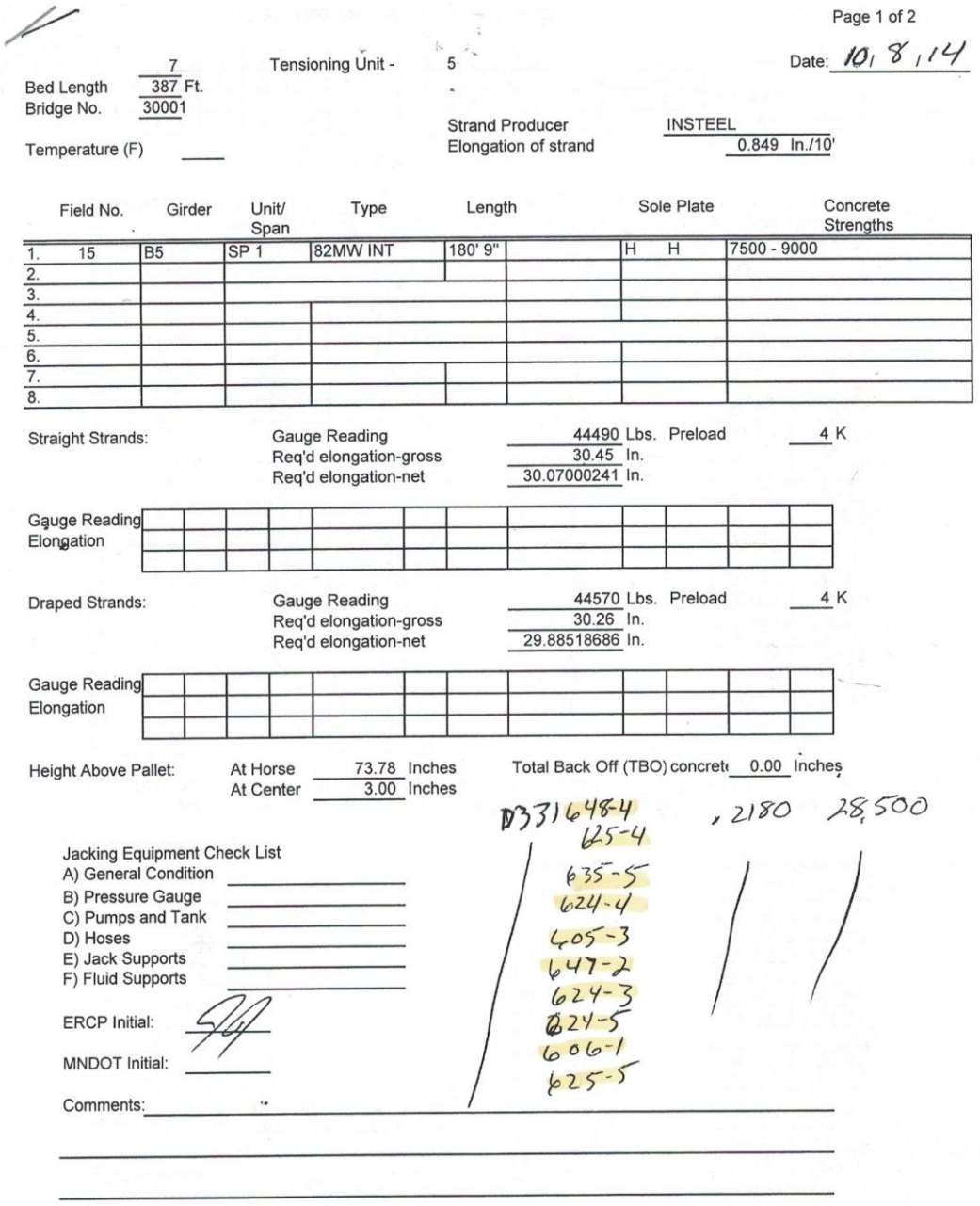

Page 1 of 2

Date: 10/8/14

7 Tensioning Unit - 5

Bed Length 387 Ft.
Bridge No. 30001

Temperature (F) ____

Strand Producer INSTEEL
Elongation of strand 0.849 In./10'

Field No.	Girder	Unit/ Span	Type	Length		Sole Plate	Concrete Strengths
1. 15	B5	SP 1	82MW INT	180' 9"		H H	7500 - 9000
2.							
3.							
4.							
5.							
6.							
7.							
8.							

Straight Strands:
Gauge Reading 44490 Lbs. Preload 4 K
Req'd elongation-gross 30.45 In.
Req'd elongation-net 30.07000241 In.

Gauge Reading												
Elongation												

Draped Strands:
Gauge Reading 44570 Lbs. Preload 4 K
Req'd elongation-gross 30.26 In.
Req'd elongation-net 29.88518686 In.

Gauge Reading												
Elongation												

Height Above Pallet: At Horse 73.78 Inches
At Center 3.00 Inches
Total Back Off (TBO) concrete 0.00 Inches

D3316484 ,2180 28,500
625-4
635-5
624-4
605-3
647-2
624-3
624-5
606-1
625-5

Jacking Equipment Check List
A) General Condition ____
B) Pressure Gauge ____
C) Pumps and Tank ____
D) Hoses ____
E) Jack Supports ____
F) Fluid Supports ____

ERCP Initial: ____
MNDOT Initial: ____

Comments: ____

Figure C.5: Test 3 tensioning sheet – page 1 of 2

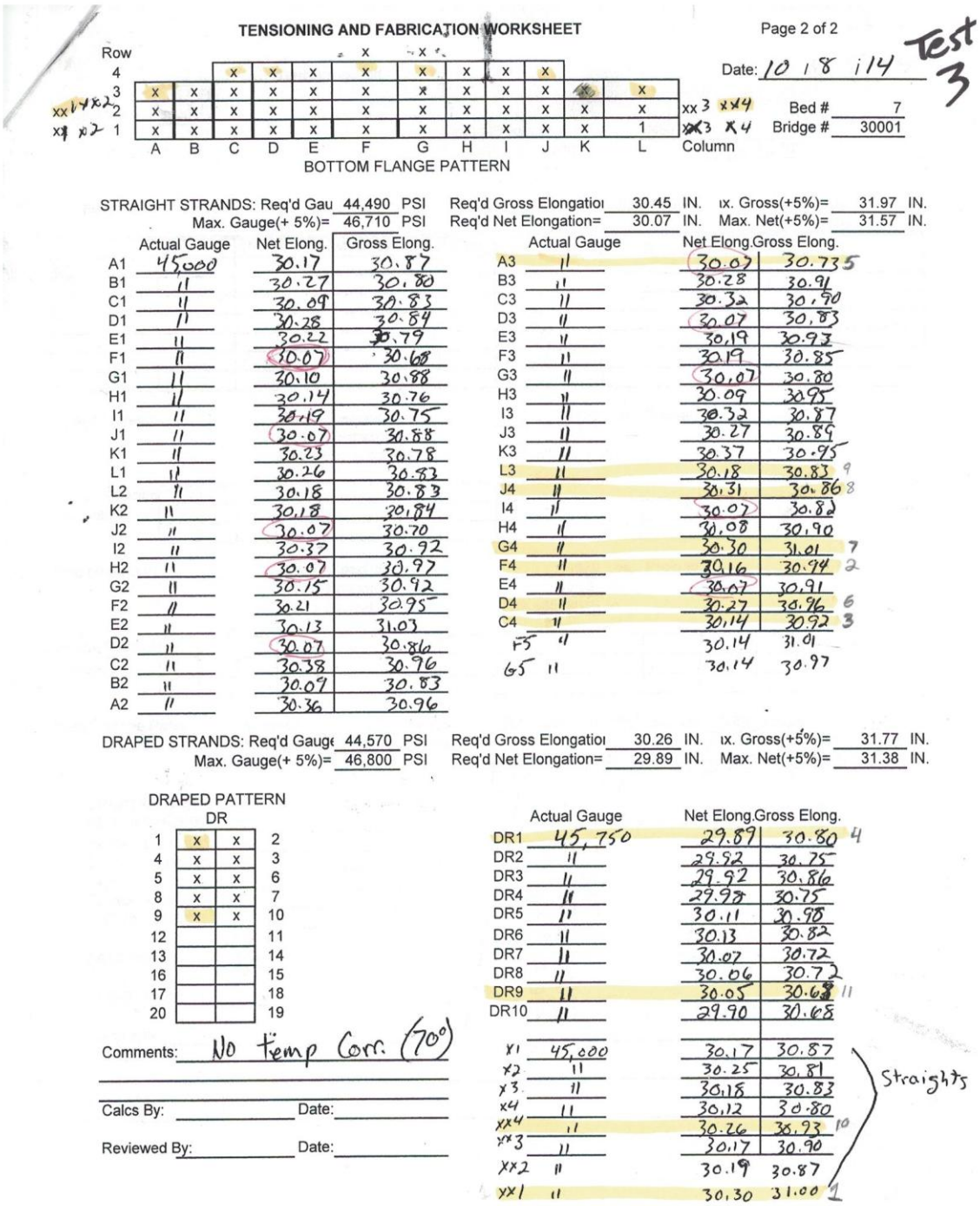

TENSIONING AND FABRICATION WORKSHEET

Page 2 of 2

Test 3

Date: 10 / 8 / 14

Bed # 7

Bridge # 30001

Row / Column

BOTTOM FLANGE PATTERN

STRAIGHT STRANDS: Req'd Gau 44,490 PSI — Max. Gauge(+ 5%)= 46,710 PSI

Req'd Gross Elongatio 30.45 IN. — Max. Gross(+5%)= 31.97 IN.

Req'd Net Elongation= 30.07 IN. — Max. Net(+5%)= 31.57 IN.

	Actual Gauge	Net Elong.	Gross Elong.
A1	45,000	30.17	30.87
B1	11	30.27	30.80
C1	11	30.09	30.83
D1	11	30.28	30.84
E1	11	30.22	30.79
F1	11	30.07	30.68
G1	11	30.10	30.88
H1	11	30.14	30.76
I1	11	30.19	30.75
J1	11	30.07	30.88
K1	11	30.23	30.78
L1	11	30.26	30.83
L2	11	30.18	30.83
K2	11	30.18	30.84
J2	11	30.07	30.70
I2	11	30.37	30.92
H2	11	30.07	30.97
G2	11	30.15	30.92
F2	11	30.21	30.95
E2	11	30.13	31.03
D2	11	30.07	30.86
C2	11	30.38	30.96
B2	11	30.09	30.83
A2	11	30.36	30.96

	Actual Gauge	Net Elong.	Gross Elong.	
A3	11	30.07	30.735	
B3	11	30.28	30.91	
C3	11	30.32	30.90	
D3	11	30.07	30.83	
E3	11	30.19	30.93	
F3	11	30.19	30.85	
G3	11	30.07	30.80	
H3	11	30.09	30.95	
I3	11	30.32	30.87	
J3	11	30.27	30.89	
K3	11	30.37	30.95	
L3	11	30.18	30.83	9
J4	11	30.31	30.86	8
I4	11	30.07	30.82	
H4	11	30.08	30.90	
G4	11	30.30	31.01	7
F4	11	30.16	30.94	2
E4	11	30.07	30.91	
D4	11	30.27	30.96	6
C4	11	30.14	30.92	3
F5	11	30.14	31.01	
G5	11	30.14	30.97	

DRAPED STRANDS: Req'd Gaug 44,570 PSI — Max. Gauge(+ 5%)= 46,800 PSI

Req'd Gross Elongatio 30.26 IN. — Max. Gross(+5%)= 31.77 IN.

Req'd Net Elongation= 29.89 IN. — Max. Net(+5%)= 31.38 IN.

DRAPED PATTERN

DR

1	x	x	2
4	x	x	3
5	x	x	6
8	x	x	7
9	x	x	10
12			11
13			14
16			15
17			18
20			19

Comments: No temp Corr. (70°)

Calcs By: _____ Date: _____

Reviewed By: _____ Date: _____

	Actual Gauge	Net Elong.	Gross Elong.	
DR1	45,750	29.89	30.80	4
DR2	11	29.92	30.75	
DR3	11	29.92	30.86	
DR4	11	29.98	30.75	
DR5	11	30.11	30.98	
DR6	11	30.13	30.82	
DR7	11	30.07	30.72	
DR8	11	30.06	30.72	
DR9	11	30.05	30.68	11
DR10	11	29.90	30.68	
X1	45,000	30.17	30.87	
X2	11	30.25	30.81	
X3	11	30.18	30.83	
X4	11	30.12	30.80	
XX4	11	30.26	30.93	10
XX3	11	30.17	30.90	
XX2	11	30.19	30.87	
XX1	11	30.30	31.00	1

Straights

Figure C.6: Test 3 tensioning sheet – page 2 of 2

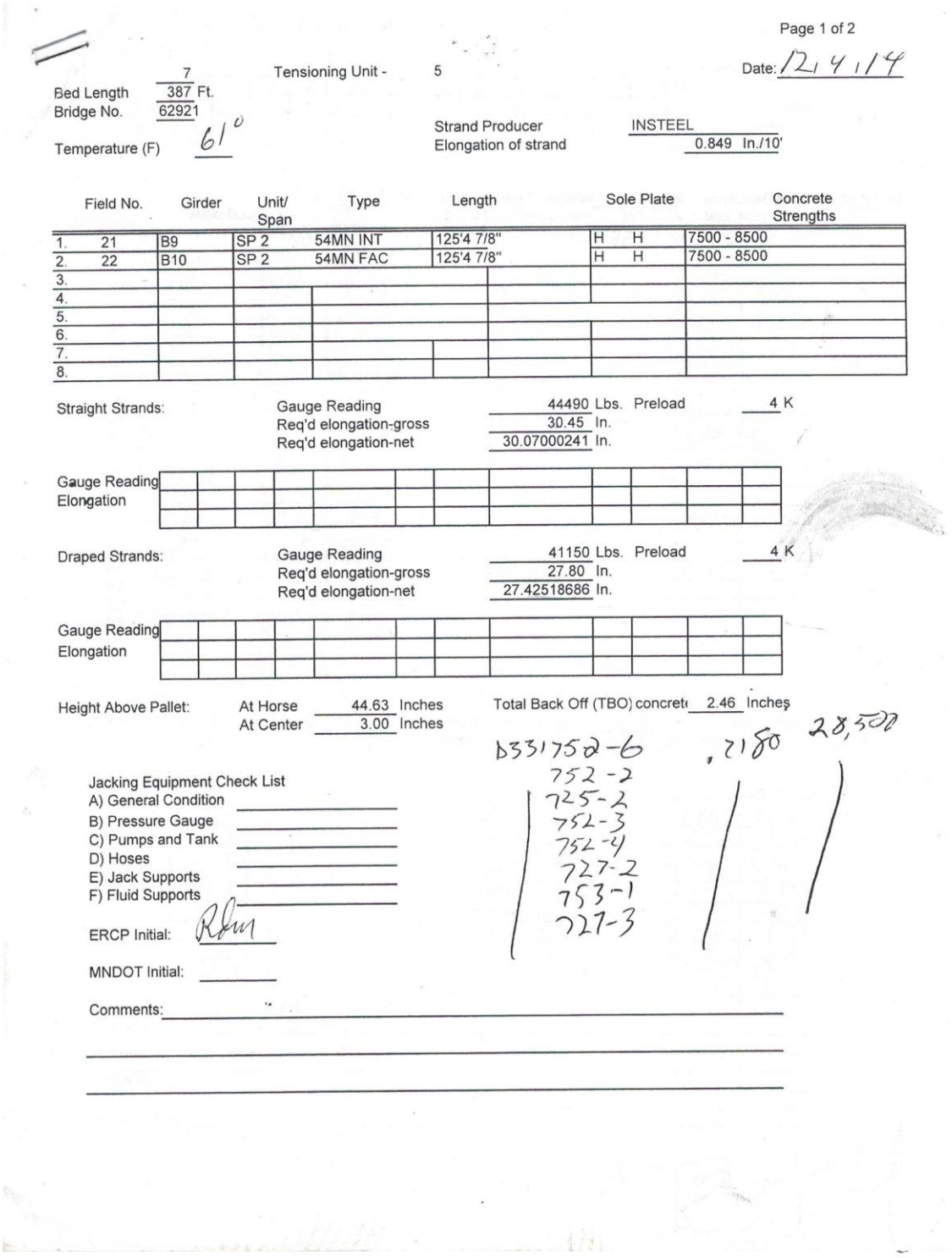

Page 1 of 2

Date: 12/4/14

Bed Length 7 387 Ft.
Bridge No. 62921
Temperature (F) 61°

Tensioning Unit - 5

Strand Producer INSTEEL
Elongation of strand 0.849 In./10'

Field No.	Girder	Unit/ Span	Type	Length	Sole Plate	Concrete Strengths
1. 21	B9	SP 2	54MN INT	125'4 7/8"	H H	7500 - 8500
2. 22	B10	SP 2	54MN FAC	125'4 7/8"	H H	7500 - 8500
3.						
4.						
5.						
6.						
7.						
8.						

Straight Strands:
Gauge Reading 44490 Lbs. Preload 4 K
Req'd elongation-gross 30.45 In.
Req'd elongation-net 30.07000241 In.

Gauge Reading												
Elongation												

Draped Strands:
Gauge Reading 41150 Lbs. Preload 4 K
Req'd elongation-gross 27.80 In.
Req'd elongation-net 27.42518686 In.

Gauge Reading												
Elongation												

Height Above Pallet: At Horse 44.63 Inches
At Center 3.00 Inches

Total Back Off (TBO) concrete 2.46 Inches

D331752-6 .2180 28,500
752-2
725-2
752-3
752-4
727-2
753-1
727-3

Jacking Equipment Check List
A) General Condition
B) Pressure Gauge
C) Pumps and Tank
D) Hoses
E) Jack Supports
F) Fluid Supports

ERCP Initial: RDM

MNDOT Initial:

Comments:

Figure C.7: Test 4 tensioning sheet – page 1 of 2

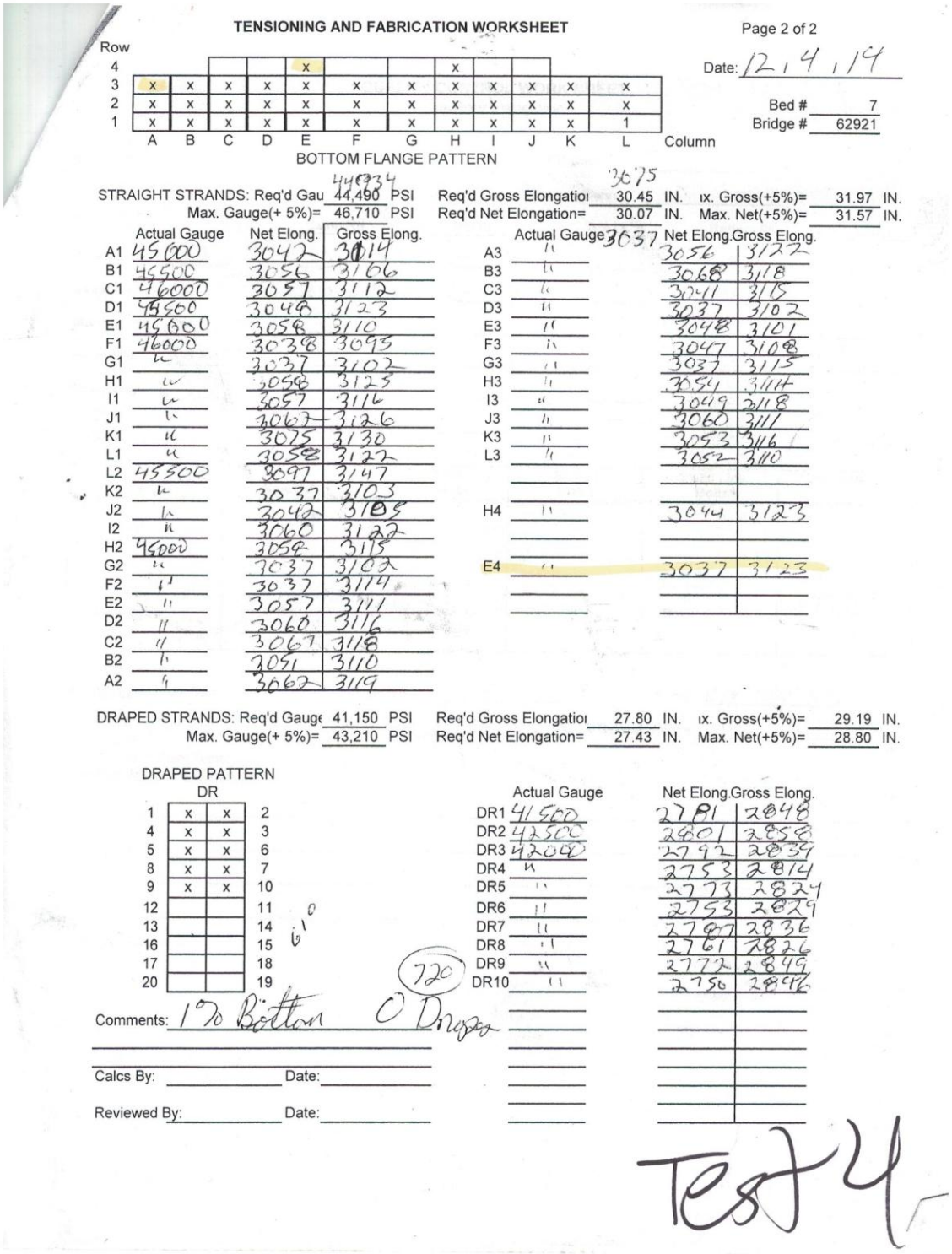

TENSIONING AND FABRICATION WORKSHEET

Page 2 of 2

Date: 12, 4, 14

Bed # 7

Bridge # 62921

Row	A	B	C	D	E	F	G	H	I	J	K	L
4					x			x				
3	x	x	x	x	x	x	x	x	x	x	x	x
2	x	x	x	x	x	x	x	x	x	x	x	x
1	x	x	x	x	x	x	x	x	x	x	x	1

Column

BOTTOM FLANGE PATTERN

STRAIGHT STRANDS: Req'd Gau 44,490 PSI (44834) Req'd Gross Elongatio 30.45 IN. (30.75) ix. Gross(+5%)= 31.97 IN.

Max. Gauge(+ 5%)= 46,710 PSI Req'd Net Elongation= 30.07 IN. Max. Net(+5%)= 31.57 IN.

	Actual Gauge	Net Elong.	Gross Elong.
A1	45600	3042	3014
B1	45500	3056	3166
C1	46000	3057	3112
D1	45500	3048	3123
E1	45600	3058	3110
F1	46000	3038	3095
G1	"	3037	3102
H1	"	3058	3123
I1	"	3057	3116
J1	"	3067	3126
K1	"	3075	3130
L1	"	3058	3122
L2	45500	3097	3147
K2	"	3037	3103
J2	"	3047	3108
I2	"	3060	3122
H2	45600	3059	3115
G2	"	3037	3102
F2	"	3037	3114
E2	"	3057	3111
D2	"	3060	3116
C2	"	3067	3118
B2	"	3051	3110
A2	"	3062	3119

	Actual Gauge (3037)	Net Elong.	Gross Elong.
A3	"	3056	3122
B3	"	3068	3118
C3	"	3041	3115
D3	"	3037	3102
E3	"	3048	3101
F3	"	3047	3108
G3	"	3037	3115
H3	"	3054	3114
I3	"	3049	3118
J3	"	3060	3111
K3	"	3053	3116
L3	"	3052	3110
H4	"	3044	3123
E4	"	3037	3123

DRAPED STRANDS: Req'd Gauge 41,150 PSI Req'd Gross Elongatio 27.80 IN. ix. Gross(+5%)= 29.19 IN.

Max. Gauge(+ 5%)= 43,210 PSI Req'd Net Elongation= 27.43 IN. Max. Net(+5%)= 28.80 IN.

DRAPED PATTERN

DR			
1	x	x	2
4	x	x	3
5	x	x	6
8	x	x	7
9	x	x	10
12			11
13			14
16			15
17			18
20			19

	Actual Gauge	Net Elong.	Gross Elong.
DR1	41500	2781	2848
DR2	42500	2801	2858
DR3	42000	2792	2834
DR4	"	2753	2814
DR5	"	2773	2824
DR6	"	2753	2829
DR7	"	2787	2836
DR8	"	2761	2826
DR9	"	2772	2849
DR10	"	2750	2846

(720)

Comments: 170 Bottom 0 Drapes

Calcs By: _____ Date: _____

Reviewed By: _____ Date: _____

Test 4

Figure C.8: Test 4 tensioning sheet – page 2 of 2

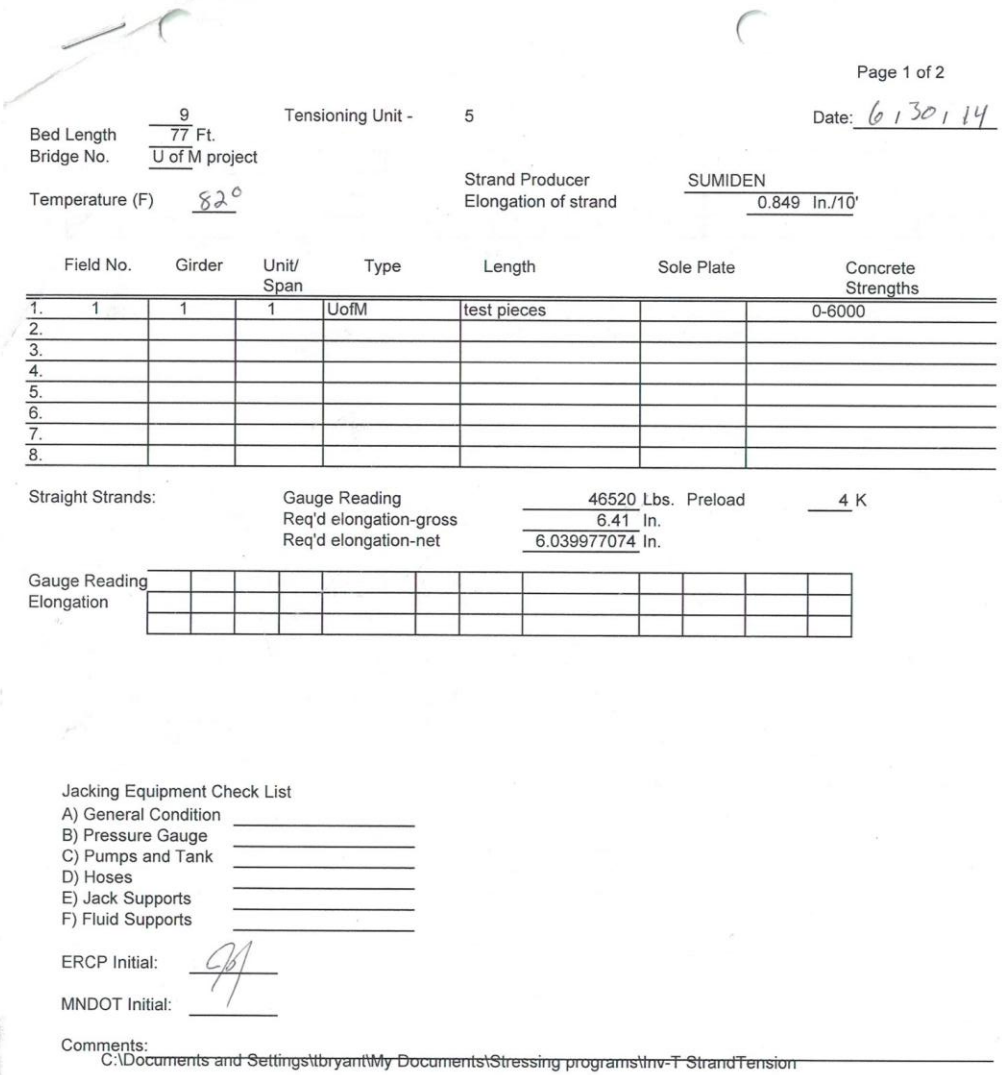

Page 1 of 2

Bed Length 9 / 77 Ft. Tensioning Unit - 5 Date: 6/30/14

Bridge No. U of M project

Temperature (F) 82° Strand Producer SUMIDEN

Elongation of strand 0.849 In./10'

	Field No.	Girder	Unit/ Span	Type	Length	Sole Plate	Concrete Strengths
1.	1	1	1	UofM	test pieces		0-6000
2.							
3.							
4.							
5.							
6.							
7.							
8.							

Straight Strands: Gauge Reading 46520 Lbs. Preload 4 K

Req'd elongation-gross 6.41 In.

Req'd elongation-net 6.039977074 In.

Gauge Reading												
Elongation												

Jacking Equipment Check List

A) General Condition _____

B) Pressure Gauge _____

C) Pumps and Tank _____

D) Hoses _____

E) Jack Supports _____

F) Fluid Supports _____

ERCP Initial: _____

MNDOT Initial: _____

Comments: C:\Documents and Settings\tbryant\My Documents\Stressing programs\Inv-T StrandTension

Figure C.9: Short girder test tensioning sheet – page 1 of 2

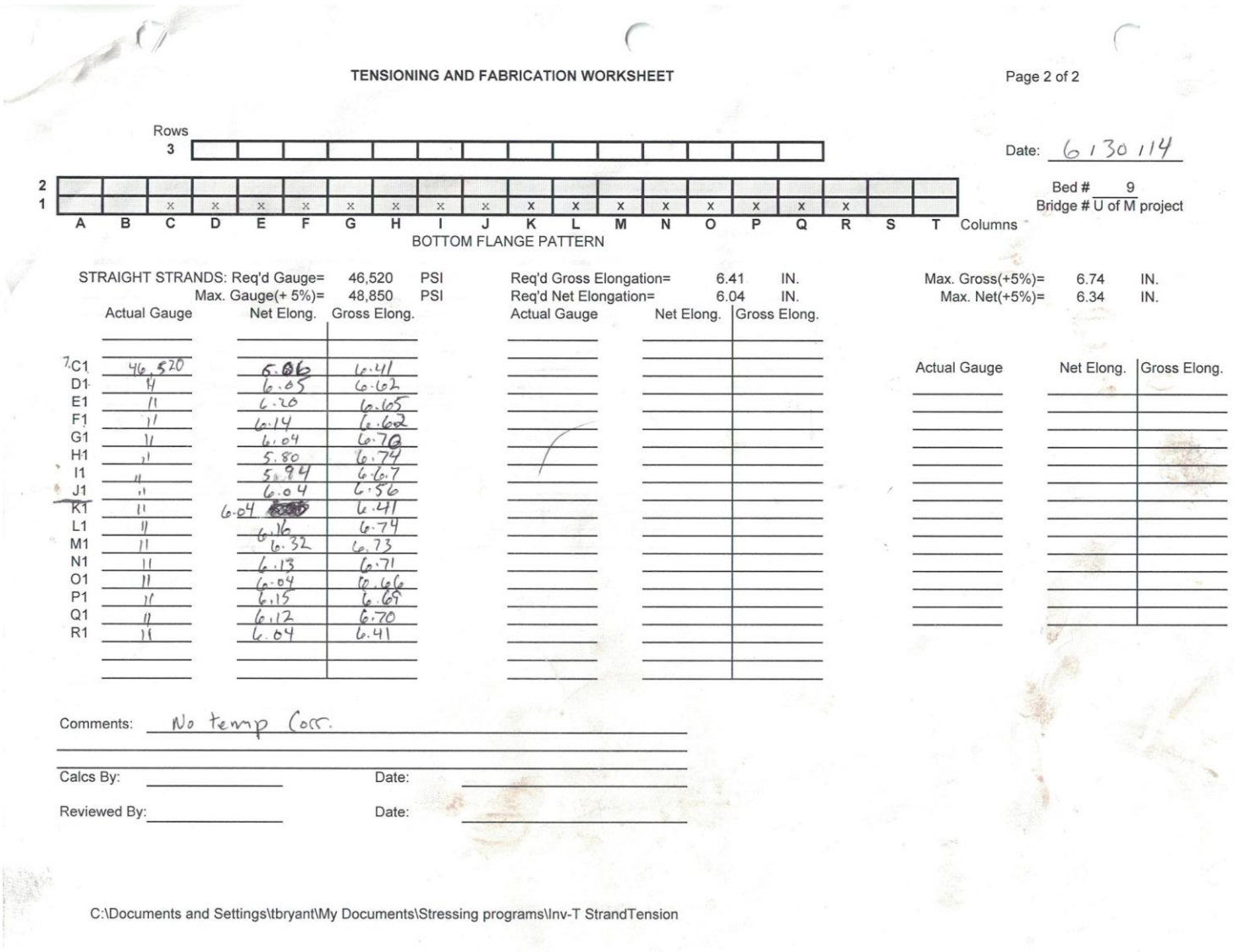

TENSIONING AND FABRICATION WORKSHEET

Page 2 of 2

Rows

3 | | | | | | | | | | | | | | | |

2 | | | | | | | | | | | | | | | | | | | | |

1 | | | x | x | x | x | x | x | x | x | x | x | x | x | x | x | x | x | | |

A B C D E F G H I J K L M N O P Q R S T Columns

Date: 6/30/14

Bed # 9

Bridge # U of M project

BOTTOM FLANGE PATTERN

STRAIGHT STRANDS: Req'd Gauge= 46,520 PSI

Max. Gauge(+ 5%)= 48,850 PSI

Req'd Gross Elongation= 6.41 IN.

Req'd Net Elongation= 6.04 IN.

Max. Gross(+5%)= 6.74 IN.

Max. Net(+5%)= 6.34 IN.

	Actual Gauge	Net Elong.	Gross Elong.
C1	46,520	6.06	6.41
D1	11	6.05	6.62
E1	11	6.20	6.65
F1	11	6.14	6.62
G1	11	6.04	6.70
H1	11	5.80	6.74
I1	11	5.94	6.67
J1	11	6.04	6.56
K1	11	6.04	6.41
L1	11	6.16	6.74
M1	11	6.32	6.73
N1	11	6.13	6.71
O1	11	6.04	6.66
P1	11	6.15	6.69
Q1	11	6.12	6.70
R1	11	6.04	6.41

Actual Gauge	Net Elong.	Gross Elong.

Comments: No temp Corr.

Calcs By: _____ Date: _____

Reviewed By: _____ Date: _____

C:\Documents and Settings\tbryant\My Documents\Stressing programs\Inv-T StrandTension

Figure C.10: Short girder test tensioning sheet – page 2 of 2

APPENDIX D. COMPARISON OF INITIAL STRAND FORCES USING ELONGATION, STRAIN GAGE, AND LOAD CELL MEASUREMENTS

Net elongation measurements recorded by the precasting plant during tensioning were used to determine the initial tensioning force that was used in the thermal effects analysis (TEA). Strain gages and load cells captured data on select strands during the tensioning process. Measured strains were converted to forces assuming an apparent modulus of 30700 ksi (212 GPa) based on tests described in Section 4.3.2. Table D.1 through Table D.4 show the differences in the strand force estimated from strain gage data and net elongation measurements for Tests 1 through 4, respectively. Figure D.1 through Figure D.3 show the differences between Strand 1 forces measured by the load cells and estimated by the net elongation measurement for full-scale Tests 2 through 4, respectively.

Table D.1: Tension forces calculated using strain gage data and elongation measurements for full-scale Test 1

Strand	Pull Order	Tension Forces [kip]				Difference** [kip]	
		Strain Gage Data*		Elongation Measurements			
		Gross	Net	Gross	Net	Gross	Net
1	1	46.3	44.8	45.8	44.8	0.5	0.0
2	28	43.3	42.8	46.2	45.1	-2.9	-2.3
3	25	47.0	46.2	45.9	44.7	1.1	1.4
4[+]	49	42.7	42.5	NA	NA	NA	NA

*Tension forces determined from strain gage readings assuming apparent elastic modulus of 30700 ksi

**Tension force from strain gage data minus corresponding tension from from elongation measurements

[+]Draped strand, elongations not recorded at full tension force

Table D.2: Tension forces calculated using strain gage data and elongation measurements for full-scale Test 2

Strand	Pull Order	Tension Forces [kip]				Difference** [kip]	
		Strain Gage Data*		Elongation Measurements			
		Gross	Net	Gross	Net	Gross	Net
1	32	46.7	46.2	45.4	44.6	1.3	1.6
2	49	NA	NA	45.4	44.3	NA	NA
3	52	45.0	44.4	45.4	44.4	-0.4	0.1
4[+]	55	44.7	44.5	NA	NA	NA	NA
5	33	45.1	44.8	45.5	44.7	-0.4	0.1
6	51	46.2	45.9	45.4	44.6	0.8	1.3
7	48	45.9	45.7	45.4	44.4	0.5	1.3
8	45	44.8	44.3	45.4	44.6	-0.7	-0.3
9	44	47.4	46.7	45.2	44.4	2.1	2.3
10	17	44.9	44.2	45.3	44.5	-0.4	-0.3
11[+]	59	43.9	43.6	NA	NA	NA	NA

*Tension forces determined from strain gage readings assuming apparent elastic modulus of 30700 ksi

**Tension force from strain gage data minus corresponding tension from from elongation measurements

[+]Draped strand, elongations not recorded at full tension force

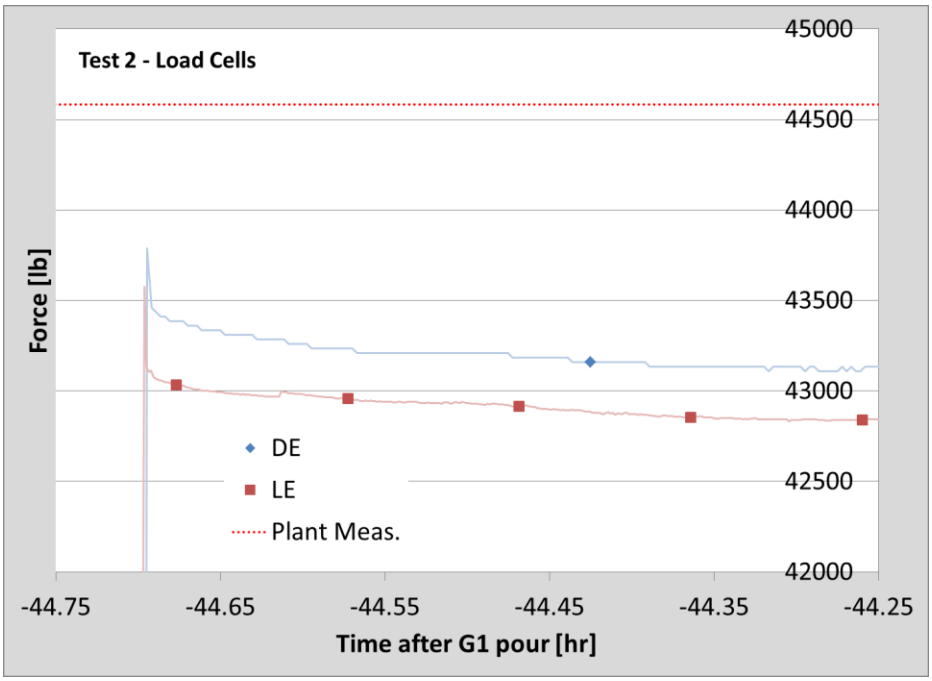

Figure D.1: Tension forces measured with load cells and calculated using elongation measurements on Strand 1 during full-scale Test 2

Table D.3: Tension forces calculated using strain gage data and elongation measurements for full-scale Test 3

Strand	Pull Order	Tension Forces [kip]				Difference** [kip]	
		Strain Gage Data*		Elongation Measurements			
		Gross	Net	Gross	Net	Gross	Net
1	32	45.9	45.1	45.5	44.6	0.4	0.5
2	49	47.6	47.4	45.4	44.4	2.1	3.0
3	52	44.0	43.7	45.4	44.4	-1.4	-0.7
4[+]	55	NA	NA	NA	NA	NA	NA
5	33	46.7	46.1	45.2	44.3	1.5	1.8
6	51	44.7	44.6	45.5	44.5	-0.7	0.0
7	48	46.9	46.4	45.5	44.6	1.4	1.8
8	45	45.6	45.5	45.3	44.6	0.3	0.9
9	44	45.7	45.2	45.3	44.4	0.4	0.7
10	17	NA	NA	NA	NA	NA	NA
11[+]	59	NA	NA	NA	NA	NA	NA

*Tension forces determined from strain gage readings assuming apparent elastic modulus of 30700 ksi

**Tension force from strain gage data minus corresponding tension from from elongation measurements

[+]Draped strand, elongations not recorded at full tension force

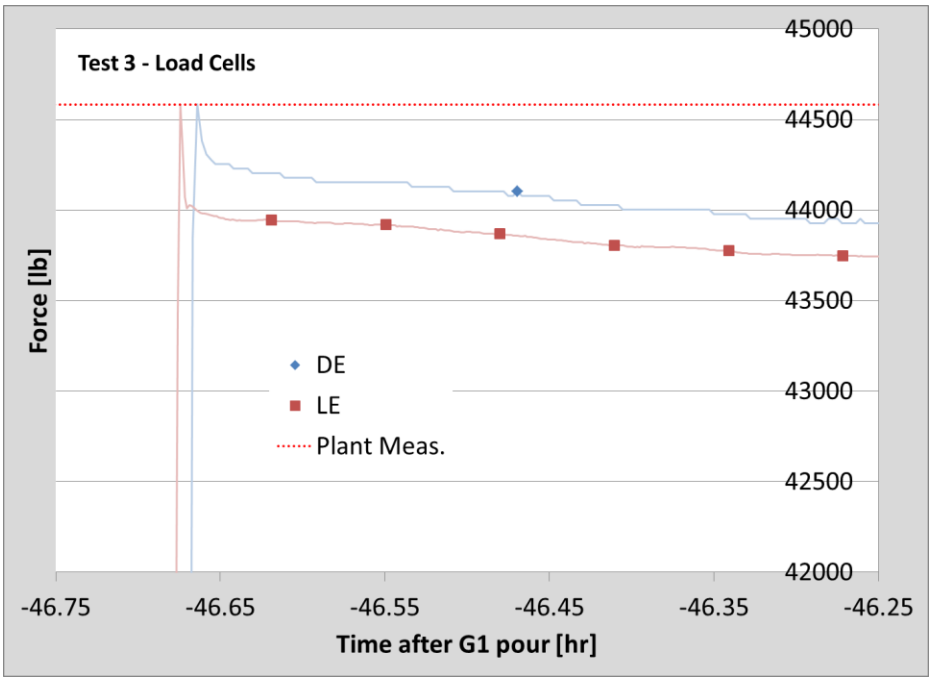

Figure D.2: Tension forces measured with load cells and calculated using elongation measurements on Strand 1 during full-scale Test 3

Table D.4: Tension forces calculated using strain gage data and elongation measurements for full-scale Test 4

Strand	Pull Order	Tension Forces [kip]				Difference** [kip]	
		Strain Gage Data*		Elongation Measurements			
		Gross	Net	Gross	Net	Gross	Net
1	38	47.5	46.7	45.8	44.7	1.6	2.1
2	25	46.8	45.7	45.8	44.9	1.0	0.8
3	37	NA	NA	45.8	44.8	NA	NA
4	1	NA	NA	45.7	44.7	NA	NA
5	12	NA	NA	45.8	45.0	NA	NA
6	27	47.1	46.6	45.7	44.7	1.4	1.8
7	30	NA	NA	45.6	44.8	NA	NA
8	36	NA	NA	45.7	44.9	NA	NA

*Tension forces determined from strain gage readings assuming apparent elastic modulus of 30700 ksi

**Tension force from strain gage data minus corresponding tension from from elongation measurements

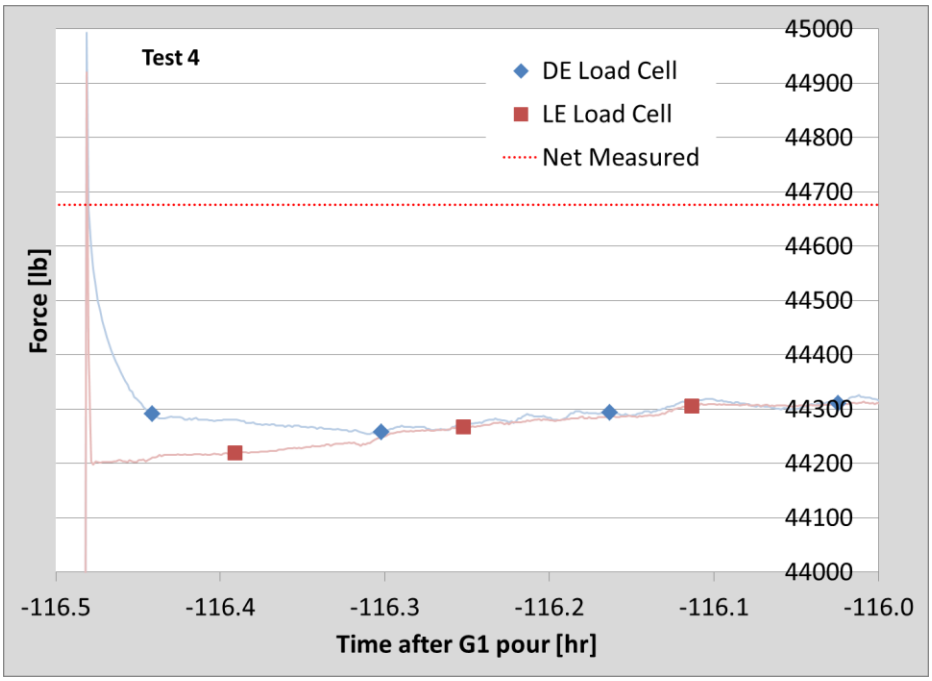

Figure D.3: Tension forces measured with load cells and calculated using elongation measurements on Strand 1 during full-scale Test 4